# Materials Science of Polymers for Engineers

## 2nd Edition

**Tim A. Osswald / Georg Menges**

**HANSER**

Tim A. Osswald / Georg Menges

# Materials Science of Polymers for Engineers

2nd Edition

*The Authors:*
Prof. Dr. Tim A. Osswald, Polymer Engineering Center, University of Wisconsin – Madison, Dept. of Mechanical Engineering, 1513 University Avenue, Madison WI 53706, USA
Prof. Dr.–Ing. Georg Menges, Am Beulardstein 19, 52072 Aachen, Germany

The use of general descriptive names, trademarks, etc., in this publication, even if the former are not especially identified, is not to be taken as a sign that such names, as understood by the Trade Marks and Merchandise Marks Act, may accordingly be used freely by anyone.

While the advice and information in this book are believed to be true and accurate at the date of going to press, neither the authors nor the editors nor the publisher can accept any legal responsibility for any errors or omissions that may be made. The publisher makes no warranty, express or implied, with respect to the material contained herein.

*For Diane, Palitos and Rudi*
*Tim A. Osswald*

*Dedicated to my wife in gratitude for her patience*
*Georg Menges*

*"Why does this applied science, which saves work and makes life easier, bring us so little happiness? The simple answer runs: Because we have not yet learned to make sensible use of it."*

Albert Einstein

## Preface to the Second Edition

The first edition of this book was adopted by several universities in North and South America, Europe, and Asia as a textbook to introduce engineering students to the materials science of polymers. The book was also translated into Japanese in 1998. The professors who taught with the first edition as well as their students liked the unified approach we took. Furthermore, it has become a reference for many practicing engineers, most of whom were introduced to the book as students. The changes and additions that were introduced in this edition are based on suggestions from these professors and their students, as well as from our own experience using it as a class textbook.

One major change that we made to this edition is the introduction of examples and problems at the end of each chapter. A new chapter containing the history of polymers replaced a few pages in the first edition. From a polymers course taught at the University of Wisconsin-Madison, we found that introducing polymers from a historical perspective not only made the topic less dry, but it also gave us a chance to show the role polymers have played, for better and for worse, while shaping today's industrial world. The mixing chapter in the first edition was replaced with a comprehensive polymer processing chapter. The first edition was praised because of the vast number of graphs and data that can be used as a reference. We have further strengthened this attribute by adding a table in the appendix that contains material property graphs for several polymers.

*Spring 2003*

Tim A. Osswald
Madison, Wisconsin, USA

Georg Menges
Aachen, Germany

## Preface to the First Edition

This book is designed to provide a polymer materials science background to engineering students and practicing engineers. It is written on an intermediate level for students, and as an introduction to polymer materials science for engineers. The book presents enough information that, in conjunction with a good design background, it will enable the engineer to design polymer components.

*Materials Science of Polymers for Engineers* is based on the German textbook, *Werkstoffkunde Kunststoffe* (G. Menges, Hanser Publishers, 1989), and on lecture notes from polymer materials science courses taught at the Technical University of Aachen, Germany, and at the University of Wisconsin-Madison. The chapters on thermal and electrical properties are loose translations from *Werkstoffkunde Kunststoffe,* and many figures throughout the manuscript were taken from this book.

We have chosen a unified approach and have divided the book into three major sections: Basic Principles, Influence of Processing on Properties, and Engineering Design Properties. This approach is often referred to as the four P's: polymer, processing, product and performance. The first section covers general topics such as historical background, basic material properties, molecular structure of polymers and thermal properties of polymers. The second section ties processing and design by discussing the effects of processing on properties of the final polymer component. Here, we introduce the reader to the rheology of polymer melts, mixing of polymer blends, development of anisotropy during processing and solidification processes. In essence, in this section we go from the melt (rheology) to the finished product (solidification). The third section covers the different properties that need to be considered when designing a polymer component, and analyzing its performance. These properties include mechanical properties, failure of polymers, electrical properties, optical properties, acoustic properties, and permeability of polymers.

The authors cannot acknowledge everyone who helped in one way or another in the preparation of this manuscript. We would like to thank the students of our polymer materials science courses who in the past few years endured our experimenting and trying out of new ideas. The authors are grateful to the staff and faculty of the Mechanical Engineering Department at the University of Wisconsin-Madison, and the Institut für Kunststoffverarbeitung (IKV) at the Technical University of Aachen for their support while developing the courses which gave the base for this book. We are grateful to Richard Theriault for proofreading the entire manuscript. We

# Table of Contents

# Part I

# Basic Principles

# Introduction to Polymers

As the word itself suggests, polymers[1] are materials composed of molecules of very high molecular weight. These large molecules are generally referred to as *macromolecules*. The unique material properties of polymers and the versatility of their processing methods are attributed to their molecular structure. The ease with which polymers and *plastics* [2] are processed makes them, for many applications, the most sought-after material today. Because of their low density and their ability to be shaped and molded at relatively low temperatures compared to traditional materials such as metals, plastics and polymers are the material of choice when integrating several parts into a single component—a design aspect usually called *part consolidation*. In fact, parts and components, which have traditionally been made of wood, metal, ceramic or glass are redesigned with plastics on a daily basis.

## 1.1 General Properties

Polymers can be placed into either a thermoplastic, thermoset, or elastomer category. Thermoplastics in turn include a special family, which is relatively new called thermoplastic elastomers. However, all these material have in common that they are made of huge molecules. Some of these molecules are uncrosslinked, which means that each molecule can move freely relative to its neighbors, and others are crosslinked, which means that "bridges", or physical links interconnect the polymer molecules. Thermoplastics and un-vulcanized elastomers are uncrosslinked. Vulcanized rubber, or elastomers, and thermosets are cross-linked.

Thermoplastics are those polymers that solidify as they are cooled, no longer allowing the long molecules to move freely. When heated, these materials regain the ability to "flow", as the molecules are able to slide past

---

[1]  From the Greek, *poli* which means many, and *meros* which means parts.

[2]  The term plastics describes a compound of polymers and various additives.

each other with ease. Furthermore, thermoplastic polymers are divided into two classes: amorphous and semi-crystalline polymers. Amorphous thermoplastics are those with molecules that remain in disorder as they cool, leading to a material with a fairly random molecular structure. An amorphous polymer solidifies, or vitrifies, as it is cooled below its glass transition temperature, $T_g$. Semi-crystalline thermoplastics, on the other hand, solidify with a certain order in their molecular structure. Hence, as they are cooled, they harden when the molecules begin to arrange in a regular order below what is usually referred to as the melting temperature, $T_m$. The molecules in semi-crystalline polymers that are not transformed into ordered regions remain as small amorphous regions. These amorphous regions within the semi-crystalline domains lose their "flowability" below their glass transition temperature. Most semi-crystalline polymers have a glass transition temperature at subzero temperatures, hence, behaving at room temperature as rubbery or leathery materials. On the other hand, thermosetting polymers solidify by being chemically cured. Here, the long macromolecules cross-link with each other during cure, resulting in a network of molecules that cannot slide past each other. The formation of these networks causes the material to lose the ability to "flow" even after reheating. The high density of cross-linking between the molecules makes thermosetting material stiff and brittle. Thermosets also exhibit a glass transition temperature which is sometimes near or above thermal degradation temperatures. Compared to thermosets, elastomers are only lightly cross-linked which permits almost full extension of the molecules. However, the links across the molecules hinder them from sliding past each other, making even large deformations reversible. One common characteristic of elastomeric materials is that the glass transition temperature is much lower than room temperature. Their ability to "flow" is lost after they are vulcanized or cross-linked. Since cross-linked elastomers at room temperature are significantly above their glass transition temperature, they are very soft and very compliant elastic solids.

Table 1.1 presents the most common amorphous and semi-crystalline thermoplastics, as well as thermosets and elastomers, with some of their applications. The abbreviations used in Table 1.1 are described in Table 1.2. Figure 1.1 presents just one example of where we can find polymers in everyday life. The young skier in the photograph is protected with a helmet that is composed of various polymer components. His skiing equipment is made up of various polymers and polymer composites, and he is keeping warm with several polymer fabrics and insulating materials. It should be pointed out that not all the polymer components the skier is wearing are listed in the figure, and that in addition to the specific polymers listed in Fig. 1.1, there are many more possibilities. For example, some skiing boots are reinforced with Aramid fibers, and there are skiing poles made of carbon fiber reinforced epoxy composites.

**Table 1.1**    Common Polymers and Some of Their Applications

| Polymer | Applications |
|---|---|
| | *Thermoplastics* |
| *Amorphous* | |
| Polystyrene | Mass-produced transparent articles, thermoformed packaging, etc. Thermal insulation (foamed), etc. |
| Polymethyl methacrylate | Skylights, airplane windows, lenses, bulletproof windows, stop lights, etc. |
| Polycarbonate | Helmets, hockey masks, bulletproof windows, blinker lights, head lights, etc. |
| Unplasticized polyvinyl chloride | Tubes, window frames, siding, rain gutters, bottles, thermoformed packaging, etc. |
| Plasticized polyvinyl chloride | Shoes, hoses, roto-molded hollow articles such as balls and other toys, calendered films for raincoats and tablecloths, etc |
| *Semi-crystalline* | |
| High density polyethylene | Milk and soap bottles, mass production of household goods of higher quality, tubes, paper coating, etc. |
| Low density polyethylene | Mass production of household goods, grocery bags, etc. |
| Polypropylene | Goods such as suitcases, tubes, engineering application (fiber-glass-reinforced), housings for electric appliances, etc. |
| Polytetrafluoroethylene | Coating of cooking pans, lubricant-free bearings, etc. |
| Polyamide | Bearings, gears, bolts, skate wheels, pipes, fishing line, textiles, ropes, etc. |
| | *Thermosets* |
| Epoxy | Adhesive, automotive leaf springs (with glass fiber), bicycle frames (with carbon fiber), etc. |
| Melamine | Decorative heat-resistant surfaces for kitchens and furniture, dishes, etc. |
| Phenolics | Heat-resistant handles for pans, irons and toasters, electric outlets, etc. |
| Unsaturated polyester | Toaster sides, iron handles, satellite dishes, breaker switch housing (with glass fiber), automotive body panels (with glass fiber), etc. |
| | *Elastomers* |
| Polybutadiene | Automotive tires (blended with natural rubber and styrene butadiene rubber), golf ball skin, etc. |
| Ethylene propylene rubber | Automotive radiator hoses and window seals, roof covering, etc. |
| Natural rubber (polyisoprene) | Automotive tires, engine mounts, etc. |
| Polyurethane elastomer | Roller skate wheels, sport arena floors, ski boots, automotive seats (foamed), shoe soles (foamed), etc. |
| Silicone rubber | Seals, flexible hoses for medical applications, etc. |
| Styrene butadiene rubber | Automotive tire treads, etc. |

**Table 1.2**    Abbreviations for Common Polymers

| Polymer | Abbrev. | Polymer | Abbrev. |
|---|---|---|---|
| Acrylonitrile-butadiene-styrene | ABS | Polyether ether ketone | PEEK |
| Butadiene rubber | BR | Polyether sulfone | PES |
| Cellulose acetate | CA | Polyethylene teraphthalate | PET |
| Cellulose acetate butyrate | CAB | Polyimide | PI |
| Cellulose nitrate | CN | Polyisobutylene | PIB |
| Epoxy | EP | Polymethyl methacrylate | PMMA |
| Ethylene-propylene-diene rubber | EPDM | Polyphenylene sulfide | PPS |
| Expanded polystyrene | EPS | Polyphenylene sulfone | PPSU |
| High density polyethylene | PE-HD | Polypropylene | PP |
| Impact resistant polystyrene | PS-HI (HIPS) | Polypropylene copolymer | PP-CO |
| Linear low density polyethylene | PE-LLD | Polystyrene | PS |
| Linear medium density polyethylene | PE-LMD | Polystyrene high impact | PS-HI |
| Liquid crystalline polymer | LCP | Polysulfone | PSU |
| Low density polyethylene | PE-LD | Polytetrafluoroethylene | PTFE |
| Melamine-formaldehyde | MF | Polyurethane | PUR |
| Metallocene catalyzed polyethylene | mPE | Polyvinylidene acetate | PVAC |
| Natural rubber | NR | Polyvinyl alcohol | PVAL |
| Olefinic thermoplastic elastomer | TPO | Polyvinyl carbazole | PVK |
| Phenol-formaldehyde (phenolic) | PF | Polyvinyl chloride | PVC |
| PF mineral filled moldings | PF-mf | Polyvinylidene fluoride | PVDF |
| PF organic filled moldings | PF-of | Rigid PVC | PVC-U |
| Plasticized PVC | PVC-P | Silicone | SI |
| Polyacetal (polyoxymethylene) | POM | Sillicone rubber | SI |
| Polyacrylate | PAR | Styrene-acrylonitrile copolymer | SAN |
| Polyacrylonitrile | PAN | Thermoplastic elastomer | TPE |
| Polyamide 6 | PA6 | Thermoplastic polyurethane elastomer | TPU |
| Polyamide 66 | PA66 | Unsaturated polyester | UP |
| Polybutylene teraphthalate | PBT | Urea-formaldehyde | UF |
| Polycarbonate | PC | Vinyl ester resin | VE |
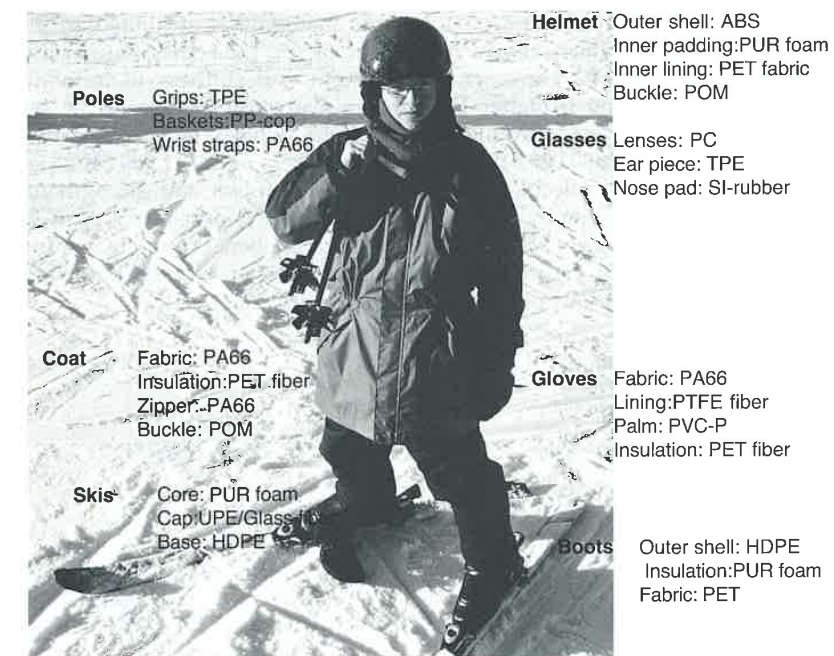
**Figure 1.1**    Polymers pervade everyday everywhere.

There are thousands of different grades of polymers available to the design engineer. These materials cover a wide range of properties, from soft to hard, ductile to brittle, and weak to tough. Figure 1.2 shows this range by plotting important average properties for selected polymers. The abbreviations used in Fig. 1.2 are described in Table 1.2. The values which correspond to each material in Fig. 1.2 only represent an average. There is a wide range in properties even for materials of the same class. The spread in properties is often increased with the different additives and fillers that a resin may contain. At this point, it is important to point out that the properties listed in Fig. 1.2 are not properties that should be used in design. The properties represent a general trend in stiffness and toughness of the various materials, and should be used only when comparing one material against another. As will be discussed in later chapters, properties that are used in design need to be time-dependent, such that loading time or speed can be included as design parameters. Today, it is very common for engineers to erroneously design a product using strength or stiffness data measured with tests such as ASTM D 638 or ASTM D790. These tests neglect the time dependence reflected in the mechanical behavior of polymers.

The relatively low stiffness of polymeric materials is attributed to their molecular structure, which allows movement of the molecules with relative ease while under stress. However, the strength and stiffness of individual polymer chains are much higher than the measured properties of the bulk polymeric material. For example, polyethylene whose molecules have a theoretical stiffness of 300,000 MPa, has a bulk stiffness of only 1,000 MPa [1, 2]. By introducing high molecular orientation, the stiffness and strength of a polymer can be substantially increased. In the case of *ultra-drawn, ultra high molecular weight high density polyethylene*, UHMHDPE, fibers can reach a stiffness of over 200,000 MPa [2]. Figure 1.2 [3] presents a plot of specific strength versus specific modulus of various polymer fibers and other materials.
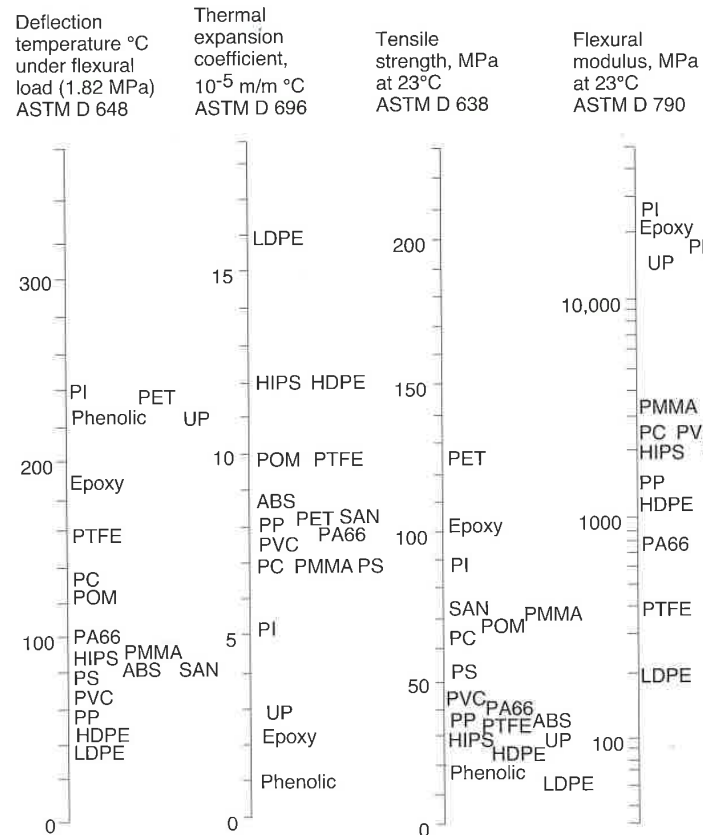


**Figure 1.2**   Average properties for common polymers. *(Continued)*
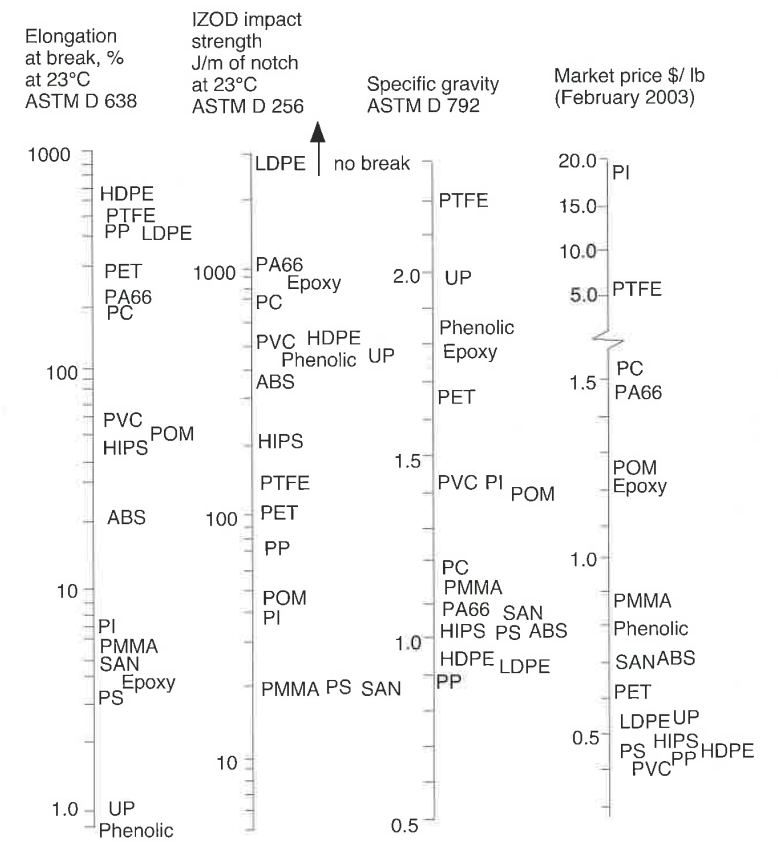


**Figure 1.2***(Continued)*   Average properties for common polymers.
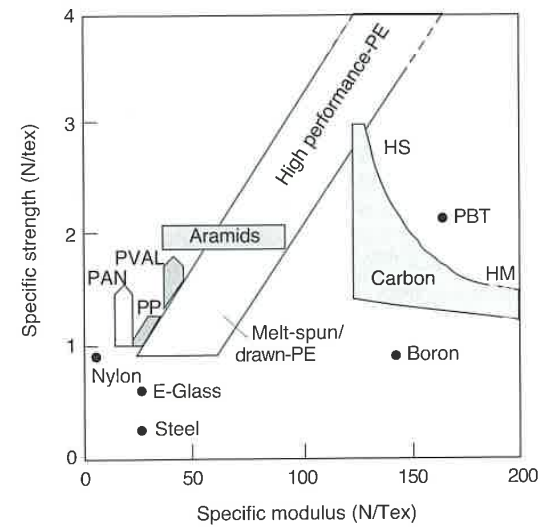
**Figure 1.3**    Specific strength versus specific modulus of fibers and other materials.

As will be discussed in more detail in Chapter 3, polymers also have a large range of molecular weights and molecular weight distributions, which affect the mechanical properties as well as the viscosity. Chapter 4 will discuss the thermal behavior of polymeric materials, and Chapters 5, 6, 7 and 8 will concentrate on rheology, processing of polymers, and how processing affects the properties of the final component through mixing, orientation, and solidification of the material during manufacturing. The important properties of the finished polymer component, such as mechanical properties, failure mechanisms, electrical properties, optical properties, permeability of polymers, etc. will be discussed in Chapters 9 through 14.

## 1.2    Identification of Polymers

Perhaps one of the most important skills a plastics design engineer needs to have is the ability to identify a specific polymer or polymer component. An experienced plastics engineers can often identify a polymer by touching, smelling, and tapping it. However, the complete identification of the chemical composition, additives, and fillers of a plastic material is an extremely complicated task. To achieve this, equipment that performs differential scanning calorimetry, infrared spectroscopy, and dynamic mechanical analysis, to name a few, is available[3]. Most process and design engineers do not have these measuring devices at hand, nor do they have the analytical experience to run them and interpret the resulting data. However, to identify a polymer often only simple means are needed in addition to basic knowledge of polymer chemistry. Through simple observation, a burn test and experience, an engineer is able to identify most plastics. Table 1.3 presents a summarized guide to aid in the identification of polymers.

Information presented in tables such as Table 1.3 must be used in conjunction with common sense and engineering insight. For example, the attribute labeled "Appearance" can sometimes be misleading. Depending on the additives or colorants added, even an amorphous thermoplastic such as polystyrene, can be opaque. The stiffness attribute is broken down into three categories: Flexible, semi-rigid and rigid. Flexible are those materials that feel rubbery or leathery, while semi-rigid are these that are strong and stiff but can deflect a substantial amount. The materials that fall under the rigid category are those that are stiff but brittle. During the burn test, as tempting as it may seem to some of us, it is not recommended to inhale the fumes released by a burning plastic, or those released soon after extinguishing the burning polymer. However, it can be said that without directly inhaling the fumes one can still discern the particular smells of the material during the burning test. Due to the benzene ring in their molecular structure, styrenic materials, such as PS, ABS and SAN have a sweet smell, while polyolefin plastics such as PE and PP smell waxy. Because of the nitrogen atoms in their structure, polyamides can smell like burning hair. When burning POM, a strong smell of formaldehyde is released. Burning PVC releases HCl. To no surprise, cellulose plastics smell like burning paper. All burn tests must be performed under a ventilation hood or in a well ventilated room.

---

3    These tests are discussed in detail in Chapters 3 and 8 of this book.

**Table 1.3**   Plastics Identification Attributes

| Polymer | Transparent | Transparent (thin film) | Translucent | Opaque | Flexible (resilient) | Semi-rigid | Rigid (brittle) | Glassy | Waxy | Dull | Black soot | Burns clean | Self extinguishing | Drips | Does not drip | Yellow flame | Blue flame | Green flame |
|---|---|---|---|---|---|---|---|---|---|---|---|---|---|---|---|---|---|---|
| PE-LD |  | • | • |  | • |  |  |  | • |  |  | • |  |  | • |  | • |  |
| PE-HD |  | • | • | • |  | • |  |  | • |  |  | • |  |  | • |  | • |  |
| PP |  | • | • |  |  | • |  |  | • |  |  | • |  |  | • |  | • |  |
| PP-CO |  | • | • |  |  | • |  |  | • |  |  | • |  |  | • |  | • |  |
| PS | • |  |  |  |  |  | • | • |  |  | • |  |  | • |  | • |  |  |
| PS-HI |  |  |  | • |  | • |  |  |  | • |  | • |  |  | • |  | • |  |
| SAN | • |  |  |  |  |  | • | • |  |  | • |  |  | • |  | • |  |  |
| ABS |  |  |  | • |  | • |  |  |  | • | • | • |  |  | • |  | • |  |
| PVC-U | • |  |  |  |  |  | • | • |  |  | • |  | • |  |  | • |  | • |
| PVC-P | • |  |  |  | • |  |  | • |  |  | • |  | • |  |  | • |  | • |
| PTFE |  |  | • | • |  |  | • | • |  |  |  | • | • |  |  |  | • | • |
| PVDF | • |  |  |  |  | • |  |  |  |  |  |  | • |  |  |  |  |  |
| PVAC |  |  |  |  |  | • |  |  |  |  | • |  |  |  |  | • |  |  |
| PVAL | • |  |  |  |  | • |  |  |  |  |  | • |  |  |  | • |  |  |
| PMMA | • |  |  |  |  |  | • | • |  |  |  | • |  | • |  |  | • |  |
| POM |  |  |  | • |  | • |  |  |  |  |  | • |  |  | • | • | • |  |
| PA6 |  | • |  |  |  | • |  | • |  |  |  | • |  |  | • |  | • |  |
| PA66 |  |  | • |  |  | • |  | • |  |  |  | • |  |  | • |  | • |  |
| PSU | • |  |  |  |  | • |  | • |  |  | • |  | • |  |  | • |  |  |
| PI |  | • |  |  |  |  | • |  |  |  |  |  | • |  |  | • |  |  |
| CA | • |  |  |  |  | • |  | • |  |  |  | • |  |  | • |  |  |  |
| CAB | • |  |  |  |  | • |  | • |  |  |  | • |  |  | • |  | • |  |
| CN | • |  |  |  |  |  | • | • |  |  | • |  |  |  |  | • |  |  |
| PC | • |  |  |  |  | • |  | • |  |  | • |  |  |  |  | • | • |  |
| PET | • |  |  |  |  | • |  | • |  |  | • |  |  |  |  | • | • |  |
| PBT | • |  |  |  |  | • |  | • |  |  | • |  |  |  |  | • | • |  |
| PF |  |  | • |  |  |  | • | • |  |  | • |  | • |  |  |  |  |  |
| PF-mf |  |  | • |  |  |  | • | • |  |  | • |  | • |  |  |  |  |  |
| PF-of |  |  | • |  |  |  | • | • |  |  | • |  | • |  |  |  |  |  |
| UP |  |  |  | • |  |  | • | • |  |  | • |  |  |  |  | • |  |  |
| EP | • |  |  |  |  |  | • | • |  |  | • |  |  |  |  | • |  |  |
| PUR |  |  |  | • | • | • | • | • |  |  | • |  |  |  | • |  |  |  |
| SI | • |  |  |  |  | • |  |  |  | • |  | • |  |  |  |  |  |  |

## Problems

1.1  Determine what material was used to fabricate the samples supplied to you by the instructor.

1.2  An opaque, semi-rigid plastic toy with a smooth surface is subjected to a burn test. It drips as it burns clean with a blue flame. There is a penetrating smell when the flame is extinguished. What material was used to manufacture this toy? Which of the above attributes should usually not be taken into account in the decision process?

1.3  A transparent and stiff cup which is involved in a Hamburger-Burger "cold juice spill" lawsuit is given to you by a group of lawyers. Of the various materials it could be made of, what is your first guess? Explain.

1.4  A competitor of yours makes a toy that is opaque, stiff, and has a smooth surface. You want to know what material it is made of. You burn a corner of the toy. The flame is yellow. What do you conclude from your tables? Which one of the attributes can you eliminate to make your decision easier.

## References

1.  Termonia, Y., and Smith, P., *High Modulus Polymers*, A.E. Zachariades, and R.S. Porter, Eds., Marcel Dekker Inc., New York, (1988).
2.  Ehrenstein, G.W., Faserverbundkunststoffe, Carl Hanser Verlag, München, (1992).
3.  Ihm, D.W., Hiltner, A., and Baer, E., *High Performance Polymers*, E. Baer and A. Moet, Eds., Hanser Publishers, Munich, (1991).

# Historical Background

Most topics are best introduced from a historical perspective. Although synthetic polymers and the plastics industry is a product of the 20th Century, the history of polymers goes back several centuries. This section presents some of the key materials and people involved in making the polymer industry into what it is known today.

## 2.1 From Natural to Synthetic Rubber

Natural polymeric materials such as rubber have been in use for several millennia. Natural rubber also known as *caoutchouc*[1] or *gummi elasticum*[2] has been used by South American Indians in the manufacture of waterproof containers, shoes, and torches (Fig. 2.1)[1]. When the natives made an incision in the bark of a tree it produced a white colored sap, composed of water and a monomer[3] called isoprene (Fig. 2.2). As the sap dried in air, and in conjunction with the sun's ultraviolet rays, the isopreme polymerizes into long chains or polymers, called polyisoprene (Fig. 2.2). This process turns the liquid into a sticky bouncy mass. Sometimes the natives performed the drying process while dipping a clay container in and out of a bat of rubber tree sap. This way, the container was slowly coated with a layer of polyisoprene, and when the layer was thick enough the clay was broken and washed out. This first dip-coating process produced a light waterproof container to carry liquids. Similarly, the indians produced rubber boots, by dip-coating their feet. A container produced by this method is shown in Fig. 2.3[1].

---

[1] From a native South American language *cahuchu: caa* (wood) and *o-chu* (tears). In French (caoutschouc) and German (Kautschuk) this word is still used to describe some elastomers.

[2] From the Latin elastic gum.

[3] While a polymer is made from many parts, a monomer is a single entity.

**Figure 2.1**    Tapping the rubber trees (1830).

$$n \; CH_2{=}CH - \underset{\underset{CH_3}{|}}{C} = CH_2$$

Isoprene

$$\left[ CH_2{-}CH = \underset{\underset{CH_3}{|}}{C} - CH_2 \right]_n$$
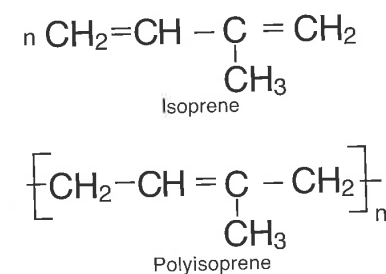
Polyisoprene

**Figure 2.2**    Isoprene and polyisoprene before and after polymerization



**Figure 2.3**    Container from the Amazon produced by an early dip-coating technique.

The first Spanish explorers of Haiti and Mexico reported that natives played games on clay courts with rubber balls [2]. Rubber trees were first mentioned in *De Orbe Novo*, originally published in Latin, by Pietro Martire d'Anghiera in 1516. The French explorer and mathematician Charles Maria de la Condamine, who was sent to Peru by the French *Académie des Sciences*, brought caoutchouc from South America to Europe in the 1740s. In his report [3] he mentions several rubber items made by native South Americans including a pistonless pump composed of a rubber pear with a hole in the bottom. He points out that the most remarkable property of natural rubber is its great elasticity. The first chemical investigations on *gummi elasticum* were published by the Frenchman Macquer in 1761. However, it was not until the 20th Century that the molecular architecture of polymers was well understood. Soon after its introduction to Europe, various uses were found for natural rubber. Gossart manufactured the first polymer tubes in 1768 by wrapping rubber sheets around glass pipes. During the same time period small rubber blocks where introduced to erase lead pencil marks from paper. In fact, the word *rubber* originates from this specific application — *rubbing*.

These new materials slowly evolved from being just a novelty thanks to new applications and processing equipment. Although the screw press, which is the predecessor of today's compression molding press, was patented in 1818 by McPherson Smith [4], the first documented *polymer processing* machinery dates back to 1820 when Thomas Hancock invented a rubber masticator. The primary use of this masticator, which consisted of a toothed rotor inside a toothed cylindrical cavity [5], was to reclaim rubber scraps which resulted from the manual manufacturing process of elastic straps[4]. In 1833, the development of the vulcanization[5] process by Charles Goodyear[6] [6] greatly enhanced

---

[4]  Perhaps the first plastics recycling program.

[5]  From the Greek *Vulcan*, god of fire.

[6]  In 1832, F. Lüdersdorff in Germany had already discovered that when incorporating sulfur into rubber it loses its tackiness if heated.

the properties of natural rubber, and in 1836, Edwin M. Chaffee invented the two roll steam-heated mill, the predecessor of the present day calender, for mixing additives into rubber for the continuous manufacturing of rubber coated textiles and leather. One of the first applications of vulcanized rubber was a set of rubber tires for Queen Victoria's carriage, but it took another 25 years for the veterinarian John Boyd Dunlop of Belfast, to develop the pneumatic tire to make his son's bicycle ride a little smoother.

As early as 1845, presses and dies were being used to mold buttons, jewelry, dominoes, and other novelties out of shellac and gutta-percha. *Gutta-percha* [7] or *gummi plasticum* [8], a gum found in trees similar to rubber, became the first wire insulation material and was used for ocean cable insulation for many years. A patent for cable coating was filed in 1846 for trans-gutta-percha and cis-hevea rubber and the first insulated wire was laid across the Hudson River for the Morse Telegraph Company in 1849. Charles Goodyear's brother, Nelson, patented hard rubber, or ebonite, in 1851 for the manufacturing of dental prostheses and combs. To allow the continuous coating of wires or textiles, the ram-type extruder was invented by Henry Bewley and Richard Brooman in 1845. The first *polymer processing* screw extruder [9], the most influential element in polymer processing, was patented by an Englishman named Mathew Gray in 1879 for the purpose of wire coating. Figure 2.4 [7] presents Mathew Gray's extruder as illustrated in his patent.

The demand for rubber grew rapidly in a world that was becoming more industrialized. In the late part of the 19th and early 20th Centuries, most of the world's rubber came from the Amazon region of South America. This not only led to a dependancy of the industrialized nations on a few local families and corporations in a relatively unstable part of the world, but also to horrible human rights abuses against the natives of the Amazon region by those entities that controlled the rubber cartel. To free themselves from the Latin-American rubber cartels, the British had planted rubber trees in Maylasia and other South East Asian colonies using seeds that had been smuggled out of South America by the 1920's. In Germany, to overcome its dependancy on rubber from other countries, and other countries' colonies, the German Kaiser, Wilhelm II, promised a 25,000 Reichsmark prize to anyone that would invent a synthetic replacement for natural rubber. By 1909, the German chemist Fritz Hoffmann, who was working at Bayer in Leverkusen had developed the first synthetic polyisoprene. The Kaiser's automobile was the first vehicle to be fitted with synthetic rubber tires (Fig 2.5[1]). When World War I broke out, the German government decided that since the war would not last long, it would drop the idea of building large polymerization plants to make synthetic rubber. Instead,

---

7    From the Malay *gettah* and *pertja* which means rubber and clump, respectively.

8    From the Latin plastic gum.

9    The screw pump is attributed to Archimedes, and the actual invention of the screw extruder by A.G. DeWolfe of the United States dates back to the early 1860s.

despite of the British embargo on Germany, the Germans smuggled natural rubber inside coffee cans from America through neutral countries. After 1916, the British blockade forced the Germans to produce synthetic rubber. In the next two years, Germany painstakingly produced 2,500 tons of synthetic rubber using polymerization processes that took several months.
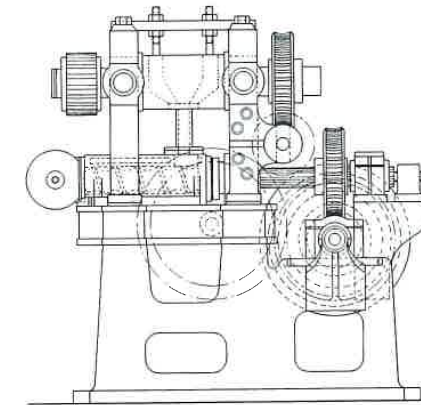


**Figure 2.4**    Mathew Gray's extruder as presented in his patent of 1879.

The low prices for rubber after the war -- 17¢ per pound in 1920 -- soon resulted in a loss of interest in continuing development of synthetic rubber. However, it did not take long for the rubber cartel to reorganize and as a result, prices of natural rubber skyrocketed again to a high of $1.21 per pound in 1925. The high rubber prices as well as being the home of the key polymer chemists of the time were the main incentives for the German government and industry to reinvest in their synthetic rubber research program.
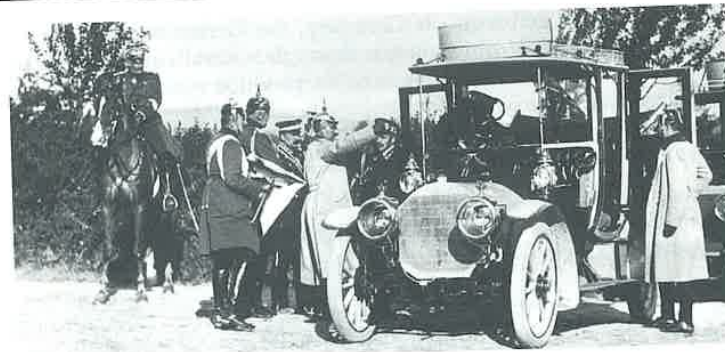
**Figure 2.5**    The Kaiser (to left wearing a white coat) and his car fitted with methyl rubber tires (1912).

Eventually, work on developing synthetic rubber became an obsession on both sides of the Atlantic ocean. By the late 1920s, the Germans had found a way to speed up the polymerization process of the butadiene monomer by using sodium as a catalyst. Their new material was marketed under the tradename Buna, made up of the first syllabi of butadiene and natrium. In the United States, Wallace Carothers (see Section 2.6), of the DuPont Company, developed polychloroprene, which was first marketed as Duprene and finally, in 1932, as Neoprene. However, by 1932, the depression had caused the prices of natural rubber to drop to an all time low of 3.5¢ per pound. By now, Germany was already in its quest of becoming self-sufficient, and intense research in the field of synthetic rubber was encouraged and funded. This resulted in styrene-butadiene rubber, marketed as Buna S, and in butadiene-acrylonitrile copolymers, marketed as Buna N. The Nazi regime saw synthetic rubber as a strategic element, and so, in addition to stockpiling natural rubber, they invested enormously in their synthetic rubber program at the IG Farbenindustrie. IG Farben was without doubt the leader in Germany's effort to become self-sufficient, and therefore enjoyed the backing of the regime. They soon started building Buna rubber plants all over Germany. During the war, to keep up with the large demand for synthetic rubber, IG Farben built the largest synthetic rubber plant in Monowitz, Silecia, just outside of Auschwitz. This was not only a very strategic place, since the location was close to the Silician coal mines that were far from Allied bombers, but undoubtedly a place that could supply prisoners for forced labor. This plant became an integral part of the Auschwitz III concentration camp and it was referred to as the Buna sub-camp. Despite of its magnitude, the Auschwitz-Monowitz Buna plant never produced a pound of rubber [8], however, it remains forever closely linked to one of the darkest hours of humanity.

## 2.2    Cellulose and the $10,000 Idea

If we step back to the 19th Century, in addition to rubber, another natural polymer, cellulose, impacted everyday life. The invention of cellulose plastics, also known as Celluloid, Parkesine, Xylonite, or Ivoride has been attributed to three people: The Swiss professor Christian Schönbein, the English inventor Alexander Parkes, and the American entrepreneur John Wesley Hyatt.

Christian Friedrich Schönbein, a chemistry professor at the University of Basel, loved to perform chemistry experiments in the kitchen of his home, much to his wife's dismay. Early one morning in the spring of 1845, Schönbein spilled a mixture of nitric and sulfuric acids, part of that day's experiment, on the kitchen counter. He quickly took one of his wife's cotton aprons and wiped the mess up, then rinsing it with water before the acid would damage the cloth. As he hung the apron to dry over the hot stove, it went into the air in a loud puff and flame. It had exploded in front of his very eyes. After he recovered from the shock, Schönbein's curiosity led him to impregnate wads of cotton with the acid mixture. Every time, he was able to ignite the mass, leading to an enormous, uncontrollable explosion. He called his invention guncotton. He had invented cellulose nitrate. Guncotton was three times as powerful as gunpowder and did not leave a black cloud after the explosion. Schönbein sold his patent to the Austrian Empire's army, but found no buyers in Prussia, Russia, or France. Finally, he sold his patent to John Taylor, his English agent, who immediately began production of guncotton in England. The production ended when his factory exploded, killing 20 workers. Although there were no buyers, several laboratories did spring up across Europe to investigate guncotton; going up into the air faster than they were being built. In addition to its bellicose applications, Schönbein envisioned other uses for the nitrated cotton mass. He added a solvent or plasticizer made of ether and alcohol and found a way to nitrate the cellulose fibers into a less explosive material which he called kollodium, glue in Greek. He reported to his friend Michael Faraday that this mass "is capable of being shaped into all sorts of things and forms…" In the spring of 1846, after accidentally cutting himself on the hand, he covered the wound with a thin elastic translucent film made of kollodium. He sold his idea to the English, who for years supplied the world with the first adhesive bandages. In England, there was one person that took particular interest in the Swiss professor's inventions. His name was Alexander Parkes.

Alexander Parkes started playing around with cellulose nitrate in 1847, and spent the next 15 years in the laboratory perfecting the formulas and processes to manufacture cellulose nitrate. His final process took the nitrated cotton and added vegetable oils and organic solvents producing a "plastic mass" that was easily molded into any shape or form after it was softened under heat. He called his plastic mass Parkesine. The new applications for this versatile

material, such as combs, knife handles, and decorations, made their debut at the 1862 World Exposition in London. In 1866, Parkes launched the Parkesine Company Ltd. Due to the low quality of its products, parkesine was not a success and the company was liquidated in 1868. The poor mixing of the additives and solvents caused Parkesine products to significantly warp only a few weeks after manufacture. In 1869, Parkes sold his patents to Daniel Spill, his chief engineer, who founded the Xylonite Company and renamed Parkesine, Xylonite. Parkes continued working on his material until his death in 1890 at the age of 77. Alexander Parkes, the inventor and engineer can be credited with improving on Schönbein's invention, paving the road for the future of the plastics industry. He is also credited with fathering a total of 20 children. A very busy man, to say the least.

At the same time as the plastics industry seemed to be going under in England, in the United States John Wesley Hyatt was launching an enterprise that finally made cellulose nitrate a success, under the name of celluloid. As the story goes, it all began when in 1865 the billiard ball manufacturer Phelan & Collendar placed an add that promised $10,000 to the person who would find a replacement for ivory in the manufacture of billiard balls. Elephants were being slaughtered at a rate of 70,000 per year, which would have led to the extinction of this great animal, exorbitant prices for the "white gold" from Africa, and reduced profits for the billiard ball industry. The $10,000 tag called the 28-year old Hyatt's attention. After returning home from his job as a printer, he worked on this project until eventually he stumbled upon nitrocellulose in 1869. After finding a way to better mix all the components as well as allowing the solvents to completely evaporate from the mass before solidification, he was soon manufacturing high quality billiard balls. Instead of cashing in on the $10,000 prize, John Hyatt founded the Albany Billiard Ball Company with his brother Isaiah, becoming a direct competitor to Phelan and Collendar. For the next thirty years, until Bakelite replaced celluloid on the billiard table, many guns were pulled in the Wild West when the volatile balls sometimes exploded upon collision. Another immediate application of celluloid were dentures (Fig. 2.6[9]), which up until then were made of hard rubber. In view of loosing a rather profitable business to plastics, the rubber industry started a propaganda campaign against cellulose in all major US newspapers. They falsely claimed that celluloid dentures could easily explode in ones mouth when coming in contact with hot food. This not only cheated people of a much prettier smile, but also started a rivalry between the two industries which has caused them to mantain as completely separate entities to this day. In fact, despite of the materials and processing similarities between plastics and rubber, the plastics industry and the rubber industry have completely separate societies and technical journals. A plastics engineer is likely to be found in meetings organized by the *Society of Plastics Engineers* (SPE) or the *Society of the Plastics Industry* (SPI), while a member of the rubber industry will attend meetings organized by their own society, the *Rubber Division of the American Chemical Society*.

With a new and versatile material, Hyatt and his coworkers needed equipment to mass-produce plastic products. Based on experience from metal injection molding, the Hyatt brothers built and patented the first injection molding machine in 1872, to mold cellulose materials [10], as well as the first blow molding machine, to manufacture hollow products. In the summer of 1869, Hyatt and Spill, respectively, filed for patents dealing with the manufacture of nitrocellulose materials. This started a lengthy and costly litigation that eventually ruled in Hyatt's favor in 1876. Spill died soon after, at age 55, of complications from diabetes. John Wesley Hyatt lived another 44 productive years in which he invented the injection molding and the blow molding machines with which he processed celluloid products. He can certainly be credited for being the first person to successfully mold a plastic mass into a useful, high quality final product. However, above all, we should credit him for saving the elephant on the road to a $10,000 prize he never claimed.



**Figure 2.6**    Celluloid dentures.

With the mass production of rubber, gutta-percha, cellulose, and shellac articles during the height of the industrial revolution, the polymer processing industry after 1870 saw the invention and development of internal kneading and mixing machines for the processing and preparation of raw materials [11]. One of the most notable inventions was the Banbury mixer, developed by Fernley Banbury in 1916. This mixer, with some modifications, is still in use today for rubber compounding.

## 2.3  Galalith -- The Milk Stone

Galalith, a popular plastic at the beginning of the 20th century, owes its discovery to a cat, a chemist, and an industrialist. Casein formaldehyde, a milk protein-based polymer is better known as casein plastic or by various trade names of which the most memorable ones are Galalith, Aladdinite, Erinoid, and Lactoid. As an industrial material it has come and gone, and all there is left are beautiful casein jewelry pieces, buttons, museum exhibits, and memories for plastic historians.

As the story goes, one night in 1897, the German chemist Adolf Spitteler's cat knocked over a small bottle of formaldehyde. The formaldehyde dripped from the chemists counter down to the floor into the cat's milk dish. The next morning, when Spitteler returned to his laboratory, he found that the formaldehyde that had dripped into the dish, had caused the milk to curdle and turn into a hard horn-like substance, much like celluloid. In fact, his cat had just invented the first semi-synthetic plastic since cellulose. Soon, Spitteler started experimenting with cheese curds (casein) and formaldehyde, and he found that the milk protein was rendered water-insoluble by letting it sit in a formaldehyde solution for extended periods of time.

Around the same time, Ernst W. Krische, who owned a small book binding and school supplies manufacturing company in Hanover, Germany, received a request from Turkey for washable, white writing boards. Pedagogists of the end of the 19th century believed that it would be better to teach children to write with black chalk on white boards rather than the other way around. However, the whiteboard had not been invented yet. Krische started experimenting by coating cardboard with casein. Casein, easily made by letting milk curdle, had been used for over 100 years as an adhesive, possibly also in Krische's book binding operation. In fact, the use of casein for non-food applications goes back even further, to at least 2 centuries B.C.E., in Egypt, where it was used as a binder for color pigments in the manufacture of paint. However, all these applications, which were well known at the end of the 19th century, did not require a water-insoluble material. In addition, there were many other hurdles that Krische had to overcome, such as the cracking and warpage which both resulted during the drying process of the wet casein.

Luckily, somehow Spitteler and Krische found each other. The chemist and the business man started playing with various materials that would soften or plasticize casein, such as glycerin and borax, and with various amounts and solutions of formaldehyde that would render the mass water-insoluble. Finally, in 1899 they were able to patent their invention. They were not only able to produce the washable whiteboards but soon their moldable plastic mass was marketed under the trade name of Galalith, from the Greek words for milk

(gala) and stone (lithos). In Britain it was marketed under the trade name of Erinoid, derived from the Gaelic word for Ireland, the source of most of the British cheese curds required in the manufacture of the new plastic mass.

Beautiful products were produced using this new semi-synthetic material. Bright colored artifacts, such as fountain pens, buttons, clock cases, combs, faux jewelry, etc., were all made out of this polymer. In addition to pigments, fish scales were often blended with casein to produce a pearlised effect. By the late 1920s, the height of casein formaldehyde production, over 10,000 tons per year of dry casein were being absorbed by the plastics industry worldwide. At the same time, 35,000 tons of cellulose were being transformed into plastic products every year. But the end of casein plastics was around the corner. In addition to phenol formaldehyde, the advent of synthetic polymers caused the casein industry to slowly disappear. The new materials were less expensive and easier to process.

Today, the use of casein as well as other protein-based polymers is very small. However, it is still, for example, possible to find very exclusive buttons being made of casein formaldehyde. Although most people regard Galalith as a historic material, the fact that protein-based plastics are made of renewable resources, offering us an unlimited supply of raw materials, should not be ignored.

## 2.4  Leo Baekeland and the Plastics Industry

Leo Hendrik Baekeland is well known for inventing the first synthetic polymer and for being the father of today's plastics industry. Dr. Baekeland, the chemist and inventor, refined and made possible Bakelite, also known as phenolic. Leo Baekeland, the sometimes mischievous, boyish, Belgian immigrant of modest origins, was an entrepreneur who created and gave momentum to what is known today as the plastics industry.

Leo Hendrik Baekeland was born November 14, 1863, in Ghent, Belgium, to poor illiterate parents. He excelled at school and at age 17 enrolled as the youngest student at the University of Ghent, where he studied chemistry. After only two years he finished his Baccalaureate in chemistry, and at age 21 he received a doctorate *summa cum laude*. Shortly after receiving his doctorate, he taught chemistry at the University of Bruges, until he was offered a professorship at the University of Ghent. That same year he married his major professor's daughter, Céline, much to the old professor's dismay. Baekeland would recount years later: "The most important discovery that I ever made was Céline." In the end, a displeased senior faculty member, and a traveling

fellowship to the United States was enough incentive for the young professor to embark for New York. During his visit, Professor Chandler at Columbia University encouraged Baekeland to stay in the United States. The 25-year-old Leo was now well aware that an academic career was not his calling. He was an entrepreneur at heart; even while an academic in Ghent he had started a small business that manufactured dry photographic plates, an enterprise that also satisfied his passion for photography. From New York, Baekeland telegraphed his resignation to the University of Ghent and soon after was offered a position as a chemist at A. & H.T. Anthony & Company, a large photographic supply house where he worked for two years. He then decided to try it on his own as a chemical consultant.

The next few years were very difficult for Baekeland. The country went into a deep recession, which adversely affected his consulting business. Worries about his finances and his future mounted, affecting Leo's health to the point that he was bedridden for an extended period of time. After recovering, he decided he would concentrate all his energies on one project where he knew he could strike it big. He returned to his old hobby, photography, and developed a photographic paper that was so light sensitive that it could be exposed using artificial light. Sunlight was the only light intense enough to expose the photographic plates of the late 1890s. *Velox*, the name he gave to his new product, was an instant success. It caught George Eastman's attention, who invited Baekeland to Rochester, NY, to negotiate the rights to this revolutionary photographic product. Baekeland had decided that he would ask Eastman for $50,000 for the rights of *Velox*, but he was willing go as low as $25,000. Before Baekeland was allowed to state his demands, the overpowering magnate took over the meeting and on the spot offered the young scientist $1 million for his invention. The year was 1899. Ten years after his arrival in the United States, the 35-year-old Leo Baekeland was wealthy beyond his wildest dreams.

Baekeland now had the necessary funds to embark on the research that would eventually lead to the development of Bakelite, the first synthetic plastic. Bakelite, also known as phenolic, results when phenol and formaldehyde undergo a condensation polymerization reaction. The reaction between these two readily available materials had been well known since 1872, when Adolf von Baeyer first reported it. Baekeland's contribution was converting the sticky useless material of the late 1800s into the chemical-resistant stiff product that could easily be shaped into any imaginable geometry during the 20th century.

Bakelite not only helped shape the streamlined pre-WWII years, but it also presented a material that made it possible to mass-produce items that made life easier in the home, office, street, field, and factory. The ability to mass-produce plastic products helped create the myth that plastics are a cheap replacement for

materials of higher quality. The reality is that phenolic is a material of superior mechanical and electrical properties with higher chemical resistance than those materials it replaced. For example, tough, lightweight, and stiff phenolic-cloth composite propellers replaced wooden aircraft propellers that easily cracked, causing catastrophic failures in the early years of aviation. In another case, Bakelite replaced wood as the material of choice for radio housings (Fig. 2.7), not because it was a cheaper material, but because it was easier and faster to form into its finished shape. In addition, phenolic offered the freedom to experiment with design and esthetics, while at the same time made products, that were previously considered luxuries, available to everyone.



**Figure 2.7**    Bakelite radios. (The Kölsch Collection).

While president of the American Chemical Society, Baekeland once said: "If academics are given the opportunities to cut their teeth on some practical problems, they may grow to be of decidedly greater service to their science or its applications." Baekeland gave himself that opportunity and certainly grew greater than anyone before or after him in the plastics industry. He died at age 80 in Beacon, New York, on February 23, 1944.

## 2.5    Herman Mark and the American Polymer Education

Herman Francis Mark has been credited for being one of the founders of the field of polymer science and for being the father of polymer education in the United States. Over his long and productive lifetime, Herman Mark published 20 books and over 500 articles. His Institute of Polymer Science at the Brooklyn Polytechnic University in New York served as the incubator for some of the most notable polymer scientists of the second half of the twentieth century.

Herman Mark was born in Vienna, Austria, on May 3, 1895, to a Jewish father and a Lutheran mother. He spent his formative years in the Viennese fourth district where his father, a physician, and his mother welcomed many turn-of-the-century intellectuals into their home. One can only imagine the impact on young Mark when among his parent's friends were the musician Johan Strauss, Sigmund Freud and Theodor Herzl, who with Chaim Weizmann went on to found the Zionist movement. As a twelve-year-old, his life and world changed during a visit to a university laboratory. When he got home, the excited boy reported of "glass bottles and glass beakers, blue flames and Bunsen burners, bubbling liquids and those long rubber tubes through which vapors are diverted." Soon after, Herman built his own laboratory in his room, where he conducted his own analyses and syntheses, starting a love affair with chemistry that lasted over 80 years.

World War I forced him into adulthood (Fig.2.8[9]). He served as a combat soldier on various fronts for a period of five years. During this time he had two short stays in Vienna, the first to recover from a bullet wound. As usual, making the most of his time, during each stay he completed a semester of chemistry at the university. During the war, his many acts of bravery made Herman Mark a national hero. On one occasion, Mark single-handedly held a dozen Russian soldiers at bay until his whole commando reached safety. At the end of the war, after a short imprisonment in Italy, Mark, now the most decorated officer of the Austrian Army, continued his chemistry studies at the University of Vienna.

After Graduating *suma cum laude* with a Ph.D. in chemistry in the summer of 1921, he moved to Berlin with his advisor Wilhelm Schlenk who succeeded Professor Emil Fischer at the University of Berlin. The year 1922 was an eventful year for Mark: he married Marie Schramek (Mimi) and joined the Kaiser Wilhelm Institute for fiber chemistry (today the Max Planck Institute), directed by R. O. Herzog. In Berlin, Mark co-authored over 30 papers, which included his work on applying the field of X-ray diffraction when analyzing crystal structures. His stay in the postwar, inflation ridden Prussian capital gave him the opportunity to work and fraternize with people of various backgrounds and nationalities, broadening his intellect and interests. He always felt that a highlight of his years in Berlin was when he conducted experiments for Albert Einstein to confirm Einstein's light-quantum hypothesis.

In the summer of 1926, Professor Kurt H. Meyer, one of the research leaders at the I.G. Farbenindustrie chemical giant's BASF labs in Ludwigshafen, visited Mark in Berlin and proposed that the young scientist move to industry to apply his basic research abilities to industrial problems. Mark accepted Meyer's offer and in January of 1927, moved to Mannheim, where he and his family would live for the next five years. This dramatic change, along with Mark's association with Meyer, his immediate boss at I.G. Farben, and his continuing collaboration with Hermann Staudinger and other German academic scientists of the time, served as one of the catalysts that propelled the field of polymer science into the spotlight. In 1924, Hermann Staudinger[10] had proposed a model that described polymers as linear molecular chains. Once this model was accepted by other scientists, the concept used to synthesize new materials was realized. For his idea of giant molecules, Staudinger was ridiculed by his conservative peers, who at the time were still convinced that polymers such as natural rubber (polyisoprene) were made of colloids. It took until 1953 for Staudinger to receive the Nobel prize for his pioneering work on polymers. The young and open-minded Hermann Mark understood Staudinger's theories from the beginning. In 1928, Mark and Meyer proposed a crystal structure for cellulose, rubber, and silk, nearly identical to the ones still accepted today. Their theory was supportive of Staudinger's high molecular weight theory and refuted the commonly accepted colloidal association theory of the time. Mark's model for polymer molecules differed from Staudinger's in that the molecules were flexible, not rigid, as Staudinger suggested. Time would prove Mark right. In the relatively short time at I.G. Farben, Mark produced an impressive list of publications, which included over 80 papers, 17 patents and 3 books.



**Figure 2.8** Hermann Mark in 1917.

---

[10]   The idea that polymers were formed by macromolecules was not well received by his peers at first. However, for this work Staudinger received the 1953 Nobel prize in chemistry.

With the political winds in Germany shifting to the right, and because of their Jewish ancestry, both Herman Mark's and Kurt Meyer's positions at I.G. Farben became uncertain in the summer of 1932. The advice that came from the top of the company was that Mark look for an academic position, preferably outside of Germany. However, since I.G. Farben did not want to loose a certain degree of control on Mark's research, he was promised financial support for his future academic work. And so, Herman Mark, his wife, Mimi, and two young children moved to Vienna in the fall of 1932, where he became director of the first Chemistry Institute at the University of Vienna. His friend and closest collaborator, Kurt Meyer, moved to Geneva that same year. With I.G. Farben funds, Mark was able to assemble an impressive team of scientists that included Eugene Guth, Robert Simha, and Fritz Eirich. In Vienna, Mark published many fundamental papers on polymer physics including groundbreaking theories on polymer relaxation, polymerization kinetics and molecular weight distribution. However, leaving Germany was not enough; during the thirties, the Austrian political airs also started turning brown, culminating March 15, 1938, when the Nazis marched into Vienna. Mark was arrested the following day, and released without his passport four days later. The next eight weeks were spent recovering his passport and securing a position in Canada, in order to get Canadian and Swiss visas. To finance his trip to North America, the resourceful Mark purchased over one kilogram of platinum wire that he carefully wrapped around coat hangers. With visas in-hand, and their precious currency, the Marks and their niece attached a Nazi flag on the hood of their car and placed rope and skis to the roof and headed up the Alps. They drove into Switzerland on May 10, 1938. After bribing their household possessions out of Austria, the Marks spent the summer in Switzerland, France, and England. Mark started his new position at the Canadian International Paper Company in September of 1938.

After almost two years in Canada, Mark moved to New York in the summer of 1940 where he founded The Institute of Polymer Science at the Brooklyn Polytechnic University in New York. This marks the official start of polymer science education in the United States. The Institute of Polymer Science was the first American institution to award the Ph.D. degree in polymer science, and thus, became the incubator of many American scientists and educators. He advised over 100 scientists that included Fritz Eirich, Edmund Immergut, Herbert Morawetz, and Charles Overberger. Some of his students went on as educators, multiplying the polymer science education all over the world. Eirich stayed at Brooklyn, Guth went to Notre Dame, Simha to Caltech and later to Case Western. Other pupils of Mark served as editors and writers such as Immergut, who had several editorial positions, including with Hanser Publishers between 1980 and 1997, which resulted in a vast polymer engineering and science book library, that has served as a reference and resource to many students, engineers, and scientists. During his years at

Brooklyn, Mark wrote hundreds of papers, many books and was the founder and editor of various journals including the Journal of Polymer Science. He also served as a consultant to DuPont, Polaroid, and others, and maintained relations with industry in his native Austria.

Herman Mark's lifetime achievements were recognized by many: he received 17 honorary doctorates, numerous medals and awards, and served as an honorary member to dozens of scientific academies and professional societies. Herman Mark, the war hero, scientist and teacher, died at age 96 in April of 1992.

## 2.6 Wallace Hume Carothers and Synthetic Polymers

Wallace Hume Carothers is perhaps the most influential American character in the history of polymers. Already as a child he was greatly admired by his grade school friends, who called him "Doc" for his ability to make, among other things, crystal radios. This was only the beginning of a short but productive life in a time when the field of polymer chemistry was still in its infancy. He went on to author over 50 technical papers, file over 100 U.S. and foreign patents, and above all, invent nylon, the world's first synthetic fiber. This specific contribution of Carothers opened the floodgates of invention in the field of thermoplastic polymers.

Born on April 27, 1896, in Burlington Iowa, Carothers was raised in Des Moines where his father taught at the Capital Cities Commercial College, which he attended after high school. He then went to Tarkio College in Missouri where he received a degree in Chemistry at age 24. From Tarkio he moved to the University of Illinois at Urbana-Champaign where he studied under Professor Roger Adams. In the summer of 1921 he received a science degree in chemistry and, after a one year teaching position at the University of South Dakota, defended his Ph.D. in the late spring of 1924. After two years as an instructor at Illinois, Carothers was recruited to teach at Harvard.

Carothers' success was also due in great part to the vision of Dr. Charles M. Stine, the Director of DuPont's Chemical Department. In 1927 Stine used his influence to accomplish something that was unheard of in a corporation of any size; he convinced the company's executive committee to fund research in pure science at the experimental station in Wilmington. With a $25,000 per month budget, Stine lured Carothers from Harvard were he had been teaching for about two years. With this practically unlimited budget and after assembling a team of extremely bright coworkers, including Paul Flory and Julian Hill, Carothers was ready to begin his 10-year tenure at DuPont. Building on his

experience as a physical chemist and on the research of his contemporaries, such as Adams, Marvel, Staudinger and Mark, Carothers and his team[11] developed polychloroprene, polyester, and of course polyamide 6 and polyamide 66. During that time he coined the terms so widely used today: *addition polymerization* and *condensation polymerization*. Polychloroprene (Fig. 2.9[9]), an elastomer, was polymerized by addition polymerization, similar to the polymerization of polyisoprene in Fig. 2.2. Polyamide 66 is polymerized by condensation polymerization as shown in Fig. 2.10.



**Figure 2.9**    Wallace Carothers stretching a sheet of polychloroprene.

---

11    Paul Flory who received the 1974 Nobel prize in chemistry worked in Carother's group at DuPont's research laboratories.

$$n \ HOOC - (CH_2)_4 - COOH \ + \ n \ H_2N - (CH_2)_6 - NH_2$$

Adipic acid                Hexamethylendiamine

$$\rightleftharpoons HO \Big[ OC - (CH_2)_4 - CO - NH - (CH_2)_6 - NH \Big] H + (2n-1)H_2O \uparrow$$
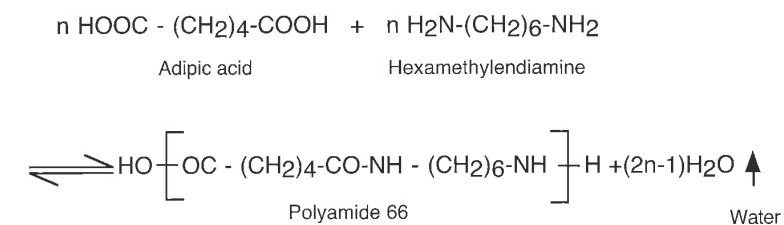
Polyamide 66                                                    Water

**Figure 2.10**    Condensation polymerization of polyamide 66.

Unfortunately, Carothers never saw the dramatic impact of his inventions. He suffered from two illnesses that in the 1930s were still considered deadly: he was both a manic-depressive and an alcoholic. And so, in spite of his own efforts, and the constant care of friends, family, and doctors, the demons finally took over. Two days after his 41st birthday he was found dead in a Philadelphia hotel room. He had taken cyanide.

In 1938, a year after Carothers's death, nylon was introduced to the world, primarily as a replacement for silk in hose and stockings and as toothbrush bristles. As the story goes, nylon is not an acronym for New York and London, as many people often believe. It evolved from the suggested name *norun* (a descriptive word that was inaccurate, since fiber 66 stockings did run), to *nuron* (which sounded too brainy), to *nulon* (which would have been hard to market as *the new nulon*), to nilon (two possible pronunciations) to, finally, nylon. In the heated pre-WWII years, it was even suggested that the word nylon was an insulting acronym for the Japanese. Though this is doubtful, it is certain that its invention gravely affected the Japanese trade balance, and in consequence, the overall position of the Japanese industry in world markets at the threshold of World War II. The influence of this miracle fiber is indisputable. Allied use of nylon in parachutes during the invasion of Normandy may have played a decisive role in the war's military outcome. The most obvious influence may come from its impact on consumer consumption. A comical example of this came after the war, the day a department store in Washington offered to sell a pair of nylon stockings to the first 1000 callers. As a result the entire phone system in the D.C. area was flooded and collapsed. This phone system had always resisted collapse, including the day Pearl Harbor was bombed, the day the war ended, and every historically significant day since. This suggests the real power of Carothers' invention: a public whose lives have been changed forever with the advent of thermoplastic polymers.

As Wallace Hume Carothers once said, he had done enough for one lifetime.

## 2.7    Polyethylene - A Product of Brain and Brawn

By the 1930s Staudinger, Carothers and Mark had paved the road of synthetic polymers for the chemical industry. At the ICI laboratories in Winnington, England, in addition to knowledge in polymers and polymerization, it took muscle power and risk-taking youths, to invent polyethylene, today's highest volume commodity plastic.

Eric William Fawcett and Reginald Oswald Gibson are the two young British scientists who can be credited with polymerizing the first few grams of polyethylene at the Winnington ICI laboratories in England. Fawcett was a young Oxford graduate who was only twenty years old and had to have his father come to the Winnington laboratories to sign for him his employment contract with ICI. Gibson had just returned from Amsterdam, where he had worked with Professor Anton Michels, the world-leading expert on high-pressure vessel design. They both worked in Lab Z, a small ICI laboratory that housed a pressure vessel that everyone called "the bomb." It was no coincidence that the assistants that worked in Lab Z were all young men in great physical shape. It took significant muscle power to operate the hand pump that could pressurize the bomb to up to 2,500 atmospheres (almost 37,000 psi). After pressurizing various liquids and finding that they remained unfazed, they decided to switch to gases, which they hoped would lead to more exiting reactions.

Late on a Friday afternoon, March 24 of 1933, they filled the bomb with ethylene gas, raised the temperature to 170 ºC and pressurized it to 1,900 atmospheres. They turned off the lights and went home for the weekend. Since they couldn't wait all weekend for their results, Fawcett and Gibson went back to the lab on Saturday morning and found that the pressure inside the vessel had dropped to 100 atmospheres, a sure sign for a chemical reaction having taken place. Again they pumped the bomb up to 1,900 atmospheres, and left for the remainder of the weekend. On Monday, they found the pressure dials marking 0 atmospheres. They found out that, in addition to the polymerization reaction that took place inside the vessel, the pressure drop was also due to a leak that sprang around an oil tube connection. After opening the vessel, they saw that its inside was covered with a waxy white powder, of which they were able to scrape out 0.4 grams; the first 0.4 grams of polyethylene. They quickly fixed the leak and repeated the experiment, recovering a total of 4 grams of polyethylene. They now had collected enough material that they were able to spin a couple of fibers and form a small thin film. In the third try, the bomb exploded. Even though the explosion did not harm anyone, the managers did not find these experiments as important as Fawcett and Gibson knew they were, and Lab Z was put to rest and the young men were given other tasks.

Two years later, Fawcett attended The Faraday Society of London polymer congress in Cambridge were Wallace Carothers, Herman Mark, Kurt Meyer, and Hermann Staudinger were the main guests and speakers. In the proceedings, Fawcett saw how the future Nobel Prize winner Staudinger claimed that it was not possible to polymerize ethylene. Fawcett got his courage together and went up to Staudinger's room at the University Arms Hotel to attempt to set him straight. There he told the prominent scientist that under certain conditions it was possible to polymerize ethylene. Staudinger ignored him and gave his talk as planned. After the talk Mark even supported Staudinger's findings. Undaunted by the prominence and belief of his opponents the young man rose and told the audience that ethylene polymerizes if maintained at 170 ºC under very high pressures. This bold move impressed Carothers, then a well-known American scientist, who offered Fawcett a job and took him to the DuPont laboratories in Wilmington, Delaware.

Soon after, ICI resumed their high-pressure vessel work, reproducing Fawcett and Gibson's experiments and patenting polyethylene in February of 1936. ICI continued to produce polyethylene using their high-pressure polymerization process. Soon, their operation had been scaled-up sufficiently to produce several kilograms of polyethylene every hour. In the meantime they had also discovered that this new plastic had excellent dielectric properties, which made it ideal for insulating thin wires for telecommunications applications.

In 1940, the British were at war. The Germans were bombing major English cities, and although ground radars detected the bombers, it was usually too late. A major breakthrough came when the British were able to reduce the weight of a radar from several tons to just under 600 pounds with the use of polyethylene as a wire insulator. This allowed them to place radars inside their fighter planes, enabling them to detect Nazi planes, before they saw them, shooting them out of the air at the same rate as they were crossing the British Channel. This put the British at an advantage, saving their cities from destruction. Similarly, the radar rendered the German submarine fleet obsolete, protecting the life saving sea transports, from the U.S.A. to England. As a result, hardly any submarines returned to Germany after 1943.

Twenty years after Fawcett and Gibson produced polyethylene inside the bomb, the German professor and future Nobel Prize winner Karl Ziegler found a way to polymerize ethylene at low pressures using catalysts. His catalysts where metal based compounds that act as vehicles as they drive through a sea of ethylene, picking up each monomer in an orderly fashion resulting in long chains of polyethylene. One was now able to produce this versatile material at much higher rates, under safer conditions, and at lower energy costs. Ziegler sold his patent to several resin producers who immediately jumped into production. However, they soon found out that their new process produced

polyethylene that cracked easily, rendering the first few thousand tons of high-density polyethylene useless. Luckily, in 1957 along came a small Californian toy manufacturer, The Wham-O Company, who proposed to use the inferior HDPE on their new toy: the Hula-Hoop (Fig. 2.11). While Wham-O was using up the world supply of imperfect polyethylene, and America was buying the hoops by the millions, the chemical companies were successfully working out the kinks in their polymerization processes. One of Ziegler's occasional co-workers, the Italian chemical engineer Giulio Natta, extended Ziegler's research on organometallic catalysts to discover polypropylene. Both, Ziegler and Natta received the Nobel Prize in chemistry in 1963, and today, Ziegler-Natta catalysts are still in use.



**Figure 2.11**   The Hula-Hoop.

Soon, polyethylene Hula-Hoops, Tupperware, and plastic bags became everyday items. As the years passed, catalysts not only produced other polymers but also allowed us to tailor an ultra-high molecular weight high-density polyethylene that can be spun into fibers that are stronger than steel. Today, UHMWHDPE is used to manufacture artificial hip joint replacements that have given many people a quality of life otherwise thought to be impossible.

Other thermoplastics were also developed during that time and in the years that followed. Polyvinyl chloride (PVC)[12] was made into a useful material in 1927 [12]. Due to its higher wear resistance, polyvinyl chloride replaced shellac as the material of choice for phonograph records in the early 1930s. Polyvinyl

12   The preparation of PVC was first recorded in 1835 by H.V. Regnault.

acetate, acrylic polymers, polystyrene (PS), polyurethanes, and polymethyl methacrylate (PMMA) were also developed in the 1930s [13], and polycarbonate (PC) in the 1950s. And the list goes on. Today, developing and synthesizing new polymeric materials has become increasingly expensive and difficult. Hence, developing new engineering materials by blending or mixing two or more polymers or by modifying existing ones with plasticizers has become a widely accepted procedure.

## 2.8   The Super Fiber and the Woman Who Invented It

When Stephanie Louise Kwolek (Fig.2.12) discovered a low viscosity and cloudy polymer in 1964, she did not discard it as a contaminated and useless polymer solution, but continued experimenting with it. Polymers in the melt state are usually not only highly viscous but also amorphous and therefore transparent or clear. Kwolek's curiosity and persistence soon showed her that she had discovered a polymer that was crystalline in the melt state; she had discovered liquid crystalline polymers or LCP's. This invention soon resulted in the discovery of Aramid fibers, probably better known by their trade name Kevlar fibers.

Kwolek, who was born in 1923 in New Kensington, Pennsylvania, had an early passion for fabrics and fashion design, which resulted in new clothes for her dolls. However, she never imagined that some day people's lives would be saved with bullet proof vests made with fabrics weaved out of her fibers. The super fibers that Stephanie Kwolek discovered were five times stronger than steel but were only a fifth of its density. Kwolek studied chemistry and biology at what is today known as Carnegie Mellon University. She wanted to continue her studies in medicine, but could not afford the high costs of medical school. To allow her to save some money, she decided to take a job at the DuPont Company. However, she soon became enamored with the work and shortly thereafter transferred to DuPont's Pioneering Research Laboratory of the Textile Fibers Department. She was in the perfect environment, working for a company that had discovered and made a name with synthetic polymer fibers. In 1964 she found herself working with a group of researchers whose main task was to develop an ultra strong fiber. The main application for this fiber would be the manufacture of lighter tires that would help reduce fuel consumption, motivated by early predictions of gasoline shortages. The main breakthrough came that same year when she discovered that extended-chain aromatic polyamides could be made into liquid crystalline solutions. These polymers could in turn be spun into fibers whose molecules were highly oriented, rendering a very stiff and strong final product.

**Figure 2.12**    Stephanie Louise Kwolek showing an Aramid molecule model.

After continued research refining her discovery, Kevlar was introduced to the market in 1971. Today, in addition to bullet proof vests, the super fiber can be found in brake pads of automobiles, trains, and aircraft as well as in safety helmets, skis, and numerous other applications.

## 2.9    One Last Word -- Plastics

The year 1967 was a significant year for plastics. One event, related to American pop culture and one that some of us tend to remember, is the advise given to the young graduate played by Dustin Hoffman in the movie *The Graduate*. The prophetic words told to the new graduate --"*I just want to say one word to you, Ben. Just one word -- plastics*"-- where a symbol of the times and a sign of things to come. The same year that the movie was showing in the theaters,   the volume of plastics' production surpassed that of all metals combined. Today, almost forty years later, plastics production is six times higher than in 1967,

while production of metals has barely doubled. However, to be fair, in the popularity contest between metals and plastics we can always present the data differently, namely by weight. This way, the tonnage of metals produced worldwide is over twice the tonnage production of polymers. Neverless, this is a book about polymers, and we like to point to the fact that today the  volume of polymers produced is three times larger than that of metals.

In fact, the world's annual production of polymer resins has experienced a steady growth since the beginning of the century, with growth predicted way into the 21st century. This can be seen in Fig. 2.13 [14] which presents the world's annual polymer production in millions of tons. There has been a steady increase throughout the years, with slight dips during the oil crisis in the mid 1970s and during the recession in the early 1980s. In developed countries, the growth in annual polymer production has diminished somewhat in recent years. However, developing countries in South America and Asia are now starting to experience tremendous growth.   With the exception of the recession years, the growth in US polymer production has been declining in  the past 20 years to  approximately 4% of annual growth rate. Since 1970, China has seen the  highest  annual  growth  in  the  world,  ranging  from  a  maximum approximately 50% between 1976 and 1977 to a low of 2% between 1980 and 1981.
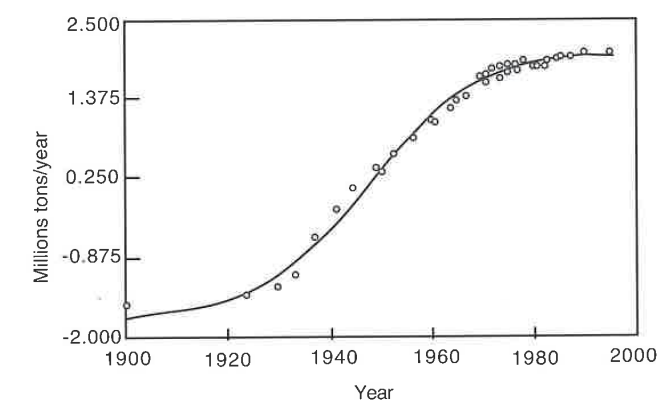


**Figure 2.13**    World annual plastics production since 1900.

In recent years, there has been a rapid increase in the demand for polymeric materials in developing countries such as Colombia. The demand for polymers in Colombia grew from 295,000 tons in 1992 to 389,000 tons in 1993. Although this number seems small when compared to the 34.4 million tons produced in

the US in 1993, Colombia has a 32% annual growth compared to the US 4% growth. It should be pointed out that Colombia produces PE, PP, PS and PVC for its own consumption and for export to other Latin American countries, while it imports most of the needed engineering thermoplastics such as SAN, ABS, PC, etc. [15] from developed countries such as the US and Germany. Similar trends exist in other Latin American countries.

There are over 18,000 different grades of polymers, available today in the US alone[13]. As pointed out in Chapter 1, they can be divided into two general categories—thermosetting and thermoplastic polymers. In 1993, 90% of polymer produced in the United States were thermoplastics. However, in a 1995 worldwide projection, thermoplastics account for 83% of the total polymer production [16]. Figure 2.13[14] shows a percentage break down of US polymer production into major polymer categories. These categories include polyethylene, polypropylene, polystyrene, polyvinyl chloride, and thermosets. Polyethylene is by far the most widely used polymeric material, accounting for 41% of the US plastic production.
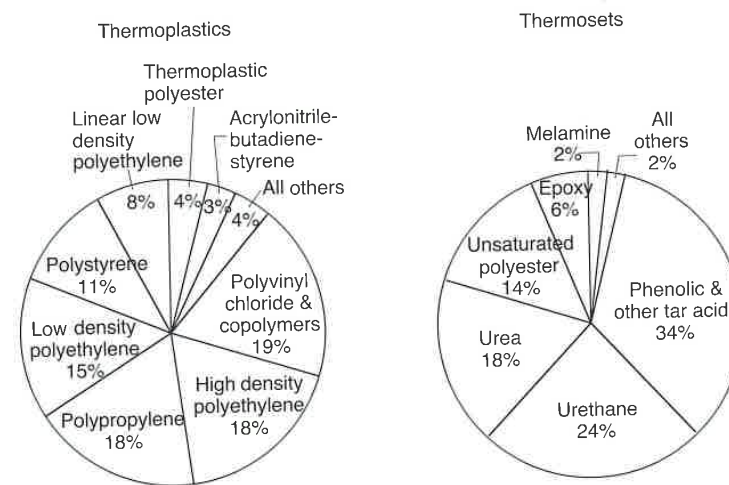


**Figure 2.14**  Break down of US polymer production into major polymer categories.

Packaging accounts for over one-third of the captive use of thermoplastics as graphically depicted in Fig. 2.15[15], whereas construction accounts for about

---

13  There are over 6,000 different polymer grades in Europe and over 10,000 in Japan.

14  Source: SPI Committee on Resin Statistics as compiled by Ernst & Young.

15  *Ibid.*

half that number, and transportation accounts for only 4% of the total captive use of thermoplastics. On the other hand, 69% of thermosets are used in building and construction, followed by 8% used in transportation. The transportation sector is one of the fastest growing areas of application for both thermoplastic and thermosetting resins. It should also be noted that 12% of the 1994 US polymer raw material production was exported.

It cannot be argued that, for some time now, polymers have become an indispensable material in everyday life. From sports to medicine, and from electronics to transportation, polymers are not only a material that is often used, but also the material that in many cases make it possible. One can sum it up with Hans Uwe Schenck's often quoted phrase -- *"Without natural polymers, there would be no life; without synthetic polymers, no standard of living."*
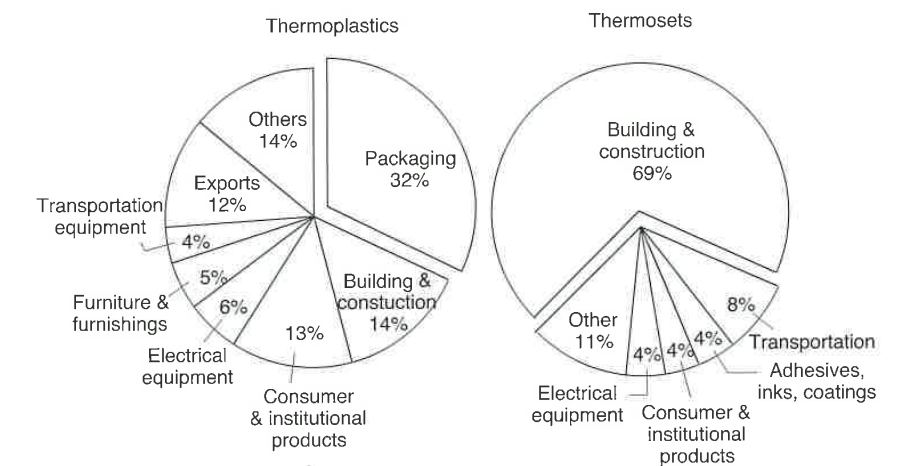


**Figure 2.15**  Break down of U.S. polymer production into major areas of application.

### References

1.  Giersch, U., and Kubisch, U., Gummi, *Die Elastische Faszination, Nicolai,* Berlin (1995).
2.  Stern, H.J., *Rubber: Natural and Synthetic,* Maclaren and Sons LDT, London, (1967).
3.  de la Condamine, C.M., Relation Abregee D'un Voyage Fait Dans l'interieur de l'Amerique Meridionale, Academie des Sciences, Paris, (1745).
4.  DuBois, J.H., *Plastics History U.S.A.,* Cahners Publishing Co., Inc., Boston, (1972).
5.  Tadmor, Z., and Gogos, C.G., *Principles of Polymer Processing,* John Wiley & Sons, New York, (1979).

6.  McPherson, A.T., and Klemin, A., *Engineering Uses of Rubber*, Reinhold Publishing Corporation, New York, (1956).
7.  Kaufman, M., The Chemistry and Industrial Production of Polyvinyl Chloride, Gordon and Beach, New York, (1969).
8.  Levi, P., *If This is a Man*, Abacus, 1995.
9.  Tschimmel, U., Die Zentausend-Dollar-Idee, ECON Verlag, Duesseldorf, (1989).
10. Sonntag, R., *Kunststoffe, 75*, 4, (1985).
11. Herrmann, H., *Kunststoffe, 75*, 2, (1985).
12. Regnault, H.V., Liebigs, A., 14, 22 (1835).
13. Ulrich, H., *Introduction to Industrial Polymers*, 2nd Ed., Hanser Publishers, Munich, (1993).
14. Utracki, L.A., *Polym. Eng. Sci.*, 35, 1, 2, (1995).
15. Noriega M. del P., ICIPC, Medellín, Colombia, Personal communication, (1994).
16. Progelhof, R.C., and Throne, J.L., *Polymer Engineering Principles*, Hanser Publishers, Munich, (1993).

# 3

# Structure of Polymers

## 3.1    Macromolecular Structure of Polymers

Polymers are macromolecular structures that are generated synthetically or through natural processes. Cotton, silk, natural rubber, ivory, amber, and wood are a few materials that occur naturally with an organic macromolecular structure, whereas natural inorganic materials include quartz and glass. The other class of organic materials with a macromolecular structure are synthetic polymers, which are generated through addition or *chain growth polymerization*, and condensation or *radical initiated polymerization*.

In addition polymerization, monomers are added to each other by breaking the double-bonds that exist between carbon atoms, allowing them to link to neighboring carbon atoms to form long chains. The simplest example is the addition of ethylene monomers, schematically shown in Fig. 3.1, to form polyethylene molecules as shown in Fig. 3.2. The schematic shown in Fig. 3.2 can also be written symbolically as shown in Fig. 3.3. Here, the subscript n represents the number of repeat units which determines the molecular weight of a polymer. The number of repeat units is more commonly referred to as the degree of polymerization. Other examples of addition polymerization include polypropylene, polyvinyl chloride and polystyrene. The side groups, such as $CH_3$ for polypropylene and $Cl$ for polyvinyl chloride, are sometimes referred to as the X groups.

Another technique to produce macromolecular materials is condensation polymerization. Condensation polymerization occurs when two components with end-groups that react with each other are mixed. When they are stoichiometric, these end-groups react, linking them to chains leaving a by-product such as water. A common polymer made by condensation polymerization is polyamide where diamine and diacid groups react to form polyamide and water, as explained n in Chapter 2.
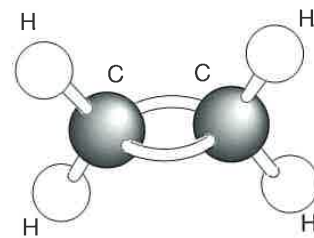
**Figure 3.1**    Schematic representation of an ethylene monomer.

At the molecular level, there are several forces that hold a polymeric material together. The most basic force present are covalent bonds which hold together the backbone of a polymer molecule, such as the -C-C bond. The energy holding together two carbon atoms is about 350 KJ/mol, which when translated would result in a polymer component strength between $1.4 \times 10^4$ and $1.9 \times 10^4$ MPa. However, as will be seen in Chapter 8, the strength of polymers only lies between 10 and 100 MPa.
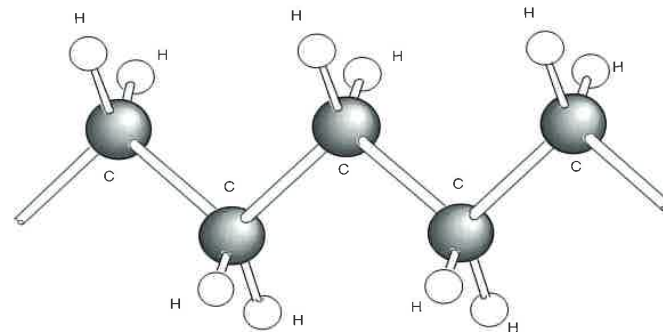


**Figure 3.2**    Schematic representation of a polyethylene molecule.
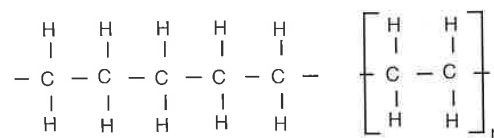


**Figure 3.3**    Symbolic representation of a polyethylene molecule.

## 3.2    Molecular Bonds and Inter-Molecular Attraction

Because of the comparatively low strength found in polymer components, it can be deduced that the forces holding a polymer component together do not come from the -C-C bonds but from intermolecular forces, or the so-called *Van-der-Waals forces*. The energy that generates the inter-molecular attraction between two polymer molecules increases, as the molecules come closer to each other by

$$F \sim \frac{1}{r^6} \tag{3.1}$$

where $F < 10\,\mathrm{kJ/mol}$ and $r$ is the distance between the molecules. Thus, it becomes clear that as a polymer sample is heated, the distance between the molecules increases as the vibration amplitude of the molecules increases. The vibration amplitude increase allows the molecules to move more freely, enabling the material to flow at the macroscopic level.

Another important point is that as solvents are introduced between the molecules, their inter-molecular separation increases which leads to a reduction in stiffness. This concept can be implemented by introducing *plasticizers* into the material, thus lowering the glass transition temperature below room temperature and bringing out rubber elastic material properties.

## 3.3    Molecular Weight

A polymeric material may consist of polymer chains of various lengths or repeat units. Hence, the molecular weight is determined by the average or mean molecular weight which is defined by

$$\overline{M} = \frac{W}{N} \tag{3.2}$$

where $W$ is the weight of the sample and $N$ the number of moles in the sample.

The properties of polymeric material are strongly linked to the molecular weight of the polymer as shown schematically in Fig. 3.4. A polymer such as polystyrene is stiff and brittle at room temperature with a degree of polymerization of 1,000. However, at a degree of polymerization of 10, polystyrene is sticky and soft at room temperature. Figure 3.5 shows the

relation between molecular weight, temperature, and properties of a typical polymeric material. The stiffness properties reach an asymptotic maximum, whereas the flow temperature increases with molecular weight. On the other hand, the degradation temperature steadily decreases with increasing molecular weight. Hence, it is necessary to find the molecular weight that renders ideal material properties for the finished polymer product, while having flow properties that make it easy to shape the material during the manufacturing process. It is important to mention that the temperature scale in Fig. 3.5 corresponds to a specific time scale, e.g., time required for a polymer molecule to flow through an extrusion die. If the time scale is reduced (e.g., by increasing the extruder throughput) the molecules have more difficulty sliding past each other. This would require a somewhat higher temperature to assure flow. In fact, at a specific temperature, a polymer melt may behave as a solid if the time scale is reduced sufficiently. Hence, for this new time scale the stiffness properties and flow temperature curves must be shifted upward on the temperature scale. A limiting factor is that the thermal degradation curve remains fixed, limiting processing conditions to remain above certain time scales. This relation between time, or time scale, and temperature will be discussed in more detail later in this chapter.
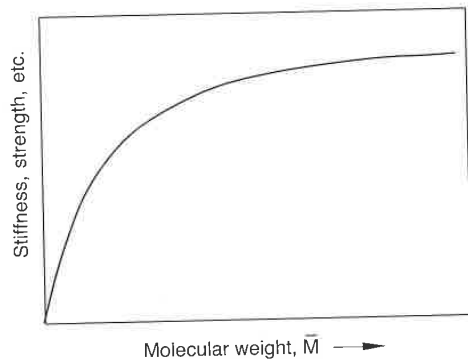


Figure 3.4    Influence of molecular weight on mechanical properties.

With the exception of maybe some naturally occurring polymers, most polymers have a molecular weight distribution such as shown in Fig. 3.6. For such a molecular weight distribution function, we can define a number average, weight average, and viscosity average[1]. The number average is the first moment and the weight average the second moment of the distribution function. In terms of mechanics this is equivalent to the center of gravity and

_____
1    There are other definitions of molecular weight which depend on the type of measuring technique.

the radius of gyration as first and second moments, respectively. The number average is defined by

$$\overline{M}_n = \frac{\sum m_i}{\sum n_i} = \frac{\sum n_i M_i}{\sum n_i}$$

(3.3)
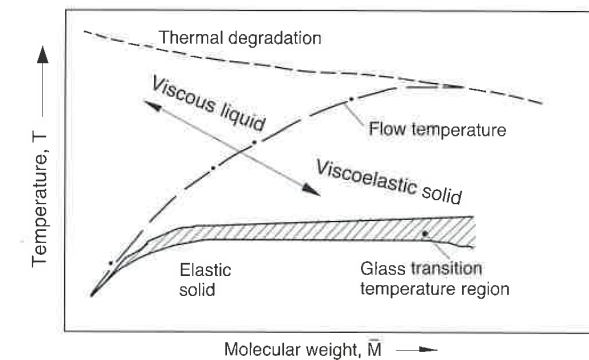


Figure 3.5    Diagram representing the relation between molecular weight, temperature, and properties of a typical thermoplastic.
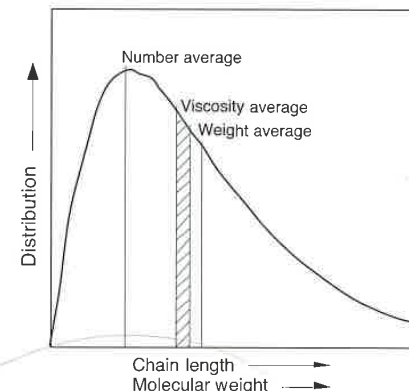


Figure 3.6    Molecular weight distribution of a typical thermoplastic.

where $m_i$ is the weight, $M_i$ the molecular weight and $n_i$ the number of molecules with $i$ repeat units. The weight average is calculated using

$$\overline{M}_W = \frac{\sum m_i M_i}{\sum m_i} = \frac{\sum n_i M_i^2}{\sum n_i M_i} \tag{3.4}$$

Another form of molecular weight average is the *viscosity average* which is calculated using

$$\overline{M}_V = \left( \frac{\sum m_i M_i^{a+1}}{\sum m_i} \right)^{1/a} \tag{3.5}$$

where $\alpha$ is a material dependent parameter which relates the *intrinsic viscosity*, $[\eta]$, to the molecular weight of the polymer. This relation is sometimes referred to as *Mark-Houwink relation* and is written as

$$[\eta] = k\overline{M}_v^{\alpha} \tag{3.6}$$

Figure 3.7 [1] presents the viscosity of various undiluted polymers as a function of molecular weight. The figure shows how for all these polymers the viscosity goes from a linear ($a$=1) to a power dependence ($a$=3.4) at some critical molecular weight. The linear relation is sometimes referred to as Staudinger's rule [2] and applies for a perfectly *monodispersed polymer* [2]. For monodispersed polymers we can write

$$\overline{M}_w = \overline{M}_n = \overline{M}_v \tag{3.7}$$

and for a polydispersed polymer [3]

$$\overline{M}_w > \overline{M}_v > \overline{M}_n \tag{3.8}$$

A measure of the broadness of a polymer's molecular weight distribution is the *polydispersity index* defined by

$$PI = \frac{\overline{M}_w}{\overline{M}_n} \tag{3.9}$$

---

[2]  A monodispersed polymer is composed of a single molecular weight species.

[3]  In most cases polymers are polydispersed systems which contain a range of molecular weights.
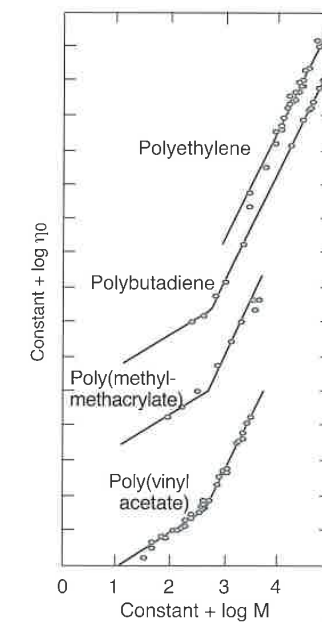
**Figure 3.7**    Zero shear rate viscosity for various polymers as a function of weight average molecular weight.

Figure 3.8 [3] presents a plot of flexural strength versus melt flow index[4] for polystyrene samples with three different polydispersity indices. The figure shows that low polydispersity index grade materials render higher strength properties and flowability, or processing ease, than high polydispersity index grades. Table 3.1 summarizes relations between polydispersity index, processing and material properties of a polymer. Figure 3.9 is a graphical representation of the relation between number average and weight average on properties of polymers. The arrows in the diagram indicate an increase in any specific property.

---

[4]  The melt flow index is the mass (grams) extruded through a capillary in a 10-min. period while applying a constant pressure. Increasing melt flow index signifies decreasing molecular weight. The melt flow index is discussed in more detail in Chapter 4.
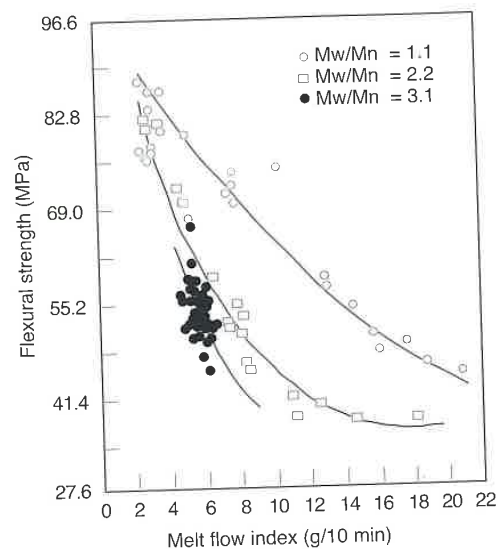
**Figure 3.8**    Effect of molecular weight on the strength-melt flow index interrelationship of polystyrene for three polydispersity indices.
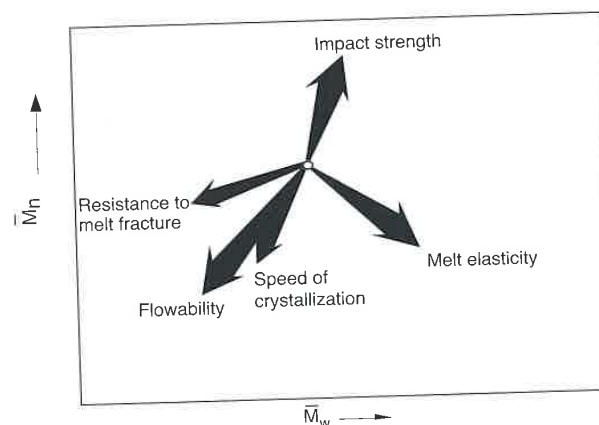


**Figure 3.9**    Influence of molecular weight number average and weight average on properties of thermoplastic polymers.

**Table 3.1**    Effect of Molecular Weight on Processing and Properties of Polymers.

| $\overline{M}_w / \overline{M}_n > 1$ | $\overline{M}_w / \overline{M}_n = 1$ |
|---|---|
| Processing | Properties |
| *Injection Molding:* | Narrow distribution leads to higher impact strength. |
| Longer cycle times caused by slow crystallization and low thermal conductivity. | Short molecules lead to easy ripping. |
| *Extrusion:* | |
| Melt fracture is less likely to occur since short molecules act as lubricants. | |
| Higher degree of extrude swell caused by the long molecules. | |

## 3.4    Conformation and Configuration of Polymer Molecules

The conformation and configuration of the polymer molecules have a great influence on the properties of the polymer component.

The conformation describes the preferential spatial positions of the atoms in a molecule, which is described by the polarity flexibility and regularity of the macromolecule. Typically, carbon atoms are tetravalent, which means that they are surrounded by four substituents in a symmetric tetrahedral geometry.

The most common example is methane, $CH_4$, schematically depicted in Fig. 3.10. As the figure demonstrates, the tetrahedral geometry sets the bond angle at 109.5º. This angle is maintained between carbon atoms on the backbone of a polymer molecule, as shown in Fig. 3.11. As shown in the figure, each individual axis in the carbon backbone is free to rotate.

The configuration gives information about the distribution and spatial organization of the molecule. During polymerization it is possible to place the X groups on the carbon-carbon backbone in different directions. The order in which they are arranged is called the *tacticity*. The polymers with side groups that are placed in a random matter are called *atactic*. The polymers whose side

groups are all on the same side are called *isotactic*, and those molecules with regularly alternating side groups are called *syndiotactic*.
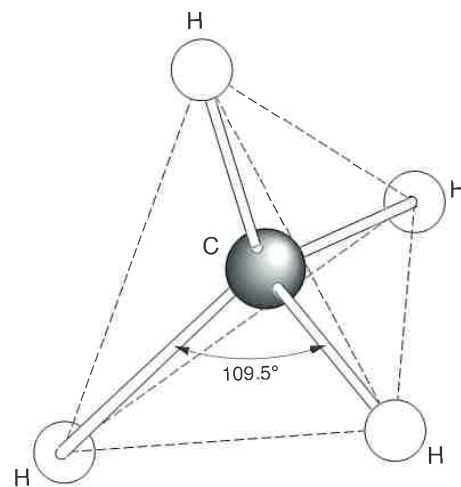


**Figure 3.10**    Schematic of tetrahedron formed by methane (CH₄).
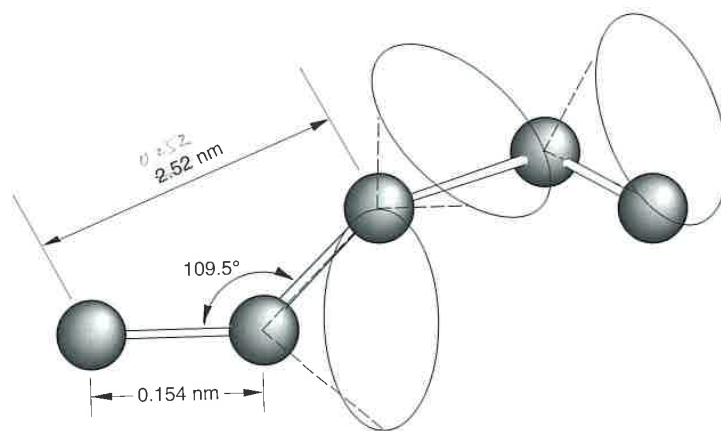


**Figure 3.11**    Random conformation of a polymer chain's carbon-carbon backbone.

Figure 3.12 shows the three different tacticity cases for polypropylene. The tacticity in a polymer determines the degree of crystallinity that a polymer can reach. For example, polypropylene with a high isotactic content will reach a high degree of crystallinity and as a result will be stiff, strong, and hard.
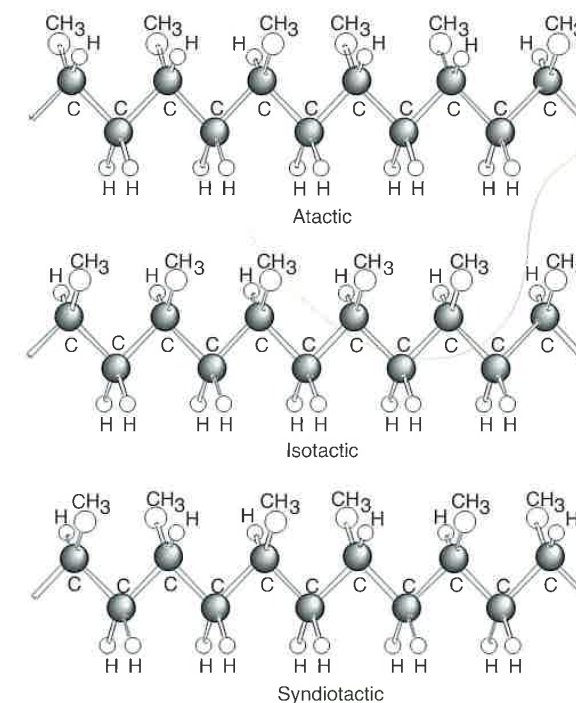


**Figure 3.12**    Different polypropylene structures.

Another type of geometric arrangement arises with polymers that have a double bond between carbon atoms. Double bonds restrict the rotation of the carbon atoms about the backbone axis. These polymers are sometimes referred to as geometric isomers. The X groups may be on the same side (*cis-*) or on opposite sides (*trans-*) of the chain as schematically shown for polybutadiene in Fig. 3.13. The arrangement in a cis-1,4- polybutadiene results in a very elastic rubbery material, whereas the structure of the trans-1,4- polybutadiene results in a leathery and tough material. A cis-1,4- polybutadiene can be used to manufacture the outer tread of an automotive tire. A trans-1,4- polybutadiene

can be used to make the outer skin of a golf ball. The same geometric arrangement is found in natural rubber, polyisoprene. The cis-1,4- polyisoprene is the elastic natural rubber used for the body of a tire, and the latex used to manufacture "rubber" gloves and condoms. The trans-1,4- polyisoprene, or the so-called *gutta percha* or *ebony*, was used to make dentures, statues, and other decorative items in the 1800s.
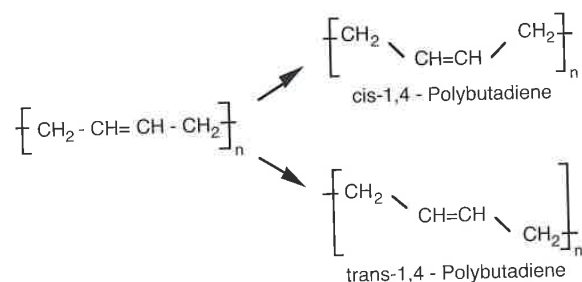


**Figure 3.13**   Symbolic representation of cis-1,4- and trans-1,4- polybutadiene molecules.

Branching of the polymer chains also influences the final structure, crystallinity, and properties of the polymeric material. Figure 3.14 shows the molecular architecture of high density, low density, and linear low density polyethylenes.
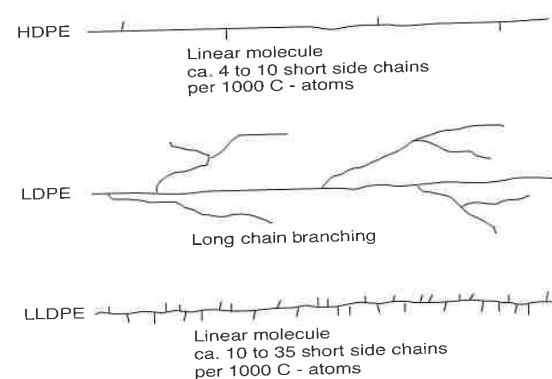


**Figure 3.14**   Schematic of the molecular structure of different polyethylenes.

The high density polyethylene has between 5 and 10 short branches every 1000 carbon atoms. The low density material has the same number of branches as HDPE; however, they are much longer and are themselves usually branched. The LLDPE has between 10 and 35 short chains every 1000 carbon atoms. Polymer chains with fewer and shorter branches can crystallize with more ease, resulting in higher density.

## 3.5   Arrangement of Polymer Molecules

As mentioned in Chapter 1, polymeric materials can be divided into two general categories: thermoplastics and thermosets. Thermoplastics are those that have the ability to remelt after they have solidified, and thermosets are those that solidify via a chemical reaction that causes polymer molecules to cross-link. These cross-linked materials cannot be remelted after solidification.

As thermoplastic polymers solidify, they take on two different types of structure: amorphous and semi-crystalline. Amorphous polymers are those where the molecules solidify in a random arrangement, whereas some of the molecules in semi-crystalline polymers align with their neighbors, forming regions with a three-dimensional order. In semi-crystalline polymers, the molecules that do not align into crystals, remain amorphous structures.

### 3.5.1   Thermoplastic Polymers

The formation of macromolecules from monomers occurs if there are unsaturated carbon atoms (carbon atoms connected with double bonds), or if there are monomers with reactive end-groups. The double bond, say in an ethylene monomer, is split, which frees two valences per monomer and leads to the formation of a macromolecule such as polyethylene. This process is often referred to as polymerization. Similarly, monomers (R) that possess two reactive end-groups (bifunctional) can react with other monomers (R') that also have two other reactive end-groups that can react with each other, also leading to the formation of a polymer chain. A list of typical reactive end-groups is given in Table 3.2.

**Table 3.2** List of Selected Reactive End-Groups

| | |
|---|---|
| Hydrogen in aromatic monomers | - H |
| Hydroxyl group in alcohols | - OH |
| Aldehyde group as in formaldehyde | $-C\overset{H}{\underset{O}{}}$ |
| Carboxyl group in organic acids | $-C\overset{OH}{\underset{O}{}}$ |
| Isocyanate group in isocyanates | -N=C=O |
| Epoxy group in polyepoxys | $-CH-CH_2$ over $O$ |
| Amido groups in amides and polyamides | $-CO-NH_2$ |
| Amino groups in amines | $-NH_2$ |

### 3.5.2 Amorphous Thermoplastics

Amorphous thermoplastics, with their randomly arranged molecular structure, are analogous to a bowl of spaghetti. Due to their random structure, the characteristic size of the largest ordered region is on the order of a carbon-carbon bond. This dimension is much smaller than the wavelength of visible light and so generally makes amorphous thermoplastics transparent.

Figure 3.15 [4] shows the shear modulus[5], $G'$, versus temperature for poly-styrene, one of the most common amorphous thermoplastics. The figure shows two general regions: one where the modulus appears fairly constant[6], and one where the modulus drops significantly with increasing temperature. With decreasing temperatures, the material enters the glassy region where the slope of the modulus approaches zero. At high temperatures the modulus is negligible and the material is soft enough to flow. Although there is not a clear transition between "solid" and "liquid," the temperature that divides the two states in an amorphous thermoplastic is referred to as the *glass transition temperature*, $T_g$. For the polystyrene in Fig. 3.15 the glass transition temperature is approximately 110 °C. Although data are usually presented in the form shown in Fig. 3.15, it should be mentioned here that the curve shown in the figure was measured at a constant frequency. If the frequency of the test is increased—reducing the time scale—the curve is shifted to the right since higher temperatures are required to achieve movement of the molecules at the new frequency. Figure 3.16 [5] demonstrates this concept by displaying the elastic modulus as a function of temperature for polyvinyl chloride at various test frequencies. A similar effect is observed if the molecular weight of the material is increased. The longer molecules have more difficulty sliding past each other, thus requiring higher temperatures to achieve "flow."
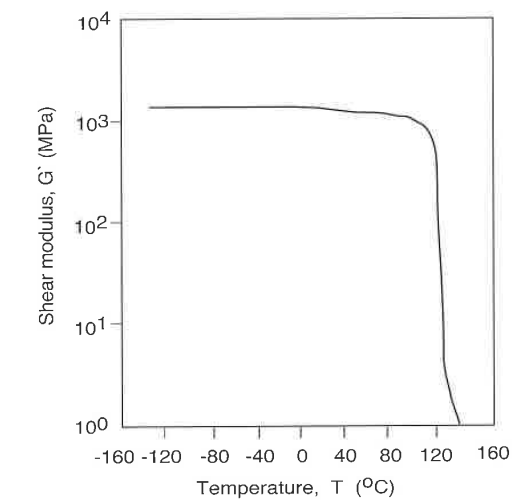


**Figure 3.15** Shear modulus of polystyrene as a function of temperature.

---

5 The dynamic shear modulus, $G'$, is obtained using the dynamic mechanical properties test described in Chapter 8.

6 When plotting $G'$ versus temperature on a linear scale, a steady decrease of the modulus is observed.
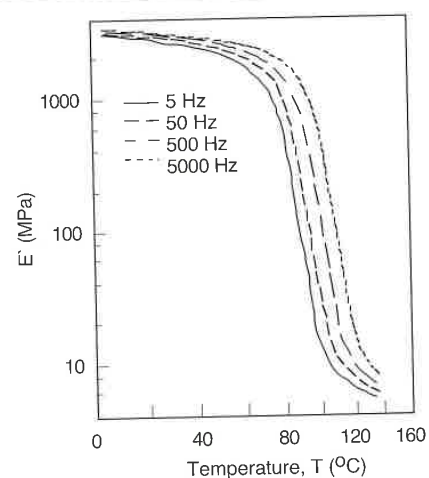
**Figure 3.16**   Modulus of polyvinyl chloride as a function of temperature at various test frequencies.

### 3.5.3 Semi-Crystalline Thermoplastics

Semi-crystalline thermoplastic polymers show more order than amorphous thermoplastics. The molecules align in an ordered crystalline form as shown for polyethylene in Fig. 3.17. The crystalline structure is part of a *lamellar crystal* which in turn forms the *spherulites*. The formation of spherulites during solidification of semi-crystalline thermoplastics is covered in Chapter 8. The schematic in Fig. 3.18 shows the general structure and hierarchical arrangement in semi-crystalline materials. The spherulitic structure is the largest domain with a specific order and has a characteristic size of 50 to 500 µm. This size is much larger than the wavelength of visible light, making semi-crystalline materials translucent and not transparent.

However, the crystalline regions are very small with molecular chains comprised of both crystalline and amorphous regions. The degree of crystallinity in a typical thermoplastic will vary from grade to grade. For example, in polyethylene the degree of crystallinity depends on the branching and the cooling rate. A low density polyethylene (LDPE) with its long branches (Fig. 3.16) can only crystallize to approximate 40-50%, whereas a high density polyethylene (HDPE) crystallizes to up to 80%. The density and strength of semi-crystalline thermoplastics increase with the degree of crystallinity as demonstrated in Table 3.3 [6], which compares low and high density polyethylenes. Figure 3.19 shows the different properties and molecular

structure that may arise in polyethylene plotted as a function of degree of crystallinity and molecular weight.

**Table 3.3**   Influence of Crystallinity on Properties for Low and High Density Polyethylene

| Property | Low density | High density |
|---|---|---|
| Density (g/cm$^3$) | 0.91-0.925 | 0.941-0.965 |
| % crystallinity | 42-53 | 64-80 |
| Melting temperature (°C) | 110-120 | 130-136 |
| Tensile modulus (MPa) | 17-26 | 41-124 |
| Tensile strength  (MPa) | 4.1-16 | 21-38 |
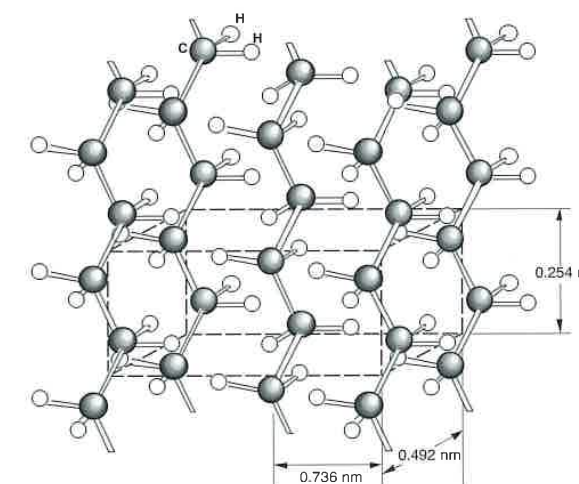


**Figure 3.17**   Schematic representation of the crystalline structure of polyethylene.

Figure 3.20 [4] shows the dynamic shear modulus versus temperature for a high density polyethylene, the most common semi-crystalline thermoplastic. Again, this curve presents data measured at one test frequency. The figure clearly shows two distinct transitions: one at about -110 °C, the *glass transition temperature*, and another near 140 °C, the *melting temperature*. Above the melting temperature, the shear modulus is negligible and the material will flow. Crystalline arrangement begins to develop as the temperature decreases below the melting point. Between the melting and glass transition temperatures, the

material behaves as a leathery solid. As the temperature decreases below the glass transition temperature, the amorphous regions within the semi-crystalline structure solidify, forming a glassy, stiff, and in some cases brittle polymer.

To summarize, Table 3.4 presents the basic structure of several amorphous and semi-crystalline thermoplastics with their melting and/or glass transition temperatures.

Furthermore, Fig. 3.21 [7] summarizes the property behavior of amorphous, crystalline, and semi-crystalline materials using schematic diagrams of material properties plotted as functions of temperature.



a = 0.736 nm
b = 0.492 nm
c = 0.254 nm

Lamella
20 to 60 nm

Crystal lamella

Spherulite
≈ 50 to 500 $\mu$m

Polymer component
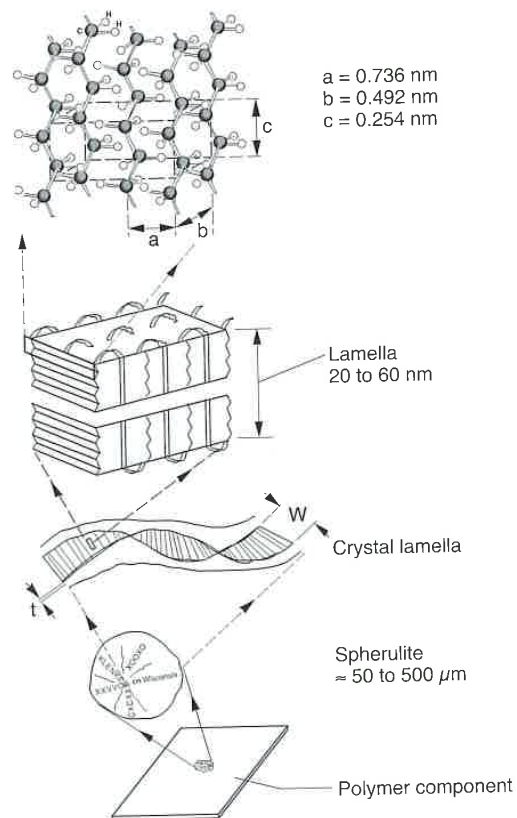
**Figure 3.18**   Schematic representation of the general molecular structure and arrangement of typical semi-crystalline materials.
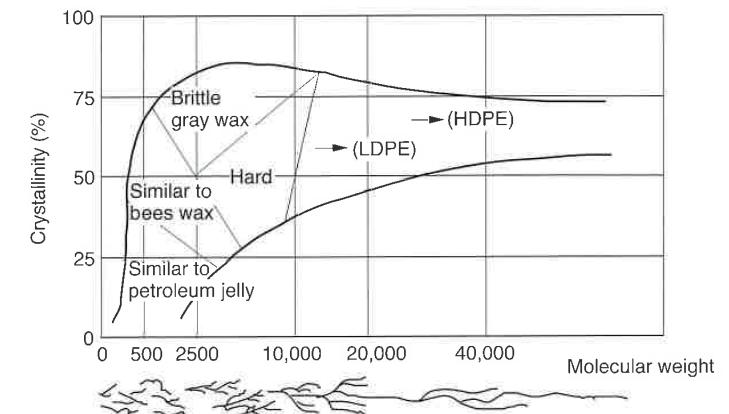
**Figure 3.19**   Influence of degree of crystallinity and molecular weight on different properties of polyethylene.
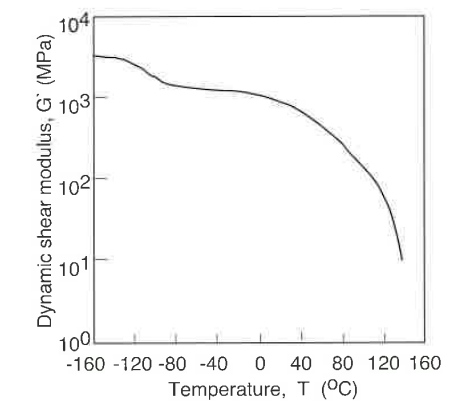


**Figure 3.20**   Shear modulus of a high density polyethylene as a function of temperature.
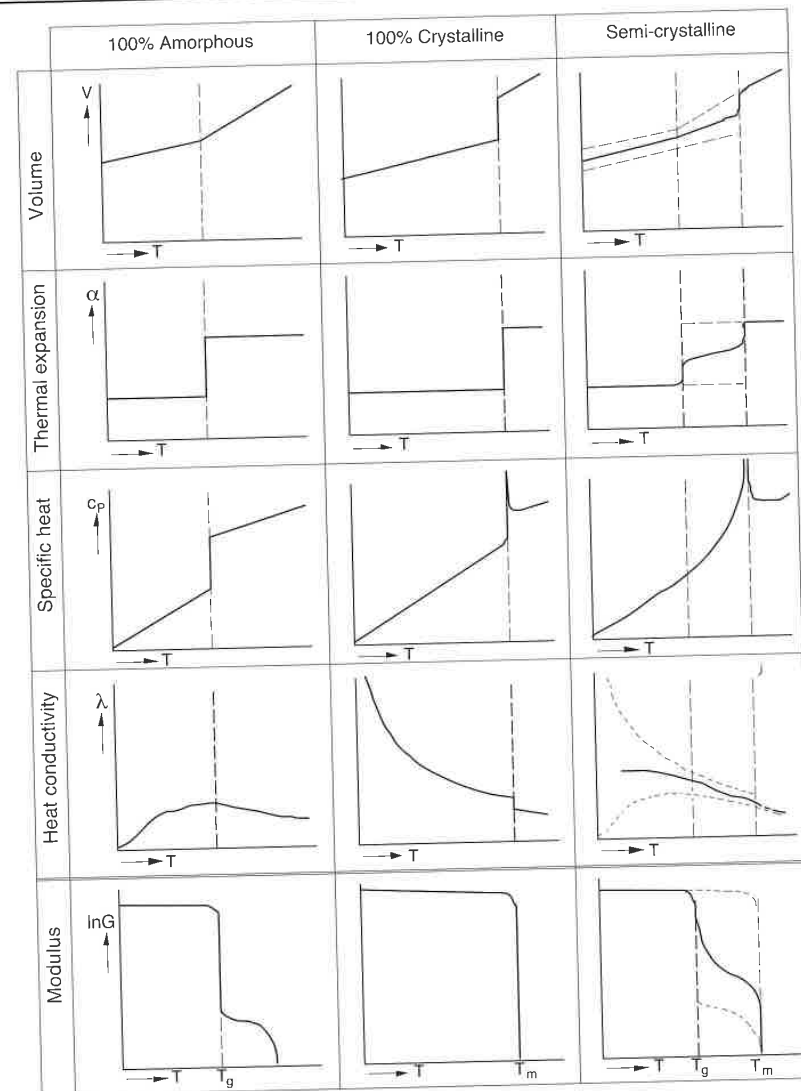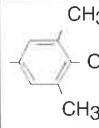
**Figure 3.21**   Schematic of the behavior of some polymer properties as a function of temperature for different thermoplastics.

**Table 3.4**   Structural Units for Selected Polymers with Glass Transition and Melting Temperatures.
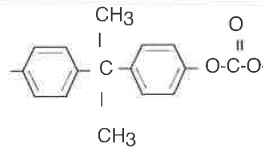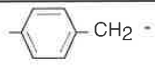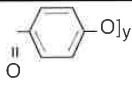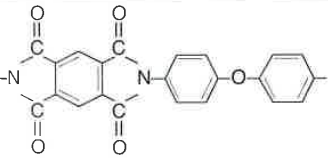
| Structural unit | Polymers | $T_g(°C)$ | $T_m(°C)$ |
|---|---|---|---|
| $-CH_2-CH_2-$ | Linear polyethylene | -125 | 135 |
| $-CH_2-CH-$ \| $CH_3$ | Isotactic polypropylene | -20 | 170 |
| $-CH_2-CH-$ \| $C_2H_5$ | Isotactic Polybutene | -25 | 135 |
| $-CH_2-CH-$ \| $CH-CH_3$ \| $CH_3$ | Isotactic poly-3-methylbutene-1 | 50 | 310 |
| $-CH_2-CH-$ \| $CH_2$ \| $CH-CH_3$ \| $CH_3$ | Isotactic poly-4-methylpentene -1 | 29 | 240 |
| $-CH_2-CH-$ (benzene ring) $C_8H_9$ | Isotactic polystyrene | 100 | 240 |
| $CH_3$ (benzene ring) $-O-$ $CH_3$   $C_8H_8O$ | Polyphenylenether (PPE) | 210 | 261 |
| $-O-CH-$ \| $CH_3$ | Polyacetaldehyde | -30 | 165 |

(continued)

**Table 3.4** Structural Units for Selected Polymers with Glass Transition and Melting Temperatures *(continued)*
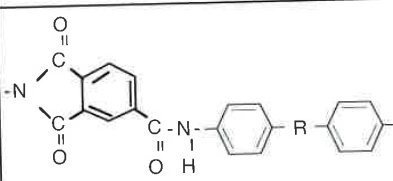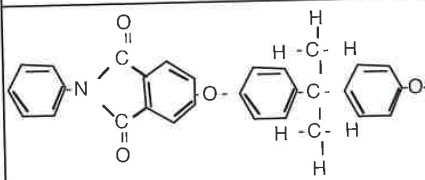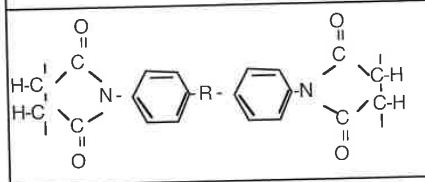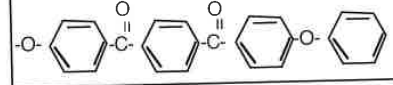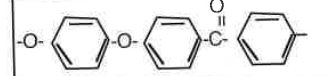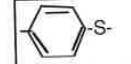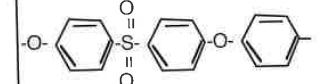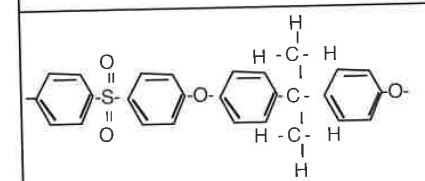
| Structural unit | Polymers | $T_g(°C)$ | $T_m(°C)$ |
|---|---|---|---|
| – O–CH$_2$– | Polyformaldehyde (polyacetal, polyoxymethylene) | -85 | 178-198 |
| – O – CH$_2$–CH– <br>         CH$_3$ | Isotactic polypropyleneoxide | -75 | 75 |
|     CH$_2$– Cl <br>      \| <br> – O– CH$_2$ – C – CH$_2$– <br>      \| <br>     CH$_2$ Cl | Poly-[2.2-bis-(chlormethyl)-trimethylene-oxide] | 5 | 181 |
|    CH$_3$ <br>     \| <br> – CH$_2$– C– <br>     \| <br>    CO$_2$ CH$_3$ | Isotactic polymethyl-methacrylate | 50 | 160 |
| Cl  F <br> \|   \| <br> – C– C– <br> \|   \| <br> F  F | Polychlortri-fluoroethylene | 45 | 220 |
| – CF$_2$– CF$_2$ | Polytetrafluoroethylene | -113,+127 | 330 |
|    Cl <br>    \| <br> – CH$_2$ – C – <br>    \| <br>    Cl | Polyvinylidenechloride | -19 | 190 |
|    F <br>    \| <br> – CH$_2$ – C – <br>    \| <br>    F | Polyvinylidenefluoride | -45 | 171 |
| – CH$_2$ – CH <br>      \| <br>      Cl | Polyvinylchloride (PVC) amorphous crystalline | 80 <br> 80 | - <br> 212 |

*(continued)*

**Table 3.4** Structural Units for Selected Polymers with Glass Transition and Melting Temperatures *(continued)*

| Structural unit | Polymers | $T_g(°C)$ | $T_m(°C)$ |
|---|---|---|---|
| – CH$_2$– CH – <br>       \| <br>       F | Polyvinylfluoride (PVF) | -20 | 200 |
| –CO$_2$ –⟨ ⟩– CO$_2$ –(CH$_2$–)$_2$ O– | Polyethylene - terephthalate (PET) (linear polyester) | 69 | 245 |
| – CO– (CH$_2$–)$_4$ CO–NH– (CH$_2$)$_6$ NH– | Polyamide 66 | 57 | 265 |
| – CO– (CH$_2$–)$_8$ CO–NH– (CH$_2$–)$_6$ NH– | Polyamide 610 | 50 | 228 |
| – CO– (CH$_2$–)$_5$ NH– | Polycaprolactam, Polyamide 6 | 75 | 233 |
|       CH$_3$       O <br>       \|          ‖ <br> –⟨ ⟩– C –⟨ ⟩– O–C–O– <br>       \| <br>       CH$_3$ | Polycarbonate (PC) | 149 | 267 |
| –CH$_2$ –⟨ ⟩– CH$_2$ - | Poly-(p-xylene) (Parylene ‖ R) | - | 400 |
| [–C–⟨ ⟩– C –O–(CH$_2$–)$_2$ O–]$_x$–[C–⟨ ⟩– O]$_y$ <br>  ‖       ‖            ‖ <br>  O       O           O <br>     35%          65% <br> \|←— PET —→\|←— PHB —→\| | Polyethylene terephthalate/p-Hydroxybenzoate-copolymers LC-PET, Polymers with flexible chains | 75 | 280 |
| (polyimide structure) | Polyimide (PI) | up to 400 | |

*(continued)*

**Table 3.4**    Structural Units for Selected Polymers with Glass Transition and Melting Temperatures *(continued)*

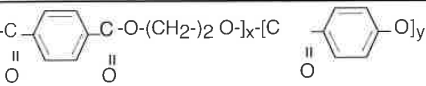| Structural unit | Polymers | $T_g(°C)$ | $T_m(°C)$ |
|---|---|---|---|
| | Polyamidimide (PAI) | ≈ 260 | |
| | Polyetherimide (PEI) | ≈ 215 | |
| | Polybismaleinimide (PBI) | ≈ 250 | |
| | Polyoxybenzoate (POB) | ≈ 290 | |
| | Polyetheretherketone (PEEK) | 145 | 335 |
| | Polyphenylenesulfide (PPS) | ~230 | |
| | Polyethersulfone (PES) | 85 | 280 |
| | Polysulfone (PSU) | ~ 180 | |

## 3.5.4  Thermosets and Cross-Linked Elastomers

Thermosets, and some elastomers, are polymeric materials that have the ability to cross-link. The cross-linking causes the material to become heat resistant after it has solidified. A more in-depth explanation of the cross-linking chemical reaction that occurs during solidification is given in Chapter 7.

The cross-linking usually is a result of the presence of double bonds that break, allowing the molecules to link with their neighbors. One of the oldest thermosetting polymers is phenol-formaldehyde, or phenolic. Figure 3.22 shows the chemical symbol representation of the reaction, and Fig. 3.23 shows a schematic of the reaction. The phenol molecules react with formaldehyde molecules to create a three-dimensional cross-linked network that is stiff and strong. The by-product of this chemical reaction is water.
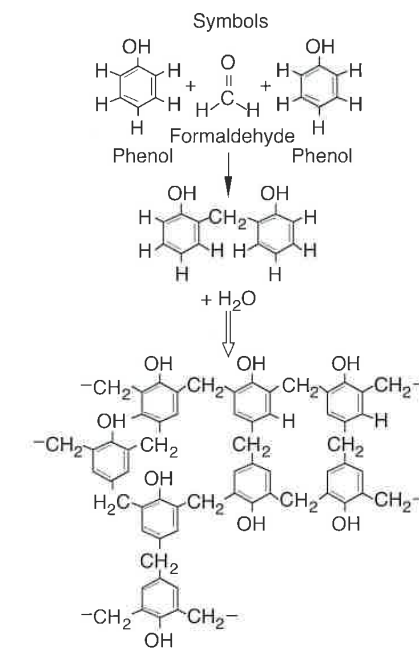


**Figure 3.22**    Symbolic representation of the condensation polymerization of phenol-formaldehyde resins.
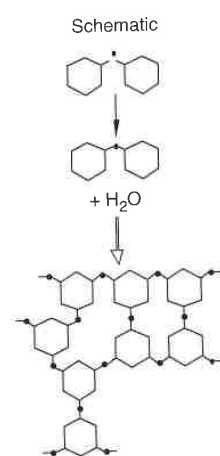
Schematic



**Figure 3.23**    Schematic representation of the condensation polymerization of phenol-formaldehyde resins.

## 3.6    Copolymers and Polymer Blends

Copolymers are polymeric materials with two or more monomer types in the same chain. A copolymer that is composed of two monomer types is referred to as a *bipolymer*, and one that is formed by three different monomer groups is called a *terpolymer*. Depending on how the different monomers are arranged in the polymer chain, one distinguishes between *random*, alternating, block, or *graft* copolymers. The four types of copolymers are schematically represented in Fig. 3.24.

A common example of a copolymer is ethylene-propylene. Although both monomers would result in semi-crystalline polymers when polymerized individually, the melting temperature disappears in the randomly distributed copolymer with ratios between 35/65 and 65/35, resulting in an elastomeric material, as shown in Fig. 3.25. In fact EPDM[7] rubbers are continuously gaining acceptance in industry because of their resistance to weathering. On the other hand, the ethylene-propylene block copolymer maintains a melting temperature for all ethylene/propylene ratios, as shown in Fig. 3.26.

---

7    The D in EP(D)M stands for the added unsaturated diene component which results in a cross-linked elastomer.

Another widely used copolymer is high impact polystyrene (PS-HI), which is formed by grafting polystyrene to polybutadiene. Again, if styrene and butadiene are randomly copolymerized, the resulting material is an elastomer called styrene-butadiene-rubber (SBR). Another classic example of copolymerization is the terpolymer acrylonitrile-butadiene-styrene (ABS).

Polymer blends belong to another family of polymeric materials which are made by mixing or blending two or more polymers to enhance the physical properties of each individual component. Common polymer blends include PP-PC, PVC-ABS, PE-PTFE.
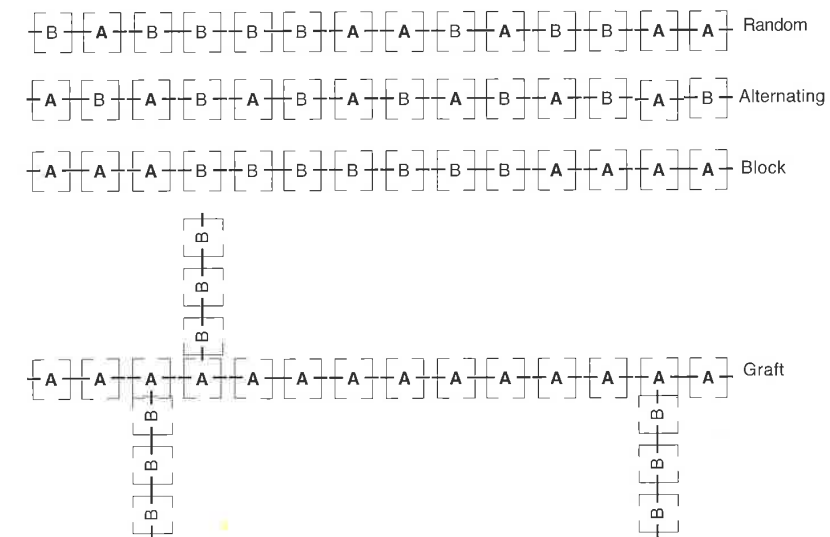


**Figure 3.24**    Schematic representation of different copolymers.
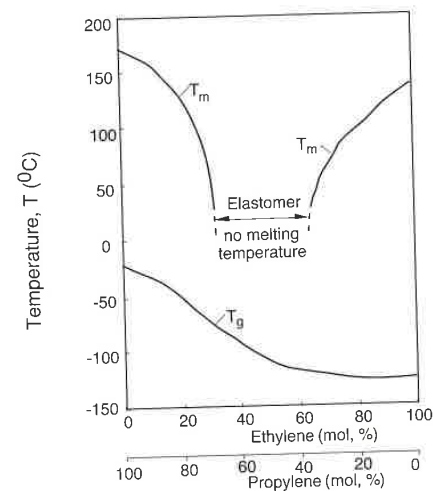
**Figure 3.25**    Melting and glass transition temperature for random ethylene-propylene copolymers.
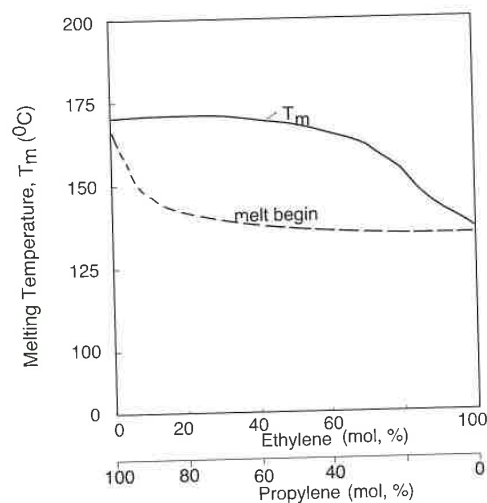


**Figure 3.26**    Melting temperature for ethylene-propylene block copolymers.

## 3.7    Polymer Additives

There are many polymer additives that are mixed into a polymer to improve the mechanical, optical, electrical, and acoustic—to name a few— performance of a component.

### 3.7.1    Flame Retardants

Since polymers are organic materials, most of them are flammable. The flammability of polymers has always been a serious technical problem. A parameter which can be used to assess the flammability of polymers is the *limiting oxygen index* (LOI), also known as the *critical oxygen index* (COI). This value defines the minimum volume percent of oxygen concentration, mixed with nitrogen, needed to support combustion of the polymer under the test conditions specified by ASTM D 2863. Since air contains 21% oxygen by volume, only those polymers with an LOI greater than 0.21 are considered self-extinguishing. In practice, an LOI value greater than 0.27 is recommended as the limiting self-extinguishing threshold. Table 3.5 presents LOI values for selected polymers.

It is impossible to make a polymer completely inflammable. However, some additives that contain halogens, such as bromine, chlorine, or phosphorous, reduce the possibility of either starting combustion within a polymer component or, once ignited, reduce the rate of flame spread. When rating the performance of flame retardants, bromine is more effective than chlorine.

In the *radical trap* theory of flame retardancy, it is believed that bromine or phosphorous containing additives compete in the reaction of a combustion process. To illustrate this we examine two examples of typical combustion reactions. These are:

$$CH_4 + OH \longrightarrow CH_3 + H_2O$$

and

$$CH_4 + O_2 \longrightarrow CH_3 + H + O_2$$

where OH and H are active chain carriers. With the presence of HBr the following reaction can take place

$$OH + HBr \longrightarrow H_2O + Br$$

**Table 3.5**    LOI Values for Selected Polymers

| Polymer | LOI |
|---|---|
| Polyformaldehyde | 0.15 |
| Polyethyleneoxide | 0.15 |
| Polymethyl methacrylate | 0.17 |
| Polyacrylonitrile | 0.18 |
| Polyethylene | 0.18 |
| Polypropylene | 0.18 |
| Polyisoprene | 0.185 |
| Polybutadiene | 0.185 |
| Polystyrene | 0.185 |
| Cellulose | 0.19 |
| Polyethylene terephthalate | 0.21 |
| Polyvinyl alcohol | 0.22 |
| Polyamide 66 | 0.23 |
| Epoxy | 0.23 |
| Polycarbonate | 0.27 |
| Aramide fibers | 0.285 |
| Polyphenylene oxide | 0.29 |
| Polysulfone | 0.30 |
| Phenolic resins | 0.35 |
| Polychloroprene | 0.40 |
| Polyvinyl chloride | 0.42 |
| Polyvinylidene fluoride | 0.44 |
| Polyvinylidene chloride | 0.60 |
| Carbon | 0.60 |
| Polytetrafluoroethylene | 0.95 |

where the active chain carrier was replaced by the less active Br radical, helping in flame extinguishment. Similarly, with the presence of Br the following reaction can take place

$$CH_4 + Br \longrightarrow HBr + CH_3$$

Table 3.6 [8] lists selected polymers with one commonly used flame retardant.

**Table 3.6**    Selected Polymers with Typical Commercial Flame Retardants

| Polymer | Flame retardants |
|---|---|
| Acrylonitrile butadiene styrene | Octabromodiphenyl oxide |
| High impact polystyrene | Decabromodiphenyl oxide |
| Polyamide | Dechlorane plus |
| Polycarbonate | Tetrabromobisphenol A carbonate oligomer |
| Polyethylene | Chlorinated paraffin |
| Polypropylene | Dechlorane plus |
| Polystyrene | Pentabromocyclododecane |
| Polyvinyl chloride | Phosphate ester |

### 3.7.2 Stabilizers

The combination of heat and oxygen will bring about thermal degradation in a polymer. Heat or energy will produce free radicals which will react with oxygen to form carbonyl compounds, which give rise to yellow or brown discolorations in the final product.

Thermal degradation can be slowed by adding stabilizers such as antioxidants or peroxide decomposers. These additives do not eliminate thermal degradation but slow down the reaction process. Once the stabilizer has been consumed by the reaction with the free radicals, the protection of the polymer against thermal degradation ends. The time period over which the stabilizer renders protection against thermal degradation is called *induction time*. A test used to measure thermal stability of a polymer is the *Oxidative Induction Time* (OIT) by differential scanning calorimetry (DSC). The OIT test is defined as the time it takes for a polymer sample to thermally degrade in an oxygen environment at a set temperature above the polymer's transition temperature. The transitions must occur in a nitrogen environment. The standard test is described by ASTM D 3895. Another test used to measure the thermal stability of a polymer and its additives is the thermal gravimetric analysis (TGA) discussed in Chapter 3.

Polyvinyl chloride is probably the polymer most vulnerable to thermal degradation. In polyvinyl chloride, scission of the C-Cl bond occurs in the weakest point of the molecule. The chlorine radicals will react with their nearest CH group, forming HCl and creating new weak C-Cl bonds. A stabilizer must therefore neutralize HCl and stop the auto catalytic reaction, as well as preventing processing equipment corrosion.

### 3.7.3 Antistatic Agents

Since polymers have such low electric conductivity they can build-up electric charges quite easily. The amount of charge build-up is controlled by the rate at which the charge is generated compared to the charge decay. The rate of charge generation at the surface of the component can be reduced by reducing the intimacy of contact, whereas the rate of charge decay is increased through surface conductivity. Hence, a good antistatic agent should be an ionizable additive that allows charge migration to the surface, at the same time as creating bridges to the atmosphere through moisture in the surroundings. Typical antistatic agents are nitrogen compounds such as long chain amines and amides, polyhydric alcohols, etc.

### 3.7.4 Fillers

Fillers can be divided into two categories: those that reinforce the polymer and improve its mechanical performance, and those that are used to take up space and so reduce the amount of actual resin to produce a part—sometimes referred to as *extenders*. A third, less common, category of filled polymers are those where fillers are dispersed into the polymer to improve its electric conductivity.

Polymers that contain fillers that improve their mechanical performance are often referred to as *composites*. Composites can be divided into two further categories: composites with *high performance* reinforcements, and composites with *low performance* reinforcements. The high performance composites are those where the reinforcement is placed inside the polymer in such a way that optimal mechanical behavior is achieved, such as unidirectional glass fibers in an epoxy resin. High performance composites usually have 50–80% reinforcement by volume and the composites are usually laminates, tubular shapes containing braided reinforcements, etc. The low performance composites are those where the reinforcement is small enough that it can be dispersed well into the matrix, allowing to process these materials the same way their unreinforced counterparts are processed. The most common filler used to reinforce polymeric materials is glass fiber. However, wood fiber, which is commonly used as an extender, also increases the stiffness and mechanical performance of some thermoplastics. To improve the bonding between the polymer matrix and the reinforcement, *coupling agents* such as *silanes* and *titanates* are often added. Polymer composites and their performance are discussed in more detail in Chapters 8 and 9.

Extenders, used to reduce the cost of the component, often come in the form of particulate fillers. The most common particulate fillers are calcium carbonate, silica flour, clay, and wood flour or fiber. As mentioned earlier, some fillers also slightly reinforce the polymer matrix, such as clay, silica flour, and wood fiber. It should be pointed out that polymers with extenders often have significantly lower toughness than when unfilled. This concept is covered in more detail in Chapter 9.

### 3.7.5 Blowing Agents

The task of blowing or foaming agents is to produce cellular polymers, also referred to as expanded plastics. The cells can be completely enclosed (closed cell) or can be interconnected (open cell). Polymer foams are produced with densities ranging from $1.6 \ kg/m^3$ to $960 \ kg/m^3$. There are many reasons for using polymer foams such as their high strength/weight ratio, excellent insulating and acoustic properties, and high energy and vibration absorbing properties.

Polymer foams can be made by mechanically whipping gases into the polymer, or by either chemical or physical means. Some of the most commonly used foaming methods are [9]:

- Thermal decomposition of chemical blowing agents which generates nitrogen and/or carbon monoxide and dioxide. An example of such a foaming agent is *azodicarbonamide* which is the most widely used commercial polyolefin foaming agent.

- Heat induced volatilization of low-boiling liquids such as pentane and heptane in the production of polystyrene foams, and methylene chloride when producing flexible polyvinyl chloride and polyurethane foams.

- Volatilization by the exothermic reaction of gases produced during polymerization. This is common in the reaction of isocyanate with water to produce carbon dioxide.

- Expansion of the gas dissolved in a polymer upon reduction of the processing pressure.

The basic steps of the foaming process are nucleation of the cells, expansion or growth of the cells, and stabilization of the cells. The nucleation of a cell occurs when, at a given temperature and pressure, the solubility of a gas is reduced, leading to saturation, expelling the excess gas to form a bubble. Nucleating agents are used for initial formation of the bubbles. The bubble

reaches an equilibrium shape when the pressure inside the bubble balances with the surface tension surrounding the cell.

## 3.8    Viscoelastic Behavior of Polymers

It was mentioned earlier in this chapter that a polymer, at a specific temperature and molecular weight, may behave as a liquid or a solid depending on the speed (time scale) at which its molecules are deformed. This behavior, which ranges between liquid and solid, is generally referred to as the viscoelastic behavior or material response. In this chapter we will limit the discussion to *linear viscoelasticity* which is valid for polymer systems that are undergoing *small deformations*. *Non-linear viscoelasticity*, required when modeling *large deformations* such as those encountered in flowing polymer melts, is covered in detail in Chapter 5.

In linear viscoelasticity the *stress relaxation test* is often used, along with the *time-temperature superposition principle* and the *Boltzmann superposition principle*, to explain the behavior of polymeric materials during deformation.

### 3.8.1   Stress Relaxation Test

In a stress relaxation test, a polymer test specimen is deformed a fixed amount, $\varepsilon_0$, and the stress required to hold that amount of deformation is recorded over time. This test is very cumbersome to perform, so the design engineer and the material scientist have tended to ignore it. In fact, several years ago the standard relaxation test ASTM D2991 was dropped by ASTM. Rheologists and scientists, however, have been consistently using the stress relaxation test to interpret the viscoelastic behavior of polymers.

Figure 3.27 [10] presents the stress relaxation modulus measured of polyisobutylene[8] at various temperatures. Here, the stress relaxation modulus is defined by

$$E_r(t) = \frac{\sigma(t)}{\varepsilon_0} \qquad (3.10)$$

where $\varepsilon_0$ is the applied strain and $\sigma(t)$ is the stress being measured. From the test results it is clear that stress relaxation is time and temperature dependent, especially around the glass transition temperature where the slope of the curve is maximal. In the case of the polyisobutylene shown in Fig. 3.27, the glass

---
[8]   Better known as chewing gum.

transition temperature is about -70 °C. The measurements were completed in an experimental time window between a few seconds and one day. The tests performed at lower temperatures were used to record the initial relaxation while the tests performed at higher temperatures only captured the end of relaxation of the rapidly decaying stresses.

It is well known that high temperatures lead to small molecular relaxation times[9] and low temperatures lead to materials with large relaxation times. This is due to the fact that at low temperatures the free volume between the molecules is reduced, restricting or slowing down their movement. At high temperatures, the free volume is larger and the molecules can move with more ease. Hence, when changing temperature, the shape of creep[10] or relaxation test results remain the same except that they are horizontally shifted to the left or right, which represent lower or higher response times, respectively.
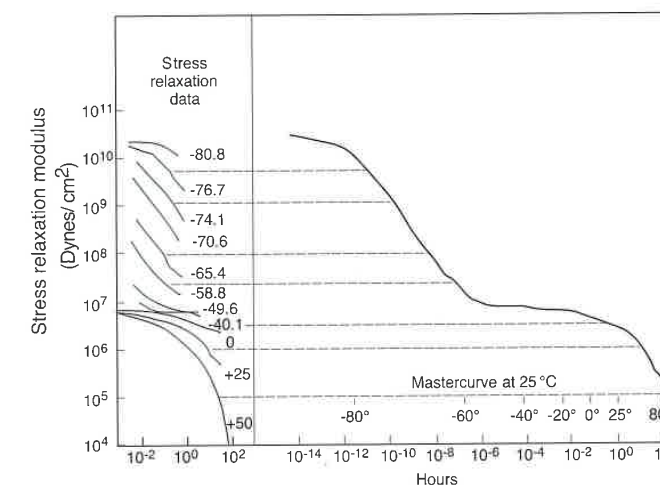


**Figure 3.27**    Relaxation modulus curves for polyisobutylene at various temperatures and corresponding master curve at 25 °C.

The same behavior is observed if the pressure is varied. As the pressure is increased, the free volume between the molecules is reduced, slowing down molecular movement. Here, an increase in pressure is equivalent to a decrease in temperature. In the melt state, the viscosity of a polymer increases with

---
[9]    By relaxation time one usually refers to the time it takes for applied stresses to relax within a material.

[10]    In a creep test the polymer specimen is loaded to a constant stress, and the strain response is recorded in time. The creep test is described in more detail in Chapter 9.

pressure. Figure 3.28 [11] is presented to illustrate the effect of pressure on stress relaxation.
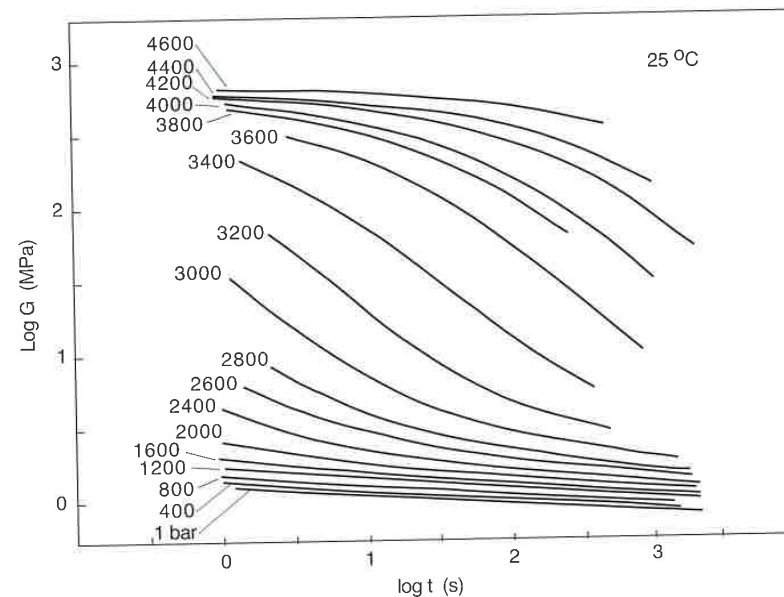


**Figure 3.28**  Shear relaxation modulus for a chlorosulfonated polyethylene at various pressures.

### 3.8.2  Time-Temperature Superposition (WLF-Equation)

The time-temperature equivalence seen in stress relaxation test results can be used to reduce data at various temperatures to one general *master curve* for a reference temperature, $T_{ref}$. To generate a master curve at the reference temperature, the curves shown in the left of Fig. 3.27 must be shifted horizontally, maintaining the reference curve stationary. Density changes are usually small and can be neglected, eliminating the need to perform tedious corrections. The master curve for the data in Fig. 3.27 is shown on the right side of the figure. Each curve was shifted horizontally until the ends of all the curves became superimposed. The amount that each curve was shifted can be plotted with respect to the temperature difference taken from the reference temperature. For the data in Fig. 3.27 the shift factor is shown in the plot in Fig. 3.29. The amounts the curves where shifted are represented by

$$\log t - \log t_{ref} = \log\left(\frac{t}{t_{ref}}\right) = \log a_T \tag{3.11}$$
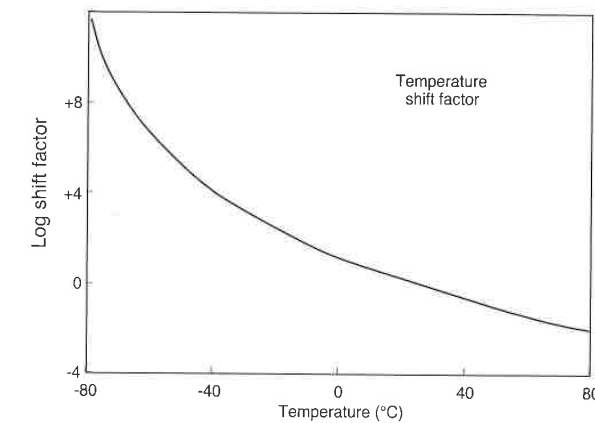


**Figure 3.29**  Plot of the shift factor as a function of temperature used to generate the master curve plotted in Fig. 3.27.

Although the results in Figure 3.29 where shifted to a reference temperature of 298 K (25 °C), Williams, Landel and Ferry [12] chose $T_{ref}$ = 243 K for

$$\log a_T = \frac{-8.86\,(T - T_{ref})}{101.6 + T - T_{ref}} \tag{3.12}$$

which holds for nearly all polymers if the chosen reference temperature is 45 K above the glass transition temperature. In general, the horizontal shift, $\log a_T$, between the relaxation responses at various temperatures to a reference temperature can be computed using the well known Williams-Landel-Ferry [12] (WLF) equation. The WLF equation is given by

$$\log a_T = -\frac{C_1\,\left(T - T_{ref}\right)}{C_2 + (T - T_{ref})} \tag{3.13}$$

where $C_1$ and $C_2$ are material dependent constants. It has been shown that with the assumption $C_1 = 17.44$ and $C_2 = 51.6$, Eq. 3.13 fits well a wide variety of polymers as long as the glass transition temperature is chosen as the reference temperature. These values for $C_1$ and $C_2$ are often referred to as universal constants. Often, the WLF equation must be adjusted until it fits the

experimental data. Master curves of stress relaxation tests are important since the polymer's behavior can be traced over much greater periods of time than those determined experimentally.

### 3.8.3 The Boltzmann Superposition Principle

In addition to the *time-temperature superposition principle* (WLF), the *Boltzmann superposition principle* is of extreme importance in the theory of linear viscoelasticity. The Boltzmann superposition principle states that the deformation of a polymer component is the sum or superposition of all strains that result from various loads acting on the part at different times. This means that the response of a material to a specific load is independent of already existing loads. Hence, we can compute the deformation of a polymer specimen upon which several loads act at different points in time by simply adding all strain responses. The Boltzmann superposition principle is schematically illustrated in Fig. 3.30. Mathematically, the Boltzmann superposition principle can be stated as follows

$$\varepsilon = \sigma_0 J(t - t_0) + (\sigma_1 - \sigma_0) J(t - t_1) + \ldots + (\sigma_i - \sigma_{i-1}) J(t - t_i) + \ldots \tag{3.14}$$

where $J$ represents the material's compliance[11]. However, not all loadings and deformations consist of finite step changes, and Eq. 3.14 can be written in integral form as

$$\varepsilon(t) = \int_{\sigma(-\infty)}^{\sigma(t)} J(t - t')\, d\sigma(t') \tag{3.15}$$

which can also be written as

$$\varepsilon(t) = \int_{-\infty}^{t} J(t - t')\, \dot{\sigma}(t')\, dt' \tag{3.16}$$

Furthermore, one can invert Eq. 3.16 and write

$$\sigma(t) = \int_{-\infty}^{t} G(t - t')\, \dot{\varepsilon}\, dt' \tag{3.17}$$

The Boltzmann superposition principle holds as long as the polymer follows a linear viscoelastic behavior.

---

[11]  The compliance is the inverse of the stiffness, $J = 1 / E$.
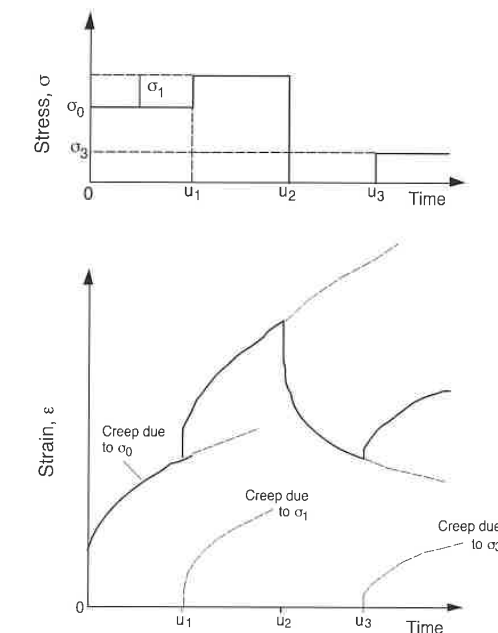
**Figure 3.30**    Schematic demonstration of Boltzmann's superposition principle. A, B, and C are sudden load changes.

### 3.8.4 Applying Linear Viscoelasticity to Describe the Behavior of Polymers

Most polymers exhibit a viscous as well as an elastic response to stress and strain. This puts them in the category of viscoelastic materials. Various combinations of elastic and viscous elements have been used to approximate the material behavior of polymeric melts. Most models are combinations of springs and dash pots— the most common one being the Maxwell model.

For clarity, let us first derive the stress-strain behavior for a Maxwell model shown in Fig. 3.31. The total strain, $\varepsilon$, in the model has an elastic, $\varepsilon_e$, and a viscous, $\varepsilon_V$, strain contribution and can be represented as follows:

$$\varepsilon = \varepsilon_e + \varepsilon_v \tag{3.18}$$
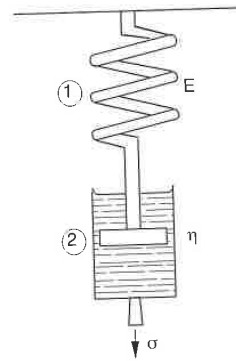
**Figure 3.31**    Schematic diagram of the Maxwell model.

Similarly, the strain rates are written as

$$\dot{\varepsilon} = \dot{\varepsilon}_e + \dot{\varepsilon}_v \tag{3.19}$$

Assuming the spring follows Hooke's law, the following relation holds

$$\dot{\varepsilon}_e = \frac{\dot{\sigma}}{E} \tag{3.20}$$

The viscous portion, represented by the dash pot, is written as follows

$$\dot{\varepsilon}_v = \frac{\sigma}{\eta} \tag{3.21}$$

Combining Eqs. 3.19–3.21 results in

$$\dot{\varepsilon} = \frac{\dot{\sigma}}{E} + \frac{\sigma}{\eta} \tag{3.22}$$

which can be rewritten as

$$\sigma + \frac{\eta}{E}\frac{d\sigma}{dt} = \eta\frac{d\varepsilon}{dt} \tag{3.23}$$

which is often referred to as the governing equation for Maxwell's model in *differential form*.

   Maintaining the material at a constant deformation, such as in the relaxation test, the differential equation, Eq. 3.23, reduces to

$$\sigma + \frac{\eta}{E}\dot{\sigma} = 0 \tag{3.24}$$

Integrating Eq. 3.24 results in

$$\sigma = \sigma_0 e^{-t/\lambda} \tag{3.25}$$

where $\lambda$ is known as the *relaxation time*. The relaxation response of the constant strain Maxwell model is depicted in Fig. 3.32. Using Eq. 3.25 one can show how after $t = \lambda$, the stresses relax to 37% of their initial value; $e^{-1} = 0.37$. When estimating relaxation of stresses, four relaxation times ($4\lambda$) are often used. Hence, by using $t = 4\lambda$ in Eq. 3.25 the stresses have relaxed to 1.8% of their original size. Using the Boltzmann superposition principle and Eq. 3.25 we can write the governing equation for the Maxwell model in *integral form* as

$$\sigma(t) = \int_{-\infty}^{t} Ee^{-(t-t')/\lambda}\dot{\varepsilon}\, dt \tag{3.26}$$

   For more accurate estimates or realistic analyses the Maxwell model is not sufficient. For a better fit with experimental data it is common to use several spring-dash pot models in parallel such as shown in Fig. 3.32 [13]. Such a configuration is often referred to as a *generalized Maxwell model*. The curve shown in the figure fits a four-parameter model with experimental relaxation and retardation data for a common polystyrene with a molecular weight of 260,000 g/mole. For this specific material, the relaxation behavior of the injected melt into a hot cavity, at a reference temperature of 113 °C, is described by

$$\frac{\varepsilon}{\varepsilon_a} = 0.25\left(e^{-8.75\,t/\lambda} + e^{-1.0\,t/\lambda} + e^{-0.28\,t/\lambda} + e^{-0.0583\,t/\lambda}\right) \tag{3.27}$$

where $\varepsilon_a$ is the strain after relaxation and is defined by

$$\varepsilon_a = \frac{l_a - l_0}{l_0} = \frac{S_0}{1 - S_0} \tag{3.28}$$

Here, $l_a$ and $l_0$ represent the length of the stretched and relaxed sample, respectively, and $S_0$ represents the total shrinkage.

   The terms $\frac{\lambda}{8.75}, \lambda, \frac{\lambda}{0.28}, \frac{\lambda}{0.0583}$, in Eq. 3.27 represent four individual relaxation times for this specific polystyrene, modeled using the four-parameter model. The relaxation time, $\lambda$, correlates with the time it takes for the initial strain to reduce, by relaxation, to one-half its initial value. This

relaxation time is also temperature dependent as shown for various polymers in Fig. 3.33. Figure 3.33 shows how the shapes of the curves are all similar, only shifted by a certain temperature. It is important to note that the relaxation and retardation behavior of all amorphous thermoplastics is similar.
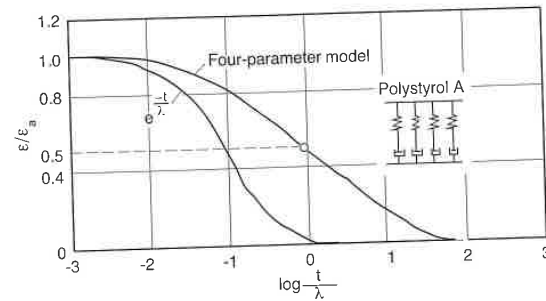


**Figure 3.32**    Relaxation response of a Maxwell model and a four-parameter Maxwell model.
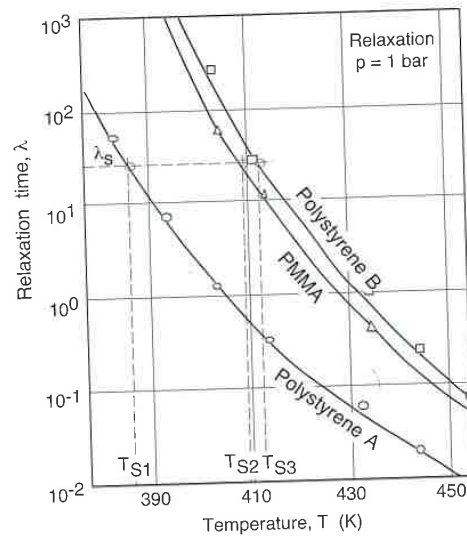


**Figure 3.33**    Relaxation time as a function of temperature for various thermoplastics.

Wübken [13] performed similar tests with different amorphous thermoplastics, and he found that, indeed, in all cases the measurements showed a correlation between time and temperature such as described by the WLF [12] equation. The data fit by the four-parameter model was generated via two different experiments: a relaxation test inside an injection mold between 100 and 180 °C, and a retardation test outside of the mold between 72 and 100 °C. The measured data are shown in Figs. 3.34 and 3.35 for the relaxation and retardation tests, respectively. The curves shown in both graphs were shifted horizontally to generate one master curve as shown in Fig. 3.36. The solid line in the figure is the four-parameter fit represented with Eq. 3.27.
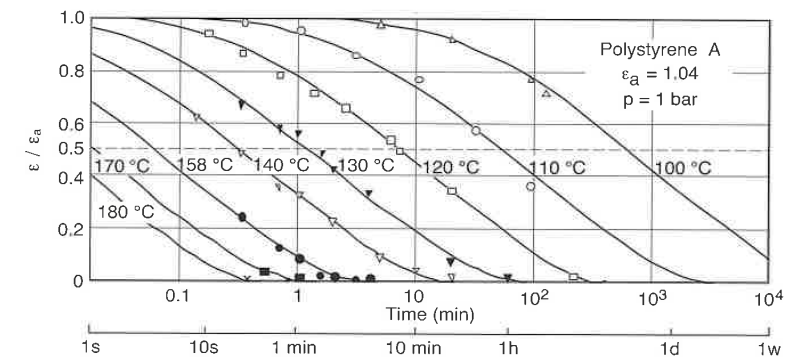


**Figure 3.34**    Relaxation response, inside an injection mold, of a polystyrene specimen at various temperatures.
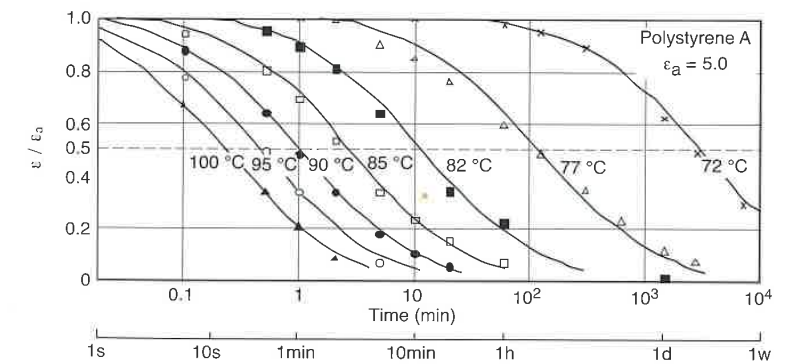


**Figure 3.35**    Recovery or retardation response after injection molding of a polystyrene specimen at various temperatures.
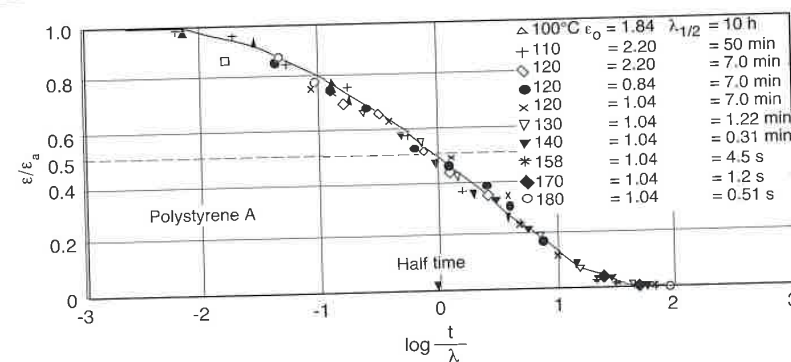
**Figure 3.36**   Master curve for the relaxation response, inside an injection mold, of a polystyrene specimen at various temperatures.

Hence, appropriate $T_{ref}$ and $l$ values must be found. However, the reference temperature is not quite independent of the relaxation behavior of the polymer but is related to the material properties. For the polystyrene A in Fig. 3.37, $T_{ref} = 113$ °C, or about 48 °C above $T_g$. For example, for the polystyrene A of Fig. 3.37, the relaxation time, $l$, can be computed by

$$\text{Relaxation}: \ \log(\lambda) = \log(27) - \frac{8.86\,(T - T_s)}{101.6 + (T - T_s)} \tag{3.29}$$

$$\text{Creep}: \ \log(\lambda) = \log(0.0018) - \frac{8.86\,(T - T_s)}{101.6 + (T - T_s)} \tag{3.30}$$

where the constants 27 and 0.0018 are the relaxation times, $\lambda$, in minutes, at the reference temperature of 113 °C.

As discussed earlier, similar to the temperature induced shift, there is also a shift due to pressure[12]. If we refer to Fig. 3.38, which shows the influence of pressure on $T_g$, we can see that this effect can easily be included into the WLF equation i.e., there is approximately a 2 °C shift in the glass transition temperature of polystyrene for every 100 bar of pressure rise [14].

Models such as the Maxwell model described by Eq. 3.23 can also be used to simulate the dynamic response of polymers. In a dynamic test[13] the strain input is given by

$$\varepsilon = \varepsilon_0 \sin(\omega t) \tag{3.31}$$

---

[12]   This is discussed in Chapters 5 and 9 for shifts in viscosity and relaxation times, respectively.

[13]   The dynamic test is discussed in more detail in Chapter 8.

where $\varepsilon_0$ is the strain amplitude and $\omega$ the frequency in radians per second. Differentiating Eq. 3.31, combining with Eq. 3.23, and integrating results in

$$\sigma = \left( \frac{E \varepsilon_a \omega \lambda}{1 + (\omega \lambda)^2} \right) \left( \omega \lambda \sin(\omega t) + \cos(\omega t) \right) \tag{3.32}$$

for a steady state response. Dividing Eq. 3.28 by the amplitude of the strain input results in a complex modulus, which is formed by an elastic component, that is in-phase with the strain input, and a viscous component. The elastic term is generally called the *storage modulus* and is defined by

$$E' = \left( \frac{E(\omega \lambda)^2}{1 + (\omega \lambda)^2} \right) \tag{3.33}$$

and the viscous term, usually referred to as the *loss modulus*, is given by

$$E'' = \left( \frac{E \omega \lambda}{1 + (\omega \lambda)^2} \right) \tag{3.34}$$
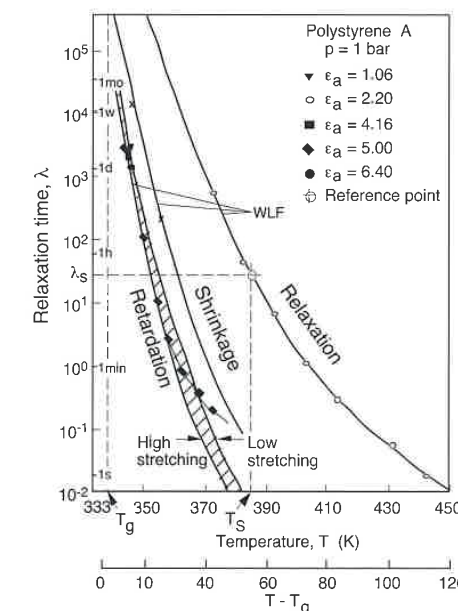


**Figure 3.37**   Relaxation and retardation times as a function of temperature for a polystyrene.
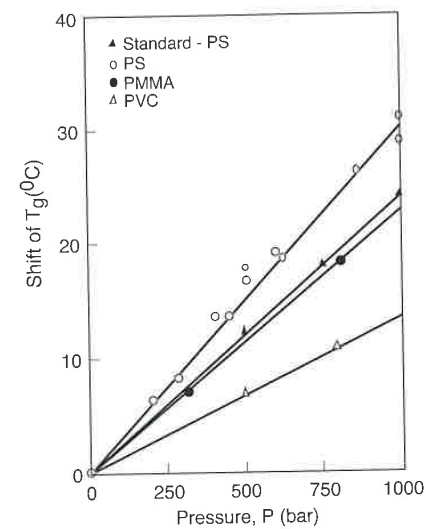
**Figure 3.38**    Influence of hydrostatic pressure on the glass transition temperature for various amorphous thermoplastics.

## Examples

3.1   What is the maximum possible separation between the ends of a high density polyethylene molecule with an average molecular weight of 100,000.

Our first task is to estimate the number of repeat units, n, in the polyethylene chain. Each repeat unit has 2 carbons and 4 hydrogen atoms. The molecular weight of carbon is 12 and that of hydrogen 1. Hence,

MW/repeat unit = 2(12)+4(1)=28.

The number of repeat units is computed as

n = MW/(MW/repeat unit) = 100,000/28 = 3,571 units.

Using the diagram presented in Fig. 3.39 we can now estimate the length of the fully extended molecule using

$$\ell = 0.252 \text{ nm}(3571) = 890 \text{ nm} = 0.89 \mu m$$

Polyethylene repeat unit
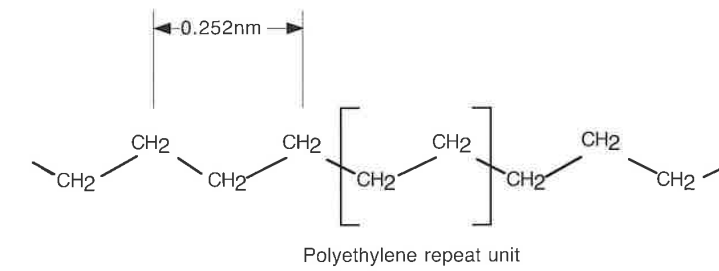
**Figure 3.39**    Schematic diagram of a polyethylene molecule.

As we know, even high density polyethylene molecules are branched and therefore our result is an overprediction.

3.2   For the poly-a-methylstyrene stress relaxation data in Fig. 3.40 [16], create a master creep curve at $T_g$ (204 °C).
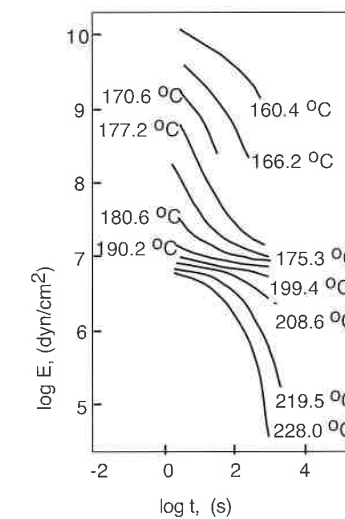


**Figure 3.40**    Stress relaxation data for poly-α-methylstyrene.

Identify the glassy, rubbery, viscous and viscoelastic regions of the master curve. Identify each region with a spring-dashpot diagram.

Develop a plot of the shift factor, $\log(a_T)$ versus T, used to create your

master curve $\log(a_T)$ is the horizontal distance that the curve at temperature T was slid to coincide with the master curve.

What is the relaxation time of the polymer at the glass transition temperature?

The master creep curve for the above data is generated by sliding the individual relaxation curves horizontally until they match with their neighbors, using a fixed scale for a hypothetical curve at 204 °C. Since the curve does not exist for the desired temperature we can interpolate between 208.6 °C and 199.4 °C. The resulting master curve is presented in Fig. 3.41.
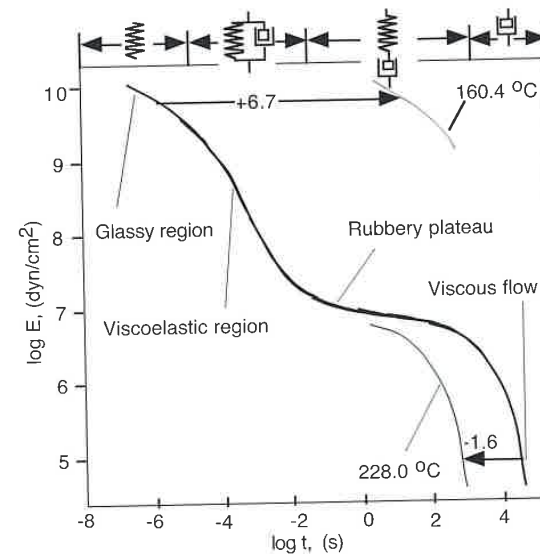


**Figure 3.41**    Master curve for poly-α-methylstyrene at 204 °C.

The amount each curve must be shifted from the master curve to their initial position is the shift factor, $\log a_T$. The graph also shows the spring-dashpot models and the shift factor for a couple of temperatures. Figure 3.42 represents the shift factor versus temperature. The solid line indicates the shift factor predicted by the WLF equation.

The relaxation time for the poly-α-methylstyrene presented here is

$10^{4.5}$ s, or 31,623 s (8.8 h). The relaxation time for the remaining temperatures can be computed using the shift factor curve.
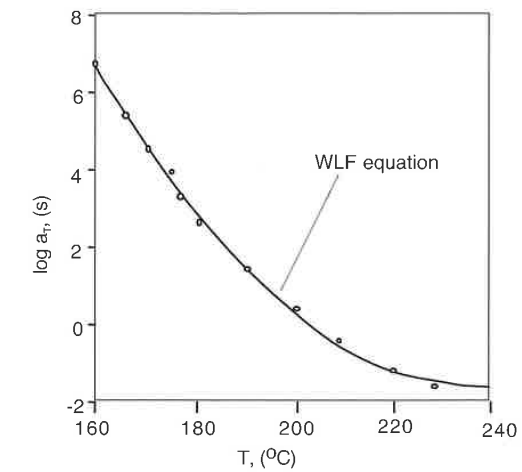


**Figure 3.42**    Shift factor and WLF curves for $T_{ref}$=204 °C.

**Problems**

3.1    Estimate the degree of polymerization of a polyethylene with an average molecular weight of 150,000. The molecular weight of an ethylene monomer is 28.

3.2    What is the maximum possible separation between the ends of a polystyrene molecule with a molecular weight of 160,000.

3.3    To enhance processability of a polymer why would you want to decrease its molecular weight?

3.4    Why would an uncrosslinked polybutadiene flow at room temperature?

3.5    Is it true that by decreasing the temperature of a polymer you can increase its relaxation time?

3.6    If you know the relaxation time of a polymer at one temperature, can you use the WLF equation to estimate the relaxation time of the same material at a different temperature? Explain.

3.7     What role does the cooling rate play in the morphological structure of semi-crystalline polymers?

3.8     Explain how cross-linking between the molecules affect the molecular mobility and elasticity of elastomers.

3.9     Increasing the molecular weight of a polymer increases its strength and stiffness, as well as its viscosity. Is too high of a viscosity a limiting factor when increasing the strength by increasing the molecular weight? Why?

3.10    Which broad class of thermoplastic polymers densifies the least during cooling and solidification from a melt state into a solid state? Why?

3.11    What class of polymers would you probably use to manufacture frying pan handles? Even though most polymers could not actually be used for this particular application, what single property do all polymers exhibit that would be considered advantageous in this particular application.

3.12    In terms of recycling, which material is easier to handle, thermosets or thermoplastics? Why?

3.13    You are to extrude a polystyrene tube at an average speed of is 0.1 m/s. The relaxation time, l, of the polystyrene, at the processing temperature, is 1 second. The die land length is 0.02 m. Will elasticity play a significant role in your process.

3.14    Figure 3.43 presents some creep compliance data for polystyrene at various temperatures [15]. Create a master curve at 109.8 °C by graphically sliding the curves at some temperatures horizontally until they line up.

        Identify the glassy, rubbery, and viscoelastic regions of the master curve.

        Develop a plot of the shift factor, $\log(a_T)$ versus T, used to create your master curve. $\log(a_T)$ is the horizontal distance that the curve at temperature T was slid to coincide with the master curve. Compare your graphical result with the WLF equation.

        **Note:** The WLF equation is for a master curve at Tg (85 °C for this PS), but your master curve is for 109.8 °C, so be sure you make a fair comparison.
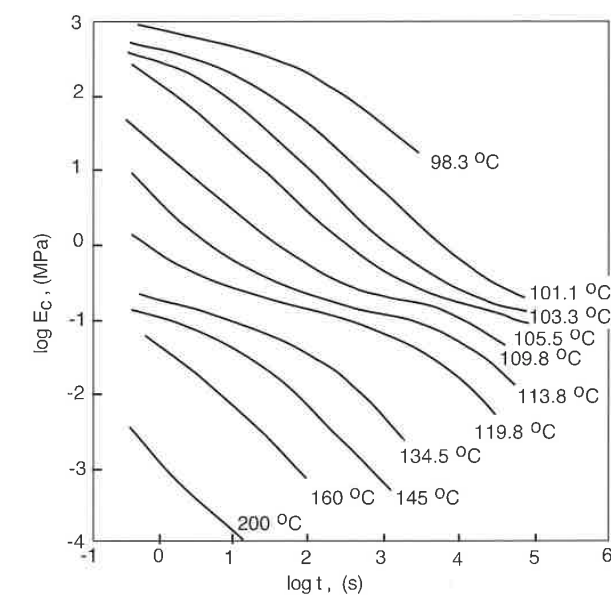
**Figure 3.43**   Creep modulus as a function of time for polystyrene.

3.15    Figure 3.44 presents relaxation data for polycarbonate at various temperatures [17]. Create a master curve at 25 °C by graphically sliding the curves at the various temperatures horizontally until they line up.

        Identify the glassy, rubbery, and viscoelastic regions of the master curve.

        Develop a plot of the shift factor, $\log(a_T)$ versus T, used to create your master curve. $\log(a_T)$ is the horizontal distance that the curve at temperature T was slid to coincide with the master curve.

        Compare your graphical result with the WLF equation. Note that the resulting master curve is far from the glass transition temperature of polycarbonate.
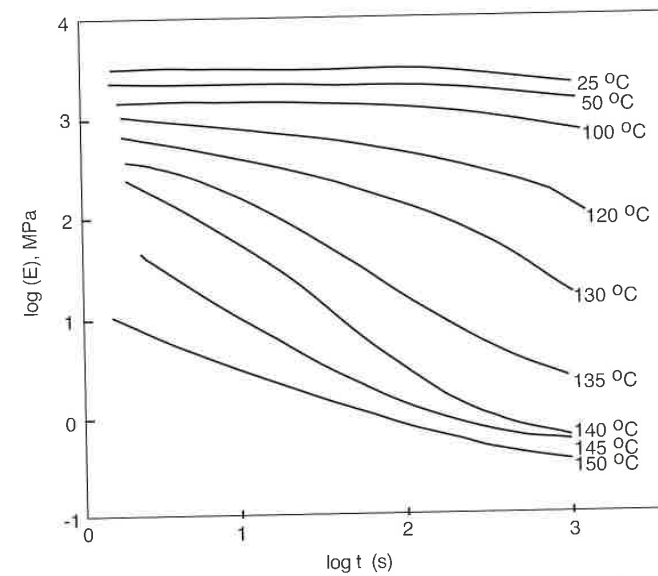
**Figure 3.44**     Relaxation modulus as a function of time for polycarbonate

3.16   Figure 3.28 presents shear relaxation data for a chlorosulfonated polyethylene at various pressures. Create a master curve at 1 bar by graphically sliding the curves at the various pressures horizontally until they line up. On the same graph draw the master curve at a pressure of 1200 bar, a high pressure encountered during injection molding.

## References

1.   Berry, G.C., and Fox, T.G., *Adv. Polymer Sci.*, 5, 261, (1968).
2.   Staudinger, H., and Huer, W., *Ber. der Deutsch. Chem Gessel.*, 63, 222, (1930).
3.   Crowder, M.L., Ogale, A.M., Moore, E.R., and Dalke, B.D.,*Polym. Eng. Sci.*, 34, 19, 1497, (1994).
4.   Domininghaus, H., *Plastics for Engineers*, Hanser Publishers, Munich, (1993).
5.   Aklonis, J.J., and MacKnight, W.J., *Introduction to Polymer Viscoelasticity*, John Wiley and Sons, New York, (1983).
6.   Rosen, S.L., *Fundamental Principles of Polymeric Materials*, John Wiley & Sons, Inc., New York, (1993).
7.   Van Krevelen, D.W., and Hoftyzer, P.J., *Properties of Polymers*, 2nd. Ed., Elsevier, Amsterdam, (1976).
8.   Green, J., *Thermoplastic Polymer Additives*, Chapter 4, J.T. Lutz, Jr., Ed., Marcel Dekker, Inc., New York, (1989).
9.   Klempner, D., and Frisch, K.C. , *Handbook of Polymeric Foams and Foam Technology*, Hanser Publishers, Munich, (1991).
10.   Castiff, E. and Tobolsky, A.V.J., *Colloid Sci.*, 10, 375, (1955).
11.   Fillers, R.W., and Tschoegl, N.W., *Trans. Soc. Rheol, 21*, 51 (1977).
12.   Williams, M.L., Landel, R.F., and Ferry, J.D., *J. Amer. Chem. Soc.*, 77, 3701, (1955).
13.   Wübken, G., Ph.D. Thesis, IKV, RWTH-Aachen, (1974).
14.   Münstedt, H., *Rheol. Acta*, 14, 1077, (1975).
15.   Pazek, D.J., *J. Polym. Sci.*, A-2, (6), 621, (1968).
16.   Fujimoto, T., Ozaki, M., and Nagasawa, M., *J. Polymer Sci.*,2, 6, (1968).
17.   Carreau, P.J., De Kee, D.C.R., and Chhabra, R.P., *Rheology of Polymeric Systems*, Hanser Publishers, Munich, (1997).

# Thermal Properties of Polymers

The heat flow through a material can be defined by Fourier's law of heat conduction. Fourier's law can be expressed as[1]

$$q_x = -k_x \frac{\partial T}{\partial x}$$ (4.1)

where $q_x$ is the energy transport per unit area in the $x$ direction, $k_x$ the thermal conductivity and the temperature gradient. At the onset of heating the polymer responds solely as a heat sink, and the amount of energy per unit volume, $Q$, stored in the material before reaching steady state conditions can be approximated by

$$Q = \rho C_p \Delta T$$ (4.2)

where $\rho$ is the density of the material, $C_p$ the specific heat, and $\Delta T$ the change in temperature.

Using the notation found in Fig. 4.1 and balancing the heat flow through the element via conduction, including the transient, convective, and viscous heating effects, the energy balance can be written as

$$\rho C_p \frac{\partial T}{\partial t} + \rho C_p \underline{v} \cdot \nabla T = (\nabla \cdot \underline{k} \cdot \nabla T) + \frac{1}{2}\mu\left(\underline{\dot{\gamma}} : \underline{\dot{\gamma}}\right) + \dot{Q}$$ (4.3)

where on the left are the transient and convective terms, and on the right the conductive, viscous heating, and an arbitrary heat generation term. The full form of the energy equation is found along with the continuity equation and momentum balance in Tables IV and V of the appendix of this book.

---

[1]  For more detailed information on transport phenomena the reader can refer to: Bird, R.B., Steward, W.E. and Lightfoot, E.N., *Transport Phenomena*, John Wiley & Sons, (1960).
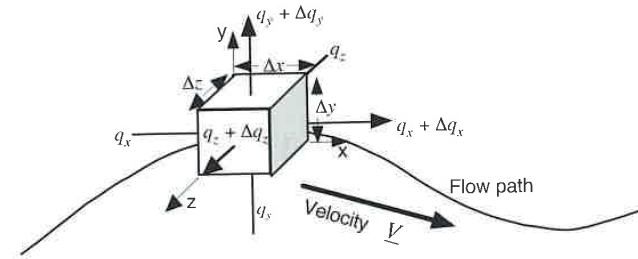
**Figure 4.1**    Heat flow through a differential material element.

The material properties found in Eqs. 4.1–4.3 are often written as one single property, namely the thermal diffusivity, a, which for an isotropic material is defined by

$$\alpha = \frac{k}{\rho C_P} \tag{4.4}$$

Typical values of thermal properties for selected polymers are shown in Table 4.1 [1]. For comparison, the properties for stainless steel are also shown at the end of the list.

It should be pointed out that the material properties of polymers are not constant and may vary with temperature, pressure or phase changes. This chapter will discuss each of these properties individually and present examples of some of the most widely used polymers and measurement techniques. For a more in-depth study of thermal properties of polymers the reader is encouraged to consult the literature [2–4].

**Table 4.1**    Thermal Properties for Selected Polymeric Materials

| Polymer | Specific gravity | Specific heat (kJ/kg°C) | Thermal conductivity (W/m/K) | Coeff. of therm. exp. (μm/m/K) | Thermal diffusivity (m²/s)x10⁷ | Max temperature (°C) |
|---|---|---|---|---|---|---|
| ABS | 1.04 | 1.47 | 0.3 | 90 | 1.7 | 70 |
| Acetal (homo-pol.) | 1.42 | 1.47 | 0.2 | 80 | 0.7 | 85 |
| Acetal (Co-pol.) | 1.41 | 1.47 | 0.2 | 95 | 0.72 | 90 |
| Acrylic | 1.18 | 1.47 | 0.2 | 70 | 1.09 | 50 |
| Cellulose acetate | 1.28 | 1.50 | 0.15 | 100 | 1.04 | 60 |
| Epoxy | 1.90 | - | 0.23 | 70 | - | 130 |
| Mod. PPO | 1.06 | - | 0.22 | 60 | - | 120 |
| PA66 | 1.14 | 1.67 | 0.24 | 90 | 1.01 | 90 |
| PA66 +30%GF | 1.38 | 1.26 | 0.52 | 30 | 1.33 | 100 |
| PET | 1.37 | 1.05 | 0.24 | 90 | - | 110 |
| PET +30%GF | 1.63 | - | - | 40 | - | 150 |
| Phenolic | 1.40 | 1.30 | 0.35 | 22 | 1.92 | 185 |
| PC | 1.15 | 1.26 | 0.2 | 65 | 1.47 | 125 |
| u-Polyester | 1.20 | 1.20 | 0.2 | 100 | - | - |
| PP | 0.905 | 1.93 | 0.24 | 100 | 0.65 | 100 |
| PS | 1.05 | 1.34 | 0.15 | 80 | 0.6 | 50 |
| LDPE | 0.92 | 2.30 | 0.33 | 200 | 1.17 | 50 |
| HDPE | 0.95 | 2.30 | 0.63 | 120 | 1.57 | 55 |
| PTFE | 2.10 | 1.00 | 0.25 | 140 | 0.7 | 50 |
| u-PVC | 1.40 | 1.00 | 0.16 | 70 | 1.16 | 50 |
| p-PVC | 1.30 | 1.67 | 0.14 | 140 | 0.7 | 50 |
| SAN | 1.08 | 1.38 | 0.17 | 70 | 0.81 | 60 |
| PS-foam | 0.032 | - | 0.032 | - | - | - |
| Steel | 7.854 | 0.434 | 60.00 | - | 14.1 | 800 |

## 4.1  Material Properties

### 4.1.1 Thermal Conductivity

When analyzing thermal processes, the thermal conductivity, $k$, is the most commonly used property that helps quantify the transport of heat through a material. By definition, energy is transported proportionally to the speed of sound. Accordingly, thermal conductivity follows the relation

$$k \approx C_p \rho u l \tag{4.5}$$

where $u$ is the speed of sound and $l$ the molecular separation. Amorphous polymers show an increase in thermal conductivity with increasing temperature, up to the glass transition temperature, $T_g$. Above $T_g$, the thermal conductivity decreases with increasing temperature. Figure 4.2 [2] presents the thermal conductivity, below the glass transition temperature, for various amorphous thermoplastics as a function of temperature.
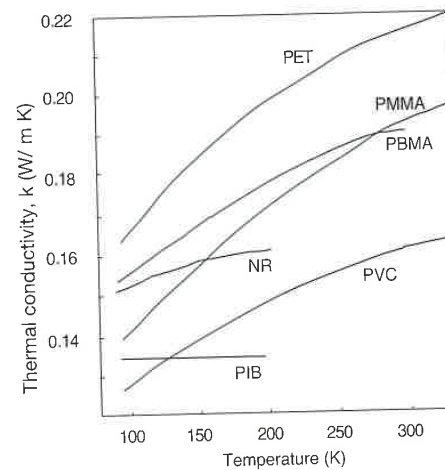


**Figure 4.2**  Thermal conductivity of various materials.

Due to the increase in density upon solidification of semi-crystalline thermoplastics, the thermal conductivity is higher in the solid state than in the melt. In the melt state, however, the thermal conductivity of semi-crystalline polymers reduces to that of amorphous polymers as can be seen in Fig. 4.3 [5]. Furthermore, it is not surprising that the thermal conductivity of melts increases with hydrostatic pressure. This effect is clearly shown in Fig. 4.4 [6].

As long as thermosets are unfilled, their thermal conductivity is very similar to amorphous thermoplastics.

Anisotropy in thermoplastic polymers also plays a significant role in the thermal conductivity. Highly drawn semi-crystalline polymer samples can have a much higher thermal conductivity as a result of the orientation of the polymer chains in the direction of the draw. For amorphous polymers, the increase in thermal conductivity in the direction of the draw is usually not higher than two. Figure 4.5 [2] presents the thermal conductivity in the directions parallel and perpendicular to the draw for high density polyethylene, polypropylene, and polymethyl methacrylate.

A simple relation exists between the anisotropic and the isotropic thermal conductivity [7]. This relation is written as

$$\frac{1}{k_\parallel} + \frac{2}{k_\perp} = \frac{3}{k} \tag{4.6}$$

where the subscripts $\parallel$ and $\perp$ represent the directions parallel and perpendicular to the draw, respectively.
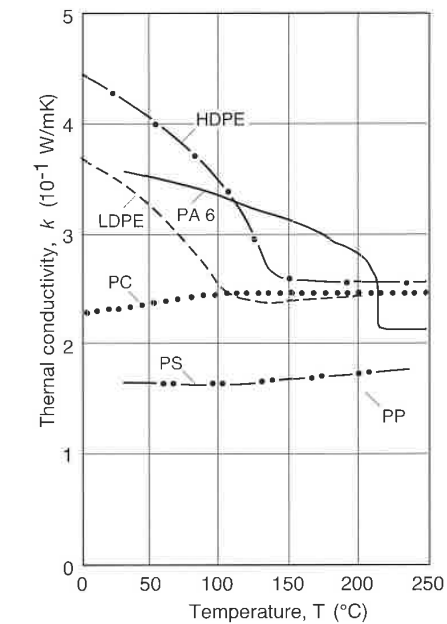


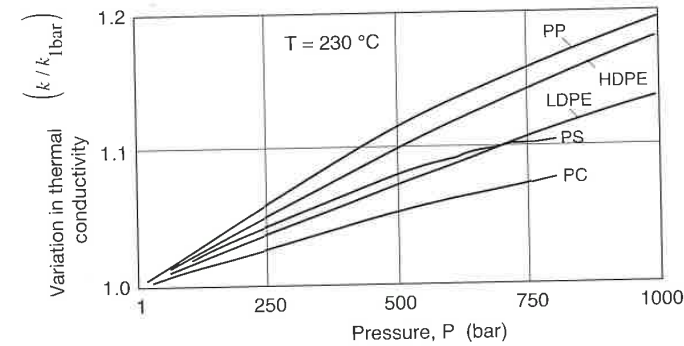**Figure 4.3**  Thermal conductivity of various thermoplastics.

**Figure 4.4**    Influence of pressure on thermal conductivity of various thermoplastics.
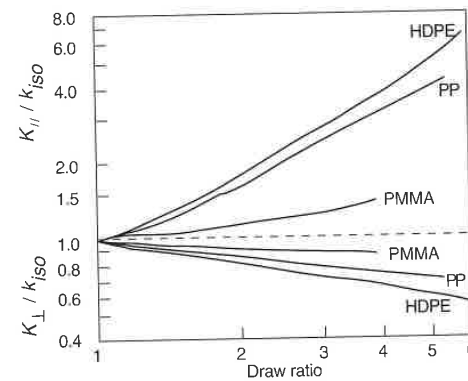


**Figure 4.5**    Thermal conductivity as a function of draw ratio in the directions perpendicular and parallel to the stretch for various oriented thermoplastics.

The higher thermal conductivity of inorganic fillers increases the thermal conductivity of filled polymers. Nevertheless, a sharp decrease in thermal conductivity around the melting temperature of crystalline polymers can still be seen with filled materials. The effect of filler on thermal conductivity of various thermoplastics is shown in Figs. 4.6 to 4.9. Figure 4.6 [8] shows the effect of fiber orientation as well as the effect of quartz powder on the thermal conductivity of low density polyethylene. Figures 4.7 to 4.9 show the effect of various volume fractions of glass fiber in polyamide 6, polycarbonate, and ABS, respectively. Figure 4.10 demonstrates the influence of gas content on expanded

or foamed polymers, and the influence of mineral content on filled polymers. There are various models available to compute the thermal conductivity of foamed or filled plastics [7, 9, 10]. A rule of mixtures, suggested by Knappe [7], commonly used to compute thermal conductivity of composite materials is written as

$$k_c = \frac{2k_m + k_f - 2\phi_f(k_m - k_f)}{2k_m + k_f + \phi_f(k_m - k_f)} k_m \tag{4.7}$$

where, $\phi_i$ is the volume fraction of filler, and $k_m$, $k_f$ and $k_c$ are the thermal conductivity of the matrix, filler and composite, respectively. Figure 4.11 compares Eq. 4.7 with experimental data [11] for an epoxy filled with copper particles of various diameters. The figure also compares the data to the classic model given by Maxwell [9] which is written as

$$k_c = \left(1 + 3\phi_f \left(\frac{k_f/k_m - 1}{k_f/k_m + 2}\right)\right) k_m \tag{4.8}$$
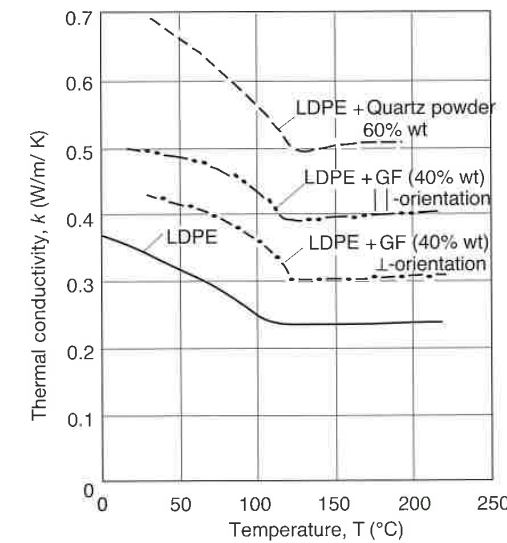


**Figure 4.6**    Influence of filler on the thermal conductivity of LDPE.
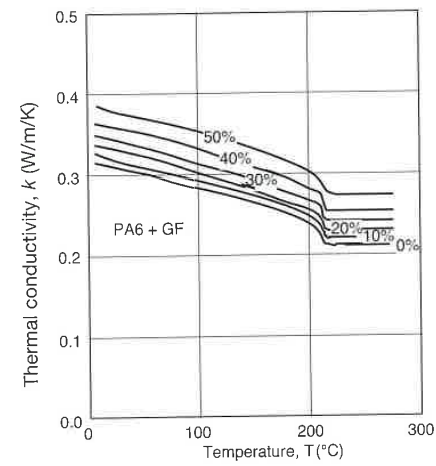
**Figure 4.7**    Influence of glass fiber on the thermal conductivity of polyamide 6. Courtesy of Bayer AG, Germany.
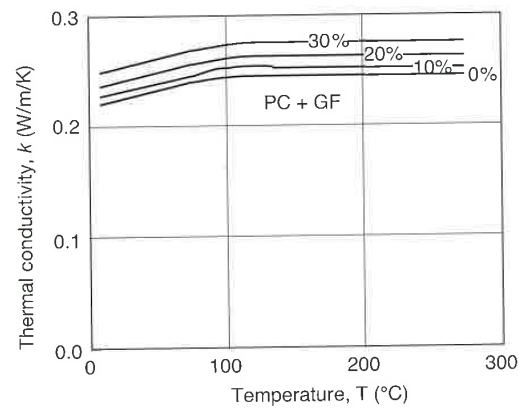


**Figure 4.8**    Influence of glass fiber on the thermal conductivity of polycarbonate. Courtesy of Bayer AG, Germany.
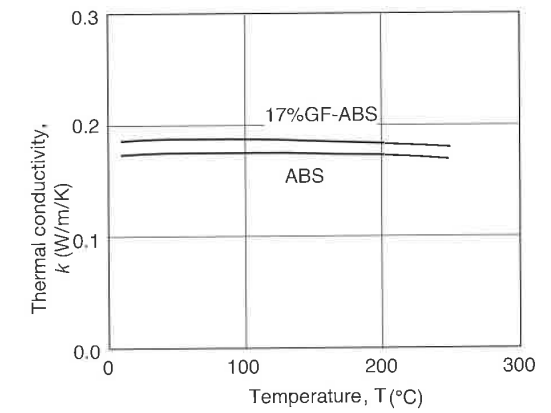


**Figure 4.9**    Influence of glass fiber on the thermal conductivity of ABS. Courtesy of Bayer AG, Germany.
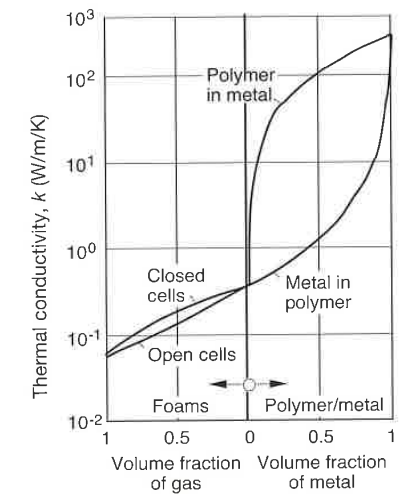


**Figure 4.10**    Thermal conductivity of plastics filled with glass or metal.
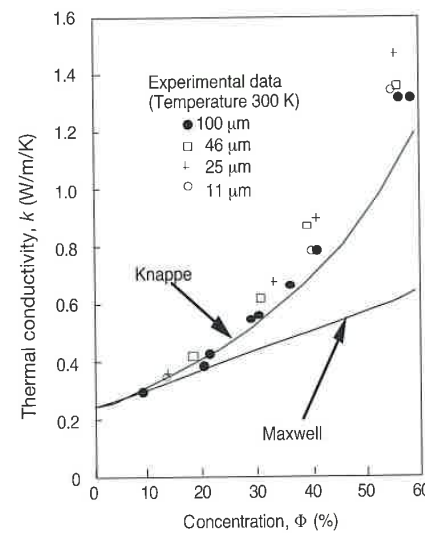
**Figure 4.11** Thermal conductivity versus volume concentration of metallic particles of an epoxy resin. Solid lines represent predictions using Maxwell and Knappe models.

In addition, a model derived by Meredith and Tobias [10] applies to a cubic array of spheres inside a matrix. Consequently, it cannot be used for volumetric concentration above 52% since the spheres will touch at that point. However, their model predicts the thermal conductivity very well up to 40% by volume of particle concentration.

When mixing several materials the following variation of Knappe's model applies

$$k_c = \frac{1 - \sum\limits_{i=1}^{n} 2\phi_i \dfrac{k_m - k_i}{2k_m + k_i}}{1 - \sum\limits_{i=1}^{n} \phi_i \dfrac{k_m - k_i}{2k_m - k_i}} k_m \qquad (4.9)$$

where $k_i$ is the thermal conductivity of the filler and $\phi_i$ its volume fraction. This relation is useful for glass fiber reinforced composites (FRC) with glass concentrations up to 50% by volume. This is also valid for FRC with unidirectional reinforcement. However, one must differentiate between the direction longitudinal to the fibers and that transverse to them. For high fiber

content one can approximate the thermal conductivity of the composite by the thermal conductivity of the fiber.

The thermal conductivity can be measured using the standard tests ASTM C177 and DIN 52612. A new method is currently being balloted, ASTM D20.30, which is preferred by most people today.

### 4.1.2 Specific Heat

The specific heat, $C$, represents the energy required to change a unit mass of material by one degree in temperature. It can be measured at either constant pressure, $C_p$, or constant volume, $C_v$. Since the specific heat at constant pressure includes the effect of volumetric change, it is larger than the specific heat at constant volume. However, the volume changes of a polymer with changing temperatures have a negligible effect on the specific heat. Hence, one can usually assume that the specific heat at constant volume or constant pressure are the same. It is usually true that specific heat only changes modestly in the range of practical processing and design temperatures of polymers. However, semi-crystalline thermoplastics display a discontinuity in the specific heat at the melting point of the crystallites. This jump or discontinuity in specific heat includes the heat that is required to melt the crystallites which is usually called the *heat of fusion*. Hence, specific heat is dependent on the degree of crystallinity. Values of heat of fusion for typical semi-crystalline polymers are shown in Table 4.2.

**Table 4.2**[2] Heat of Fusion of Various Thermoplastic Polymers

| Polymer | $\lambda$ (kJ /kg) | $T_m$ (°C) |
|---|---|---|
| Polyethylene | 268- 300 | 141 |
| Polypropylene | 209- 259 | 183 |
| Polyvinyl-chloride | 181 | 285 |
| Polybutadiene | 170- 187 | 148 |
| Polyamide 6 | 193- 208 | 223 |
| Polyamide 66 | 205 | 265 |

The chemical reaction that takes place during solidification of thermosets also leads to considerable thermal effects. In a hardened state, their thermal data are similar to the ones of amorphous thermoplastics. Figure 4.12 shows the specific heat graphs for the three polymer categories.

---

[2] The values for heat of fusion were computed using data taken from: van Krevelen, D.W., and Hoftyzer, P.J., *Properties of Polymers*, Elsevier Scientific Publishing Company, Amsterdam, (1976).

For filled polymer systems with inorganic and powdery fillers a rule of mixtures[3] can be written as

$$C_P(T) = (1 - \psi_f)C_{PM}(T) + \psi_f C_{Pf}(T) \qquad (4.10)$$

where $\psi_f$ represents the weight fraction of the filler and $C_{PM}$ and $C_{Pf}$ the specific heat of the polymer matrix and the filler, respectively. As an example of using Eq. 4.10, Fig. 4.13 shows a specific heat curve of an unfilled polycarbonate and its corresponding computed specific heat curves for 10%, 20%, and 30% glass fiber content. In most cases temperature dependence of $C_P$ of inorganic fillers is minimal and need not be taken into consideration.

The specific heat of copolymers can be calculated using the mole fraction of the polymer components.

$$C_{Pcopolymer} = \sigma_1 C_{P1} + \sigma_2 C_{P2} \qquad (4.11)$$

where $\sigma_1$ and $\sigma_2$ are the mole fractions of the comonomer components and $C_{P1}$ and $C_{P2}$ the corresponding specific heats.
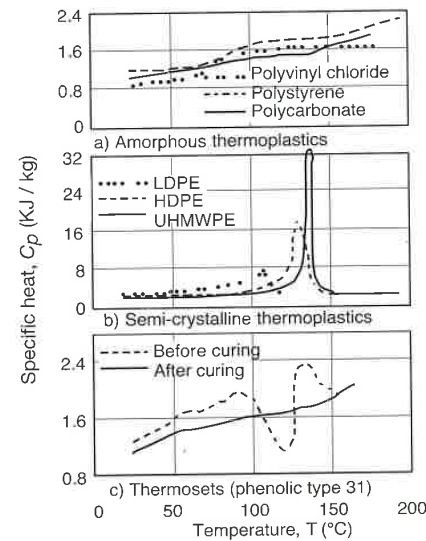


**Figure 4.12**    Specific heat curves for selected polymers of the three general polymer categories.

3    Valid up to 65% filler content by volume.
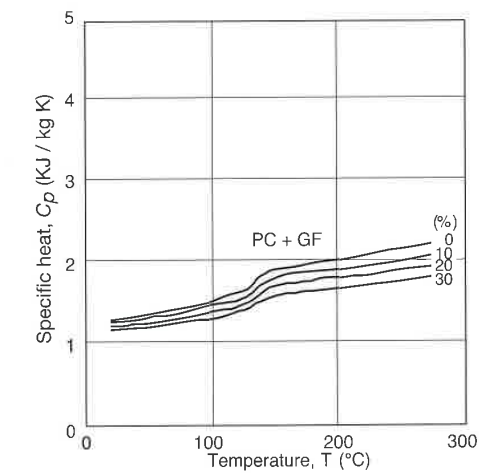
**Figure 4.13**    Generated specific heat curves for a filled and unfilled polycarbonate. Courtesy of Bayer AG, Germany.

### 4.1.3  Density

The density or its reciprocal, the specific volume, is a commonly used property for polymeric materials. The specific volume is often plotted as a function of pressure and temperature in what is known as a p-v-T diagram. A typical p-v-T diagram for an unfilled and filled amorphous polymer is shown, using polycarbonate as an example, in Figs. 4.14 to 4.16. The two slopes in the curves represent the specific volume of the melt and of the glassy amorphous polycarbonate, separated by the glass transition temperature. Figure 4.17 presents the p-v-T diagram for polyamide 66 as an example of a typical semi-crystalline polymer. Figure 4.18 shows the p-v-T diagram for polyamide 66 filled with 30% glass fiber. The curves clearly show the melting temperature (i.e., $T_m \approx 250\,°C$ for the unfilled PA66 cooled at 1 bar, which marks the beginning of crystallization as the material cools). It should also come as no surprise that the glass transition temperatures are the same for the filled and unfilled materials.

When carrying out die flow calculations, the temperature dependence of the specific volume must often be dealt with analytically. At constant pressures, the density of pure polymers can be approximated by

$$\rho(T) = \rho_0 \frac{1}{1 + \alpha_l(T - T_s)} \qquad (4.12)$$

where $\rho_o$ is the density at reference temperature, $T_o$, and $\alpha_t$ is the linear coefficient of thermal expansion.



**Figure 4.14**    p-v-T diagram for a polycarbonate. Courtesy of Bayer AG, Germany.



**Figure 4.15**    p-v-T diagram for a polycarbonate filled with 10% glass fiber. Courtesy of Bayer AG, Germany.



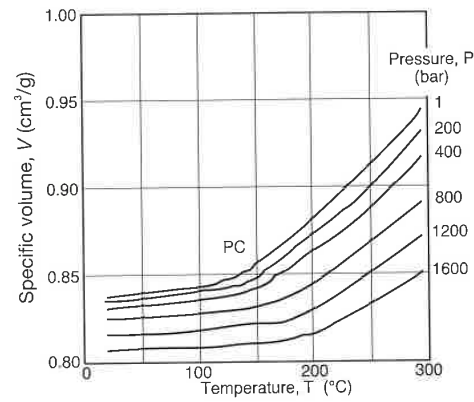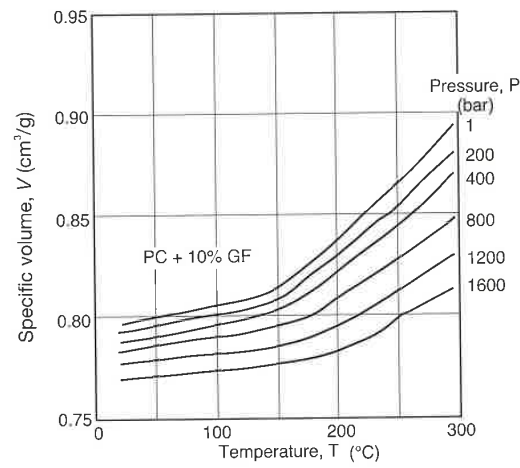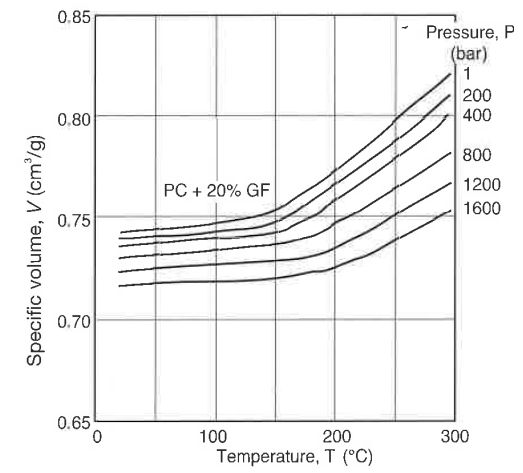**Figure 4.16**    p-v-T diagram for a polycarbonate filled with 20% glass fiber. Courtesy of Bayer AG, Germany.
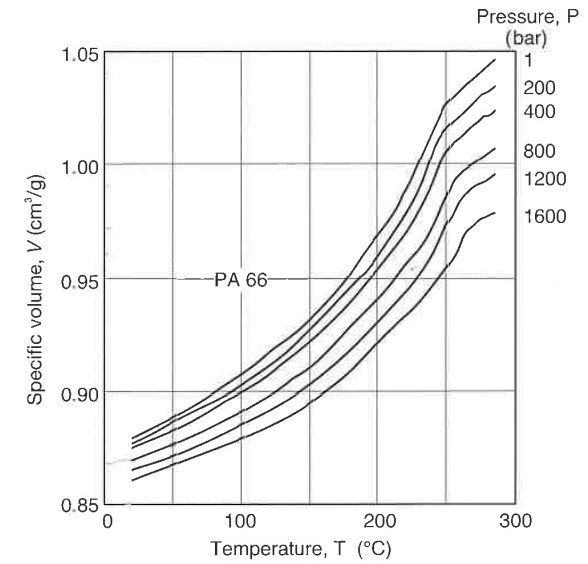


**Figure 4.17**    p-v-T diagram for a polyamide 66. Courtesy of Bayer AG, Germany.
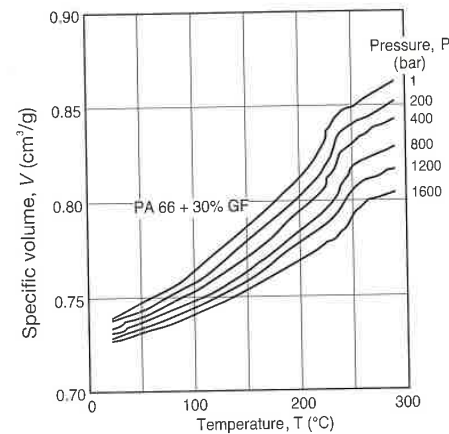
**Figure 4.18**    p-v-T diagram for a polyamide 66 filled with 30% glass fiber. Courtesy of Bayer AG, Germany.

For amorphous polymers, Eq. 4.12 is valid only for the linear segments (i.e., below or above $T_g$), and for semi-crystalline polymers it is only valid for temperatures above $T_m$.

The density of polymers filled with inorganic materials can be computed at any temperature using the following rule of mixtures

$$\rho_c(T) = \frac{\rho_m(T)\rho_f}{\psi\rho_m(T) + (1-\psi)\rho_f} \tag{4.13}$$

where $\rho_c$, $\rho_m$ and $\rho_f$ are the densities of the composite, polymer and filler, respectively, and $\psi$ the weight fraction of filler.

### 4.1.4 Thermal Diffusivity

Thermal diffusivity, defined in Eq. 4.4, is the material property that governs the process of thermal diffusion over time. The thermal diffusivity in amorphous thermoplastics decreases with temperature. A small jump is observed around the glass transition temperature due to the decrease in heat capacity at $T_g$. Figure 4.19 [2] presents the thermal diffusivity for selected amorphous thermoplastics.
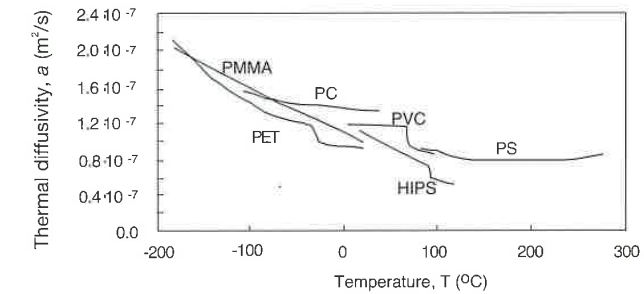
**Figure 4.19**    Thermal diffusivity as a function of temperature for various amorphous thermoplastics.

A decrease in thermal diffusivity, with increasing temperature, is also observed in semi-crystalline thermoplastics. These materials show a minimum at the melting temperature as demonstrated in Fig. 4.20 [2] for a selected number of semi-crystalline thermoplastics. It has also been observed that the thermal diffusivity increases with increasing degree of crystallinity and that it depends on the rate of crystalline growth, hence, on the cooling speed.
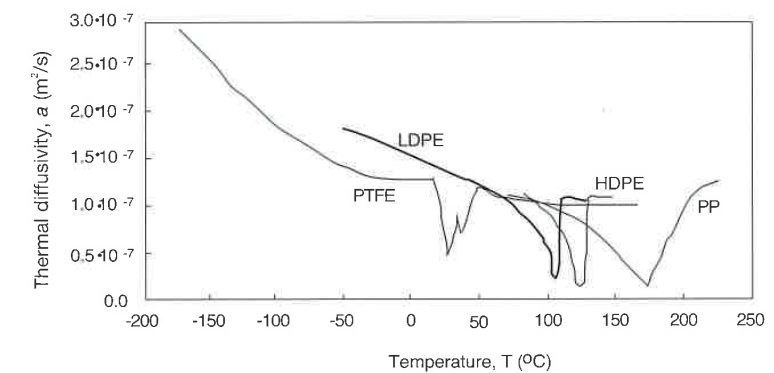


**Figure 4.20**    Thermal diffusivity as a function of temperature for various semi-crystalline thermoplastics.

### 4.1.5 Linear Coefficient of Thermal Expansion

The linear coefficient of thermal expansion is related to volume changes that occur in a polymer due to temperature variations and is well represented in the

p-v-T diagram. For many materials, thermal expansion is related to the melting temperature of that material, clearly demonstrated for some important polymers in Fig. 4.21. Although the linear coefficient of thermal expansion varies with temperature, it can be considered constant within typical design and processing conditions. It is especially high for polyolefins where it ranges from $1.5 \times 10^{-4}$/K to $2 \times 10^{-4}$/K, however fibers and other fillers significantly reduce thermal expansion. A rule of mixtures is sufficient to calculate the thermal expansion coefficient of polymers that are filled with powdery and small particles as well as with short fibers. For this case the rule of mixtures is written as

$$\alpha_c = \alpha_p (1 - \phi_f) + \alpha_f \phi_f \tag{4.14}$$

where $\phi_f$ is the volume fraction of the filler, and $\alpha_c$, $\alpha_p$ and $\alpha_f$ are coefficients for the composite, the polymer and the filler, respectively. In case of continuous fiber reinforcement, the rule of mixtures presented in Eq. 4.14 applies for the coefficient perpendicular to the reinforcing fibers. In the fiber direction, however, the thermal expansion of the fibers determines the linear coefficient of thermal expansion of the composite. Extensive calculations are necessary to determine coefficients in layered laminated composites.
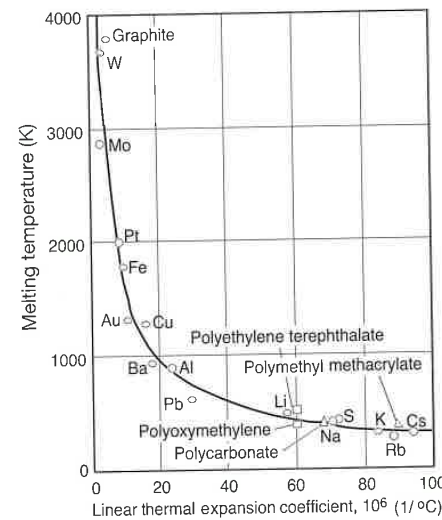


**Figure 4.21**    Relation between thermal expansion of some metals and plastics at 2 °C and their melting temperature.

### 4.1.6 Thermal Penetration

In addition to thermal diffusivity, the thermal penetration number is of considerable practical interest. It is given by

$$b = \sqrt{k\, C_p\, \rho} \tag{4.15}$$

If the thermal penetration number is known, the contact temperature $T_C$ which results when two bodies A and B, which are at different temperatures, touch can easily be computed using

$$T_C = \frac{b_A T_A + b_B T_B}{b_A + b_B} \tag{4.16}$$

where $T_A$ and $T_B$ are the temperatures of the touching bodies and $b_A$ and $b_B$ are the thermal penetrations for both materials. The contact temperature is very important for many objects in daily use (e.g., from the handles of heated objects or drinking cups made of plastic, to the heat insulation of space crafts). It is also very important for the calculation of temperatures in tools and molds during polymer processing. The constants used to compute temperature dependent thermal penetration numbers for common thermoplastics are given in Table 4.3 [12].

**Table 4.3** Thermal Penetration of Some Plastics

| Plastic | Coefficients to calculate the thermal penetration $b = a_b T + b_b$ (W/s$^{1/2}$/m$^2$K) | |
|---------|:---:|:---:|
| | $a_b$ | $b_b$ |
| HDPE | 1.41 | 441.7 |
| LDPE | 0.0836 | 615.1 |
| PMMA | 0.891 | 286.4 |
| POM | 0.674 | 699.6 |
| PP | 0.846 | 366.8 |
| PS | 0.909 | 188.9 |
| PVC | 0.649 | 257.8 |

### 4.1.7 Glass Transition Temperature

The glass transition temperature, $T_g$, is closely related to the secondary forces. Typical values for the glass transition temperature of common thermoplastics

are listed in   Chapter 2. If a polymer is mixed with a solvent, the glass transition temperature can be lowered and we can compute it with the following rule of mixtures[4]

$$T_{gM} = \frac{\phi_p \alpha_{tp} T_{gp} - (1 - \phi_p) T_{gs}}{\alpha_{tp} \phi_p + (1 - \phi_p) \alpha_{ts}} \qquad (4.17)$$

where $\alpha_{tp}$ and $\alpha_{ts}$ are the linear coefficients of thermal expansion for the polymer and the solvent, respectively; $T_{gM}$, $T_{gp}$ and $T_{gs}$ are the glass transition temperatures of the mixture, polymer and solvent, respectively; and $\phi_p$ is the volume fraction of polymer in the mixture. Stabilizers, plasticizers, and similar auxiliary processing agents work the same way. Usually, the rule of thumb applies that 1% by volume of plasticizer reduces the glass transition temperature by 2 K .

When mixing two incompatible polymers, two glass transition temperatures result, which are visible when measuring the elastic or loss modulus of the polymer blend.

### 4.1.8  Melting Temperature

The melting temperature, $T_m$ is the highest temperature at which crystalline structures can exist. Above this temperature the polymer can be considered a viscous or viscoelastic liquid, depending on the molecular weight . of the polymer and the time scale associated with its deformation. An interesting observation made is the relation between the melting and the glass transition temperatures. This relation can be written as

$$\frac{T_g}{T_m} \approx \frac{2}{3} \qquad (4.18)$$

where the temperatures are expressed in degrees Kelvin.

## 4.2    Measuring Thermal Data

Thanks to modern analytical instruments it is possible to measure thermal data with a high degree of accuracy. These data allow a good insight into chemical and manufacturing processes. Accurate thermal data or properties are necessary for everyday calculations and computer simulations of thermal processes. Such

---

4    This rule of mixtures only applies for compatible or miscible materials.

analyses are used to design polymer processing installations and to determine and optimize processing conditions.

In the last twenty years several physical thermal measuring devices have been developed to determine thermal data used to analyze processing and polymer component behavior.

### 4.2.1  Differential Thermal Analysis (DTA)

The differential thermal analysis test serves to examine transitions and reactions which occur on the order between seconds and minutes, and involve a measurable energy differential of less than 0.04 J/g. Usually the measuring is done dynamically (i.e., with linear temperature variations in time). However, in some cases isothermal measurements are also done. The DTA is mainly used to determine the transition temperatures. The principle is shown schematically in Fig. 4.22. Here, the sample, S, and an inert substance, I, are placed in an oven that has the ability to raise its temperature linearly. Two thermocouples that monitor the samples are connected opposite to one another such that no voltage is measured as long as S and I are at the same temperature:

$$\Delta T = T_S - T_I = 0 \qquad (4.19)$$

However, if a transition or a reaction occurs in the sample at a temperature, $T_c$, then heat is consumed or released, in which case $\Delta T \neq 0$. This thermal disturbance in time can be recorded and used to interpret possible information about the reaction temperature, $T_c$, the heat of transition or reaction, $\Delta H$, or simply about the existence of a transition or reaction.
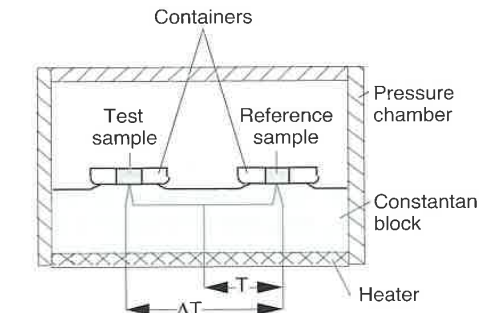


**Figure 4.22**    Schematic of a differential thermal analysis test.

Figure 4.23 presents the temperature history in a sample with an endothermic melting point (i.e., such as the one that occurs during melting of semi-crystalline polymers). The figure also shows the functions $\Delta T(T_I)$ and $\Delta T(T_S)$ which result from such a test. A comparison between Figs. 4.23 (b) and (c) demonstrates that it is very important to record the sample temperature, $T_S$, to determine a transition temperature such as the melting or glass transition temperature.
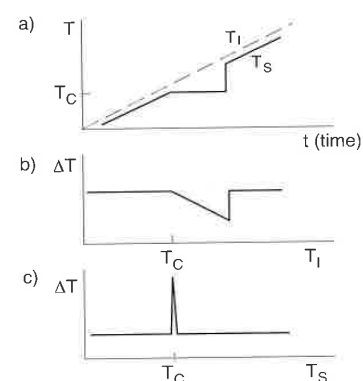


**Figure 4.23**    Temperature and temperature differences measured during melting of a semi-crystalline polymer sample.

### 4.2.2 Differential Scanning Calorimeter (DSC)

The differential scanning calorimeter permits us to determine thermal transitions of polymers in a range of temperatures between -180 and +600 °C. Unlike the DTA cell in the DSC device, thermocouples are not placed directly inside the sample or the reference substance. Instead, they are embedded in the specimen holder or stage on which the sample and reference pans are placed; the thermocouples make contact with the containers from the outside. A schematic diagram of a differential scanning calorimeter is very similar to the one shown in Fig. 4.22. Materials that do not show or undergo transition or react in the measuring range (e.g., air, glass powder, etc.) are placed inside the reference container. For standardization one generally uses mercury, tin, or zinc, whose properties are exactly known. In contrast to the DTA test, where samples larger than 10 g are needed, the DSC test requires samples that are in the mg range (< 10 mg). Although DSC tests are less sensitive than the DTA tests, they are the most widely used tests for thermal analysis. In fact, DTA tests are rarely used in the polymer industry.

Figure 4.24 [4] shows a typical DSC curve measured using a partly crystalline polymer sample. In the figure, the area which is enclosed between the trend line (bold) and the base line is a direct measurement for the amount of heat, $\Delta H$, needed for transition. In this case, the transition is melting and the area corresponds to the *heat of fusion*.

The degree of crystallinity, $x$, is determined from the ratio of the heat of fusion of a polymer sample, $\Delta H_{SC}$, and the enthalpy of fusion of a 100% crystalline sample $\Delta H_C$.

$$\chi = \frac{\Delta H_{SC}}{\Delta H_C} \tag{4.20}$$

In a DSC analysis of a semi-crystalline polymer, a jump in the specific heat curve, as shown in Fig. 4.24, becomes visible; a phenomenon which can easily be traced with a DSC. The glass transition temperature, $T_g$, is determined at the inflection point of the specific heat curve. The release of residual stresses as a material's temperature is raised above the glass transition temperature is often observed in a DSC analysis.

Specific heat, $C_p$, is one of the many material properties that can be measured with the DSC. During a DSC temperature sweep, the sample pan and the reference pan are maintained at the same temperature. This allows the measurement of the differential energy required to maintain identical temperatures. The sample with the higher heat capacity will absorb a larger amount of heat, which is proportional to the difference between the heat capacity of the measuring sample and the reference sample.

It is also possible to determine the purity of a polymer sample when additional peaks or curve shifts are detected in a DSC measurement.

Thermal degradation is generally accompanied by an exothermic reaction which may result from oxidation. Such a reaction can easily be detected in a DSC output. By further warming of the test sample, cross-linking may take place and, finally, chain breakage, as shown in Fig. 4.24.

An important aspect in DSC data interpretation is the finite heat flow resistance between the sample pan and the furnace surface. Recent studies by Janeschitz-Kriegl, Eder and co-workers [13, 14] have demonstrated that the heat transfer coefficient between the sample pan and furnace is of finite value, and cannot be disregarded while interpreting the data. In fact, with materials that have a low thermal conductivity, such as polymers, the finite heat transfer coefficient will significantly influence the temperature profiles of the samples.
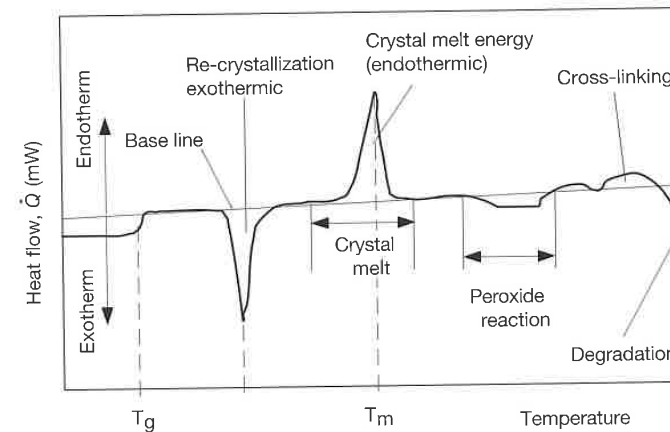
**Figure 4.24**    Typical DSC heat flow for a semi-crystalline polymer.

### 4.2.3 Thermomechanical Analysis (TMA)

The thermomechanical analysis (TMA) measures shape stability of a material at elevated temperatures by physically penetrating it with a metal rod. A schematic diagram of TMA equipment is shown in Fig. 4.25. In TMA, the test specimen's temperature is raised at a constant rate, the sample is placed inside the measuring device, and a rod with a specified weight is placed on top of it. To allow for measurements at low temperatures, the sample, oven, and rod can be cooled with liquid nitrogen. The TMA also allows one to measure the Vicat temperature described in Chapter 8.

Most instruments are so precise that they can be used to measure the melting temperature of the material and, by using linear dilatometry, to measure the thermal expansion coefficients. The thermal expansion coefficient can be measured using

$$\alpha_l = \frac{1}{L_0}\frac{\Delta L}{\Delta T} \tag{4.21}$$

where $L_0$ is the initial dimension of the test specimen, $\Delta L$ the change in size and $\Delta T$ the temperature difference. For isotropic materials a common relation between the linear and the volumetric thermal expansion coefficient can be used:

$$\gamma = 3\alpha_l \tag{4.22}$$
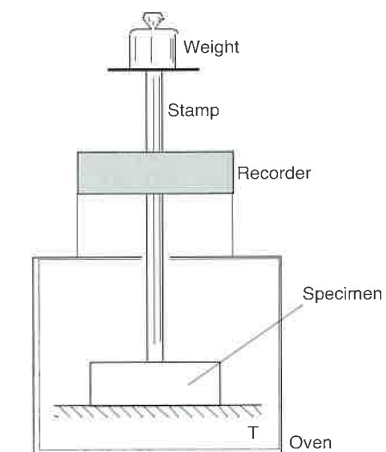


**Figure 4.25**    Schematic diagram of the thermomechanical analysis (TMA) device.

### 4.2.4 Thermogravimetry (TGA)

A thermogravimetric analyzer can measure weight changes of less than 10 μg as a function of temperature and time. This measurement technique, typically used for thermal stability, works on the principle of a beam balance. The testing chamber can be heated (up to approximate 1200 °C) and rinsed with gases (inert or reactive). Measurements are performed on isothermal reactions or at temperatures sweeps of less than 100 K/min. The maximum sample weight used in thermogravimetric analyses is 500 mg. Thermogravimetry is often used to identify the components in a blend or a compound based on the thermal stability of each component. Figure 4.26[5] shows results from a TGA analysis on a PVC fabric. The figure clearly shows the transitions at which the various components of the compound decompose. The percent of the original sample weight is recorded along with the change of the weight with respect to temperature. Five transitions representing (1) the decomposition of volatile components, (2) decomposition of the DOP plasticizer, (3) formation of HCl, (4) carbon-carbon scission, and (5) the forming of $CO_2$, are clearly visible.

---

[5]    Courtesy of the ICIPC, Medellín, Colombia.

**Figure 4.26**  TGA analysis on a PVC fabric. (1) volatiles: humidity, monomers, solvents etc., (2) DOP plasticizer, (3) HCl formation, (4) carbon-carbon scission, and (5) $CO_2$ formation.
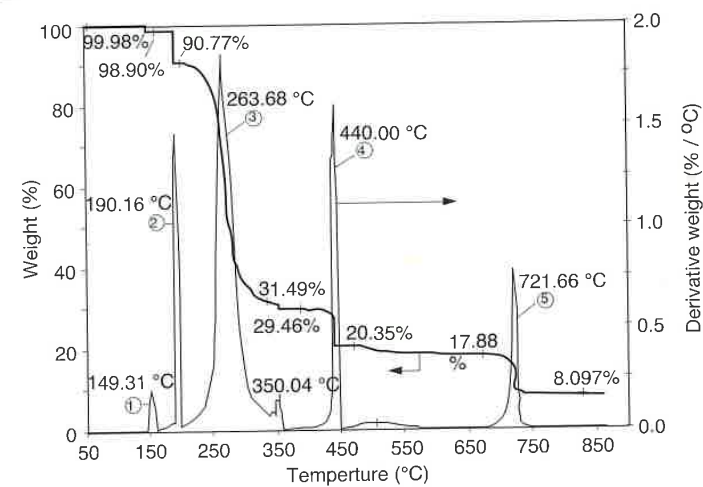
### 4.2.5  Density Measurements

One simple form of calculating the density of a polymer sample is to first weigh the sample immersed in water. Assuming the density of water to be 1.0 g/cm³ we can use the relation

$$\rho = \frac{m}{(m - m_i)\left(1 \, cm^3 / g\right)} \tag{4.23}$$

where $m$ is mass of the specimen, $m_i$ is the mass of the immersed specimen and $(m - m_i)$ is the mass of the displaced body of water.

Some common ways of determining density of polymeric materials are described by the ASTM D792, ISO 1183, and DIN 53 479 test methods. Another common way of measuring density is the "through flow density meter." Here, the density of water is changed to that of the polymer by adding ethanol until the plastic shavings are suspended in the solution. The density of the solution is then measured in a device which pumps the liquid through a U-pipe, where it is measured using ultrasound techniques. A density gradient technique is described by the standard ASTM D1505 test method.

### Examples

4.1  A differential scanning calorimetry (DSC) test was performed on a 25 mg polyethylene terephthalate (PET) sample taken from the screw-top of a soda bottle. The test was performed using a heating rate of 5K/minute (5K rise every minute). The DSC output is presented in Fig. 4.27.
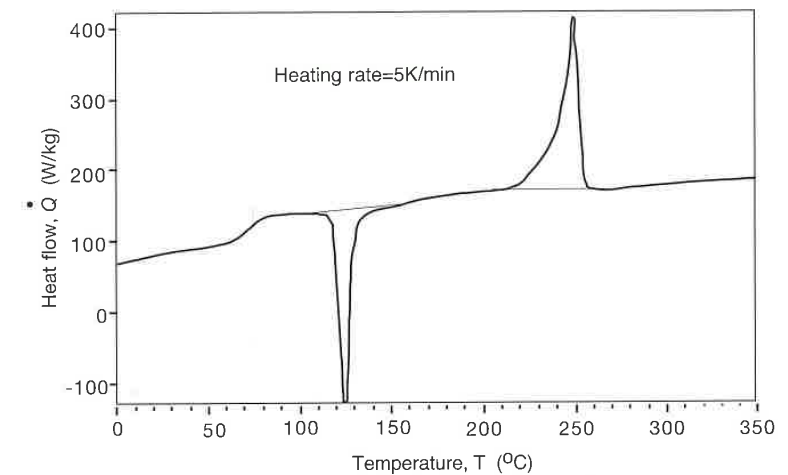


**Figure 4.27**    DSC scan of a PET bottle screw-top sample

From the curve estimate the glass transition temperature, $T_g$, the melting temperature, $T_m$, the crystallization temperature, $T_c$ and the heat of fusion, $\lambda$, for this specific PET sample during the temperature ramp-up.

If the heat of fusion for a hypothetically 100% crystalline PET sample is 137 kJ/kg [15], what was the degree of crystallinity in the PET bottle screw-top?

From the curve presented in Fig. 4.27 we can deduce that the glass transition temperature is around 72 °C, the crystallization temperature at 125 °C and the melting temperature at 250 °C. Note that in all three cases there is range of temperatures at which the transition occurs. To compute the heat of fusion during the ramp-up we need to find the area between $\dot{Q}$ and the base-line for the endothermic deviation around the melting point, between 210 and 260 °C. To do this we must first transform the temperature scale to time by dividing it by the heating rate as

$$t = \frac{T}{5\text{K/min}} \frac{60\,s}{1\,\text{min}}$$

Hence, 50 °C becomes 600 s, 100 °C becomes 1200 s, etc. The integral equals 37.8 kJ/kg, which represents the heat of fusion of the sample during the temperature ramp-up. However, one must consider that this melting energy includes the extra crystallization that occurs between 108 and 155 °C. The exothermic energy is computed by integrating the curve between those two temperatures in a transformed time scale. The integral equals 22.9 kJ/kg. We can also find the area under the curve by transforming the heat flow, $\dot{Q}$, to heat capacity, $C_p$, and integrating using the temperature scale instead of a time scale. Heat capacity can be computed using

$$C_p = \frac{\dot{Q}}{5\text{K/min}} \frac{60\,s}{\text{min}}$$

The degree of crystallinity of the initial PET bottle screw-top can now easily be computed using

$$\chi = \frac{37.8\,\text{kJ/kg} - 22.9\,\text{kJ/kg}}{137\,\text{kJ/kg}} = 0.109 \quad \text{or} \quad 10.9\%$$

## Problems

4.1  Does the coefficient of linear expansion of a polymer increase or decrease upon the addition of glass fibers?

4.2  Plot $T_g$ versus $T_m$ for several polymers. What trend or relation do you observe?

4.3  In a soda bottle, how does the degree of crystallinity in the screw-top region compare to the degree of crystallinity in the wall? Explain.

4.4  A 5K/min heating and 5K/min cooling differential scanning calorimetry (DSC) test (Fig. 4.28) was performed on a 10.8 mg sample of PE-LD. What is the specific heat of the PE-LD just after melting during heating and just before crystallization during cooling. What is the degree of crystallinity of the initial and the final samples.
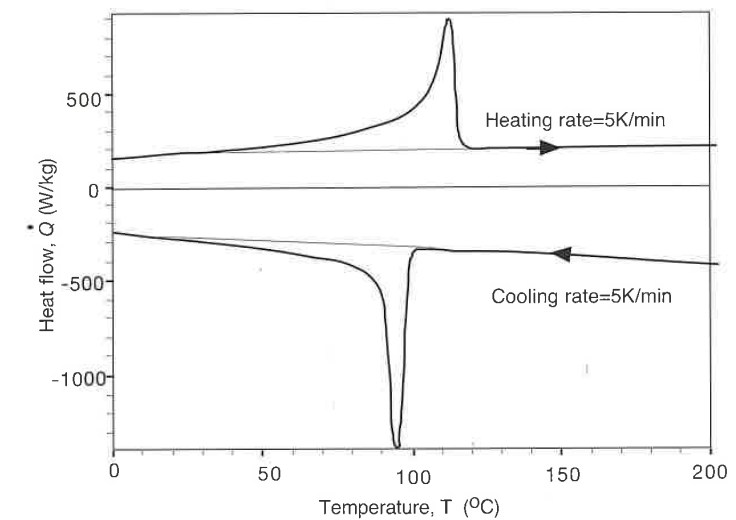
**Figure 4.28**   Heating and cooling DSC scans of a PE-LD sample

4.5  A differential scanning calorimetry (DSC) test was performed on an 11.4 mg polyethylene terephthalate (PET) sample using the standard ASTM D 3417 test method. The ASTM test calls for a temperature heating rate of 20 °C/minute (20 °C rise every minute). The DSC output is presented below[6].

From the curve in Fig. 4.29 estimate the glass transition temperature, $T_g$, the melting temperature, $T_m$, the crystallization temperature, $T_c$ and the heat of fusion, $\lambda$, for this specific PET sample during the temperature ramp-up. Note that the heat flow scale has already been transformed to heat capacity. How do $T_g$ and $T_m$ compare to the "book values" ?

If the heat of fusion for a hypothetically 100% crystalline PET is 137 kJ/kg, what was the degree of crystallinity of the original PET sample.

On the same graph below sketch a hypothetical DSC output for the original PET sample with a temperature heating rate that is too fast to allow any additional crystallization during heating.

6   Courtesy of ICIPC, Medellín, Colombia.

**Figure 4.29**  DSC scan of a PET sample.



**Figure 4.30**  Isothermal DSC measurements of UPE samples.
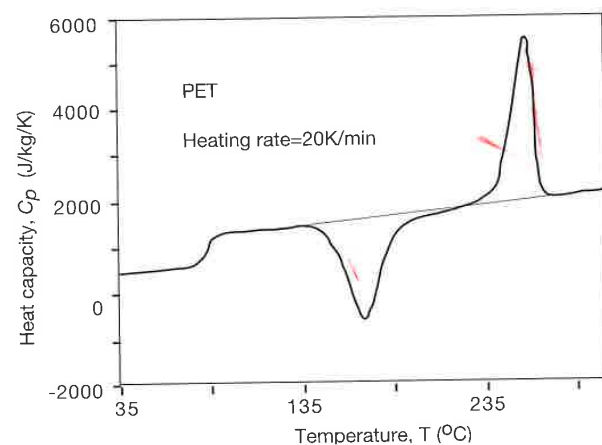
4.6  A typical injection pack/hold pressure during injection molding of polyamide 66 components is 1000 bar and the injection temperature is 280 °C. The gate freezes shut when the average temperature inside the mold reaches 225 °C.

Draw the process on the pvT diagram given in Fig. 4.17.

What volume shrinkage should be taken into account when designing the mold? Note that the shrinkage is mostly taken up by a thickness reduction.

4.7  Isothermal differential scanning calorimetry (DSC) tests were performed on three unsaturated polyester (UPE) samples at three different temperatures (100 °C, 110 °C, and 120 °C). The output for the three DSC tests are presented in the figure below[7]. On the graph, label which curve is associated with which test temperature. From the curves in Fig. 4.30 estimate the total heat of reaction, $Q_T$.

4.8  A differential scanning calorimetry (DSC) test (Fig. 4.31) was performed on an 18.3 mg sample of polystyrene. What is the glass transition temperature of the sample. Determine the specific heat of this PS just before the glass transition temperature has been reached. What is $C_p$ just after $T_g$? Why is the heat larger as the temperature increases?
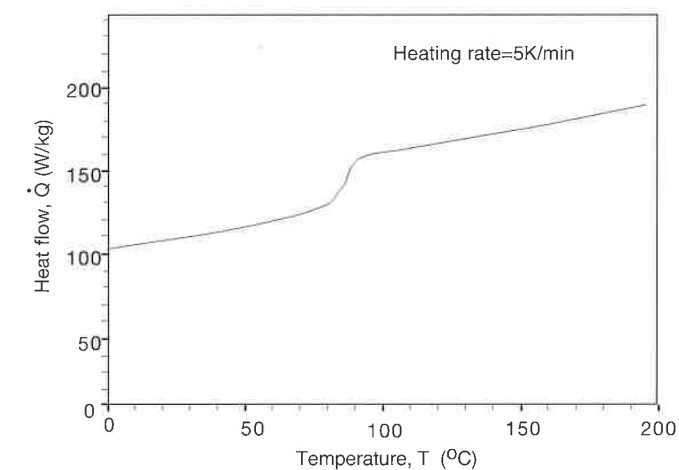


**Figure 4.31**  DSC scan of a PS sample.

---

7  Courtesy of GenCorp Research, Akron, OH.

4.9  Sketch the pvT diagrams for a semi-crystalline polymer with a high and a low cooling rate.

### References

1.  Crawford, R.J., *Plastics Engineering*, 2nd Ed., Pergamon Press, Oxford, (1987).
2.  Godovsky, Y.K., *Thermophysical Properties of Polymers*, Springer-Verlag, Berlin, (1992)
3.  Mathot, V.B.F., *Calorimetry and Thermal Analysis of Polymers*, Hanser Publishers, Munich, (1994).
4.  van Krevelen, D.W., and Hoftyzer, P.J., *Properties of Polymers*, 2nd. Ed., Elsevier, Amsterdam, (1976).
5.  Knappe, W., *Kunststoffe, 66*, 5, 297, (1976).
6.  Dietz, W., *Kunststoffe, 66*, 3, 161, (1976)
7.  Knappe, W., *Adv. Polym. Sci., 7*, 477, (1971).
8.  Fischer, F., *Gummi-Asbest-Kunststoffe*, 32, 12, 922, (1979).
9.  Maxwell, J.C., *Electricity and Magnetism*, Clarendon Press, Oxford, (1873).
10. Meredith, R.E., and Tobias, C.W., *J. Appl. Phys. ,31*, 1270, (1960).
11. Araujo, F.F.T., and Rosenberg, H.M., *J. Phys. D:Appl. Phys.*, 9, 665, (1976).
12. Catic, I., Ph.D. Thesis, IKV, RWTH-Aachen, Germany, (1972).
13. Janeschitz-Kriegl, H., Wippel, H., Paulik, Ch., and Eder, G., *Colloid Polym. Sci.*, 271, 1107, (1993).
14. Wu, C.H., Eder, G., and Janeschitz-Kriegl, H.,*Colloid Polym. Sci.*, 271, 1116, (1993).
15. Tadmor, Z., and Gogos, C.G., *Principles of Polymer Processing*, John Wiley & Sons, New York, (1979).

# Rheology of Polymer Melts

## 5.1  Introduction

Rheology is the field of science that studies fluid behavior during flow-induced deformation. From the variety of materials that rheologists study, polymers have been found to be the most interesting and complex. Polymer melts are shear thinning, viscoelastic, and their flow properties are temperature dependent. Viscosity is the most widely used material parameter when determining the behavior of polymers during processing. Since the majority of polymer processes are shear rate dominated, the viscosity of the melt is commonly measured using shear deformation measurement devices. However, there are polymer processes, such as blow molding, thermoforming, and fiber spinning, which are dominated by either elongational deformation or by a combination of shear and elongational deformation. In addition, some polymer melts exhibit significant elastic effects during deformation. This chapter will concentrate on shear deformation models but, for completeness, elongational flows, concentrated suspensions, and viscoelastic fluids will also be covered. Modeling and simulation of polymer flows will be briefly discussed. For further reading on rheology of polymer melts, the reader should consult the literature [1–6]. For more detail on polymer flow and processing simulation the literature [7, 8] should also be reviewed.

### 5.1.1  Continuum Mechanics

When analyzing the flow or deformation of polymers during processing, a balance of energy, mass and forces must be preserved.

Using the notation found in Fig. 5.1 and performing a mass balance on the differential element, for an incompressible liquid[1] one can write

---

1  It is clear that a polymer melt is not incompressible. However, assuming incompressibility simplifies the analysis significantly without losing accuracy in flow predictions.

$$\nabla \cdot \underline{v} = 0 \tag{5.1}$$

where Eq. 5.1 represents the divergence of the velocity vector and is presented in Appendix A in expanded form for various coordinate systems.

Using a similar differential element that is moving with the fluid, as shown in Fig. 5.2, a force balance results in

$$\rho \frac{D\underline{v}}{Dt} = \left[ \nabla \cdot \underline{\sigma} \right] + \rho \underline{g} \tag{5.2}$$
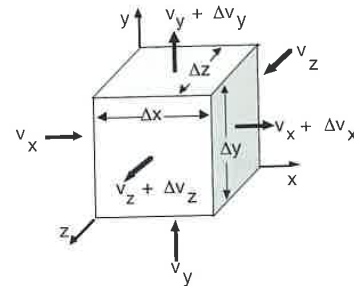


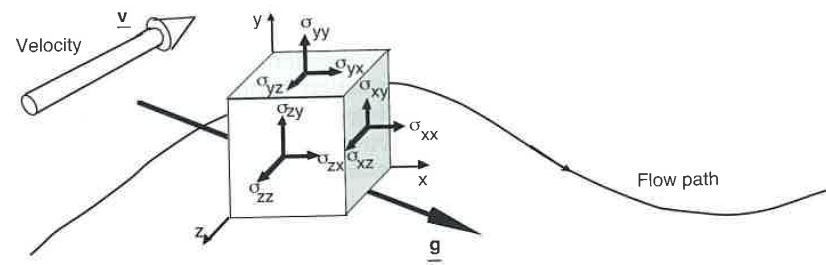**Figure 5.1**    Differential element used for mass balance.



**Figure 5.2**    Differential element used for force balance.

where the term on the left side represents the inertia of the polymer melt, the first term on the right is the divergence of the stress tensor and represents viscous and elastic forces, and the second term on the right represents the gravitational effects. The operator $D/Dt$ is the *substantial* or *material derivative* defined by

$$\frac{D}{Dt} = \frac{\partial}{\partial t} + \underline{v} \cdot \nabla \tag{5.3}$$

which represents a convective or embedded frame of reference that moves with a material particle.

The stress, $\underline{\sigma}$, sometimes referred to as the *total stress*, can be split into *hydrostatic pressure*, $\underline{\sigma}_H$, and *deviatoric stress*, $\underline{\tau}$. The hydrostatic pressure is a stress vector that acts only in the normal direction to the surfaces and can be represented by $-p\underline{\delta}$, where p is the pressure and $\underline{\delta}$ is a unit tensor. The momentum balance can now be written as

$$\rho \frac{D\underline{v}}{Dt} = -\nabla p + \left[ \nabla \cdot \underline{\tau} \right] + \rho g \tag{5.4}$$

The full form of Eq. 5.4 is presented in Table VI of the appendix.

### 5.1.2 The Generalized Newtonian Fluid

The viscosity of most polymer melts is *shear thinning* and temperature dependent. The shear thinning effect is the reduction in viscosity at high rates of deformation. This phenomenon occurs because at high rates of deformation the molecules are stretched out, enabling them to slide past each other with more ease, hence, lowering the bulk viscosity of the melt. Figure 5.3 clearly shows the shear thinning behavior and temperature dependance of the viscosity a specific general purpose polystyrene. To take into consideration these *non-Newtonian effects*, it is common to use a viscosity which is a function of the strain rate and temperature to calculate the stress tensor[2] in Eq. 5.4:

$$\underline{\tau} = \eta(\dot{\gamma}, T)\dot{\underline{\gamma}} \tag{5.5}$$

where $\eta$ is the viscosity and $\dot{\underline{\gamma}}$ the *strain rate* or *rate of deformation tensor* defined by

$$\dot{\underline{\gamma}} = \nabla \underline{v} + \nabla \underline{v}^t \tag{5.6}$$

where $\nabla \underline{v}$ represents the velocity gradient tensor. This model describes the *Generalized Newtonian Fluid*. In Eq. 5.5, $\dot{\gamma}$ is the magnitude of the strain rate tensor and can be written as

$$\dot{\gamma} = \sqrt{\frac{1}{2}II} \tag{5.7}$$

where $II$ is the second invariant of the strain rate tensor defined by

$$II = \sum_i \sum_j \dot{\gamma}_{ij}\dot{\gamma}_{ji} \tag{5.8}$$

---

2    As will be shown later, this is only true when the elastic effects are negligible during deformation of the polymeric material.

The strain rate tensor components in Eq. 5.8 are defined by

$$\dot{\gamma}_{ij} = \frac{\partial v_i}{\partial x_j} + \frac{\partial v_j}{\partial x_i} \tag{5.9}$$

The temperature dependence of the polymer's viscosity is normally factored out as

$$\eta(T, \dot{\gamma}) = f(T)\eta(\dot{\gamma}) \tag{5.10}$$

where for small variations in temperature $f(T)$ can be approximated using an exponential function such as

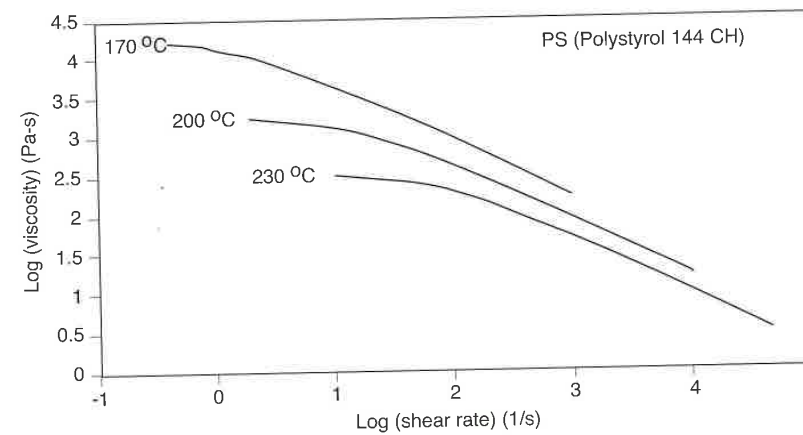$$f(T) = \exp\left(-a(T - T_0)\right). \tag{5.11}$$

**Figure 5.3**    Viscosity curves for a polystyrene.

However, as mentioned in Chapter 2, a variation in temperature corresponds to a shift in the time scale. A shift commonly used for semi-crystalline polymers is the Arrhenius shift, which is written as

$$a_T(T) = \frac{\eta_0(T)}{\eta_0(T_0)} = \exp\left(\frac{E_0}{R}\left(\frac{1}{T} - \frac{1}{T_0}\right)\right) \tag{5.12}$$

where $E_0$ is the activation energy, $T_0$ a reference temperature, and $R$ the gas constant. Using this shift, one can translate viscosity curves measured at different temperatures to generate a master curve at a specific temperature. Figure 5.4 [9] presents the viscosity of a low density polyethylene with

measured values shifted to a reference temperature of 150 °C. For the shift in Fig. 5.4, an activation energy $E_0 = 54$ kJ/mol was used.
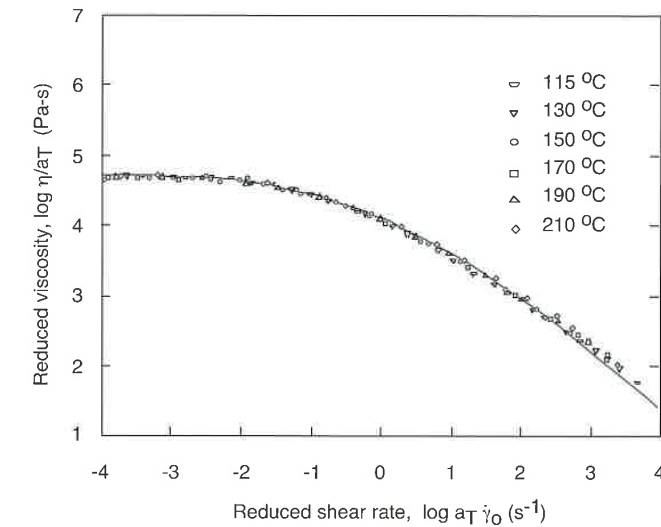
**Figure 5.4**    Reduced viscosity curve for a low density polyethylene at a reference temperature of 150 °C.

Several models that are used to represent the strain rate dependence of polymer melts are presented later in this chapter.

### 5.1.3  Normal Stresses in Shear Flow

The tendency of polymer molecules to "curl-up" while they are being stretched in shear flow results in normal stresses in the fluid. For example, shear flows exhibit a deviatoric stress defined by

$$\tau_{xy} = \eta(\dot{\gamma})\dot{\gamma}_{xy} \tag{5.13}$$

Measurable normal stress differences, $N_1 = \tau_{xx} - \tau_{yy}$ and $N_2 = \tau_{yy} - \tau_{zz}$ are referred to as the *first* and *second normal stress differences*. The first and second normal stress differences are material dependent and are defined by

$$N_1 = \tau_{xx} - \tau_{yy} = -\psi_1(\dot{\gamma}, T)\dot{\gamma}_{xy}^2 \tag{5.14}$$

$$N_2 = \tau_{yy} - \tau_{zz} = -\psi_2(\dot{\gamma},T)\dot{\gamma}_{xy}^2 \qquad (5.15)$$

The material functions, $\psi_1$ and $\psi_2$, are called the primary and secondary normal stress coefficients, and are also functions of the magnitude of the strain rate tensor and temperature. The first and second normal stress differences do not change in sign when the direction of the strain rate changes. This is reflected in Eqs. 5.14 and 5.15. Figure 5.5 [9] presents the first normal stress difference coefficient for the low density polyethylene melt of Fig. 5.4 at a reference temperature of 150 °C. The second normal stress difference is difficult to measure and is often approximated by

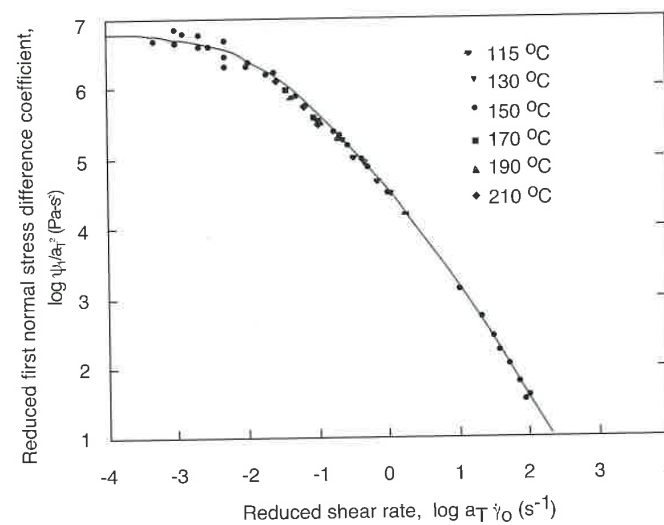$$\psi_2(\dot{\gamma}) \approx -0.1\psi_1(\dot{\gamma}) \qquad (5.16)$$



**Figure 5.5**    Reduced first normal stress difference coefficient for a low density polyethylene melt at a reference temperature of 150 °C.

### 5.1.4  Deborah Number

A useful parameter often used to estimate the elastic effects during flow is the Deborah number[3], De. The Deborah number is defined by

3    From the Song of Deborah, Judges 5:5–"The mountains flowed before the Lord." M. Reiner is credited for naming the Deborah number; *Physics Today*, (January 1964).

$$De = \frac{\lambda}{t_p} \qquad (5.17)$$

where $\lambda$ is the relaxation time of the polymer and $t_p$ is a characteristic process time. The characteristic process time can be defined by the ratio of characteristic die dimension and average speed through the die. A Deborah number of zero represents a viscous fluid and a Deborah number of $\infty$ an elastic solid. As the Deborah number becomes > 1, the polymer does not have enough time to relax during the process, resulting in possible extrudate dimension deviations or irregularities such as *extrudate swell* [4], *shark skin*, or even *melt fracture*.

Although many factors affect the amount of extrudate swell, fluid "memory" and normal stress effects are the most significant ones. However, abrupt changes in boundary conditions, such as the separation point of the extrudate from the die, also play a role in the swelling or cross section reduction of the extrudate. In practice, the fluid memory contribution to die swell can be mitigated by lengthening the land length of the die. This is schematically depicted in Fig. 5.6. A long die land separates the polymer from the manifold for enough time to allow it to "forget" its past shape.
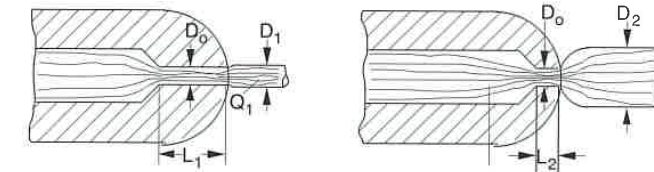


**Figure 5.6**    Schematic diagram of extrudate swell during extrusion.

Waves in the extrudate may also appear as a result of high speeds during extrusion, where the polymer is not allowed to relax. This phenomenon is generally referred to as *shark skin* and is shown for a high density polyethylene in Fig. 5.7a [10]. It is possible to extrude at such high speeds that an intermittent separation of melt and inner die walls occurs as shown in Fig. 5.7b. This phenomenon is often referred to as the *stick-slip effect* or *spurt flow* and is attributed to high shear stresses between the polymer and the die wall. This phenomena occurs when the shear stress is near the critical value of 0.1 MPa [11–13]. If the speed is further increased, a helical geometry is extruded as

4    It should be pointed out that Newtonian fluids, which do not experience elastic or normal stress effects, also show some extrudate swell or reduction. A Newtonian fluid that is being extruded at high shear rates reduces its cross-section to 87% of the diameter of the die, whereas if extruded at very low shear rate it swells to 113% of the diameter of the die. This swell is due to inertia effects caused by the change from the parabolic velocity distribution inside the die to the flat velocity distribution of the extrudate.

shown for a polypropylene extrudate in Fig. 5.7c. Eventually, the speeds are so high that a chaotic pattern develops such as the one shown in Fig. 5.7d. This well known phenomenon is called *melt fracture*. The shark skin effect is frequently absent and spurt flow seems to occur only with linear polymers.

The critical shear stress has been reported to be independent of the melt temperature but to be inversely proportional to the weight average molecular weight [14, 12]. However, Vinogradov et al. [15] presented results where the critical stress was independent of molecular weight except at low molecular weights. Dealy and co-workers [16], and Denn [17] give an extensive overview of various melt fracture phenomena which is recommended reading.

To summarize, the Deborah number and the size of the deformation imposed upon the material during processing determine how the system can most accurately be modeled. Figure 5.8 [1] helps visualize the relation between time scale, deformation and applicable model. At small Deborah numbers, the polymer can be modeled as a Newtonian fluid, and at very high Deborah numbers the material can be modeled as a Hookean solid. In between, the viscoelastic region is divided in two: the linear viscoelastic region for small deformations, and the non-linear viscoelastic region for large deformations. Linear viscoelasticity was briefly discussed in Chapter 2.
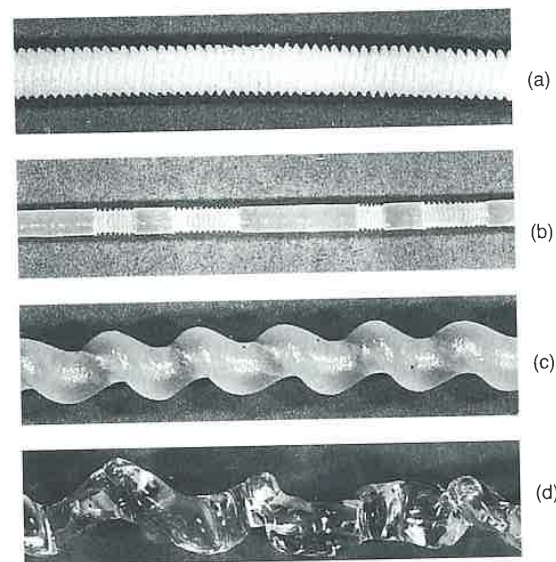


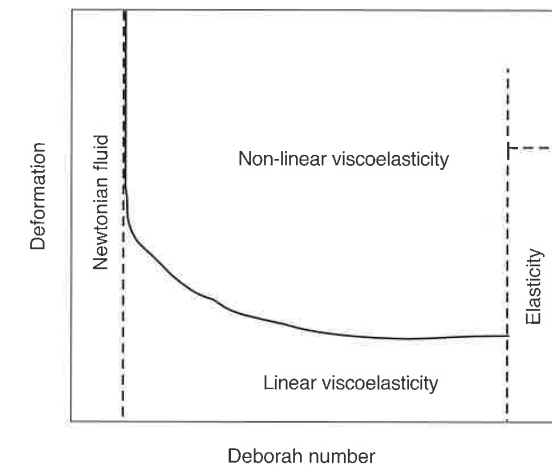**Figure 5.7**   Various shapes of extrudates under melt fracture.

**Figure 5.8**   Schematic of Newtonian, elastic, linear, and non-linear viscoelastic regimes as a function of deformation and Deborah number during deformation of polymeric materials.

## 5.2   Viscous Flow Models

Strictly speaking, the viscosity $\eta$, measured with shear deformation viscometers, should not be used to represent the elongational terms located on the diagonal of the stress and strain rate tensors. Elongational flows are briefly discussed later in this chapter. A rheologist's task is to find the models that best fit the data for the viscosity represented in Eq. 5.5. Some of the models used by polymer processors on a day-to-day basis to represent the viscosity of industrial polymers are presented in the next section.

### 5.2.1   The Power Law Model

The power law model proposed by Ostwald [18] and de Waale [19] is a simple model that accurately represents the shear thinning region in the viscosity versus strain rate curve but neglects the Newtonian plateau present at small strain rates. The power law model can be written as follows:

$$\eta = m(T)\dot{\gamma}^{n-1} \tag{5.18}$$

where $m$ is referred to as the *consistency index* and $n$ the *power law index*. The consistency index may include the temperature dependence of the viscosity such as represented in Eq. 5.11, and the power law index represents the shear thinning behavior of the polymer melt. Figure 5.9 presents normalized velocity distributions inside a tube for a fluid with various power law indices calculated using the power law model. It should be noted that the limits of this model are

$$\eta \to 0 \; as \; \dot{\gamma} \to \infty \; and$$

$$\eta \to \infty \; as \; \dot{\gamma} \to 0$$

The infinite viscosity at zero strain rates leads to an erroneous result in problems where there is a region of zero shear rate, such as at the center of a tube. This results in a predicted velocity distribution that is flatter at the center than the experimental profile. In computer simulation of polymer flows, this problem is often overcome by using a truncated model such as

$$\eta = m_0(T)\dot{\gamma}^{n-1} \quad for \quad \dot{\gamma} > \dot{\gamma}_0 \; and \tag{5.19a}$$

$$\eta = m_0(T) \quad for \quad \dot{\gamma} \le \dot{\gamma}_0 \tag{5.19b}$$

where $m_0$ represents a zero shear rate ($\dot{\gamma}_0$) viscosity. Table 5.1 presents a list of typical power law and consistency indices for common thermoplastics.
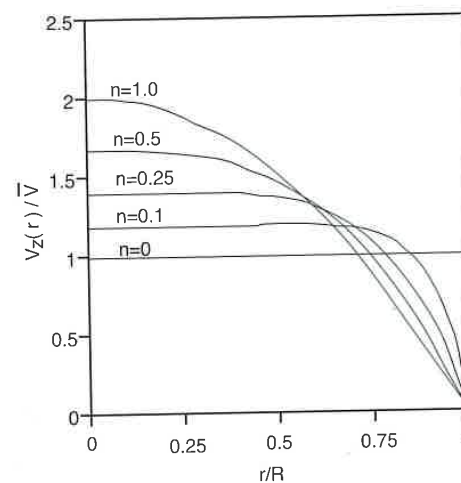
**Table 5.1**    Power Law and Consistency Indices for Common Thermoplastics

| Polymer | m(Pa-s$^n$) | n | T($^oC$) |
|---|---|---|---|
| Polystyrene | $2.80 \times 10^4$ | 0.28 | 170 |
| High density polyethylene | $2.00 \times 10^4$ | 0.41 | 180 |
| Low density polyethylene | $6.00 \times 10^3$ | 0.39 | 160 |
| Polypropylene | $7.50 \times 10^3$ | 0.38 | 200 |
| Polyamide 66 | $6.00 \times 10^2$ | 0.66 | 290 |
| Polycarbonate | $6.00 \times 10^2$ | 0.98 | 300 |
| Polyvinyl chloride | $1.70 \times 10^4$ | 0.26 | 180 |



**Figure 5.9**    Pressure flow velocity distributions inside a tube for fluids with various power law indices.

### 5.2.2  The Bird–Carreau–Yasuda Model

A model that fits the whole range of strain rates was developed by Bird and Carreau [20] and Yasuda [21] and contains five parameters:

$$\frac{\eta - \eta_0}{\eta_0 - \eta_\infty} = \left[1 + |\lambda\dot{\gamma}|^a\right]^{(n-1)/a} \tag{5.20}$$

where $\eta_0$ is the zero shear rate viscosity, $\eta_\infty$ is an infinite shear rate viscosity, $\lambda$ is a time constant and $n$ is the power law index. In the original Bird–Carreau model, the constant $a = 2$. In many cases, the infinite shear rate viscosity is negligible, reducing Eq. 5.20 to a three parameter model. Equation 5.20 was modified by Menges, Wortberg and Michaeli [22] to include a temperature dependence using a WLF relation. The modified model, which is used in commercial polymer data banks, is written as follows:

$$\eta = \frac{k_1 a_T}{\left[1 + k_2 \dot{\gamma} a_T\right]^{k_3}} \tag{5.21}$$

where the shift $a_T$ applies well for amorphous thermoplastics and is written as

$$\ln a_T = \frac{8.86(k_4 - k_5)}{101.6 + k_4 - k_5} - \frac{8.86(T - k_5)}{101.6 + T - k_5} \tag{5.22}$$

Table 5.2 presents constants for Carreau–WLF (amorphous) and Carreau–Arrhenius models (semi-crystalline) for various common thermoplastics. In addition to the temperature shift, Menges, Wortberg and Michaeli [22] measured a pressure dependence of the viscosity and proposed the following model, which includes both temperature and pressure viscosity shifts:

$$\log \eta(T,p) = \log \eta_0 + \frac{8.86\left(T^* - T_s\right)}{101.6 + T^* - T_s} - \frac{8.86\left(T^* - T_s + 0.02p\right)}{101.6 + \left(T^* - T_s + 0.02p\right)}$$    (5.23)

where $p$ is in bar, and the constant 0.02 represents a 2 °C shift per bar.

Table 5.2    Constants for Carreau-WLF (Amorphous) and Carreau-Arrhenius (Semi-Crystalline) Models for Various Common Thermoplastic

| Polymer | K1 (Pa-s) | K2 (s) | K3 | K4 (°C) | K5 (°C) | T0 (°C) | E0 (J/mol) |
|---|---|---|---|---|---|---|---|
| Polystyrene | 1777 | 0.064 | 0.73 | 200 | 123 | - | - |
| High density polyethylene | 24198 | 1.38 | 0.60 | - | - | 200 | 22272 |
| Low density polyethylene | 317 | 0.015 | 0.61 | - | - | 189 | 43694 |
| Polypropylene | 1386 | 0.091 | 0.68 | - | - | 220 | 427198 |
| Polyamide 66 | 44 | 0.00059 | 0.40 | - | - | 300 | 123058 |
| Polycarbonate | 305 | 0.00046 | 0.48 | 320 | 153 | - | - |
| Polyvinyl chloride | 1786 | 0.054 | 0.73 | 185 | 88 | - | - |

### 5.2.3  The Bingham Fluid

The Bingham fluid is an empirical model that represents the rheological behavior of materials that exhibit a "no flow" region below certain yield stresses, $\tau_Y$, such as polymer emulsions and slurries. Since the material flows like a Newtonian liquid above the yield stress, the Bingham model can be represented by

$$\eta = \infty \quad \text{or} \quad \dot{\gamma} = 0 \quad \tau \leq \tau_Y$$    (5.24a)

$$\eta = \mu_0 + \frac{\tau_y}{\dot{\gamma}} \qquad \tau \geq \tau_Y$$    (5.24b)

Here, $\tau$ is the magnitude of the deviatoric stress tensor and is computed in the same way as in Eq. 5.7.

### 5.2.4  Elongational Viscosity

In polymer processes such as fiber spinning, blow molding, thermoforming, foaming, certain extrusion die flows, and compression molding with specific processing conditions, the major mode of deformation is elongational.

To illustrate elongational flows, consider the fiber spinning process shown in Fig. 5.10.
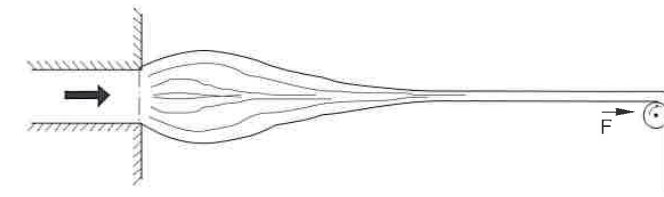


Figure 5.10    Schematic diagram of a fiber spinning process.

A simple elongational flow is developed as the filament is stretched with the following components of the rate of deformation:

$$\dot{\gamma}_{11} = -\dot{\varepsilon}$$    (5.25a)

$$\dot{\gamma}_{22} = -\dot{\varepsilon}$$    (5.25b)

$$\dot{\gamma}_{33} = +2\dot{\varepsilon}$$    (5.25c)

where $\dot{\varepsilon}$ is the elongation rate, and the off-diagonal terms of $\dot{\gamma}_{ij}$ are all zero. The diagonal terms of the total stress tensor can be written as

$$\sigma_{11} = -p - \eta\dot{\varepsilon}$$    (5.26a)

$$\sigma_{22} = -p - \eta\dot{\varepsilon}$$    (5.26b)

and

$$\sigma_{33} = -p + 2\eta\dot{\varepsilon}$$    (5.26c)

Since the only outside forces acting on the fiber are in the axial or 3 direction, for the Newtonian case, $\sigma_{11}$ and $\sigma_{12}$ must be zero. Hence,

$$p = -\eta\dot{\varepsilon} \quad \text{and}$$    (5.27)

$$\sigma_{33} = 3\eta\dot{\varepsilon} = \overline{\eta}\dot{\varepsilon}$$    (5.28)

which is known as *elongational viscosity or Trouton viscosity* [23]. This is analogous to elasticity where the following relation between elastic modulus, $E$, and shear modulus, $G$, can be written

$$\frac{E}{G} = 2(1 + \nu)$$    (5.29)

where $v$ is Poisson's ratio. For the incompressibility case, where $v = 0.5$, Eq. 5.29 reduces to

$$\frac{E}{G} = 3 \tag{5.30}$$

Figure 5.11 [24] shows shear and elongational viscosities for two types of polystyrene. In the region of the Newtonian plateau, the limit of 3, shown in Eq. 5.28, is quite clear. Figure 5.12 presents plots of elongational viscosities as a function of stress for various thermoplastics at common processing conditions. It should be emphasized that measuring elongational or extensional viscosity is an extremely difficult task. For example, in order to maintain a constant strain rate, the specimen must be deformed uniformly exponentially. In addition, a molten polymer must be tested completely submerged in a heated neutrally buoyant liquid at constant temperature.
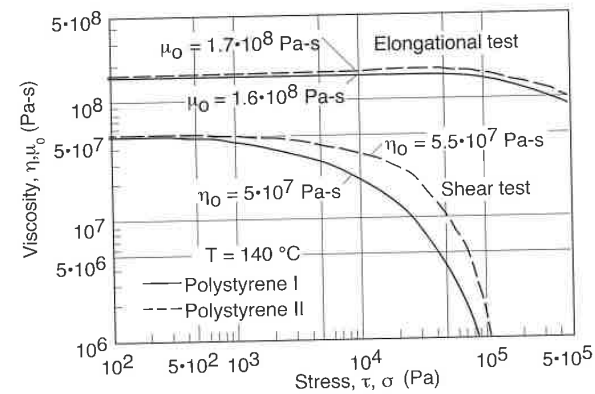


**Figure 5.11**    Shear and elongational viscosity curves for two types of polystyrene.

### 5.2.5  Rheology of Curing Thermosets

A curing thermoset polymer has a conversion or cure dependent viscosity that increases as the molecular weight of the reacting polymer increases. For the vinyl ester whose curing history[5] is shown in Fig. 5.13 [25], the viscosity behaves as shown in Fig. 5.14 [25]. Hence, a complete model for viscosity of a reacting polymer must contain the effects of strain rate, $\dot{\gamma}$, temperature, $T$, and degree of cure, $c$, such as

$$\eta = \eta(\dot{\gamma}, T, c) \tag{5.31}$$

---

5    A more in-depth view of curing and solidification processes of thermosetting polymers is given in Chapter 7.
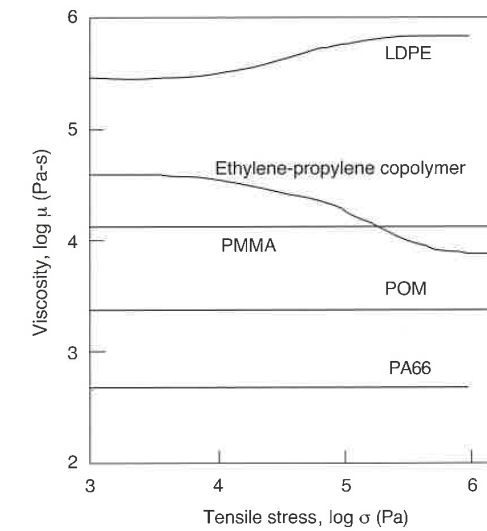


**Figure 5.12**    Elongational viscosity curves as a function of tensile stress for several thermoplastics.
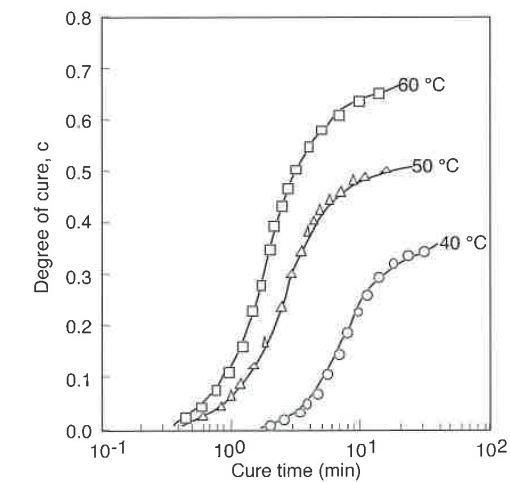


**Figure 5.13**    Degree of cure as a function of time for a vinyl ester at various isothermal cure temperatures.

There are no generalized models that include all these variables for thermosetting polymers. However, extensive work has been done on the viscosity of polyurethanes [26, 27] used in the reaction injection molding process. An empirical relation which models the viscosity of these mixing-activated polymers, given as a function of temperature and degree of cure, is written as

$$\eta = \eta_0 e^{E/RT}\left(\frac{c_g}{c_g - c}\right)^{c_1 + c_2 c} \tag{5.32}$$

where $E$ is the activation energy of the polymer, $R$ is the ideal gas constant, $T$ is the temperature, $c_g$ is the gel point[6], $c$ the degree of cure, and $C_1$ and $C_2$ are constants that fit the experimental data. Figure 5.15 shows the viscosity as a function of time and temperature for a 47% MDI-BDO P(PO-EO) polyurethane, and Fig. 5.16 shows the viscosity as a function of degree of cure.
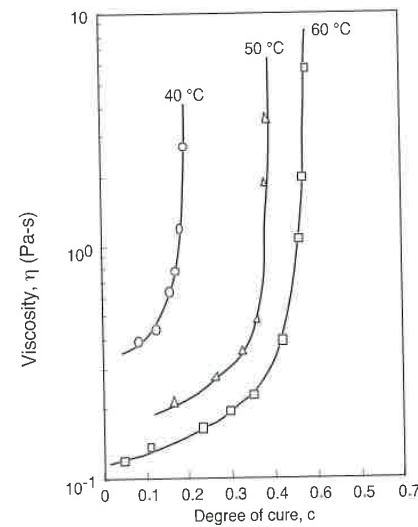


**Figure 5.14**    Viscosity as a function of degree of cure for a vinyl ester at various isothermal cure temperatures.



**Figure 5.15**    Viscosity as a function of time for a 47% MDI-BDO P(PO-EO) polyurethane at various isothermal cure temperatures.



**Figure 5.16**    Viscosity as a function of degree of cure for a 47% MDI-BDO P(PO-EO) polyurethane at various isothermal cure temperatures.

---

6    At the gel point the change of the molecular weight with respect to the degree of cure goes to infinity. Hence, it can be said that at this point all the molecules are interconnected.
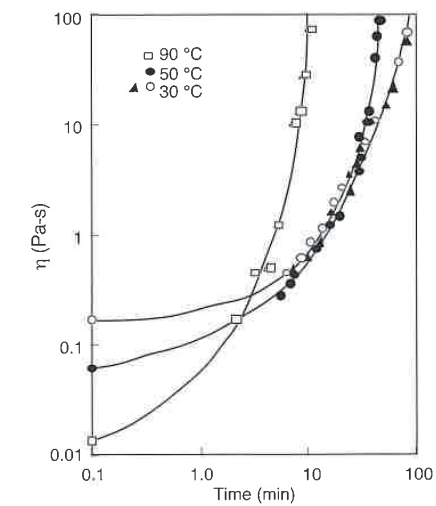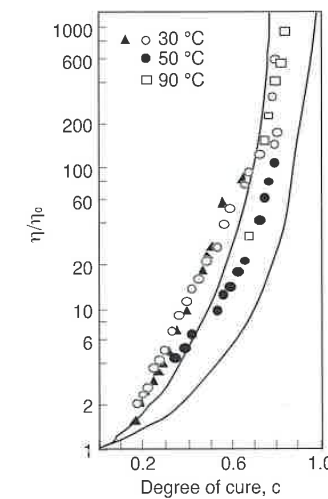
### 5.2.6  Suspension Rheology

Particles suspended in a material, such as in filled or reinforced polymers, have a direct effect on the properties of the final article and on the viscosity during processing. Numerous models have been proposed to estimate the viscosity of filled liquids [28–32]. Most models proposed are a power series of the form[7]

$$\frac{\eta_f}{\eta_0} = 1 + a_1\phi + a_2\phi^2 + a_3\phi^3 + \dots \tag{5.33}$$

The linear term in Eq. 5.33 represents the narrowing of the flow passage caused by the filler that is passively entrained by the fluid and sustains no deformation as shown in Fig. 5.17. For instance, Einstein's model, which only includes the linear term with $a_1 = 2.5$, was derived based on a viscous dissipation balance. The quadratic term in the equation represents the first-order effects of interaction between the filler particles. Geisbüsch suggested a model with a yield stress and, where the strain rate of the melt increases by a factor $\kappa$ as

$$\eta_f = \frac{\tau_0}{\dot{\gamma}} + \kappa\eta_0(\kappa\dot{\gamma}) \tag{5.34}$$

For high deformation stresses, which are typical in polymer processing, the yield stress in the filled polymer melt can be neglected. Figure 5.18 compares Geisbüsch's experimental data to Eq. 5.33 using the coefficients derived by Guth [30]. The data and Guth's model seem to agree well. A comprehensive survey on particulate suspensions was recently given by Gupta [33], and on short-fiber suspensions by Milliken and Powell [34].
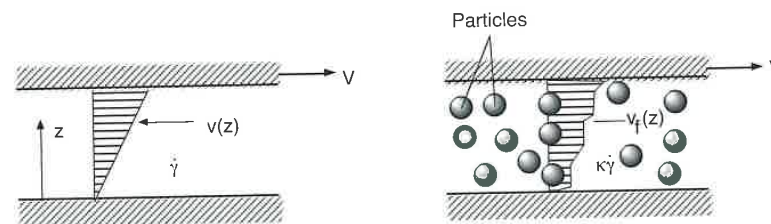
**Figure 5.17**    Schematic diagram of strain rate increase in a filled system.

---

[7]    The model which best fits experimental data is the one given by Guth (1938): $\dfrac{\eta_f}{\eta_0} = 1 + 2.5\phi + 14.1\phi^2$

However, a full analysis of the first-order particle interactions gives an analytical value for the quadratic term of 6.96.
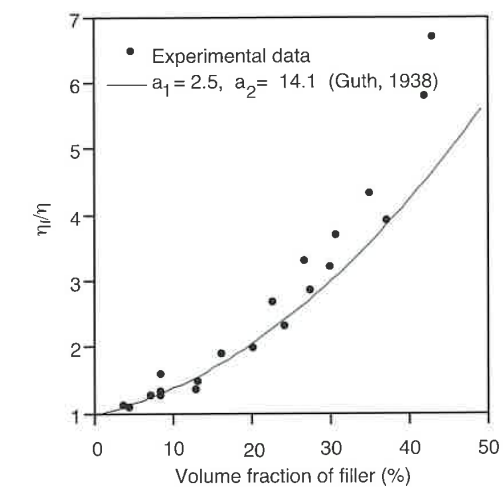
**Figure 5.18**    Viscosity increase as a function of volume fraction of filler for polystyrene and low density polyethylene containing spherical glass particles with diameters ranging between 36 μm and 99.8 μm.

### 5.3    Simplified Flow Models Common in Polymer Processing

Many polymer processing operations can be modeled using simplified geometries and material models. This section presents several isothermal flow models in simple geometries using a Newtonian viscosity and a power-law viscosity as described in Eq. 5.18. Although it is very common to simplify analyses of polymer processes by assuming isothermal conditions, most operations are non-isothermal since they include melting and are often influenced by viscous dissipation. Hence, the temperature of the polymer melt lies between $T_g$ (amorphous polymers) or $T_m$ (semi-crystalline polymers) and the heater temperature, $T_w^{s}$, and often exceeds $T_w$ due to viscous dissipation. An estimate of the maximum temperature rise due to viscous heating is

$$\Delta T_{\max} = \frac{\eta v_0^2}{8k} \tag{5.35}$$

where $v_0$ represents a characteristic velocity in the flow system, such as plate velocity in a simple shear flow, and $k$ represents the thermal conductivity. To

---

[8]    The subscript $w$ is often used for "wall."

estimate the importance of viscous dissipation, the Brinkman number, $Br$, is often computed

$$Br = \frac{\eta v_0^2}{k\left(T_w - T_{g\ or\ m}\right)} \tag{5.36}$$

The Brinkman number is the ratio of the heat generated via viscous dissipation and the heat conducted out of the system via conduction. A Brinkman number > 1 implies that the temperature field will be affected by viscous dissipation. The choice of temperatures in the denominator of the equation depends on the type of material and problem being analyzed.

### 5.3.1   Simple Shear Flow

Simple shear flows as represented in Fig. 5.19 are very common in polymer processing, such as inside extruders as well as in certain coating flows. The flow field in simple shear is the same for all fluids and is described by

$$v_z = v_0 \frac{y}{h} \tag{5.37}$$

for the velocity distribution and

$$Q = \frac{v_0 h W}{2} \tag{5.38}$$

for the volumetric throughput, where $W$ represents the width of the plates.
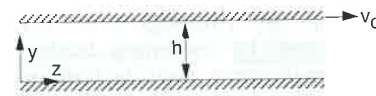


**Figure 5.19**    Schematic diagram of a simple shear flow.

### 5.3.2   Pressure Flow Through a Slit

The pressure flow through a slit, as depicted in Fig. 5.20, is encountered in flows through extrusion dies or inside injection molds. The flow field for a Newtonian fluid is described by

$$v_z(y) = \left(\frac{h^2 \Delta p}{8\mu L}\right)\left[1 - \left(\frac{2y}{h}\right)^2\right] \tag{5.39}$$

and

$$Q = \frac{W h^3 \Delta p}{12 \mu L} \tag{5.40}$$

for the net volumetric throughput. When using the power-law model the flow field is described by

$$v_z(y) = \left(\frac{h}{2(s+1)}\right)\left(\frac{h\Delta p}{2mL}\right)^s\left[1 - \left(\frac{2y}{h}\right)^{s+1}\right] \tag{5.41}$$

and

$$Q = \frac{W h^2}{2(s+2)}\left(\frac{h\Delta p}{2mL}\right)^s \tag{5.42}$$

for the throughput, where $s = 1/n$, and $n$ the power-law index.
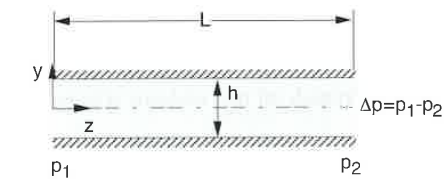


**Figure 5.20**    Schematic diagram of pressure flow through a slit.

### 5.3.3   Pressure Flow through a Tube - Hagen-Poiseuille Flow

Pressure flow through a tube (Fig. 5.21), or Hagen-Poiseuille flow, is the type that exists inside the runner system in injection molds, as well as extrusion dies and inside the capillary viscometer. For a Newtonian fluid, the flow field inside a tube is described by

$$v_z(r) = \frac{R^2 \Delta p}{4\mu L}\left[1 - \left(\frac{r}{R}\right)^2\right] \tag{5.43}$$

and

$$Q = \frac{\pi R^4 \Delta p}{8 \mu L} \qquad (5.44)$$

for the throughput.

Using the power law model, the flow though a tube is described by

$$v_z(r) = \frac{R}{1+s}\left(\frac{R\Delta p}{2mL}\right)^s\left[1-\left(\frac{r}{R}\right)^{s+1}\right] \qquad (5.45)$$

and

$$Q = \left(\frac{\pi R^3}{s+3}\right)\left(\frac{R\Delta p}{2mL}\right)^s \qquad (5.46)$$
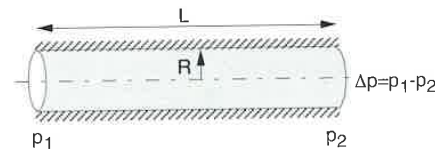
for the throughput.



**Figure 5.21**    Schematic diagram of pressure flow through a tube.

### 5.3.4  Couette Flow

The Couette device, as depicted in Fig. 5.22, is encountered in bearings and in certain types of rheometers. It is also used as a simplified flow model for mixers and extruders. The Newtonian flow field in a Couette device is described by

$$v_\theta(r) = \frac{\Omega}{\kappa^2 - 1}\left(\frac{R_0^2 - r^2}{r}\right) \qquad (5.47)$$

where $\kappa = R_0/R_i$. Using the power law model, the flow field inside a Couette device is described by

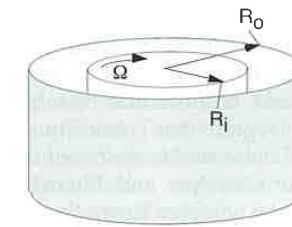$$v_\theta(r) = \frac{\Omega}{\kappa^{2s} - 1}\left(\frac{R_0^{2s} - r^{2s}}{r^{2s-1}}\right) \qquad (5.48)$$

**Figure 5.22**    Schematic diagram of a Couette device

## 5.4    Viscoelastic Flow Models

Viscoelasticity has already been introduced in Chapter 3, based on linear viscoelasticity. However, in polymer processing large deformations are imposed on the material, requiring the use of non-linear viscoelastic models. There are two types of general non-linear viscoelastic flow models: the differential type and the integral type.

### 5.4.1    Differential Viscoelastic Models

Differential models have traditionally been the choice for describing the viscoelastic behavior of polymers when simulating complex flow systems. Many differential viscoelastic models can be described with the general form

$$\mathbf{Y}\underline{\tau} + \lambda_1\underline{\tau}_{(1)} + \lambda_2\left(\underline{\dot{\gamma}}\cdot\underline{\tau} + \underline{\tau}\cdot\underline{\dot{\gamma}}\right) + \lambda_3\left(\underline{\tau}\cdot\underline{\tau}\right) = \eta_0\underline{\dot{\gamma}} \qquad (5.49)$$

where $\underline{\tau}_{(1)}$ is the *first contravariant convected time derivative* of the deviatoric stress tensor and represents rates of change with respect to a convected coordinate system that moves and deforms with the fluid. The *convected derivative* of the deviatoric stress tensor is defined as

$$\underline{\tau}_{(1)} = \frac{D\underline{\tau}}{D_t} - \left(\nabla\underline{v}^t\cdot\underline{\tau} + \underline{\tau}\cdot\nabla\underline{v}\right) \qquad (5.50)$$

The constants in Eq. 5.49 are defined in Table 5.3 for various viscoelastic models commonly used to simulate polymer flows. A recent review by Bird and Wiest [6] gives a more complete list of existing viscoelastic models.

The *upper convective model* and the *White–Metzner model* are very similar with the exception that the White–Metzner model incorporates the strain rate effects

of the relaxation time and the viscosity. Both models provide a first order approximation to flows in which shear rate dependence and memory effects are important. However, both models predict zero second normal stress coefficients. The *Giesekus model* is molecular-based, non-linear in nature and describes the power law region for viscosity and both normal stress coefficients. The *Phan-Thien Tanner models* are based on network theory and give non-linear stresses. Both the Giesekus and Phan-Thien Tanner models have been successfully used to model complex flows.

**Table 5.3**   Definition of Constants in Eq. 5.49

| Constitutive model | Y | $\lambda_1$ | $\lambda_2$ | $\lambda_2$ |
|---|---|---|---|---|
| Generalized Newtonian | 1 | 0 | 0 | 0 |
| Upper convected Maxwell | 1 | $\lambda_1$ | 0 | 0 |
| White–Metzner | 1 | $\lambda_1(\dot{\gamma})$ | 0 | 0 |
| Phan-Thien Tanner-1 | $\exp\left(-\varepsilon\left(\lambda/\eta_0\right)tr\underline{\underline{\tau}}\right)$ | $\lambda$ | $\frac{1}{2}\xi\lambda$ | 0 |
| Phan-Thien Tanner-2 | $1-\varepsilon\left(\lambda/\eta_0\right)tr\underline{\underline{\tau}}$ | $\lambda$ | $\frac{1}{2}\xi\lambda$ | 0 |
| Giesekus | 1 | $\lambda_1$ | 0 | $-\left(\alpha\lambda_1/\eta_0\right)$ |

An overview of numerical simulation of viscoelastic flow systems and an extensive literature review on the subject was given by Keunings [35], and detail on numerical implementation of viscoelastic models are given by Crochet et al. [36] and Debbaut et al. [37]. As an example of the application of differential models to predict flow of polymeric liquids, it is worth mentioning recent work by Dietsche and Dooley [38], who evaluated the White–Metzner, the Phan-Thien Tanner-1, and the Giesekus models by comparing finite element[9] and experimental results of the flow inside multi-layered coextrusion dies. Figure 5.23 [39] presents the progression of a matrix of colored circular polystyrene strands flowing in an identical polystyrene matrix down a channel with a square cross section of 0.95 x 0.95 cm. The cuts in the figure are shown at intervals of 7.6 cm.

The circulation pattern caused by the secondary normal stress differences inside non-circular dies were captured well by the Phan-Thien Tanner and Giesekus models but, as expected, not by the White–Metzner model. Figure 5.24 presents flow patterns predicted by the Phan-Thien Tanner model along with the experimental rearrangement of 165 initially horizontal layers of polystyrene in square, rectangular, and tear-drop shaped dies[10]. In all three

---

9    For their simulation they used the commercially available code POLYFLOW.

10    These geometries are typical for distribution manifolds used in sheeting dies.

cases, the shape of the circulation patterns were predicted accurately. The flow simulation of the square die predicted a velocity on the order of $10^{-5}$ m/s along the diagonal of the cross section, which was in agreement with the experimental results. Also worth mentioning is work recently done by Baaijens [40], who evaluated the Phan-Thien Tanner models 1 and 2, and the Giesekus models. He compared finite element results to measured isochromatic birefringence patterns using complex experiments with polymer melts and solutions. His simulation results predicted the general shape of the measured birefringence patterns. He found that at high Deborah numbers, the Phan-Thien Tanner models converged much more easily than the Giesekus model.
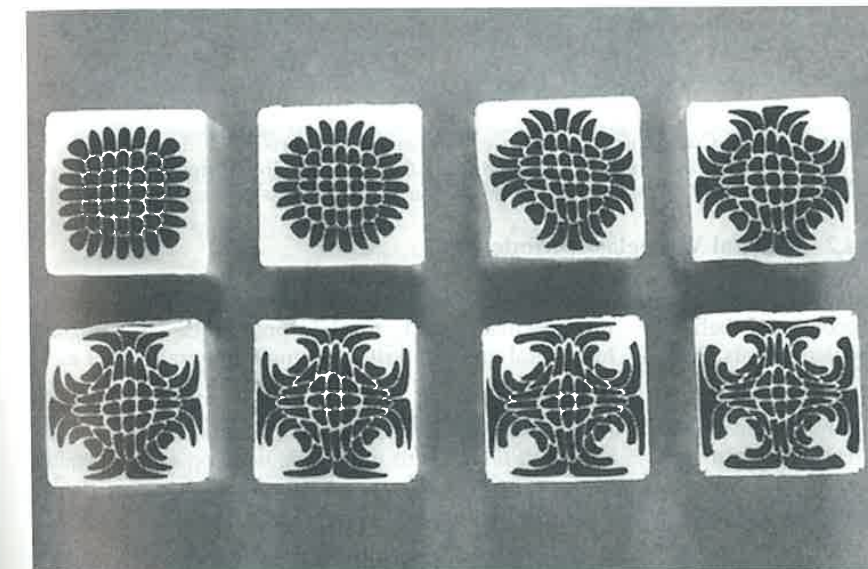


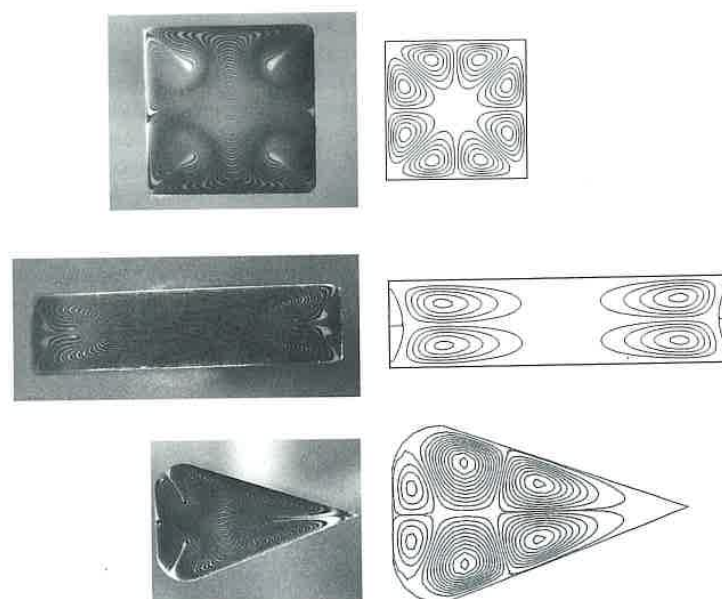**Figure 5.23**   Polystyrene strand profile progression in a square die.

**Figure 5.24**    Comparison between experimental and predicted flow patterns of polystyrene in square, rectangular, and tear-drop shaped dies.

### 5.4.2  Integral Viscoelastic Models

Integral models with a memory function have been widely used to describe the viscoelastic behavior of polymers and to interpret their rheological measurements [9,41,42]. In general one can write the single integral model as

$$\underline{\underline{\tau}} = \int_{-\infty}^{t} M(t - t')\underline{\underline{S}}(t')dt' \tag{5.51}$$

where $M(t - t')$ is a memory function  and a deformation dependent tensor defined by

$$\underline{\underline{S}}(t') = \phi_1\left(I_1,I_2\right)\underline{\underline{\gamma}}_{[0]} + \phi_2\left(I_1,I_2\right)\underline{\underline{\gamma}}^{[0]} \tag{5.52}$$

where $I_1$ and $I_2$ are the first invariant of the Cauchy and Finger strain tensors respectively.

Table 5.4 [43–47] defines the constants $\phi_1$ and $\phi_2$ for various models. In Eq.

5.52, $\underline{\underline{\gamma}}_{[0]}$ and $\underline{\underline{\gamma}}^{[0]}$ are the *finite strain tensors* given by

$$\underline{\underline{\gamma}}_{[0]} = \underline{\underline{\Delta}}^{t} \cdot \underline{\underline{\Delta}} - \underline{\underline{\delta}} \quad \text{and} \tag{5.53}$$

$$\underline{\underline{\gamma}}^{[0]} = \underline{\underline{\delta}} - \underline{\underline{E}} \cdot \underline{\underline{E}}^{t} \tag{5.54}$$

**Table  5.4.**    Definition of Constants in Eq. 5.52

| Constitutive model | $\phi_1$ | $\phi_2$ |
|---|---|---|
| Lodge rubber-like liquid | 1 | 0 |
| K-BKZ* | $\dfrac{\partial W}{\partial I_1}$ | $\dfrac{\partial W}{\partial I_2}$ |
| Wagner** | $\exp(-\beta)\sqrt{\alpha I_1 + (1-\alpha)I_2 - 3}$ | 0 |
| Papanastasiou–Scriven–Macosko*** | $\dfrac{\alpha}{(\alpha - 3) + \beta I_1 + (1 - \beta)I_2}$ | 0 |

\*    W(I1,I2) represents a potential function which can be derived from empiricisms or molecular theory.
\*\*    Wagner's model is a special form of the K-BKZ model
\*\*\*    The Papanastasiou-Scriven Macosko model is also a special form of the K-BKZ model.

The terms  and are displacement gradient tensors[11] defined by

$$\Delta_{ij} = \frac{\partial x_i'\left(x,t,t'\right)}{\partial x_j} \quad \text{and} \tag{5.55}$$

$$E_{ij} = \frac{\partial x_i\left(x',t',t\right)}{\partial x_j'} \tag{5.56}$$

where the components $\Delta_{ij}$ measure the displacement of a particle at past time $t'$ relative to its position at present time $t$, and the terms $E_{ij}$ measure the material displacements at time $t$ relative to the positions at time $t'$.

A memory function $M(t-t')$ which is often applied and which leads to commonly used constitutive equations is written as

$$M\left(t - t'\right) = \sum_{k=1}^{n} \frac{\eta_k}{\lambda_{k^2}}\exp\left(-\frac{t - t'}{\lambda_k}\right) \tag{5.57}$$

[11]  Another combination of the displacement gradient tensors which are often used are the *Cauchy strain tensor* and the *Finger strain tensor* defined by $\underline{\underline{B}}^{-1} = \underline{\underline{\Delta}}^{t} \cdot \underline{\underline{\Delta}}$ and  $\underline{\underline{B}} = \underline{\underline{E}} \cdot \underline{\underline{E}}^{t}$ respectively.

where $\lambda_k$ and $\eta_k$ are relaxation times and viscosity coefficients at the reference temperature $T_{ref}$, respectively.

Once a memory function has been specified one can calculate several material functions using [4]

$$\eta(\dot{\gamma}) = \int_0^\infty M(s)s(\phi_1 + \phi_2)\,ds \qquad (5.58)$$

$$\psi_1(\dot{\gamma}) = \int_0^\infty M(s)s^2(\phi_1 + \phi_2)\,ds \quad \text{and} \qquad (5.59)$$

$$\psi_2(\dot{\gamma}) = \int_0^\infty M(s)s^2(\phi_2)\,ds \qquad (5.60)$$

For example, Figs. 5.25 and 5.26 present the measured [48] viscosity and first normal stress difference data, respectively, for three blow molding grade high density polyethylenes along with a fit obtained from the Papanastasiou–Scriven–Macosko [47] form of the K-BKZ equation. A memory function with a relaxation spectrum of 8 relaxation times was used. The coefficients used to fit the data are summarized in Table 5.5 [41]. The viscosity and first normal stress coefficient data presented in Figs. 5.4 and 5.5 where fitted with the Wagner [9] form of the K-BKZ equation [9]. Luo and Mitsoulis used the K-BKZ model with the data in Table 5.5 to simulate the flow of HDPE through annular dies. Figure 5.27 [41] shows simulation results for a converging, a straight, and a diverging die geometry. The results shown in Fig. 5.27 were in good agreement with experimental results[12].

**Table 5.5**    Material Parameter Values in Eq. 5.57 for Fitting Data of High Density Polyethylene Melts at 170 °C

| k | $\lambda_k$ (s) | $\eta_k$ (Pa-s) |
|---|---|---|
| 1 | 0.0001 | 52 |
| 2 | 0.001 | 148 |
| 3 | 0.01 | 916 |
| 4 | 0.1 | 4210 |
| 5 | 1.0 | 8800 |
| 6 | 10.0 | 21,200 |
| 7 | 100.0 | 21,000 |
| 8 | 1000.0 | 600 |

---

12  The quality of the agreement between experiment and simulation varied between the resins.
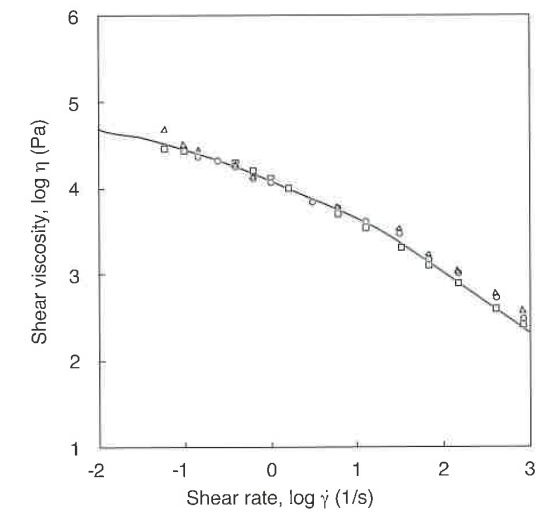


**Figure 5.25**    Measured and predicted shear viscosity for various high density polyethylene resins at 170 °C.
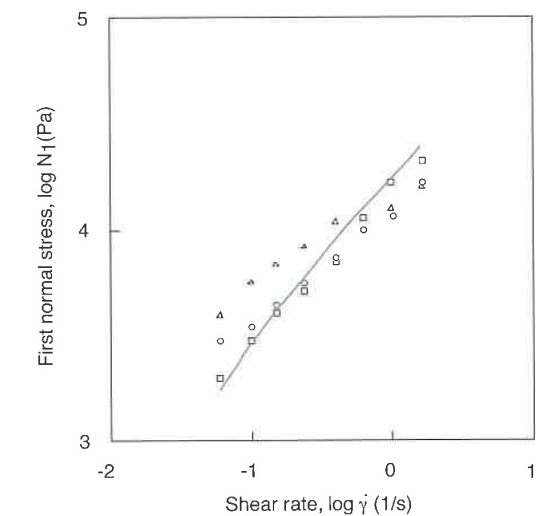


**Figure 5.26**    Measured and predicted first normal stress difference for various high density polyethylene resins at 170 °C.
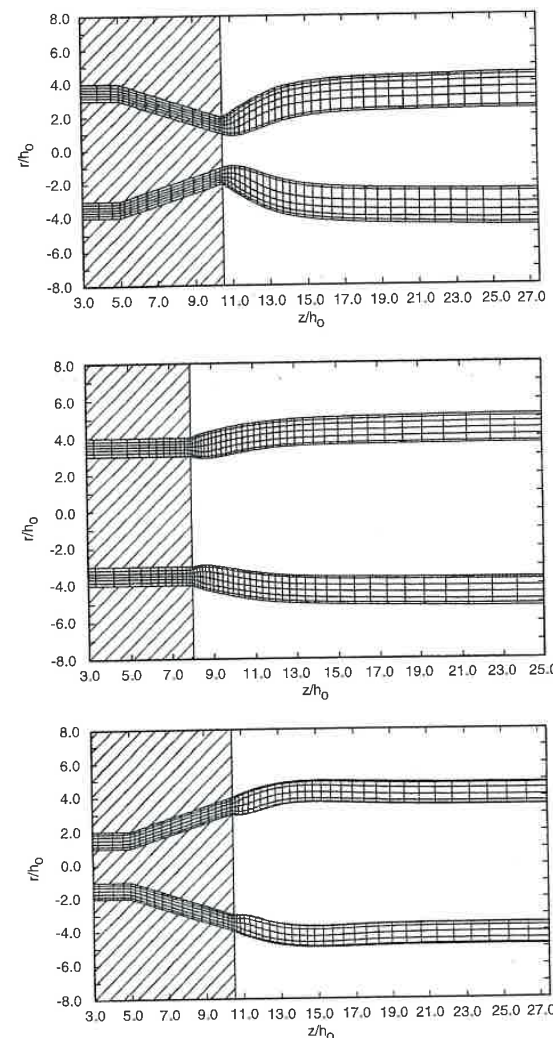
**Figure 5.27**    Predicted extrudate geometry for: (a) converging, (b) straight, and (c) diverging annular dies.

## 5.5    Rheometry

In industry there are various ways to qualify and quantify the properties of the polymer melt. The techniques range from simple analyses for checking the consistency of the material at certain conditions, to more complex measurements to evaluate viscosity, and normal stress differences. This section includes three such techniques, to give the reader a general idea of current measuring techniques.

### 5.5.1    The Melt Flow Indexer

The melt flow indexer is often used in industry to characterize a polymer melt and as a simple and quick means of quality control. It takes a single point measurement using standard testing conditions specific to each polymer class on a ram type extruder or extrusion plastometer as shown in  Fig. 5.28. The standard procedure for testing the flow rate of thermoplastics using a extrusion plastometer is described in the ASTM D1238 test [49]. During the test, a sample is heated in the barrel and extruded from a short cylindrical die using a piston actuated by a weight. The weight of the polymer in grams extruded during the 10-minute test is the melt flow index (MFI) of the polymer.

### 5.5.2    The Capillary Viscometer

The most common and simplest device for measuring viscosity is the capillary viscometer. Its main component is a straight tube or capillary, and it was first used to measure the viscosity of water by Hagen [50] and Poiseuille [51]. A capillary rheometer has a pressure driven flow for which the velocity gradient or strain rate and also the shear rate will be maximum at the wall and zero at the center of the flow, making it a non-homogeneous flow.

Since pressure driven viscometers employ non-homogeneous flows, they can only measure steady shear functions such as viscosity, $\eta(\dot{\gamma})$. However, they are widely used because they are relatively inexpensive to build and simple to operate. Despite their simplicity, long capillary viscometers give the most accurate viscosity data available. Another major advantage is that the capillary rheometers has no free surfaces in the test region, unlike other types of rheometers such as the cone and plate rheometers, which we will discuss in the next section. When the strain rate dependent viscosity of polymer melts is measured, capillary rheometers may be the only satisfactory method of obtaining such data at shear rates > 10 s$^{-1}$. This is important for processes with higher rates of deformation like mixing, extrusion, and injection molding. Because its design is basic and it only needs a pressure head at its entrance,

capillary rheometers can easily be attached to the end of a screw- or ram-type extruder for on-line measurements. This makes the capillary viscometer an efficient tool for industry.
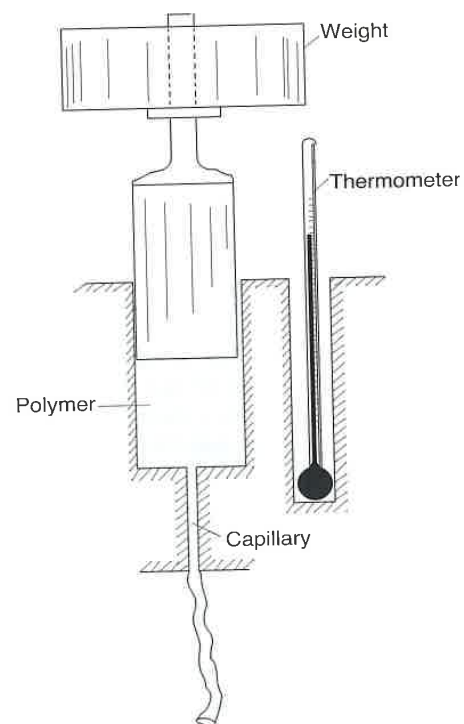


**Figure 5.28**    Schematic diagram of an extrusion plastometer used to measure melt flow index.

The basic features of the capillary rheometers are shown in Fig. 5.29. A capillary tube of radius R and length L is connected to the bottom of a reservoir. Pressure drop and flow rate through this tube are used to determine the viscosity.

To derive the viscosity relation, the following assumptions are made:
- no velocity in the r and $\theta$ directions,
- the polymer is incompressible, and
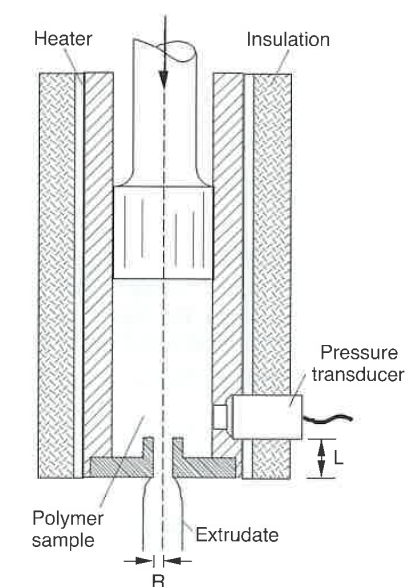- fully developed, steady, isothermal, laminar flow.

**Figure 5.29**    Schematic diagram of a capillary viscometer.

The capillary viscometer can be modeled using the z-component of the equation of motion in terms of stress, $\tau$, as

$$0 = \frac{dp}{dz} + \frac{1}{r}\frac{d}{dr}\left(r\tau_{rz}\right) \tag{5.61}$$

where,

$$\frac{dp}{dz} = \frac{p_0 - p_L}{L} \tag{5.62}$$

Integrating for the shear stress term gives:

$$\tau_{rz} = \frac{(p_0 - p_L)r}{2L} + \frac{C_1}{r} \tag{5.63}$$

The constant $C_1$ is taken to be zero since the stress can not be infinite at the tube axis.

### 5.5.3 Computing Viscosity Using the Bagley and Weissenberg–Rabinowitsch Equations

At the wall the shear stress is:

$$\tau_{r=R} = \tau_w = \frac{R}{2}\frac{(p_0 - p_L)}{L} = \frac{R}{2}\frac{\Delta p}{L} \tag{5.64}$$

Equation 5.64 requires that the capillary be sufficiently long to assure a fully developed flow where end effects are insignificant. However, due to end effects the actual pressure profile along the length of the capillary exhibits a curvature. The effect is shown schematically in Fig. 5.30 [52] and was corrected by Bagley [53] using the end correction $e$ as,

$$\tau_w = \frac{1}{2}\frac{(p_0 - p_L)}{\left(L/R + e\right)} \tag{5.65}$$

The correction factor $e$ at a specific shear rate can be found by plotting pressure drop for various capillary $L/D$ ratios as shown in Fig. 5.31 [52].
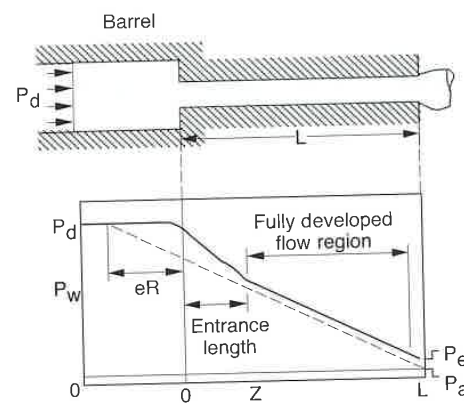


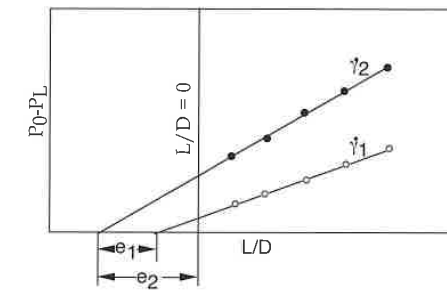**Figure 5.30**   Entrance effects in a typical capillary viscometer.

**Figure 5.31**   Bagley plots for two shear rates.

The equation for shear stress can now be written as

$$\tau_{rz} = \frac{r}{R}\tau_w \tag{5.66}$$

To obtain the shear rate at the wall, $\frac{dv_z}{dr}$, the Weissenberg–Rabinowitsch [54] equation can be used

$$-\frac{dv_z}{dr} = \dot{\gamma}_w = \frac{1}{4}\dot{\gamma}_{aw}\left(3 + \frac{d(\ln Q)}{d(\ln \tau)}\right) \tag{5.67}$$

where, $\dot{\gamma}_{aw}$ is the apparent or Newtonian shear rate at the wall and is written as

$$\dot{\gamma}_{aw} = \frac{4Q}{\pi R^3} \tag{5.68}$$

The shear rate and shear stress at the wall are now known. Therefore, using the measured values of the flow rate, $Q$, and the pressure drop, $p_0 - p_L$, the viscosity can be calculated using

$$\eta = \frac{\tau_w}{\dot{\gamma}_w} \tag{5.69}$$

### 5.5.4 Viscosity Approximation Using the Representative Viscosity Method

A simplified method to compute viscosity, developed by Schümmer and Worthoff [55], takes advantage of the fact that the Newtonian and the shear thinning materials have a common streamline at which the strain rate is the same. This is schematically represented in Fig. 5.32 where the common

streamline is located at $r_s$. The position of that streamline is related to the power law index and varies between $0.7715R$ and $0.8298R$ for power law indices between 1.4 and 0.25. A close approximation is given by[13]

$$r_s \approx \frac{\pi}{4} R = 0.7854 R \tag{5.70}$$

and the strain rate at that point is given by

$$\bar{\dot{\gamma}} = \frac{4}{\pi} \frac{Q}{R^4} r_s \approx \frac{Q}{R^3} \tag{5.71}$$

The shear stress at the location $r_s$ can be calculated using

$$\bar{\tau} = \left( \frac{p_0 - p_L}{L} \right) \frac{r_s}{2} \approx \frac{\pi}{8} R \left( \frac{p_0 - p_L}{L} \right) \tag{5.72}$$
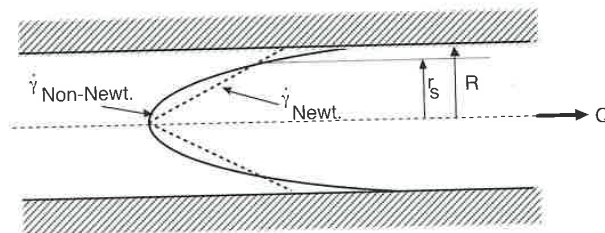


Figure 5.32    Strain rate distribution in Newtonian and non-Newtonian fluids flowing through a capillary.

## 5.5.5  The Cone-Plate Rheometer

The cone-plate rheometer is often used when measuring the viscosity and the primary and secondary normal stress coefficient functions as a function of shear rate and temperature. The geometry of a cone-plate rheometer is shown in Fig. 5.33. Since the angle $\theta_0$ is very small, typically $< 5^\circ$, the shear rate can be considered to be constant and is given by

$$\dot{\gamma}_{\theta\phi} = \frac{\Omega}{\theta_0} \tag{5.73}$$

where $\Omega$ is the angular velocity of the cone. The shear stress can also be considered to be constant and can be related to the measured torque, $T$,

---

13   The value $\pi/4$ was not mathematically derived but offers a significant simplification to the equations with a final error in viscosity of less than 5%.

$$\tau_{\theta\phi} = \frac{3T}{2\pi R^3} \tag{5.74}$$

The viscosity function can now be obtained from

$$\eta\left(\dot{\gamma}_{\theta\phi}\right) = \frac{\tau_{\theta\phi}}{\dot{\gamma}_{\theta\phi}} \tag{5.75}$$

The primary normal stress coefficient function, $\psi_1$, can be calculated by measuring the force, $F$, required to maintain the cone in place and can be computed using

$$\psi_1 = \frac{2F}{\pi R^2 \dot{\gamma}^2} \tag{5.76}$$

Although it is also possible to determine the secondary stress coefficient function from the normal stress distribution across the plate, it is very difficult to get accurate data.
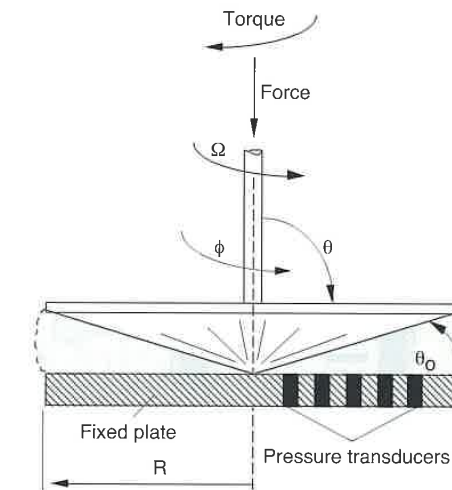


Figure 5.33    Schematic diagram of a cone-plate rheometer.

### 5.5.6  The Couette Rheometer

Another rheometer commonly used in industry is the concentric cylinder or Couette flow rheometer schematically depicted in Fig. 5.34. The torque, $T$, and rotational speed, $\Omega$, can easily be measured. The torque is related to the shear stress that acts on the inner cylinder wall and can be computed as follows:

$$\tau_i = \frac{T}{2\pi r_i^2 L} \tag{5.77}$$

If we consider a power-law fluid confined between the outer and inner cylinder walls of a Couette device, the shear rate at the inner wall can be computed using

$$\dot{\gamma}_i = \frac{2\Omega}{n\left(1 - \left(r_i/r_0\right)^{2/n}\right)} \tag{5.78}$$

The power-law index can be determined with experimental data using

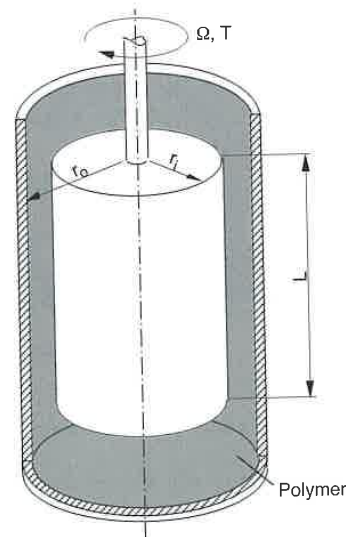$$n = \frac{d\log \tau_i}{d\log \Omega} \tag{5.79}$$



**Figure 5.34**    Schematic diagram of a Couette rheometer.

Once the shear strain rate and stress are known the viscosity can be computed using

$$\eta = \frac{\tau_i}{\dot{\gamma}} \tag{5.80}$$

The major sources of error in a concentric cylinder rheometer are the end-effects. One way of minimizing these effects is by providing a large gap between the inner cylinder end and the bottom of the closed end of the outer cylinder.

### 5.5.7  Extensional Rheometry

It should be emphasized that the shear behavior of polymers measured with the equipment described in the previous sections cannot be used to deduce the extensional behavior of polymer melts. Extensional rheometry is the least understood field of rheology. The simplest way to measure extensional viscosities is to stretch a polymer rod held at elevated temperatures at a speed that maintains a constant strain rate as the rod reduces its cross-sectional area. The viscosity can easily be computed as the ratio of instantaneous axial stress to elongational strain rate. The biggest problem when trying to perform this measurement is to grab the rod at its ends as it is pulled apart. The most common way to grab the specimen is with toothed rotary clamps to maintain a constant specimen length [56]. A schematic of Meissner's extensional rheometer incorporating rotary clamps is shown in Fig. 5.35 [56].
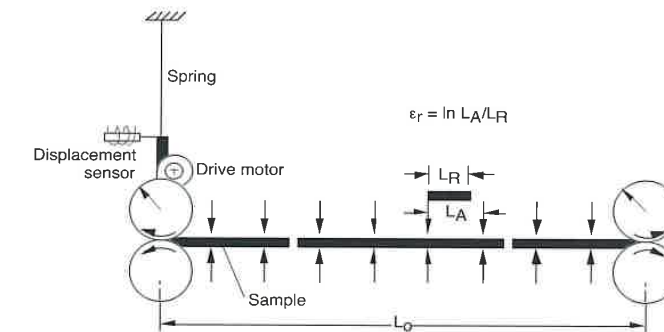


**Figure 5.35**    Schematic diagram of an extensional rheometer.

Another set-up that can be used to measure extensional properties without clamping problems and without generating orientation during the measurement is the lubricating squeezing flow [57], which generates an equibiaxial deformation. A schematic of this apparatus is shown in Fig. 5.36.

It is clear from the apparatus description on Fig. 5.35 that carrying out tests to measure extensional rheometry is a very difficult task. One of the major problems arises because of the fact that, unlike shear tests, it is not possible to achieve steady state condition with elongational rheometry tests. This is simply because the cross-sectional area of the test specimen is constantly diminishing. Figure 5.37 [56] shows this effect by comparing shear and elongational rheometry data on polyethylene.
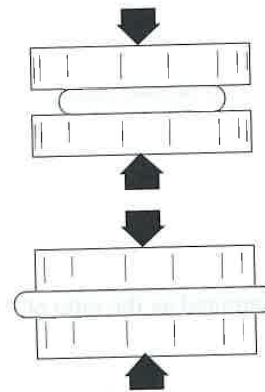


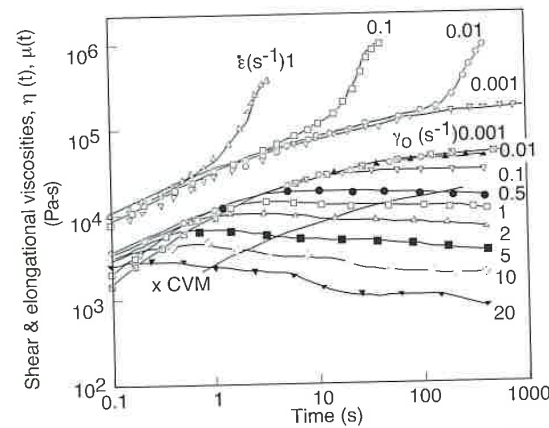**Figure 5.36**    Schematic diagram of squeezing flow.



**Figure 5.37**    Development of elongational and shear viscosities during deformation for polyethylene samples.

Finally, another equibiaxial deformation test is carried out by blowing a bubble and measuring the pressure required to blow the bubble and the size of the bubble during the test. This test has been successfully used to measure extensional properties of polymer membranes for blow molding and thermoforming applications. Here, a sheet is clamped between two plates with circular holes and a pressure differential is introduced to deform it. The pressure applied and deformation of the sheet are monitored with time and related to extensional properties of the material. Assuming an incompressible material, the instantaneous thickness of the sheet can be computed using the notation shown in Fig. 5.38:

$$t = t_0 \left( \frac{D^2}{8Rh} \right) \tag{5.81}$$

The instantaneous radius of curvature of the sheet is related to bubble height by

$$R = \frac{D^2}{8h} + \frac{h}{2} \tag{5.82}$$

The biaxial strain can be computed using

$$\varepsilon_B = \ln \left( \frac{2\alpha R}{D} \right) \tag{5.83}$$

and the biaxial stress can be calculated using

$$\sigma_B = \frac{R\Delta P}{2t} \tag{5.84}$$

For more detail on extensional rheometry, beyond the scope of this book, the reader should refer to the literature [58].
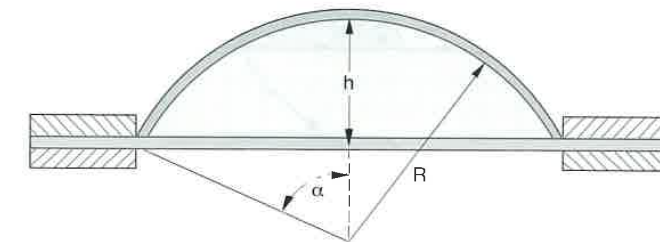


**Figure 5.38**    Schematic diagram of sheet inflation.

## 5.6   Surface Tension

Although surface tension is generally not included in rheology chapters, it does play a significant role in the deformation of polymers during flow, especially in dispersive mixing of polymer blends. Surface tension, $\sigma_s$, between two materials appears as a result of different intermolecular interactions. In a liquid-liquid system, surface tension manifests itself as a force that tends to maintain the surface between the two materials to a minimum. Thus, the equilibrium shape of a droplet inside a matrix which is at rest is a sphere. When three phases touch, such as liquid, gas, and solid, we get different contact angles depending on the surface tension between the three phases. Figure 5.45 schematically depicts three different cases. In case 1, the liquid perfectly wets the surface with a continuous spread, leading to a wetting angle of zero. Case 2, with moderate surface tension effects, shows a liquid that has a tendency to flow over the surface with a contact angle between zero and $\pi/2$. Case 3, with a high surface tension effect, is where the liquid does not wet the surface which results in a contact angle greater than $\pi/2$. In Fig. 5.39, $\sigma_s$ denotes the surface tension between the gas and the solid, $\sigma_l$ the surface tension between the liquid and the gas, and $\sigma_{sl}$ the surface tension between the solid and liquid. Using geometry one can write

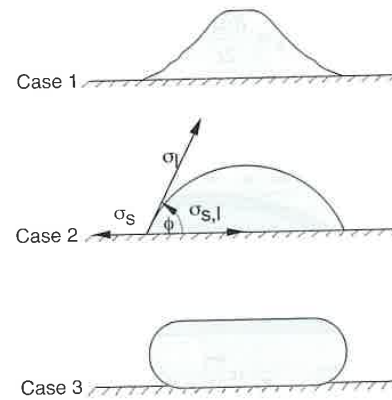$$\cos\theta = \frac{\sigma_s - \sigma_{sl}}{\sigma_l} \qquad (5.85)$$



**Figure 5.39**   Schematic diagram of contact between liquids and solids with various surface tension effects.

The wetting angle can be measured using simple techniques such as a projector, as shown schematically in Fig. 5.40. This technique, originally developed by Zisman [59], can be used in the ASTM D2578 [60] standard test. Here, droplets of known surface tension, $\sigma_l$ are applied to a film. The measured values of $\cos\phi$ are plotted as a function of surface tension, $\sigma_l$, as shown in Fig. 5.41, and extrapolated to find the *critical surface tension*, $\sigma_c$, required for wetting.

For liquids of low viscosity, a useful measurement technique is the tensiometer, schematically represented in Fig. 5.42. Here, the surface tension is related to the force it takes to pull a platinum ring from a solution. Surface tension for selected polymers are listed in Table 5.6 [61], for some solvents in Table 5.7 [62] and between polymer-polymer systems in Table 5.8 [61].

Furthermore, Hildebrand and Scott [63] found a relationship between the solubility parameter[14], $\delta$, and surface tension, $\sigma_s$ for polar and non-polar liquids. Their relationship can be written as [64]
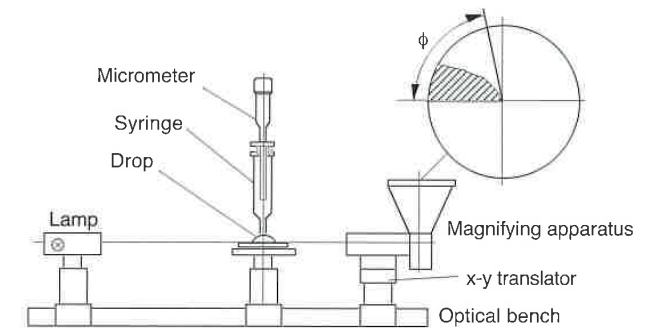


**Figure 5.40**   Schematic diagram of apparatus to measure contact angle between liquids and solids.
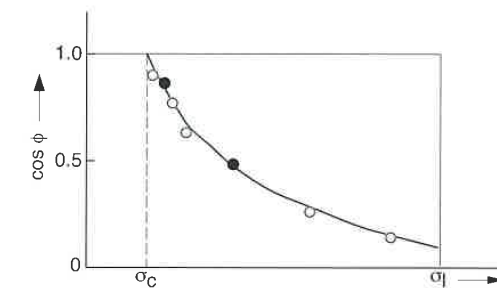


**Figure 5.41**   Contact angle as a function of surface tension.

---

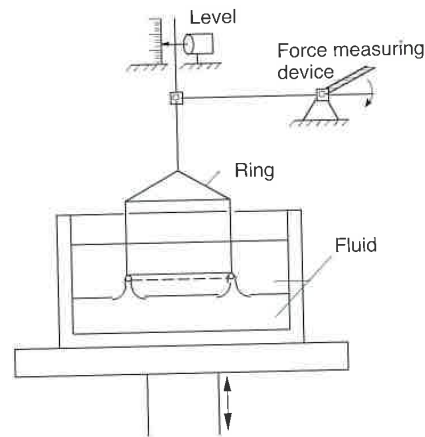[14] Solubility parameter is defined in Chapter 6.

**Figure 5.42**   Schematic diagram of a tensiometer used to measure surface tension of liquids.

$$\sigma_s = 0.24\,\delta^{2.33}\,V^{0.33} \qquad (5.86)$$

where $V$ is the molar volume of the material. The molar volume is defined by

$$V = \frac{M}{\rho} \qquad (5.87)$$

where $M$ is the molar weight. It should be noted that the values in Eqs. 5.86 and 5.87 must be expressed in cgs units.

There are many areas in polymer processing and in engineering design with polymers where surface tension plays a significant role. These are mixing of polymer blends, which is discussed in detail in Chapter 6 of this book, adhesion, treatment of surfaces to make them non-adhesive and sintering.

During manufacturing it is often necessary to coat and crosslink a surface with a liquid adhesive or bonding material. To enhance adhesion it is often necessary to raise surface tension by oxidizing the surface, by creating COOH groups, using flames, etching or releasing electrical discharges. This is also the case when enhancing the adhesion properties of a surface before painting.

On the other hand it is often necessary to reduce adhesiveness of a surface such as required when releasing a product from the mold cavity or when coating a pan to give it nonstick properties. A material that is often used for this purpose is polytetrafluoroethylene (PTFE), mostly known by its tradename of teflon.

**Table 5.6**  Typical Surface Tension Values of Selected Polymers at 180 °C

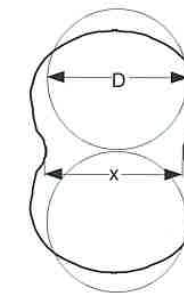| Polymer | $\sigma_S$ (N/m) | $\partial\sigma_S/\partial T$ (N/m/°C) |
|---|---|---|
| Polyamide resins (290 °C) | 0.0290 | — |
| Polyethylene (linear) | 0.0265 | -5.7 x 10$^{-5}$ |
| Polyethylene terephthalate (290 °C) | 0.027 | — |
| Polyisobutylene | 0.0234 | -6.6 x 10$^{-5}$ |
| Polymethyl methacrylate | 0.0289 | -7.6 x 10$^{-5}$ |
| Polypropylene | 0.0208 | -5.8 x 10$^{-5}$ |
| Polystyrene | 0.0292 | -7.2 x 10$^{-5}$ |
| Polytetrafluoroethylene | 0.0094 | -6.2 x 10$^{-5}$ |
| Polyvinyl acetate | 0.0259 | -6.6 x 10$^{-5}$ |



**Figure 5.43**   Schematic of the sintering process.

Finally, during the sintering process, surface tension plays a key role, especially when bringing together pairs of particles at high temperatures without applying pressure. Using the notation for the sintering process presented in Fig. 5.43, Menges and Reichstein [65] develop the relation

$$x^2 \approx \frac{\sigma_s D t}{\eta} \qquad (5.88)$$

where, $\sigma_s$ is the surface tension, $t$ is time and $\eta$ the viscosity.

**Examples**

5.1  Derive the equation that describes the pressure driven velocity field inside a tube of constant diameter (Eq. 5.43).
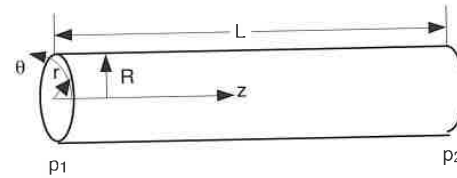


**Figure 5.44** Tube geometry and coordinate system.

In our solution scheme, we must first choose a coordinate system:

Next we must state our assumptions:

- no variations in the $\theta$ direction: $\dfrac{\partial}{\partial\theta} = v_\theta = 0$,

- steady state: $\dfrac{\partial}{\partial t} = 0$,
- no velocity in the radial direction: $v_r = 0$.

The continuity equation (Appendix 1) reduces to

$$\frac{\partial v_z}{\partial z} = 0$$

Using the reduced continuity equation and the above assumptions, only the z-component of the equation of motion (Appendix 1) is needed

$$0 = -\frac{\partial p}{\partial z} + \mu\left[\frac{1}{r}\frac{\partial}{\partial r}\left(r\frac{\partial v_z}{\partial r}\right)\right]$$

Letting $\dfrac{\partial p}{\partial z} = \dfrac{\Delta p}{L}$ and integrating gives

$$r\frac{\partial v_z}{\partial r} = \frac{r^2}{2\mu}\left(\frac{\Delta p}{L}\right) + C_1$$

Since $\dfrac{\partial v_z}{\partial r} = 0$ at $r = 0$, $C_1 = 0$. Integrating again, we get

$$v_z = \frac{r^2}{4\mu}\left(\frac{\Delta p}{L}\right) + C_2$$

Since $v_z = 0$ at $r = R$, the above equation becomes

$$v_z = \frac{R^2\Delta p}{4\mu L}\left[1 - \left(\frac{r}{R}\right)^2\right]$$

5.2  Derive the equation that describes the annular flow in a wire coating process. The wire travels through the annulus at a speed, $V$, and we assume that the pressure inside the die equals atmospheric pressure. Use the notation presented in Fig. 5.45. Assume a power law viscosity.
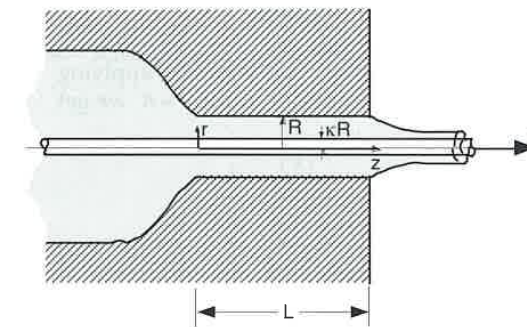


**Figure 5.45**  Wire coating process geometry and coordinate system.

When solving this problem we make similar assumptions as in Example 5.1. This results in $\dfrac{\partial}{\partial\theta} = v_\theta = 0$, $\dfrac{\partial}{\partial t} = 0$ and $v_r = 0$. Here too, the continuity equation reduces to

$$\frac{\partial v_z}{\partial z} = 0$$

However, the pressure gradient, $\dfrac{\partial p}{\partial z}$, can be neglected. Since this problem is non-Newtonian we need to use the general equation of motion (Appendix 1). The z-component reduces to

$$\frac{\partial}{\partial r}\left(r\tau_{rz}\right) = 0$$

Next, we define the deviatoric stress as a function of rate of deformation using

$$\tau_{rz} = \eta(T,\dot{\gamma})\dot{\gamma}_{rz} = m_0\dot{\gamma}^{n-1}\dot{\gamma}_{rz}$$

Since the only deformation that occurs is the shear deformation in the rz-plane the magnitude of the rate of deformation tensor is given by

$$\dot{\gamma} = \dot{\gamma}_{rz} = \frac{\partial v_z}{\partial r}$$

The equation of motion, can now be written as

$$\frac{\partial}{\partial r}\left(rm_0\left[\frac{\partial v_z}{\partial r}\right]^n\right) = 0$$

Integrating this equation twice, and applying two boundary conditions, $v_z = V$ at $r = \kappa R$, and $v_z = 0$ at $r = R$ we get

$$v_z = V\frac{\left[\dfrac{r}{R}\right]^{1-\frac{1}{n}} - 1}{\kappa^{1-\frac{1}{n}} - 1}$$

5.3  Formulate a design equation for the end-fed sheeting die shown in Fig. 5.46 so that the extruded sheet is of uniform thickness. Your job is to specify the length of the approach zone or die land as a function of the manifold direction to achieve uniform flow. The manifold diameter is constant and the flow can be assumed isothermal with a Newtonian viscosity of $\eta$.

After assigning a coordinate system, and assuming the notation presented in Fig. 5.46, the flow of the manifold can be represented using the Hagen-Poiseuille equation as

$$Q = \frac{\pi R^4}{8\eta}\left(-\frac{dp}{dz}\right)$$

and the flow in the die land (per unit width) using slit flow

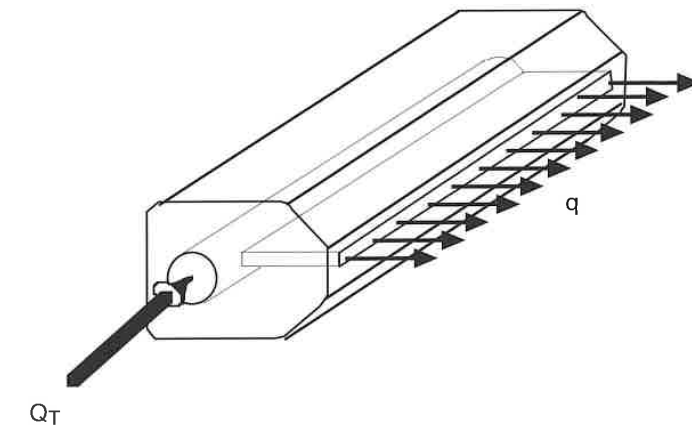$$q = \frac{h^3}{12\eta}\left(-\frac{dp}{dl}\right) = \frac{h^3}{12\eta}\left(\frac{p}{L_l}\right)$$



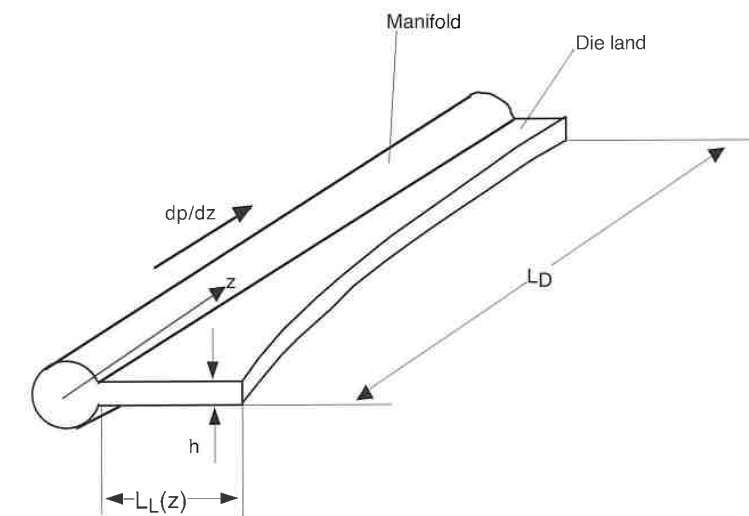**Figure 5.46**    Schematic of an end-fed sheeting die.



**Figure 5.47**    End-fed sheeting die coordinates and dimensions.

A manifold that leads to a uniform sheet must deliver a constant throughput along the die land. Performing a flow balance within the differential element shown in Fig. 5.48 results in
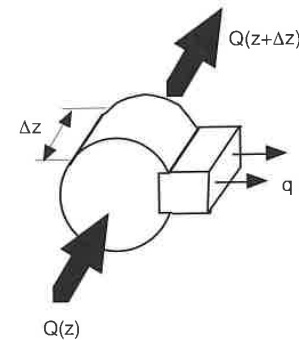
**Figure 5.48**   Differential element of an end-fed sheeting die.

$$Q(z + \Delta z) - Q(z) - q(z)\Delta z = 0$$

and letting $\Delta z \to 0$ results in

$$\frac{dQ}{dz} = -q = \text{constant}$$

If we integrate and let $Q = Q_T$ at $z = 0$ and $Q = 0$ at $z = L_D$ we get

$$Q(z) = Q_T\left(1 - \frac{z}{L_D}\right)$$

Hence,

$$\frac{dQ}{dz} = -\frac{Q_T}{L_D} = -\frac{h^3}{12\eta}\frac{p(z)}{L_l(z)}$$

which results in

$$L_l(z) = \frac{h^3}{12\eta}\frac{L_D}{Q_T}p(z)$$

where $p(z)$ is unknown. We can now rewrite the manifold equation as

$$\frac{dp}{dz} = -\frac{8\eta}{\pi R^4}Q_T\left(1 - \frac{z}{L_D}\right)$$

and then, letting $p = p_0$ at $z = 0$, we get

$$p = p_0 - \frac{8\eta Q_T L_D}{\pi R^4}\left[\left(\frac{z}{L_D}\right) - \frac{1}{2}\left(\frac{z}{L_D}\right)^2\right]$$

which leads to a land length of

$$L_l = \frac{h^3 L_D p_0}{12\eta Q_T} - \frac{2h^3 L_D^2}{3\pi R^4}\left[\left(\frac{z}{L_D}\right) - \frac{1}{2}\left(\frac{z}{L_D}\right)^2\right]$$

**Problems**

5.1   During the filling stage of the injection molding cycle, would the pressure requirements for a PP with a MFI = 10 be larger or smaller, relative to a PP with a MFI = 4? Why?

5.2   Model the viscosity of the PE-LD shown in Fig. 5.4 using the power law model and the Bird–Carreau model.

5.3   Derive the equation that predicts the volumetric throughput during pressure flow through a slit, assuming a Newtonian viscosity (Eq. 5.40).

5.4   Derive the Hagen-Poiseuille equation for a power law fluid (Eq. 5.46).

5.5   You are to extrude a polystyrene sheet through a die with a land length of 0.1 m. What is the maximum speed you can extrude the sheet if you are extruding a polystyrene with the viscoelastic properties presented in Fig. 3.44 of Chapter 3.

5.6   The metering section of a single screw extruder can be modeled using a combination of shear flow and pressure flow between parallel plates. Derive the relation between volumetric throughput versus pressure build-up, $\Delta p$, in a melt extruder of a Newtonian fluid. Hint: Use the notation given in Chapter 6.

5.7   In Example 5.2 obtain an expressions for the flowrate, coating thickness, and the axial force required to pull the wire through the die.

5.8   Formulate the design equation for an end-fed sheeting die such as the one in Example 3. Unlike the example, the new die should have a variable radius manifold as in Fig. 5.48. In this case, the axial distance from the manifold center to the die exit must be constant.
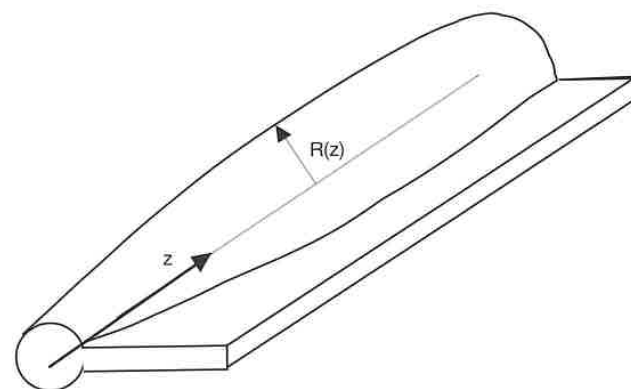
**Figure 5.49**    End-fed variable diameter manifold sheeting die coordinates and dimensions.

## References

1. Macosko, C.W., Rheology: Principles, Measurements and Applications, VCH, (1994).
2. Dealy, J.M., and Wissbrun, K.F., *Melt Rheology and Its Role in Plastics Processing*, Van Nostrand, New York, (1990).
3. Carreau, P.J., De Kee, D.C.R., and Chhabra, R.P., *Rheology of Polymeric Systems*, Hanser Publishers, Munich, (1997).
4. Bird, R.B., Armstrong, R.C., and Hassager, O., *Dynamics of Polymeric Liquids*, 2nd Ed., Vol.1, John Wiley & Sons, New York, (1987).
5. Gordon, G.V., and Shaw, M.T., *Computer Programs for Rheologists*, Hanser Publishers, Munich, (1994).
6. Bird, R.B., and Wiest, J.M., *Annu. Rev. Fluid Mech.*, 27, 169, (1995).
7. Tucker III, C.L., *Fundamentals of Computer Modeling for Polymer Processing*, Hanser Publishers, Munich, (1989).
8. Isayev, A.I., *Modeling of Polymer Processing*, Hanser Publishers, Munich, (1991).
9. Laun, H.M., *Rheol. Acta, 17*, 1, (1978).
10. Agassant, J.-F., Avenas, P., J.-Ph. Sergent, and P.J. Carreau, *Polymer Processing: Principles and Modeling*, Hanser Publishers, Munich, (1991).
11. Vinogradov, G.V., Malkin, A.Y., Yanovskii, Y.G., Borisenkova, E.K., Yarlykov, B.V., and Berezhnaya, G.V., *J. Polym. Sci. Part A-2, 10*, 1061, (1972).
12. Vlachopoulos, J., and Alam, M., *Polym. Eng. Sci., 12*, 184, (1972).
13. Hatzikiriakos, S.G., and Dealy, J.M., *ANTEC Tech. Papers, 37*, 2311 (1991).
14. Spencer, R.S., and Dillon, R.D., *J. Colloid Inter. Sci., 3*, 163, (1947).
15. Vinogradov, G.V., Malkin, A.Y., Yanovskii, Y.G., Borisenkova, E.K., Yarlykov, B.V., and Berezhnaya, G.V., *J. Polym. Sci. Part A-2, 10*, 1061, (1972).
16. Hatzikiriakos, S.G., and Dealy, J.M., *J. Rheol., 36*, 845, (1992).
17. Denn, M.M., *Annu. Rev. Fluid Mech., 22*, 13, (1990).
18. Ostwald, W., *Kolloid-Z., 36*, 99, (1925).
19. de Waale, A., *Oil and Color Chem. Assoc. Journal, 6*, 33, (1923).
20. Carreau, P.J., Ph.D. Thesis, University of Wisconsin-Madison, USA, (1968).
21. Yasuda, K., Armstrong, R.C., and Cohen, R.E., *Rhel. Acta, 20*, 163, (1981).
22. Menges, G., Wortberg, F., and Michaeli, W., *Kunststoffe, 68*, 71, (1978).
23. Trouton, F.T., *Proc. Roy. Soc., A77*, (1906).
24. Münstedt, H., *Rheologica Acta, 14*, 1077, 92, (1975).
25. Han, C.D. and Lem, K.W., *J. Appl. Polym. Sci., 29*, 1879, (1984).
26. Castro, J.M. and Macosko, C.W., *AIChe J., 28*, 250, (1982).
27. Castro, J.M., Perry, S.J., and Macosko, C.W., *Polymer Comm., 25*, 82, (1984).
28. Einstein, A., *Ann. Physik, 19*, 549, (1906).
29. Guth, E., and Simha, R., *Kolloid-Zeitschrift, 74*, 266, (1936).
30. Guth, E., *Proceedings of the American Physical Society*, (1937); *Physical Review, 53*, 321, (1938).
31. Batchelor, G.K., *Annu. Rev. Fluid Mech.*, 6, 227, (1974).
32. Geisbüsch, P., Ph.D. Thesis, IKV, RWTH-Aachen, Germany, (1980).
33. Gupta, R.K., *Flow and Rheology in Polymer Composites Manufacturing*, Ed. S.G. Advani, Elsevier, Amsterdam, (1994).
34. Milliken, W.J., and Powell, R.L., *Flow and Rheology in Polymer Composites Manufacturing*, Ed. S.G. Advani, Elsevier, Amsterdam, (1994).
35. Keunings, R., *Simulation of Viscoelastic Fluid Flow*, in *Computer Modeling for Polymer Processing*, Ed. C.L. Tucker III, Hanser Publishers, Munich, (1989).
36. Crocket, MJ., Davies, A.R., and Walters, K., *Numerical Simulation of Non-Newtonian Flow*, Elsevier, Amsterdam, (1984).
37. Debbaut, B., Marchal, J.M., and Crochet, M.J., *J. Non-Newtonian Fluid Mech., 29*, 119, (1988).
38. Dietsche, L., and Dooley, J., *SPE ANTEC, 53*, 188, (1995).
39. Dooley, J., and Hughes, K., *SPE ANTEC, 53*, 69, (1995).
40. Baaijens, J.P.W., *Evaluation of Constitutive Equations for Polymer Melts and Solutions in Complex Flows*, Ph.D. Thesis, Eindhoven University of Technology, Eindhoven, The Netherlands, (1994).
41. Luo, X.-L., and Mitsoulis, E., *J. Rheol., 33*, 1307, (1989).
42. Kiriakidis, D.G., and Mitsoulis, E., *Adv. Polym. Techn., 12*, 107, (1993).
43. Lodge, A.S., *Elastic Liquids*, Academic Press, London, (1960).
44. Kaye, A., *Non-Newtonian Flow in Incompressible Fluids*, CoA Note No.134, The College of Aeronautics, Cranfield, (1962).
45. Bernstein, B., Kearsley, E., and Zapas, L., *Trans. Soc. Rheol., 7*, 391, (1963).
46. Wagner, M.H., *Rheol. Acta, 18*, 33, (1979).
47. Papanastasiou, A.C., Scriven, L.E., and Macosko, C.W., *J. Rheol., 27*, 387, (1983).
48. Orbey, N., and Dealy, J.M., *Polym. Eng. Sci., 24*, 511, (1984).
49. ASTM, 8.01, Plastics (I), ASTM, Philadelphia, (1994).
50. Hagen, G.H.L., *Annalen der Physik, 46*, 423, (1839).
51. Poiseuille, L.J., *Comptes Rendus 11*, 961, (1840).
52. Dealy, J.M., *Rheometers for Molten Plastics*, Van Nostrand Reinhold Company, New York, (1982).

53. Bagley, E.B., *J. Appl. Phys.*, 28, 624, (1957).
54. Rabinowitsch, B., *Z. Phys. Chem.*, 145, 1, (1929).
55. Schümmer, P., and Worthoff, R.H., *Chem. Eng. Sci.*, 38, 759, (1978).
56. Meissner, J., *Rheol. Acta*, 10 , 230, (1971)..
57. Chatrei, Sh., Macosko, C.W., and Winter, H.H., *J. Rheol.*, 25 , 433, (1981).
58. Macosko, C.W., *Rheology: Principles, Measurements and Applications*, VCH, (1994).
59. Zisman, W.A., *Ind. Eng. Chem.*, 55, 19, (1963).
60. ASTM, 8.02, Plastics (II), ASTM, Philadelphia, (1994).
61. Wu, S., *J. Macromol. Sci. - Revs. Macromol. Chem.*, C10, 1, (1974).
62. Owens, D.K. and Wendt, R.C., *J. Appl. Polymer Sci.*, 13, 1741, (1969).
63. Hildebrand, J. and Scott, R.L., *The Solubility of Non-Electrolytes*, 3rd Ed., Reinhold Publishing Co., New York, (1949).
64. Van Krevelen, D.W., and Hoftyzer, P.J., *Properties of Polymers*, Elsevier, Amsterdam, (1976).
65. Reichstein, H., Ph.D. thesin, IKV, RWTH-Aachen, (1982).

# Part II

# Influence of Processing Properties

# Introduction to Processing

The mechanical properties and the performance of a finished product are always the result of a sequence of events. Manufacturing of a plastic part begins with material choice in the early stages of part design. Processing follows this, at which time properties of the final part are made and frozen into place. During design and manufacturing of any plastic product one must always be aware that material, processing and design properties all go hand-in-hand and cannot be decoupled. This approach is often referred to as the four P's: polymer, processing, product and performance. This chapter presents the most important polymer processing techniques available today[1]. Extrusion[2] is covered first, followed by mixing processes and injection molding[3]. Secondary shaping shaping operations are discussed next. At the end of the chapter other processes such as calendering, coating, compression molding, and rotational molding are presented.

## 6.1 Extrusion

During extrusion, a polymer melt is pumped through a shaping die and formed into a profile. This profile can be a plate, a film, a tube, or have any shape for its cross section. Ram-type extruders were first built by J. Bramah in 1797 to extrude seamless lead pipes. The first ram-type extruders for rubber were built by Henry Bewley and Richard Brooman in 1845. In 1846, a patent for cable coating was filed for trans-gutta-percha and cis-hevea rubber and the first insulated wire was laid across the Hudson River for the Morse Telegraph Company in 1849. The first screw extruder was patented by Mathew Gray in 1879 for the purpose of wire coating. However, the screw pump can be attributed to Archimedes, and the actual invention of the screw extruder in

---

[1]   An in-depth view of polymer processing is given by Tadmor and Gogos [1].
[2]   For further reading in area of extrusion we recommend Rauwendaal's book [2].
[3]   For further reading in the area of injection molding we recommend Osswald, Turng and Gramann [3]

polymer processing by A.G. DeWolfe of the United States dates to the early 1860s. The first extrusion of thermoplastic polymers was done at the Paul Troester Maschinenfabrik in Hannover, Germany in 1935.

Although ram and screw extruders are both used to pump highly viscous polymer melts through passages to generate specified profiles, they are based on different principles. The schematic in Fig. 6.1 shows under what principles ram extruders, screw extruders, and other pumping systems work.
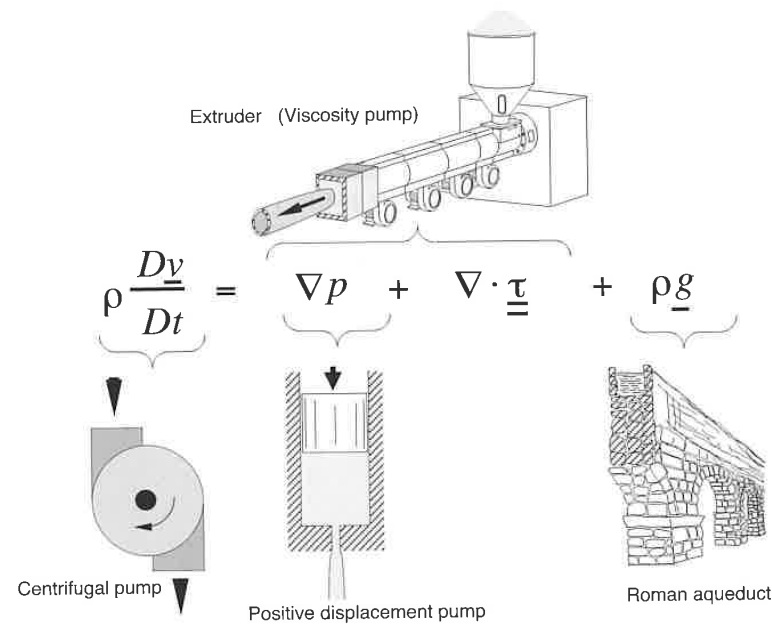
Extruder   (Viscosity pump)

$$\rho \frac{D\underline{v}}{Dt} = \nabla p + \nabla \cdot \underline{\underline{\tau}} + \rho \underline{g}$$

Centrifugal pump

Positive displacement pump

Roman aqueduct

**Figure 6.1**    Schematic of pumping principles.

The ram extruder is a positive displacement pump based on the pressure gradient term of the equation of motion. Here, as the volume is reduced, the fluid is displaced from one point to the other, resulting in a pressure rise. The gear pump, widely used in the polymer processing industry, also works on this principle. On the other hand, a screw extruder is a viscosity pump that works based on the pressure gradient term and the deformation of the fluid, represented as the divergence of the deviatoric stress tensor in Fig. 6.1. The centrifugal pump, based on the fluid inertia, and the Roman aqueduct, based on the potential energy of the fluid, are also represented in the figure and are typical of low viscosity liquids.

In today's polymer industry, the most commonly used extruder is the single screw extruder, schematically depicted in Fig. 6.2. The single screw extruder can either have a smooth inside barrel surface, called a conventional single screw extruder, or a grooved feed zone, called a grooved feed extruder. In some cases, an extruder can have a degasing zone, required to extract moisture, volatiles, and other gases that form during the extrusion process.
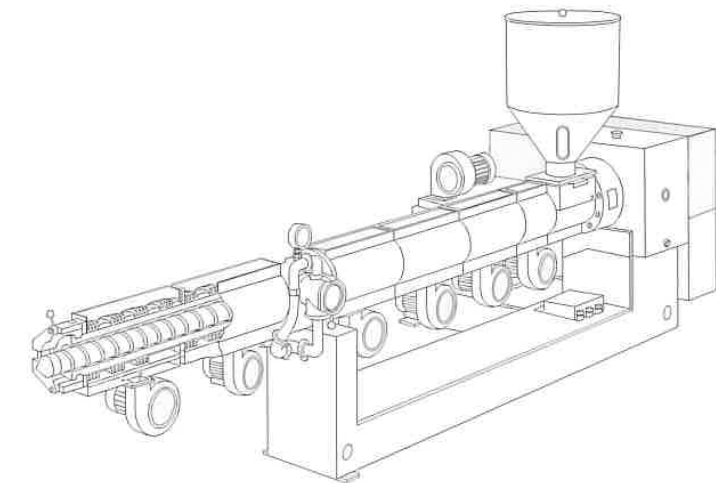
**Figure 6.2**    Schematic of a single screw extruder (Reifenhäuser).

Another important class of extruders are the twin screw extruders, schematically depicted in Fig. 6.3. Twin screw extruders can have co-rotating or counter-rotating screws, and the screws can be intermeshing or non-intermeshing. Twin screw extruders are primarily employed as mixing and compounding devices, as well as polymerization reactors. The mixing aspects of single and twin screw extruders are detailed later in this chapter.
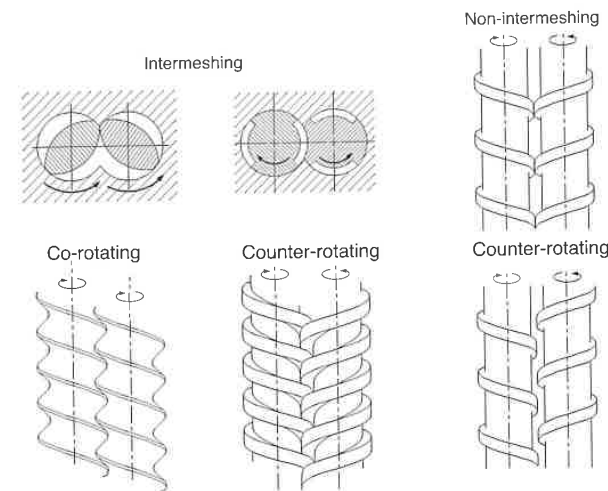
**Figure 6.3**   Schematic of different twin screw extruders.

### 6.1.1  The Plasticating Extruder

The plasticating single screw extruder is the most common equipment in the polymer industry. It can be part of an injection molding unit and found in numerous other extrusion processes, including blow molding, film blowing, and wire coating. A schematic of a plasticating or three-zone, single screw extruder, with its most important elements is given in Fig. 6.4. Table 6.1 presents typical extruder dimensions and relationships common in single screw extruders.
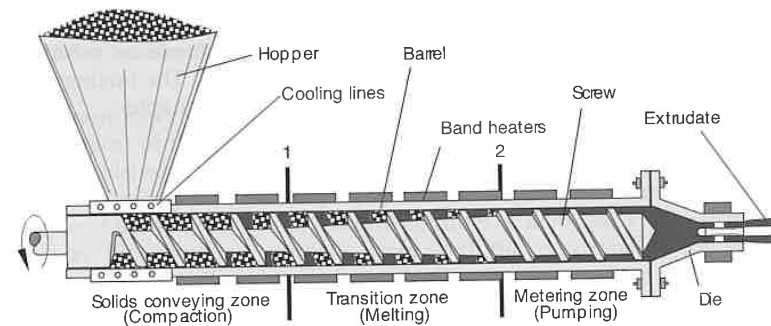


**Figure 6.4**   Schematic of a plasticating single screw extruder.

**Table 6.1**   Typical Extruder Dimensions and Relationships (the Notation for Table 6.1 is Defined in Fig. 6.5.)

| | |
|---|---|
| L/D | Length to Diameter ratio<br>20 or less for feeding or melt extruders<br>25 for blow molding, film blowing, and injection molding<br>30 or higher for vented extruders or high output extruders |
| D<br>US (inches)<br>Europe (mm) | Standard diameter<br>0.75, 1.0, 1.5, 2, 2.5, 3.5, 4.5, 6, 8, 10, 12, 14, 16, 18, 20, and 24<br>20, 25, 30, 35, 40, 50, 60, 90, 120, 150, 200, 250, 300, 350, 400, 450, 500,  and 600 |
| $\phi$ | Helix angle<br>$17.65^\circ$ for a square pitch screw where $L_S=D$<br>New trend: $0.8 < L_S/D < 1.2$ |
| h | Channel depth in the metering section<br>$(0.05-0.07)D$ for $D<30$ mm<br>$(0.02-0.05)D$ for $D>30$ mm |
| $\beta$ | Compression ratio:<br>$h_{feed} = \beta h$<br>2 to 4 |
| $\delta$ | Clearance between the screw flight and the barrel<br>0.1 mm for $D<30$ mm<br>0.15 mm for $D>30$ mm |
| N | Screw speed<br>1-2 rev/s (60-120 rpm) for large extruders<br>1-5 rev/s (60-300 rpm) for small extruders |
| $V_b$ | Barrel velocity (relative to screw speed) = $\pi DN$<br>0.5 m/s for most polymers<br>0.2 m/s for unplasticized PVC<br>1.0 m/s for LDPE |

The plasticating extruder can be divided into three main zones:

- The solids conveying zone
- The melting or transition zone
- The metering or pumping zone

The tasks of a plasticating extruder are to:

- Transport the solid pellets or powder from the hopper to the screw channel
- Compact the pellets and move them down the channel
- Melt the pellets
- Mix the polymer into a homogeneous melt
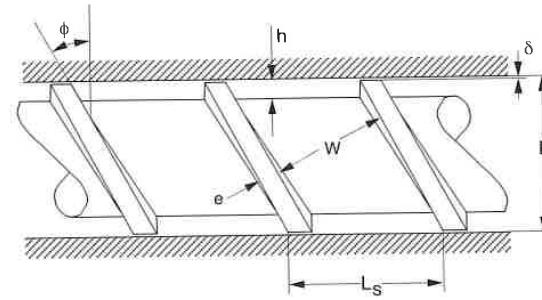- Pump the melt through the die

**Figure 6.5**    Schematic diagram of a screw section.

The pumping capability and characteristic of an extruder can be represented with sets of die and screw characteristic curves. Figure 6.6 presents such curves for a conventional (smooth barrel) single screw extruder.
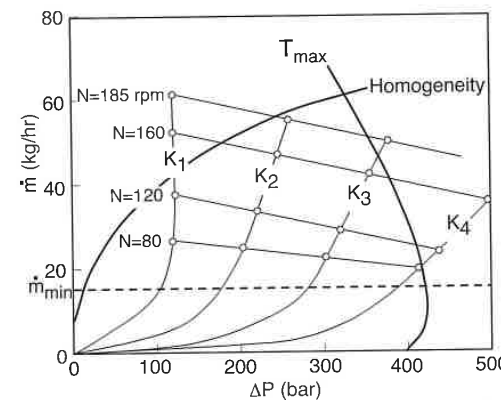


**Figure 6.6**    Screw and die characteristic curves for a 45 mm diameter extruder with an LDPE.

The die characteristic curves are Land $_e$l K $_1$, K2, K3, and K4 in ascending order of die restriction. Here, K1 represents a low resistance die such as for a thick plate, and K4 represents a restrictive die, such as is used for film. The different screw characteristic curves represent different screw rotational speeds. In a screw characteristic curve the point of maximum throughput and no pressure build-up is called the point of open discharge. This occurs when there is no die. The point of maximum pressure build-up and no throughput is called the point of closed discharge. This occurs when the extruder is plugged.

Shown in Fig. 6.6 are also lines that represent critical aspects encountered during extrusion. The curve labeled Tmax represents the conditions at which excessive temperatures are reached as a result of viscous heating. The feasibility line ($\dot{m}_{min}$) represents the throughput required to have an economically feasible system. The processing conditions to the right of the homogeneity line render a thermally and physically heterogeneous polymer melt.

#### 6.1.1.1   The Solids Conveying Zone

The task of the solids conveying zone is to move the polymer pellets or powders from the hopper to the screw channel. Once the material is in the screw channel, it is compacted and transported down the channel. The process to compact the pellets and to move them can only be accomplished if the friction at the barrel surface exceeds the friction at the screw surface. This can be visualized if one assumes the material inside the screw channel to be a nut sitting on a screw. As we rotate the screw without applying outside friction, the nut (polymer pellets) rotates with the screw without moving in the axial direction. As we apply outside forces (barrel friction), the rotational speed of the nut is less than the speed of the screw, causing it to slide in the axial direction. Virtually, the solid polymer is then "unscrewed" from the screw.

To maintain a high coefficient of friction between the barrel and the polymer, the feed section of the barrel must be cooled, usually with cold water cooling lines. The frictional forces also result in a pressure rise in the feed section. This pressure compresses the solids bed which continues to travel down the channel as it melts in the transition zone. Figure 6.7 presents the pressure build-up in a conventional, smooth barrel extruder. In these extruders, most of the pressure required for pumping and mixing is generated in the metering section.
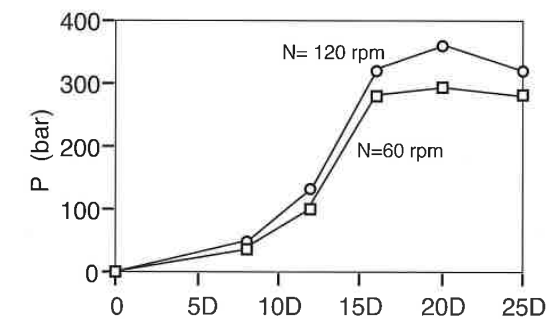


**Figure 6.7**    Conventional extruder pressure distribution.

The simplest mechanism for ensuring high friction between the polymer and the barrel surface is grooving its surface in the axial direction [4, 5]. Extruders with a grooved feed section where developed by Menges and Predöhl [4, 5] in 1969, and are called grooved feed extruders. To avoid excessive pressures that can lead to barrel or screw failure, the length of the grooved barrel section must not exceed 3.5D. A schematic diagram of the grooved section in a single screw extruder is presented in Fig. 6.8. The key factors that propelled the development and refinement of the grooved feed extruder were the processing problems, excessive melt temperature, and reduced productivity posed by high viscosity and low coefficients of friction typical of high molecular weight polyethylenes and polypropylenes.
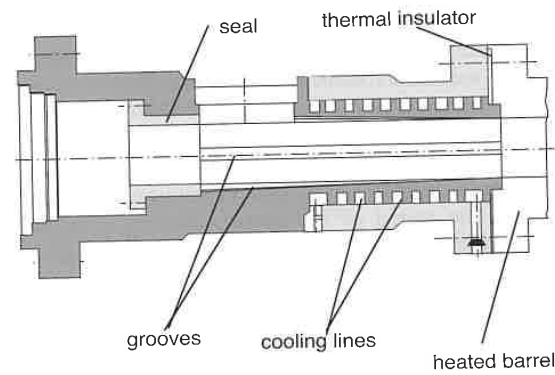


Figure 6.8    Schematic diagram of the grooved feed section of a single screw extruder.

In a grooved feed extruder, the conveying and pressure build-up tasks are assigned to the feed section. Figure 6.9 presents the pressure build-up in a single screw extruder with a grooved feed section. The high pressures in the feed section lead to the main advantages over conventional systems. With grooved feed systems, there is a higher productivity and a higher melt flow stability and pressure invariance. This is demonstrated with the screw characteristic curves in Fig. 6.10, which presents screw characteristic curves for a 45 mm diameter grooved feed extruder with comparable mixing sections and die openings as shown in Fig. 6.6.
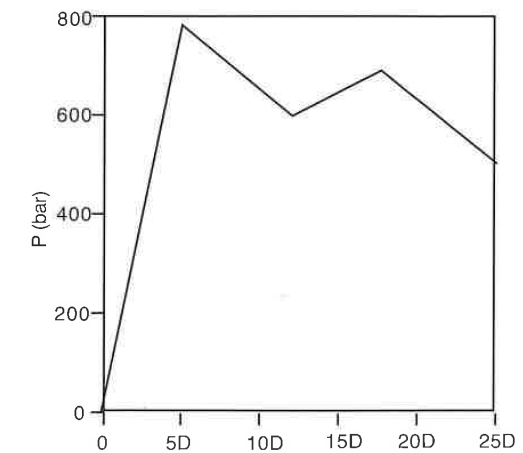


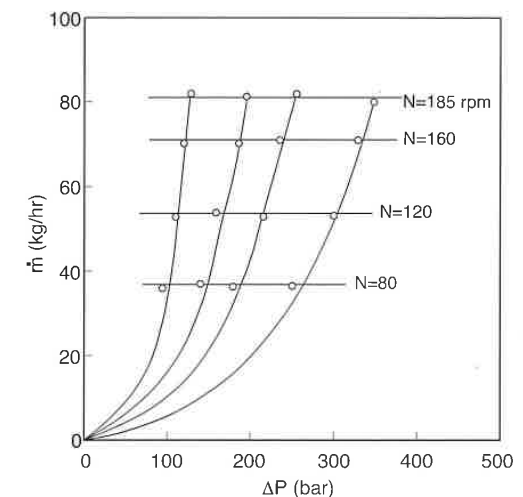Figure 6.9    Grooved feed extruder pressure distribution.



Figure 6.10    Screw and die characteristic curves for a grooved feed 45 mm diameter extruder with an LDPE.

The behavior of the two extruders in Figs. 6.6 and 6.10 are best compared if the throughput and the pressure build-up are non-dimensionalized. The dimensionless throughput is

$$\hat{m} = \frac{\dot{m}}{\rho N D^3} \tag{6.1}$$

and the dimensionless pressure build-up is

$$\Delta\hat{p} = \frac{\Delta p D}{m N^n L_c} \tag{6.2}$$

where $L$ represents the total channel length and for a $25\,L/D$ extruder is

$$L_c = \frac{25D}{\sin(\phi)} \tag{6.3}$$

where f is assumed to be 17.65° (square pitch). Figure 6.11 presents the results shown in Figs. 6.6 and 6.10 after having been non-dimensionalized using Eqs. 6.2 and 6.3. The figure clearly shows the higher productivity of the grooved feed extruder where the throughput is at least 50% more than that observed with the conventional system for a comparable application. Used with care, Fig. 6.11 can also be used for scale-up.
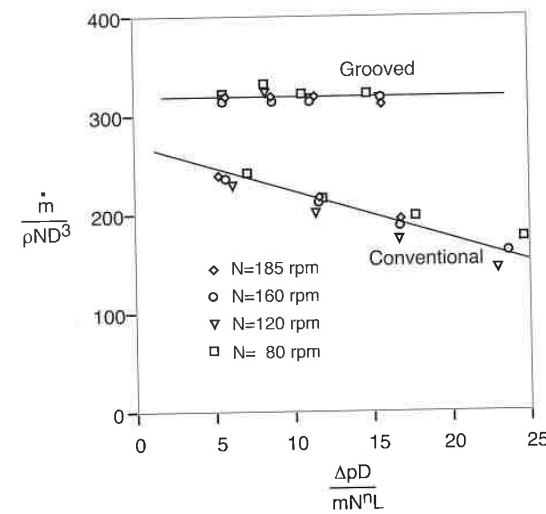


**Figure 6.11**   Dimensionless screw characteristic curves for conventional and grooved feed extruders.

#### 6.1.1.2   The Melting Zone

The melting or transition zone is the portion of the extruder were the material melts. The length of this zone is a function of the material properties, screw geometry, and processing conditions. During melting, the size of the solid bed shrinks as a melt pool forms at its side, as depicted in Fig. 6.12a which shows the polymer unwrapped from the screw channel.
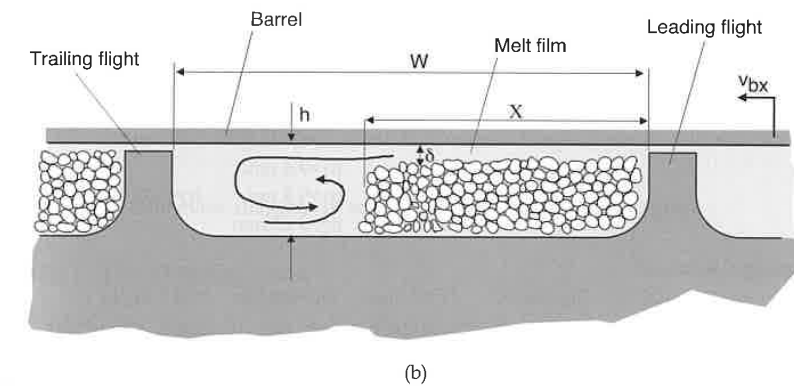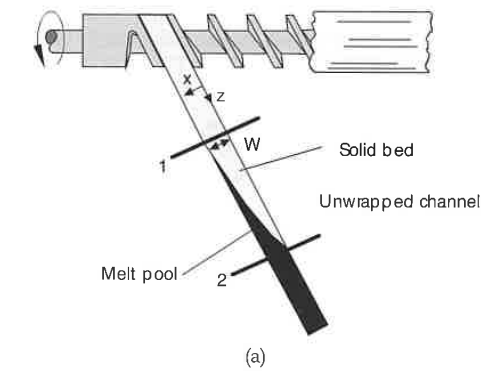


(a)



(b)

**Figure 6.12**   (a) Solids bed in an unwrapped screw channel and   (b) screw channel cross section.

Figure 6.12b presents a cross section of the screw channel in the melting zone. The solid bed is pushed against the leading flight of the screw as freshly molten polymer is wiped from the melt film into the melt pool by the relative motion between the solids bed and the barrel surface.

Knowing where the melt starts and ends is important when designing a screw for a specific application. The most widely used model to predict melting in a plasticating single screw extruder is the well known Tadmor Model [5]. Using the Tadmor Model, one can accurately predict the solid bed profile in the single screw extruder. Figure 6.13 presents the experimental and predicted solids bed profile of an LDPE in a single screw extruder. The material properties and processing conditions used in the calculations are given in Table 6.2.
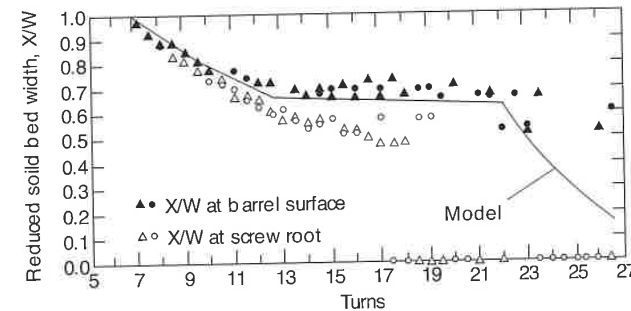


**Figure 6.13**    Predicted (Tadmor Model) and experimental solids bed profile.

**Table 6.2**    Extruder Parameters, Processing Conditions, and Material Properties for the Solids Bed Profile Results in Fig. 6.13.

*Extruder Geometry:*

Square pitch screw, D=63.5 mm, L/D=26.5, W=54.16 mm

| | | |
|---|---|---|
| Feed zone        - 12.5 turns | $h_1$=9.4 mm | |
| Transition zone - 9.5 turns | $h_1$=9.4 mm | $h_2$=3.23 mm |
| Metering zone   - 4.5 turns | $h_2$=3.23 mm | |

*Processing Conditions:*

$T_0$=24 °C    $T_b$=149 °C    N=60 rpm    $D_p$=204 bar    $\dot{m}$=61.8 kg/hr

*Material properties (LDPE):*

Viscosity:    n=0.345    a=0.01 °C$^{-1}$    $m_0$=5.6x10$^4$ Pa-s$^n$    $T_m$=110 °C

Thermal:
$k_m$=0.1817 W/m°C    $C_m$=2.596 kJ/kg°C    $C_s$=2.763 kJ/kg°C
$\rho_{bulk}$=595 kg/m$^3$    $\rho_s$=915.1 kg/m$^3$    $\rho_m$=852.7 + 5.018x10$^{-7}$p - 0.4756T
$\lambda$=129.8 kJ/kg

From experiment to experiment there are always large variations in the experimental solids bed profiles. The variations in this section of the extruder are caused by slight variations in processing conditions and by the uncontrolled solids bed break-up towards the end of melting. This effect can be eliminated by introducing a screw with a barrier flight that separates the solids bed from the melt pool. The Maillefer screw and barrier screw in Fig. 6.14 are commonly used for high quality and reproducibility. The Maillefer screw maintains a constant solids bed width, using most effectively the melting with melt-removal mechanism, while the barrier screw uses a constant channel depth with a gradually decreasing solids bed width.
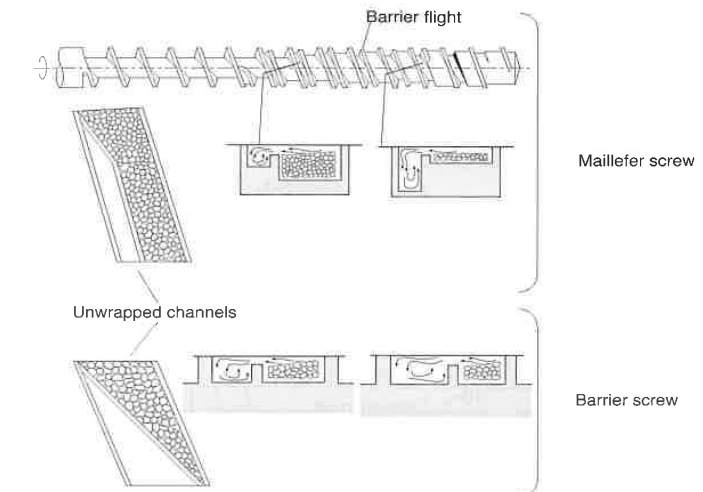


**Figure 6.14**    Schematic diagram of screws with different barrier flights.

### 6.1.1.3    The Metering Zone

The metering zone is the most important section in melt extruders and conventional single screw extruders that rely on it to generate pressures sufficient for pumping. The pumping capabilities in the metering section of a single screw extruder can be estimated by solving the equation of motion with appropriate constitutive laws. For a Newtonian fluid in an extruder with a constant channel depth, the screw and die characteristic curves for different cases are represented in Fig. 6.15. The figure shows the influence of the channel depth on the screw characteristic curves. A restrictive extrusion die would clearly work best with a shallow channel screw, and a less restrictive die would render the highest productivity with a deep channel screw.
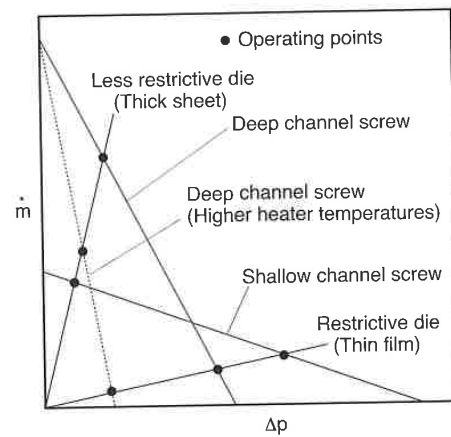
**Figure 6.15**  Screw characteristic curves (Newtonian).

In both the grooved barrel and the conventional extruder, the diameter of the screw determines the metering or pumping capacity of the extruder. Figure 6.16 presents typical normalized mass throughput as a function of screw diameter for both systems.
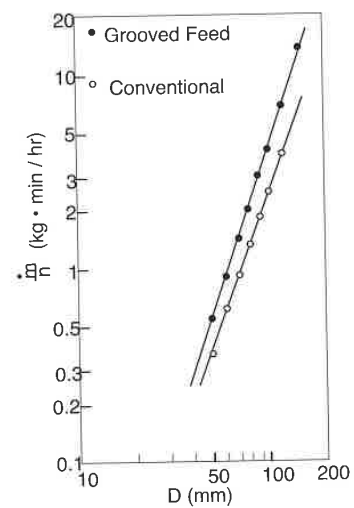


**Figure 6.16**  Throughput for conventional and grooved feed extruders.

### 6.1.2  Extrusion Dies

The extrusion die shapes the polymer melt into its final profile. The extrusion die is located at the end of the extruder and its used to extrude

- Flat films and sheets
- Pipes and tubular films for bags
- Filaments and strands
- Hollow profiles for window frames
- Open profiles

As shown in Fig. 6.17, depending on the functional needs of the product, several rules of thumb can be followed when designing an extruded plastic profile. These are:

- Avoid thick sections. Thick sections add to the material cost and increase sink marks caused by shrinkage.
- Minimize the number of hollow sections. Hollow sections add to die cost and make the die more difficult to clean.
- Generate profiles with constant wall thickness. Constant wall thickness in a profile makes it easier to control the thickness of the final profile and results in a more even crystallinity distribution in semi-crystalline profiles.
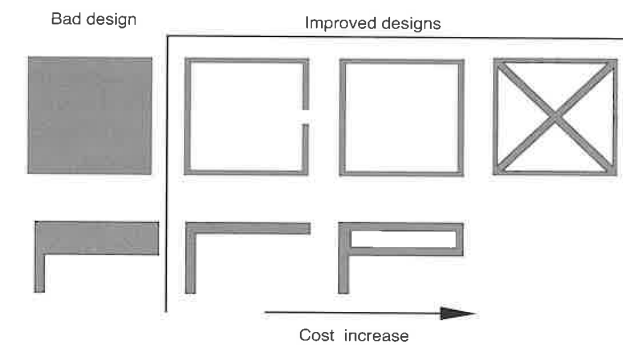


**Figure 6.17**  Extrusion profile designs.

### 6.1.2.1  Sheeting Dies

One of the most widely used extrusion dies is the coat-hanger sheeting die. A sheeting die, such as depicted in Fig. 6.18, is formed by the following elements:

- Manifold: evenly distributes the melt to the approach or land region
- Approach or land: carries the melt from the manifold to the die lips
- Die lips: perform the final shaping of the melt
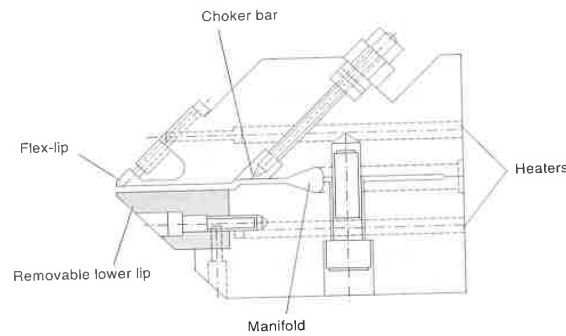- Flex lips: for fine tuning when generating a uniform profile



**Figure 6.18**    Cross section of a coat-hanger die.

To generate a uniform extrudate geometry at the die lips, the geometry of the manifold must be specified appropriately. Figure 6.19 presents the schematic of a coat-hanger die with a pressure distribution that corresponds to a die that renders a uniform extrudate. It is important to mention that the flow though the manifold and the approach zone depend on the non-Newtonian properties of the polymer extruded. So the design of the die depends on the shear thinning behavior of the polymer. Hence, a die designed for one material does not necessarily work for another.
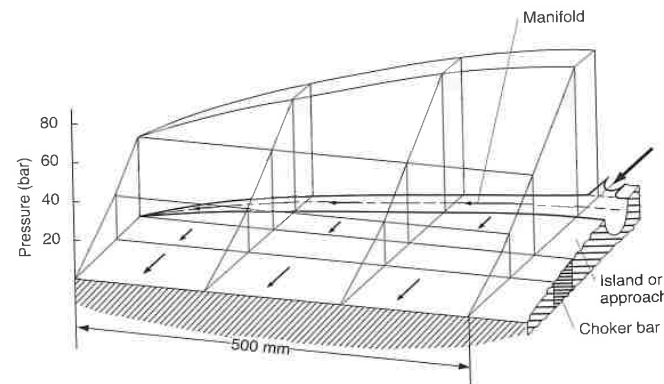


**Figure 6.19**    Pressure distribution in a coat-hanger die.

### 6.1.2.2   Tubular Dies

In a tubular die, the polymer melt exits through an annulus. These dies are used to extrude plastic pipes and tubular film. The film blowing operation is discussed in more detail later in this chapter.

The simplest tubing die is the spider die, depicted in Fig. 6.20. Here, a symmetric mandrel is attached to the body of the die by several legs. The polymer must flow around the spider legs causing weld lines along the pipe or film. These weld lines, visible streaks along the extruded tube, are weaker regions.
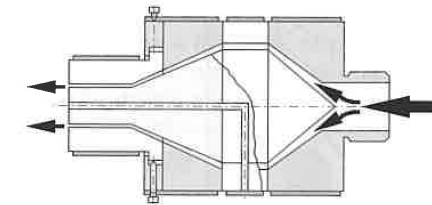


**Figure 6.20**    Schematic of a spider leg tubing die.

To overcome weld line problems, the cross-head tubing die is often used. Here, the die design is similar to that of the coat-hanger die, but wrapped around a cylinder. This die is depicted in Fig. 6.21. Since the polymer melt must flow around the mandrel, the extruded tube exhibits one weld line. In addition, although the eccentricity of a mandrel can be controlled using adjustment screws, there is no flexibility to perform fine tuning such as in the coat-hanger die. This can result in tubes with uneven thickness distributions.
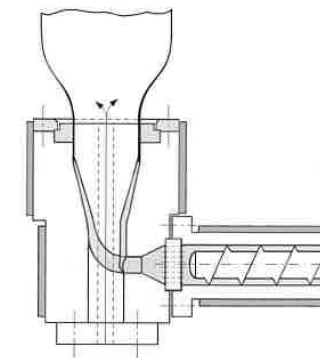


**Figure 6.21**    Schematic of a cross-head tubing die used in film blowing.

The spiral die, commonly used to extrude tubular blown films, eliminates weld line effects and produces a thermally and geometrically homogeneous extrudate. The polymer melt in a spiral die flows through several feed ports into independent spiral channels wrapped around the circumference of the mandrel. This type of die is schematically depicted in Fig. 6.22.
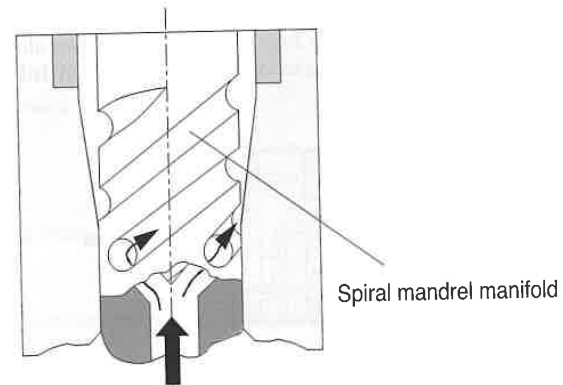


**Figure 6.22**  Schematic of a spiral die.

## 6.2  Mixing Processes

Today, most processes involve some form of mixing. As discussed in the previous section, an integral part of a screw extruder is a mixing zone. In fact, most twin screw extruders are primarily used as mixing devices. Similarly, the plasticating unit of an injection molding machine often has a mixing zone. This is important because the quality of the finished product in almost all polymer processes depends in part on how well the material was mixed. Both the material properties and the formability of the compound into shaped parts are highly influenced by the mixing quality. Hence, a better understanding of the mixing process helps to optimize processing conditions and increase part quality.

The process of polymer blending or mixing is accomplished by distributing or dispersing a minor or secondary component within a major component serving as a matrix. The major component can be thought of as the continuous phase, and the minor components as distributed or dispersed phases in the form of droplets, filaments, or agglomerates.

When creating a polymer blend, one must always keep in mind that the blend will probably be remelted in subsequent processing or shaping processes. For example, a rapidly cooled system, frozen as a homogenous mixture, can separate into phases because of coalescence when re-heated. For all practical purposes, such a blend is not processable. To avoid this problem, compatibilizers, which are macromolecules used to ensure compatibility in the boundary layers between the two phases, are common [6].

The mixing can be distributive or dispersive. The morphology development of polymer blends is determined by three competing mechanisms: distributive mixing, dispersive mixing, and coalescence. Figure 6.23 presents a model, proposed by Macosko and co-workers [6], that helps us visualize the mechanisms governing morphology development in polymer blends. The process begins when a thin tape of polymer is melted away from the pellet. As the tape is stretched, surface tension causes it to rip and to form into threads. These threads stretch and reduce in radius, until surface tension becomes significant enough which leads to Rayleigh disturbances. These cause the threads to break down into small droplets.
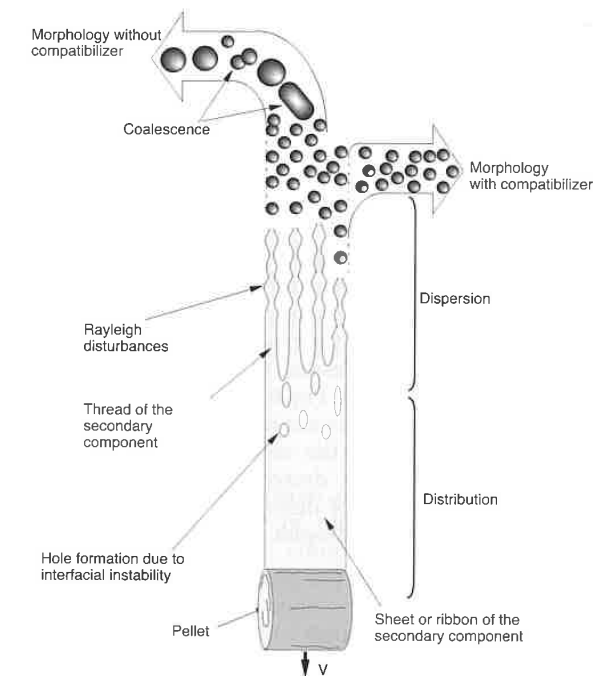


**Figure 6.23**  Mechanism for morphology development in polymer blends.

There are three general categories of mixtures that can be created:

- Homogeneous mixtures of compatible polymers,
- Single phase mixtures of partly incompatible polymers, and
- Multi-phase mixtures of incompatible polymers.

Table 6.3 lists examples of compatible, partially incompatible, and incompatible polymer blends.

**Table 6.3**   Common Polymer Blends

Compatible polymer blends

> Natural rubber and polybutadiene
> Polyamides (e.g., PA 6 and PA 66)
> Polyphenylene ether (PPE) and polystyrene

Partially incompatible polymer blends

> Polyethylene and polyisobutylene
> Polyethylene and polypropylene (5% PE in PP)
> Polycarbonate and polybutylene terephthalate

Incompatible polymers blends

> Polystyrene/polyethylene blends
> Polyamide/polyethylene blends
> Polypropylene/polystyrene blends

### 6.2.1  Distributive Mixing

Distributive mixing or laminar mixing of compatible liquids is usually characterized by the distribution of the droplet or secondary phase within the matrix. This distribution is achieved by imposing large strains on the system such that the interfacial area between the two or more phases increases and the local dimensions, or striation thicknesses, of the secondary phases decrease. This concept is shown schematically in Fig. 6.24 [7]. The figure shows a Couette flow device with the secondary component having an initial striation thickness of $\delta_0$. As the inner cylinder rotates, the secondary component is distributed through the systems with constantly decreasing striation thickness; striation thickness depends on the strain rate of deformation which makes it a function of position. The total strain that a droplet or secondary phase undergoes is defined by

$$\gamma(\tau) = \int_0^\tau \dot{\gamma}(t)\,dt \tag{6.4}$$

where $\dot{\gamma}$ is the magnitude of the strain rate of deform tion defined by Eqs. 4.7

and 4.8, and $\tau$ is an arbitrary point in time. For a sphere, which is deformed into an ellipsoid, the total strain can be related to the striation thickness using

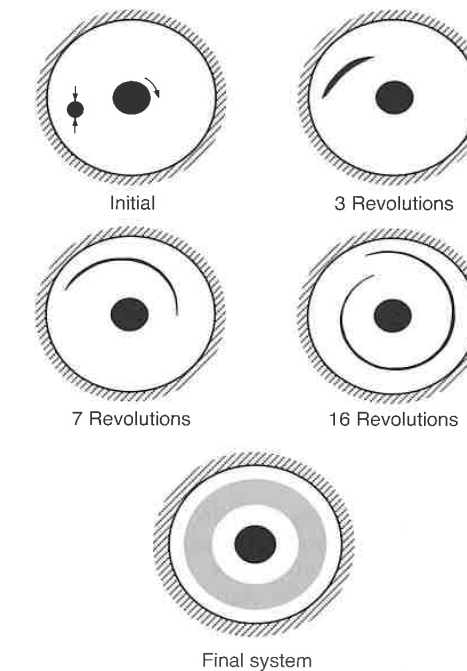$$\delta = 2R\left(1 + \gamma^2\right)^{-0.25} \tag{6.5}$$



Figure 6.24   Experimental results of distributive mixing in Couette flow, and schematic of the final mixed system.

### 6.2.1.1  Effect of Orientation

Imposing large strains on the system is not always sufficient to achieve a homogeneous mixture. The type of mixing device, initial orientation and position of the two or more fluid components play a significant role in the quality of the mixture. For example the mixing problem shown in Fig. 6.24 homogeneously distributes the melt within the region contained by the streamlines cut across by the initial secondary component. The final mixed system is shown in Fig. 6.24. Figure 6.25 [8] shows another variation of initial orientation and arrangement of the secondary component. Here, the secondary

phase cuts across all streamlines, which leads to a homogeneous mixture throughout the Couette device, under appropriate conditions.
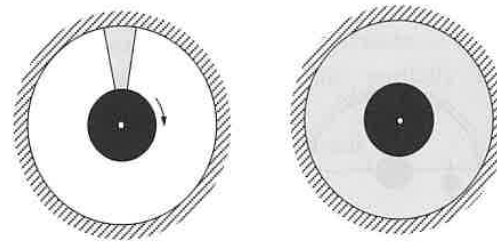


**Figure 6.25**    Schematic of distributive mixing in Couette flow.

A common way of quantifying mixing is by following the growth of the interface between the primary and secondary fluids. In a simple shear flow, a simple expression exists that relates the growth of the interface, the strain, and the orientation of the area of the secondary fluid with respect to the flow direction [9]:

$$\frac{A}{A_0} = \gamma \cos \alpha \tag{6.6}$$

where $A_0$ is the initial interface area, $A$ is the final interface area, $\gamma$ is the total strain and $\alpha$ the angle that defines the orientation of the surface, or normal vector, with respect to the direction of flow. Figure 6.26 [2] demonstrates this concept. Here, both cases (a) and (b) start with equal initial areas, $A_0$, and undergo the same amount of strain, $\gamma = 10$. The circular secondary component in (a) has a surface that is randomly oriented, between 0 and $2\pi$, whereas most of the surface of the elongated secondary component in (b) is oriented at $\pi/2$ leading to negligible growth of the interface area. An ideal case would have been a long slender secondary component with a surface oriented in the direction of flow or vertically between the parallel plates. Hence, the maximum interface growth inside a simple shear mixer can be achieved if the direction of the interface is maintained in an optimal orientation ($\cos \alpha = 1$). In a simple shear flow this would require a special stirring mechanism that would maintain the interface between the primary and secondary fluid components in a vertical position. Erwin [10] and Ng [11] demonstrated this in an experimental study that involved placing black and white polyethylene blocks in a Couette device (Fig. 6.27a). Figure 6.27b shows that after applying a small amount of shear, the surfaces that were originally oriented in the radial direction have stretched a certain amount and have changed their orientation. It is clear from the photograph that the same surface tends to align with the planes of shear,

reducing the mixing efficiency of the process. Hence, in order to increase the effectiveness of the mixer Ng [11] took the Couette content and cut it into new blocks, that were placed inside the Couette device rotated by 90º (Fig. 6.27c). This changed the orientation of the surfaces back to a position where they can more effectively feel the effects of deformation. By repeating this procedure several times, Erwin and co-workers [10, 11] were able to demonstrate that the area growth is also a function of the number of re-orientation that occur during the mixing process. If $N$ is the total number of shearing stages, separated by a re-orientation, the area growth can be computed using

$$\frac{A}{A_0} = \left( \frac{\gamma_{Total}}{N} \right)^N \tag{6.7}$$

where $\gamma_{Total}$ is the total strain applied during the process. Using this concept, Erwin [10] demonstrated that the upper bound for the ideal mixer is found in a mixer that applies a plane strain extensional flow or pure shear flow to the fluid and where the surfaces are maintained ideally oriented during the whole process; this occurs when $N = \infty$ and each time an infinitesimal amount of shear is applied. In such a system the growth of the interfacial areas follows the relation given by

$$\frac{A}{A_0} = e^{\gamma_{Total}/2} \tag{6.8}$$

In Erwin's ideal mixer the amount of mixing increases in an exponential fashion, compared to a linear increase if the orientation of the fluids' interfaces remain undisturbed.
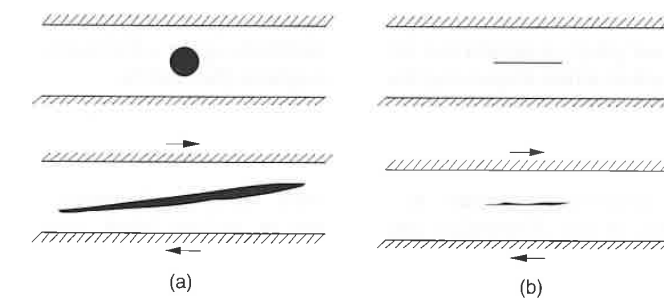


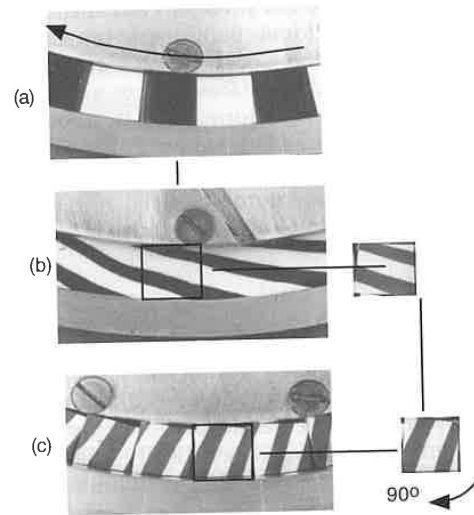**Figure 6.26**    Effect of initial surface orientation on distributive mixing.

**Figure 6.27**   Couette deformation and reorientation scheme.

## 6.2.2  Dispersive Mixing

Dispersive mixing in polymer processing involves breaking a secondary immiscible fluid or an agglomerate of solid particles and dispersing them throughout the matrix. Here, the imposed strain is not as important as the imposed stress which causes the system to break-up. Hence, the type of flow inside a mixer plays a significant role on the break-up of solid particle clumps or fluid droplets when dispersing them throughout the matrix.

### 6.2.2.1  Break-Up of Particulate Agglomerates

The most common example of dispersive mixing of particulate solid agglomerates is the dispersion and mixing of carbon black into a rubber compound. The dispersion of such a system is schematically represented in Fig. 6.28. However, the break-up of particulate agglomerates is best explained using an ideal system of two small spherical particles that need to be separated and dispersed during a mixing process.

If the mixing device generates a simple shear flow, as shown in Fig. 6.29, the maximum separation forces that act on the particles as they travel on their streamline occur when they are oriented in a 45⁰ position as they continuously rotate during flow. The magnitude of the force trying to separate the "agglomerate" is given by [12]
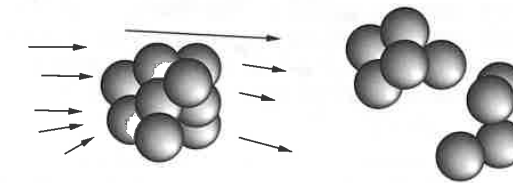


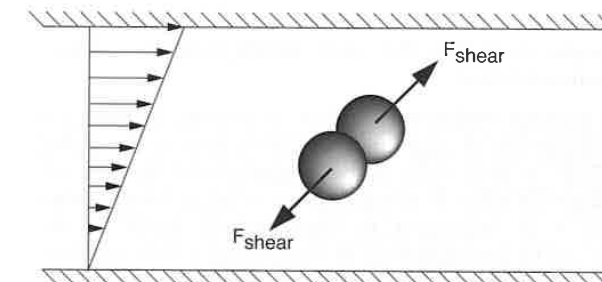**Figure 6.28**   Break-up of particulate agglomerates during flow.



**Figure 6.29**   Force applied to a two-particle agglomerate in a simple shear flow.

$$F_{shear} = 3\pi\eta\dot{\gamma}r^2 \qquad (6.9)$$

where $\eta$ is the viscosity of the carrier fluid, $\dot{\gamma}$ the magnitude of the strain rate tensor, and r are the radii of the particles.

However, if the flow field generated by the mixing device is a pure elongational flow, such as shown in Fig. 6.30, the particles will always be oriented at 0⁰; the position of maximum force. The magnitude of the force for this system is given by
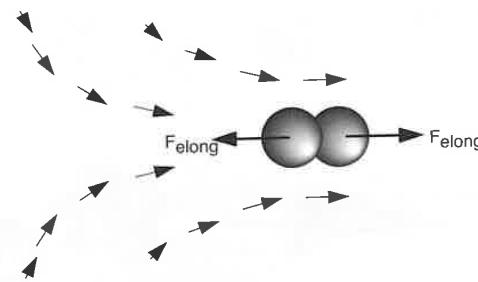
**Figure 6.30**     Force applied to a two-particle agglomerate in an elongational flow.

$$F_{shear} = 6\pi\eta\dot{\gamma}r^2 \qquad (6.10)$$

which is twice as large as the maximum force generated by the system that produces a simple shear flow. In addition, in an elongational flow, the agglomerate is always oriented in the direction of maximum force generation, whereas in simple shear flow the agglomerate tumbles quickly through the position of maximum force[4].

The above analysis makes it clear that for mixing processes which require break-up and dispersion of agglomerates, elongation is the preferred mode of deformation. This is only valid if the magnitude of the rate of deformation tensor can be kept the same in elongation as in shear. Hence, when optimizing mixing devices it is important to know which mode of deformation is dominant. This can be accomplished by computing a flow number [13], defined by

$$\lambda = \frac{\dot{\gamma}}{\dot{\gamma} - \omega} \qquad (6.11)$$

where $\dot{\gamma}$ is the magnitude of the rate of deformation tensor and $\omega$ the magnitude of the vorticity tensor. A flow number of 0 implies pure rotational flow, a value of 0.5 represents simple shear flow, and pure elongational flow is implied when l is 1.

---

4   A full description of the relation between flow field and rotation of fibers and agglomerates is given in Chapter 7.

### 6.2.2.2   Break-Up of Fluid Droplets

In general, droplets inside an incompatible matrix tend to stay or become spherical due to the natural tendencies of the drop trying to maintain the lowest possible surface to volume ratio. However, a flow field within the mixer applies a stress on the droplets, causing them to deform. If this stress is high enough, it will eventually cause the drops to disperse. The droplets will disperse when the surface tension can no longer maintain their shape in the flow field and the filaments break-up into smaller droplets. This phenomenon of dispersion and distribution continues to repeat itself until the deviatoric stresses of the flow field can no longer overcome the surface tension of the new droplets formed.

As can be seen, the mechanism of fluid agglomerate break-up is similar in nature to solid agglomerate break-up in the sense that both rely on forces to disperse the particulates. Hence, elongation is also the preferred mode of deformation when breaking up fluid droplets and threads, making the flow number, $\lambda$, an indispensable quantity when quantifying mixing processes that deal with such systems.

A parameter commonly used to determine whether a droplet will disperse is the capillary number defined by

$$Ca = \frac{\tau R}{\sigma_s} \qquad (6.12)$$

where $\tau$ is the flow induced or deviatoric stress, $R$ the characteristic dimension of the droplet and $\sigma_s$ the surface tension that acts on the drop. The capillary number is the ratio of flow stresses to droplet surface stresses. Droplet break-up occurs when a critical capillary number, $Ca_{crit}$, is reached. This break-up is clearly shown in Fig. 6.31 [1], which shows the disintegration of a Newtonian thread in a Newtonian matrix. Because of the continuously decreasing thread radius, the critical capillary number will be reached at some specific point in time. Due to the competing deviatoric stresses and surface forces, the cylindrical shape becomes unstable and small disturbances at the surface lead to a growth of capillary waves. These waves are commonly referred to as Rayleigh disturbances. Disturbances with various wavelengths form on the cylinder surface, but only those with a wavelength greater than the circumference $(2\pi R_0)$ of the thread lead to a monotonic decrease of the interfacial area.

Figure 6.32 [14] shows the critical capillary number as a function of viscosity ratio, $\phi$, and flow type, described by the mixing parameter $\lambda$. For a viscosity ratio of 1 the critical capillary number is of order 1 [1]. Distributive mixing is implied when $Ca$ is much greater than $Ca_{crit}$ since the
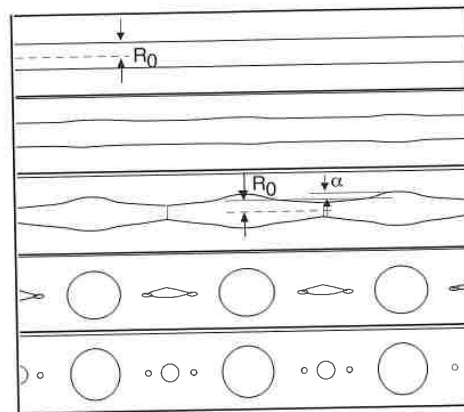
**Figure 6.31**   Disintegration of a Newtonian 0.35 mm diameter castor oil thread in a Newtonian silicon oil matrix. Redrawn from photographs taken every second.
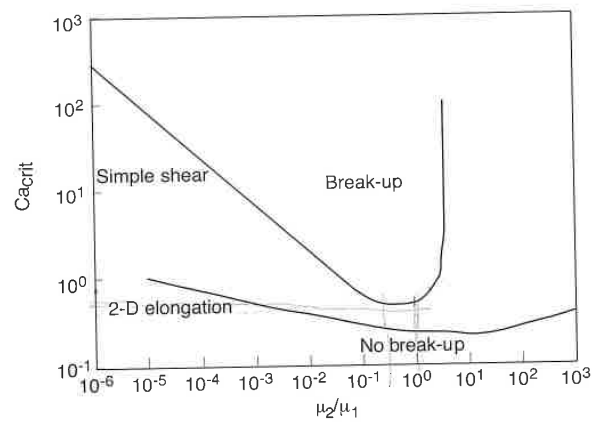


**Figure 6.32**   Critical capillary number for drop break-up as a function of viscosity ratio in a simple shear and a 2-D elongational flow.

interfacial stress is much smaller than shear stresses. For such a case the capillary waves which would cause droplet break-up would not develop. Dispersive mixing is implied when $Ca$ is close to the value of the critical $Ca$ or when interfacial stresses are almost equal to the deviatoric stresses causing droplet break-up. In addition, break-up can only occur if enough time is given for this to happen. The disturbance amplitude, $\alpha$, is assumed to grow exponentially as

$$\alpha = \alpha_0 e^{qt} \tag{6.13}$$

where $\alpha_0$ is the initial disturbance amplitude, sometimes assumed to be 0.3% of the thread radius, and the growth rate $q$ defined by

$$q = \frac{\sigma_s \Omega}{2\eta_1 R_0} \tag{6.14}$$

In the above equation $R_0$ represents the initial radius of the thread and $\Omega$ a dimensionless growth rate presented in Fig. 6.33 as a function of viscosity ratio for the wavelength disturbance amplitude which leads to break-up. The time required for break-up, $t_b$, can now be computed using the above equations as

$$t_b = \frac{1}{q}\ln\left(\alpha_b / \alpha_0\right) \tag{6.15}$$



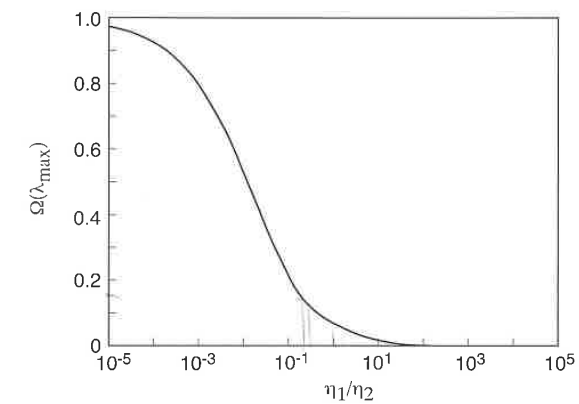**Figure 6.33**   Dominant growth rate of interfacial disturbances as a function of viscosity ratio.

where $\alpha_b$ is the amplitude at break-up which for a sinusoidal disturbance is $\alpha_b = \sqrt{2/3} R_0$. The break-up time decreases as the critical capillary number is exceeded. The reduced break-up time $t_b^*$ can be approximated using [14]

$$t_b^* = t_b \left(\frac{Ca}{Ca_{crit}}\right)^{-0.63} \tag{6.16}$$

As mentioned before, surface tension plays a large role in the mixing process, especially when dealing with dispersive mixing, when the capillary number approaches its critical value. Because of the stretching of the interfacial area, due to distributive mixing, the local radii of the suspended components decrease, causing surface tension to play a role in the process. It should also be noted that once the capillary number assumes a value below the critical $Ca$, only slight deformations occur and internal circulation maintains an equilibrium elliptical droplet shape in the flow field as schematically represented in Fig. 6.34. At that point, the mixing process reduces to the distribution of the dispersed droplets. Analytical and numerical investigations of stable droplet shapes, for $Ca < Ca_{crit}$ in simple shear flow have been made by several investigators [15–17]. Figure 6.32 also shows that at viscosity ratios above 4 simple shear flows are not able to break-up fluid droplets.
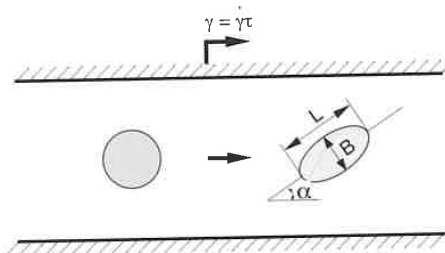


Figure 6.34    Schematic of droplet deformation in simple shear flow.

### 6.2.3    Mixing Devices

The final properties of a polymer component are heavily influenced by the blending or mixing process that takes place during processing or as a separate step in the manufacturing process. As mentioned earlier, when measuring the quality of mixing it is also necessary to evaluate the efficiency of mixing. For example, the amount of power required to achieve the highest mixing quality for a blend may be unrealistic or unachievable. This section presents some of the most commonly used mixing devices encountered in polymer processing.

In general, mixers can be classified in two categories: internal batch mixers and continuous mixers. Internal batch mixers, such as the Banbury type mixer, are the oldest type of mixing devices in polymer processing and are still widely used in the rubber compounding industry. Industry often also uses continous mixers because they combine mixing in addition to their normal processing tasks. Typical examples are single and twin screw extruders that often have mixing heads or kneading blocks incorporated into their system.

#### 6.2.3.1    Static Mixers

Static mixers or motionless mixers are pressure-driven continuous mixing devices through which the melt is pumped, rotated, and divided, leading to effective mixing without the need for movable parts and mixing heads. One of the most commonly used static mixers is the twisted tape static mixer schematically shown in Fig. 6.35. Figure 6.36 [19] shows computed streamlines relative to the twist in the wall. As the fluid is rotated by the dividing wall, the interfaces between the fluids increase. The interfaces are then re-oriented by $90^\circ$ once the material enters a new section. Figure 6.36 shows a typical trajectory of a particle as it travels on a streamline in section $N$ of the static mixer and ends on a different streamline after entering the next section, $N+1$. The stretching-re-orientation sequence is repeated until the number of striations is so high that a seemingly homogeneous mixture is achieved. Figure 6.37 shows a sequence of cuts down a Kenics static mixer[5]. From the figure it can be seen that the number of striations increases from section to section by 2, 4, 8, 16, 32, etc., which can be computed using

$$N = 2^n \qquad (6.17)$$

where $N$ is the number of striations and $n$ is the number of sections in the mixer.
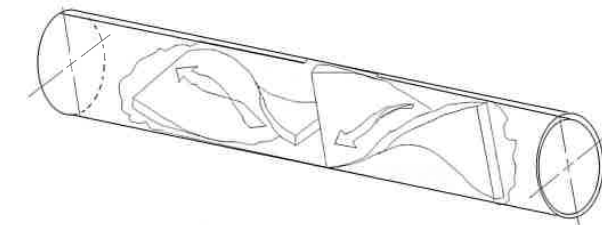


Figure 6.35    Schematic diagram of a Kenics static mixer.

---

[5]    Courtesy Chemineer, Inc., North Andover, Massachusetts.
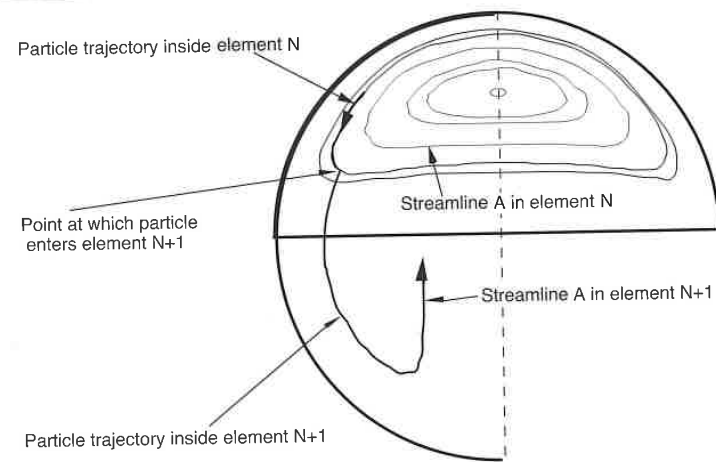
**Figure 6.36**    Simulated streamlines inside a Kenics static mixer section.



**Figure 6.37**    Experimental progression of the layering of colored resins in a Kenics static mixer.

### 6.2.3.2   Banbury Mixer

The Banbury type mixer, schematically shown in Fig. 6.38, is perhaps the most commonly used internal batch mixer. Internal batch mixers are high intensity mixers that generate complex shearing and elongational flows which work especially well in the dispersion of solid particle agglomerates within polymer matrices. One of the most common applications for high intensity internal batch mixing is the break-up of carbon black agglomerates into rubber compounds. The dispersion of agglomerates is strongly dependent on mixing time, rotor speed, temperature, and rotor blade geometry [18]. Figure 6.39 [15, 21] shows the fraction of undispersed carbon black as a function of time in a Banbury mixer at 77 rpm and 100 °C. The broken line in the figure represents the fraction of particles smaller than 500 nm.
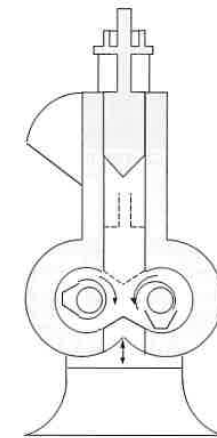


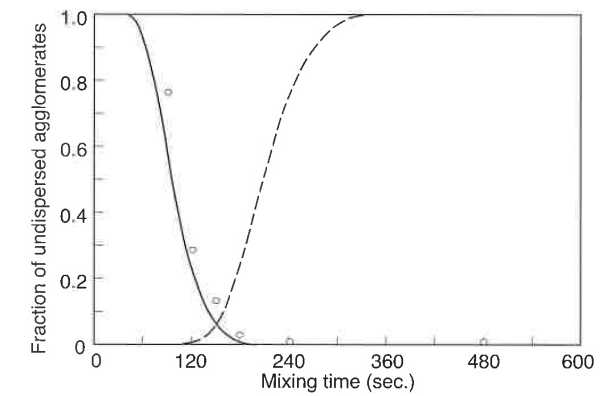**Figure 6.38**    Schematic diagram of a Banbury type mixer.



**Figure 6.39**    Fraction of undispersed carbon black, of size above 9 μm, as a function of mixing time inside a Banbury mixer. (O) denotes experimental results and solid line theoretical predictions. Broken line denotes the fraction of aggregates of size below 500 nm.

### 6.2.3.3    Mixing in Single Screw Extruders

Mixing caused by the cross-channel flow component can be further enhanced by introducing pins in the flow channel. These pins can either sit on the screw as shown in Fig. 6.40 [22] or on the barrel as shown in Fig. 6.41 [23]. The extruder with the adjustable pins on the barrel is generally referred to as QSM-extruder[6]. In both cases the pins disturb the flow by re-orienting the surfaces between fluids and by creating new surfaces by splitting the flow. Figure 6.42 presents a photograph of the channel contents of a QSM-extruder[7]. The photograph clearly demonstrates the re-orientation of the layers as the material flows past the pins. The pin type extruder is especially necessary for the mixing of high viscosity materials such as rubber compounds; thus, it is often called a cold feed rubber extruder. This machine is widely used in the production of rubber profiles of any shape and size.
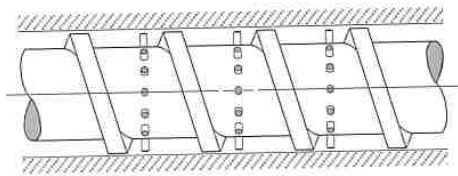


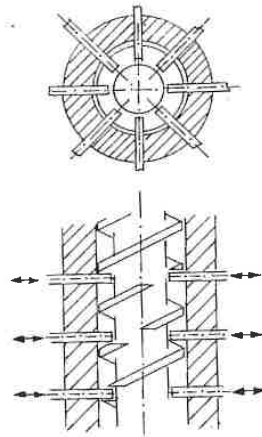**Figure 6.40**    Pin mixing section on the screw of a single screw extruder.



**Figure 6.41**    Pin barrel extruder (Quer Strom Misch Extruder).

---

6    QSM comes from the German *Quer Strom Misch* which translates into cross-flow mixing.
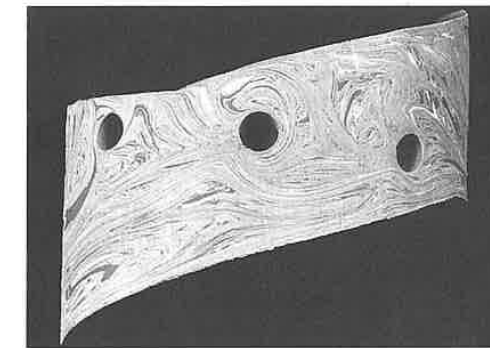7    Courtesy of Paul Troester Maschinenfabrik, Hannover, Germany.



**Figure 6.42**    Photograph of the unwrapped channel contents of a pin barrel extruder.

For lower viscosity fluids, such as thermoplastic polymer melts, the mixing action caused by the cross-flow is often not sufficient to re-orient, distribute, and disperse the mixture, making it necessary to use special mixing sections. Re-orientation of the interfaces between primary and secondary fluids and distributive mixing can be induced by any disruption in the flow channel. Figure 6.43 [22] presents commonly used distributive mixing heads for single screw extruders. These mixing heads introduce several disruptions in the flow field which have proven to perform well in mixing.
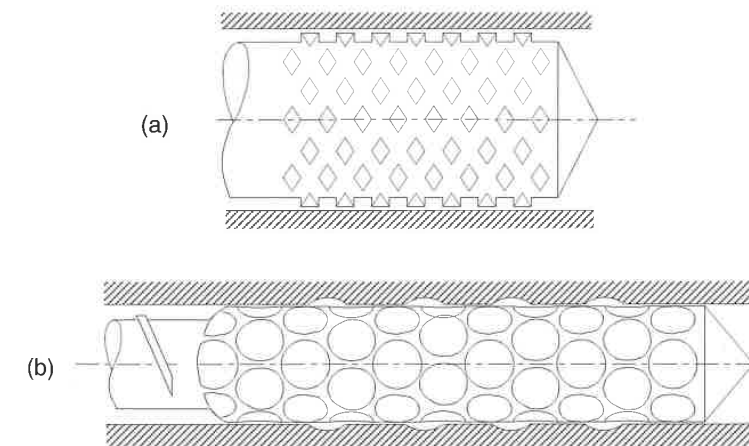


**Figure 6.43**    Distributive mixing sections: (a) Pineapple mixing section, (b) cavity transfer mixing section.

As mentioned earlier, dispersive mixing is required when breaking down particle agglomerates or when surface tension effects exist between primary and secondary fluids in the mixture. To disperse such systems, the mixture must be subjected to large stresses. Barrier-type screws are often sufficient to apply high stresses to the polymer melt. However, more intensive mixing can be applied by using a mixing head. When using barrier-type screws or a mixing head as shown in Fig. 6.44 [22] the mixture is forced through narrow gaps, causing high stresses in the melt. It should be noted that dispersive as well as distributive mixing heads result in a resistance to the flow, which results in viscous heating and pressure losses during extrusion.
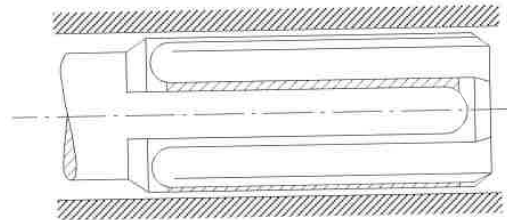


**Figure 6.44**     Maddock or Union Carbide mixing section.

#### 6.2.3.4   Cokneader

The cokneader is a single screw extruder with pins on the barrel and a screw that oscillates in the axial direction. Figure 6.45 shows a schematic diagram of a cokneader. The pins on the barrel practically wipe the entire surface of the screw, making it the only self-cleaning single-screw extruder. This results in a reduced residence time, which makes it appropriate for processing thermally sensitive materials. The pins on the barrel also disrupt the solid bed creating a dispersed melting [24] which improves the overall melting rate while reducing the overall temperature in the material.
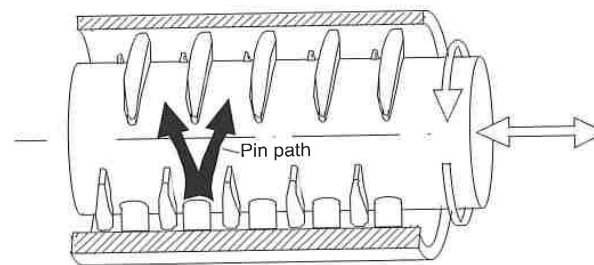


**Figure 6.45**     Schematic diagram of a cokneader.

A simplified analysis of a cokneader gives a number of striations per $L/D$ of [25]

$$N_s = 2^{12} \qquad\qquad (6.18)$$

which means that over a section of 4D the number of striations is $2^{12}(4) = 2.8E14$. A detailed discussion on the cokneader is given by Rauwendaal [25] and Elemans [26].
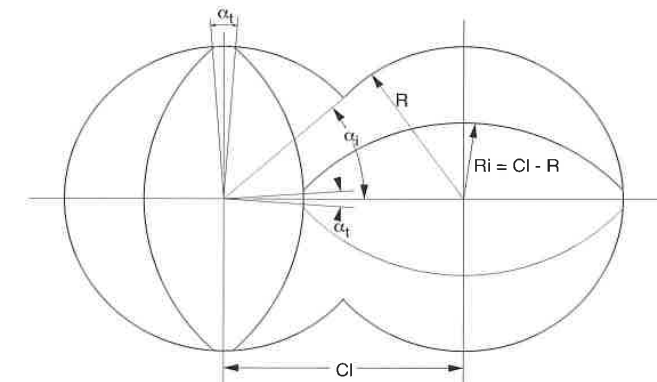


**Figure 6.46**     Geometry description of a double-flighted, co-rotating, self-cleaning, twin screw extruder.

#### 6.2.3.5   Twin Screw Extruders

In the past two decades, twin screw extruders have developed into the best available continuous mixing devices. In general, they can be classified into intermeshing or non-intermeshing, and co-rotating or counter-rotating twin screw extruders[8]. The intermeshing twin screw extruders render a self-cleaning effect which evens-out the residence time of the polymer in the extruder. The self-cleaning geometry for a co-rotating double flighted twin screw extruder is shown in Fig. 6.46. The main characteristic of this type of configuration is that the surfaces of the screws are sliding past each other, constantly removing the polymer that is stuck to the screw.

In the last two decades, the co-rotating twin screw extruder systems have established themselves as efficient continuos mixers, including reactive extrusion. In essence, the co-rotating systems have a high pumping efficiency caused by the double transport action of the two screws. Counter-rotating

---

[8]   A complete overview of twin screw extruders is given by White, J.L., *Twin Screw Extrusion-Technology and Principles*, Hanser Publishers, Munich, (1990).

systems generate high stresses because of the calendering action between the screws, making them efficient machines to disperse pigments and lubricants[9].

Several studies have been performed to evaluate the mixing capabilities of twin screw extruders. Noteworthy are two recent studies performed by Lim and White [27, 28] that evaluated the morphology development in a 30.7 mm diameter screw co-rotating [17] and a 34 mm diameter screw counter-rotating [18] intermeshing twin screw extruder. In both studies they dry-mixed 75/25 blend of polyethylene and polyamide 6 pellets that were fed into the hopper at 15 kg/h. Small samples were taken along the axis of the extruder and evaluated using optical and electron microscopy.

Figure 6.47 shows the morphology development along the screws at positions marked A, B, C, and D for a counter-rotating twin screw extruder configuration without special mixing elements. The dispersion of the blend becomes visible by the reduction of the characteristic size of the polyamide 6 phase. Figure 6.48 is a plot of the weight average and number average domain size of the polyamide 6 phase along the screw axis. The weight average phase size at the end of the extruder was measured to be 10 μm and the number average 6 μm. By replacing sections of the screw with one kneading-pump element and three special mixing elements, the final weight average phase size was reduced to 2.2 μm and the number average to 1.8 μm, as shown in Fig. 6.49.
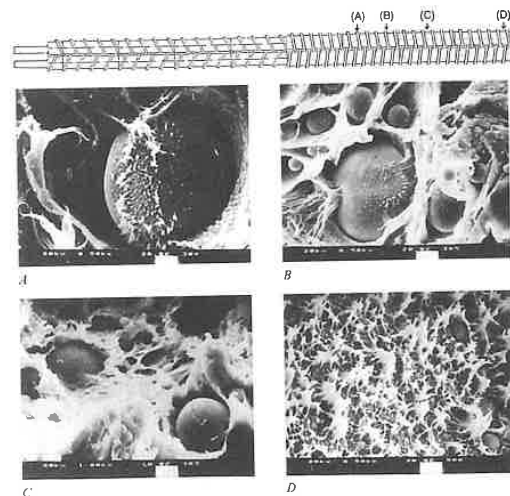


**Figure 6.47**    Morphology development inside a counter-rotating twin screw extruder.

9    There seems to be considerable disagreement about co- versus counter-rotating twin screw extruders between different groups in the polymer processing industry and academic community.
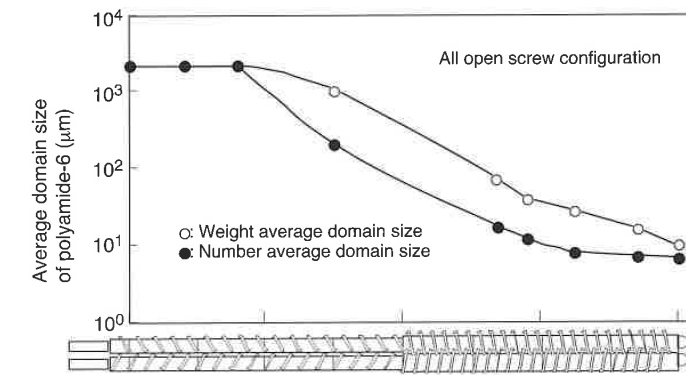


**Figure 6.48**    Number and weight average of polyamide 6 domain sizes along the screws for a counter-rotating twin screw extruder.
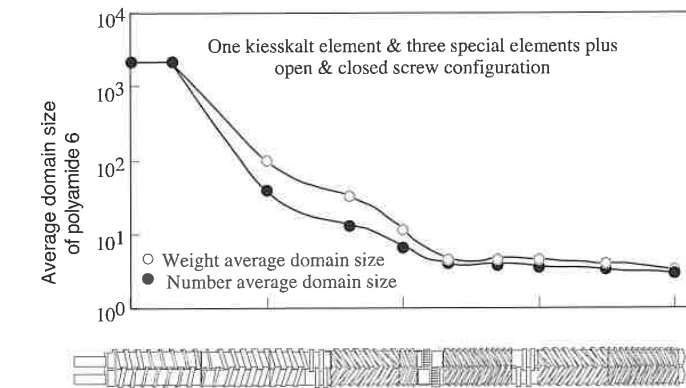


**Figure 6.49**    Number and weight average of polyamide 6 domain sizes along the screws for a counter-rotating twin screw extruder with special mixing elements.

Using a co-rotating twin screw extruder with three kneading disk blocks, a final morphology with polyamide 6 weight average phase sizes of 2.6 μm was achieved. Figure 6.50 shows the morphology development along the axis of the screws. When comparing the outcome of both counter-rotating (Fig. 6.49) and co-rotating (Fig. 6.50), it is clear that both extruders achieve a similar final mixing quality. However, the counter-rotating extruder achieved the final morphology much earlier in the screw than the co-rotating twin screw

extruder. A possible explanation for this is that the blend traveling through the counter-rotating configuration melted earlier than in the co-rotating geometry. In addition the phase size was slightly smaller, possibly due to the calendering effect between the screws in the counter-rotating system.
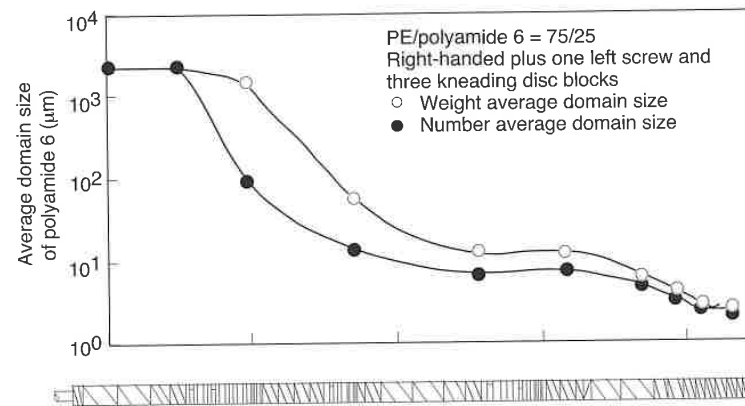


**Figure 6.50**   Number and weight average of polyamide 6 domain sizes along the screws for a co-rotating twin screw extruder with special mixing elements.

### 6.2.4  Energy Consumption During Mixing

Energy consumption is of extreme importance when assessing and comparing various mixing devices. High energy requirements for optimal mixing mean high costs and expensive equipment. The power consumption per unit volume of a deforming Newtonian fluid is given by [29]

$$p = 2\mu\left[\left(\frac{\partial v_x}{\partial x}\right)^2 + \left(\frac{\partial v_y}{\partial y}\right)^2 + \left(\frac{\partial v_z}{\partial z}\right)^2\right] + \mu\left[\left(\frac{\partial v_x}{\partial y} + \frac{\partial v_y}{\partial x}\right)^2 + \left(\frac{\partial v_y}{\partial z} + \frac{\partial v_z}{\partial y}\right)^2 + \left(\frac{\partial v_x}{\partial z} + \frac{\partial v_z}{\partial x}\right)^2\right] \quad (6.19)$$

Erwin [30] used the above equation to assess the energy input requirements for different types of mixing flows: simple shear, pure shear, and extensional flows. Table 6.4 presents flow fields and energy requirements for various flows described by Erwin [30]. For example, to produce a mixture such that $A/A_0 = 10^4$ in time $t_0 = 100$ s, for a fluid with viscosity $\mu = 10^4 \text{Pa} - \text{s}$, in a mixer which deforms the fluid with an elongational flow, one needs 96 kJ/m$^3$ of energy input. Since the flow is steady, this requires a power input of 0.96 kW/m$^3$ for 100 s. In a mixer that deforms the fluid in a biaxial extensional flow the energy

required is 24 kJ/m$^3$ with 0.24 kW/m$^3$ of power input. For the same amount of mixing, a mixer which deforms the fluid in pure shear requires an energy input of 40 kJ/m$^3$ or a steady power input of 0.4 kW/m$^3$ for 100 s. A device that deforms the fluid in simple shear requires a total energy input of 4x107 kJ/m$^3$ or a steady power input of 40,000 kW/m$^3$ for a 100 second period to achieve the same amount of mixing.

**Table 6.4**   Energy Input Requirements for Various Flow Mixers

| Flow type | Flow field | Power | Energy input |
|---|---|---|---|
| Extensional flow (elongational) | $v_x = Gx$ $v_y = -Gy/2$ $v_z = -Gz/2$ | $3\mu G^2$ | $\frac{12\mu}{t_0}\left(\ln\left(\frac{5A}{4A_0}\right)\right)^2$ |
| Extensional flow (biaxial) | $v_x = -Gx$ $v_y = Gy/2$ $v_z = Gz/2$ | $3\mu G^2$ | $\frac{3\mu}{t_0}\left(\ln\left(\frac{5A}{4A_0}\right)\right)^2$ |
| Pure shear | $v_x = -hx$ $v_y = -Hy$ $v_z = 0$ | $2\mu(h^2 + H^2)$ | $\frac{4\mu}{t_0}\left(\ln\left(2\frac{A}{A_0}\right)\right)^2$ |
| Simple shear | $v_x = -Gy$ $v_y = 0$ $v_z = 0$ | $\mu G^2$ | $\frac{4\mu}{t_0}\left(\frac{A}{A_0}\right)^2$ |

From this it is clear that, in terms of energy and power consumption, simple shear flows are significantly inferior to extensional flows.

### 6.2.5  Mixing Quality and Efficiency

In addition to the flow number, strain, and capillary number, several parameters have been developed by various researchers in the polymer industry to quantify the efficiency of the mixing processes. Some have used experimentally measured parameters while others have used mixing parameters which are easily calculated from computer simulation.

A parameter used in visual experiments is the batch homogenization time (BHT). This parameter is defined as the time it takes for a material to become homogeneously colored inside the mixing chamber after a small sample of colored pigment is placed near the center of the mixer. A downfall to this technique is that the observed homogenized time can be quite subjective.

To describe the state of the dispersion of fillers in a composite material, Suetsugu [31] used a dispersion index defined as:

$$\text{Dispersion index} = 1 - \phi_a \tag{6.20}$$

where $\phi_a$ is a dimensionless area that the agglomerates occupy and is defined by:

$$\phi_a = \frac{\pi}{4 A \phi} \sum d_i^2 n_i \tag{6.21}$$

where $A$ is the area under observation, $\phi$ the volume fraction of the filler, $d_i$ the diameter of the agglomerate and $n_i$ the number agglomerates. The dispersion index ranges between 0 for the worst case of dispersion and 1 where no agglomerates remain in the system.

A commonly used method to analyze the mixing capabilities of the extruder is the residence time distribution (RTD). It is calculated by monitoring the output of the extruder with the input of a secondary component. Two common response techniques are the step input response and the pulse input response shown in Fig. 6.51 [22]. The response of the input gives information on the mixing and conveying performance of the extruder. The RTD response to a pulse input for an ideal mixing situation is shown in Fig. 6.52. The figure shows a quick response to the input with a constant volume fraction of the secondary component until there is no material left.
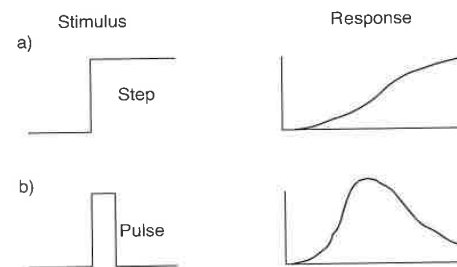


**Figure 6.51**    Step input and pulse input residence time distribution responses.
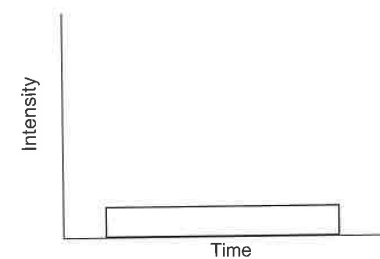


**Figure 6.52**    Ideal residence time distribution response to a pulse input.

By the use of a computer simulation, velocities, velocity gradients, and particle tracking can be computed with some degree of accuracy — depending on the computational method and assumptions made. Using information from a computer simulation, several methods to quantify mixing have been developed. Poincaré sections are often used to describe the particle paths during the mixing process. The Poincaré section shows the trajectory of several particles during the mixing process. They can be very useful in locating stagnation points, recirculation regions, and detecting symmetric flow patterns where no exchange exists across the planes of symmetry — all issues that hinder mixing.

### 6.2.6  Plasticization

Solvents, commonly referred to as plasticizers, are sometimes mixed into a polymer to dramatically alter its rheological and/or mechanical properties. Plasticizers are used as a processing aid since they have the same impact as raising the temperature of the material. Hence, the lowered viscosities at lower temperatures reduce the risk of thermal degradation during processing. For example, cellulose nitrite would thermally degrade during processing without the use of a plasticizer.

Plasticizers are more commonly used to alter a polymer's mechanical properties such as stiffness, toughness, and strength. For example, adding a plasticizer such as dioctylphthalate (DOP) to PVC can reduce its stiffness by three orders of magnitude and lower its glass transition temperature to -35 °C. In fact, a highly plasticized PVC is rubbery at room temperature. Table 6.5 [45] presents some common plasticizers with the polymers they plasticize, and their applications.

Since moisture is easily absorbed by polyamides, slightly modifying their mechanical behavior, it can be said that water acts as a plasticizing agent with these materials. Figure 6.53 shows the equilibrium water content for polyamide 6 and 66 as a function of the ambient relative humidity[10]. This moisture absorption causes the polyamide to expand or swell as shown in Fig. 6.54[11].

---

[10]    Courtesy of Bayer AG, Germany.
[11]    *Ibid.*

**Table 6.5**    Commercial Plasticizers and Their Applications

| Plasticizer | Polymers | Plasticizer type |
|---|---|---|
| Di-octyl phthalate (DOP) | Polyvinyl chloride and copolymers | General purpose, primary plasticizer |
| Tricresyl phosphate (TCP) | Polyvinyl chloride and copolymers, cellulose acetate, cellulose nitrate | Flame retardant, primary plasticizer |
| Di-octyl adipate (DOA) | Polyvinyl chloride, cellulose acetate, butyrate | Low temperature plasticizer |
| Di-octyl sebacate (DOS) | Polyvinyl chloride , cellulose acetate, butyrate | Secondary plasticizer |
| Adipic acid polyesters (MW = 1500-3000) | Polyvinyl chloride | Non-migratory secondary plasticizer |
| Sebacic acid polyesters (MW = 1500-3000) | Polyvinyl chloride | Non-migratory secondary plasticizer |
| Chlorinated paraffins (%CI = 40-70) (MW = 600-1000) | Most polymers | Flame retardant, plasticizer extenders |
| Bi- and terphenyls (also hydrogenated) | Aromatic polyesters | Various |
| N-ethyl-toluene sulphonamide | Polyamides | General purpose, primary plasticizer |
| Sulphonamide-formaldehyde resins | Polyamides | Non-migratory secondary plasticizers |
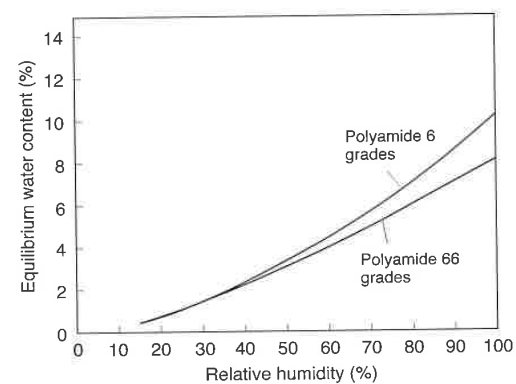


**Figure 6.53**    Equilibrium water content as a function of relative humidity for polyamide 6 and polyamide 66.
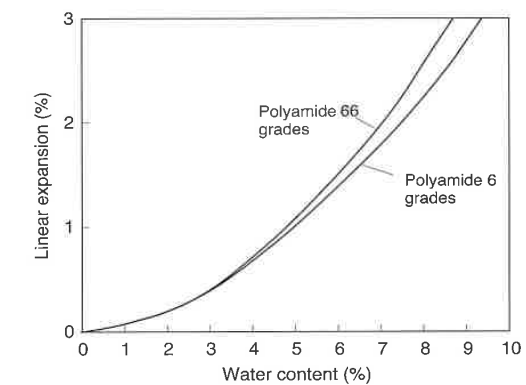


**Figure 6.54**    Linear expansion as a function of water content for polyamide 6 and polyamide 66.

The behavior of polymers toward solvents depends in great part on the nature of the solvent and on the structure of the polymer molecules. If the basic building block of the macromolecule and the solvent molecule are the same or of similar nature, then the absorption of a solution will lead to swelling. If a sufficient amount is added, the polymer will dissolve  in the solvent. Crystalline regions of a semi-crystalline thermoplastic are usually not affected by solvents, whereas amorphous regions are easily penetrated. In addition, the degree of cross-linking in thermosets and elastomers has a great influence on whether a material can be permeated by solvents. The shorter the distances between the linked molecules, the less solvent molecules can permeate and give mobility to chain segments. While elastomers can swell in the presence of a solvent, highly cross-linked thermosets do not swell or dissolve.

The amount of solvent that is absorbed depends not only on the chemical structure of the two materials but also on the temperature. Since an increase in temperature reduces the covalent forces of the polymer, solubility becomes higher. Although it is difficult to determine the solubility of polymers, there are some rules to estimate it. The simplest rule is: same dissolves same (i.e., when both—polymer and solvent—have the same valence forces, solubility exists).

The solubility of a polymer and a solvent can be addressed from a thermodynamic point of view using the familiar Gibbs free energy equation

$$\Delta G = \Delta H - T\Delta S \tag{6.22}$$

where $\Delta G$ is the change in free energy, $\Delta H$ is the change in enthalpy, $\Delta S$ the change in entropy and $T$ the temperature. If $\Delta G$ in Eq. 6.22 is negative

solubility, is possible. A positive $\Delta H$ suggests that polymer and the solvent do not "want" to mix, which means solubility can only occur if $\Delta H < T \Delta S$. On the other hand, $\Delta H \approx 0$ implies that solubility is the natural lower energy state. Since the entropy change when dissolving a polymer is very small, the determining factor if a solution will occur or not is the change in enthalpy, $\Delta H$. Hildebrand and Scott [46] proposed a useful equation that estimates the change in enthalpy during the formation of a solution. The Hildebrand equation is stated by

$$\Delta H = V\left(\left(\frac{\Delta E_1}{V_1}\right)^{1/2} - \left(\frac{\Delta E_2}{V_2}\right)^{1/2}\right)^2 \phi_1 \phi_2 \qquad (6.23)$$

where $V$ is the total volume of the mixture, $V_1$ and $V_2$ the volumes of the solvent and polymer, $\Delta E_1$ and $\Delta E_2$ their energy of evaporation and, $\phi_1$ and $\phi_2$ their volume fractions. Equation 6.23 can be simplified to

$$\Delta H = V\left(\delta_1 - \delta_2\right)^2 \phi_1 \phi_2 \qquad (6.24)$$

where $\delta$ is called the solubility parameter and is defined by

$$\delta = \left(\frac{\Delta E}{V}\right)^{1/2} \qquad (6.25)$$

If the solubility parameter of the substances are nearly equal they will dissolve. A rule-of-thumb can be used that if $|\delta_1 - \delta_2| < 1$ $(cal/cm^3)^{1/2}$ solubility will occur [47]. The units $(cal/cm^3)^{1/2}$ are usually referred to as Hildebrands. Solubility parameters for various polymers are presented in Table 6.6 [48], and for various solvents in Table 6.7 [48].

Figure 6.55 [49] shows a schematic diagram of swelling and dissolving behavior of cross-linked and uncross-linked polymers as a function of the solubility or *solubility parameter*, $\delta_s$, of the solvent. When the solubility parameter of the polymer and the solvent approach each other, the uncross-linked polymer becomes unconditionally soluble. However, if the same polymer is cross-linked then it is only capable of swelling. The amount of swelling depends on the degree of cross-linking.

**Table 6.6**  Solubility Parameter for Various Polymers

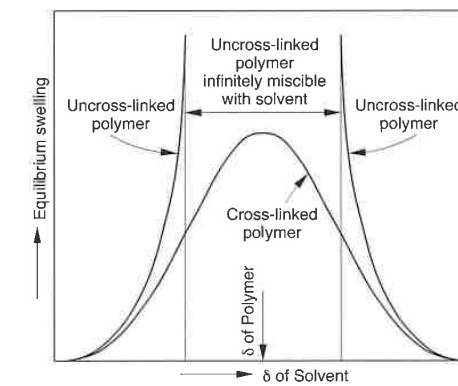| Polymer | $\delta \left(cal/cm^3\right)^{1/2}$ |
|---|---|
| Polytetrafluoroethylene | 6.2 |
| Polyethylene | 7.9 |
| Polypropylene | 8.0 |
| Polyisobutylene | 8.1 |
| Polyisoprene | 8.3 |
| Polybutadiene | 8.6 |
| Polystyrene | 9.1 |
| Poly(vinyl acetate) | 9.4 |
| Poly(methyl methacrylate) | 9.5 |
| Polycarbonate | 9.9 |
| Polysulphone | 9.9 |
| Poly(vinyl chloride) | 10.1 |
| Polyethylene terephthalate | 10.2 |
| Polyamide 6 | 11.0 |
| Cellulose nitrate | 11.5 |
| Poly(vinylidene chloride) | 12.2 |
| Polyamide 66 | 13.6 |
| Polyacrylonitrile | 15.4 |



**Figure 6.55**  Equilibrium swelling as a function of solubility parameter for cross-linked and uncross-linked polymers.

**Table 6.7**   Solubility Parameter of Various Plasticizers and Solvents

| Solvent | $\delta \left( cal/cm^3 \right)^{1/2}$ |
|---|---|
| Acetone | 10.0 |
| Benzene | 9.1 |
| Di-butoxyethyl phthalate (Dronisol) | 8.0 |
| n-butyl alcohol | 11.4 |
| Sec-butyl alcohol | 10.8 |
| Butyl stearate | 7.5 |
| Chlorobenzene | 9.6 |
| Cyclohexanone | 9.9 |
| Dibutyl phenyl phosphate | 8.7 |
| Dibutyl phthalate | 9.3 |
| Dibutyl sebacate | 9.2 |
| Diethyl phthalate | 10.0 |
| Di-n-hexyl phthalate | 8.9 |
| Diisodecyl phthalate | 7.2 |
| Dimethyl phthalate | 10.7 |
| Dioctyl adipate | 8.7 |
| Dioctyl phthalate (DOP) | 7.9 |
| Dioctyl sebacate | 8.6 |
| Dipropyl phthalate | 9.7 |
| Ethyl acetate | 9.1 |
| Ethyl alcohol | 12.7 |
| Ethylene glycol | 14.2 |
| 2-ethylhexyl diphenyl phosphate (Santicizer 141) | 8.4 |
| N-ethyl-toluenesulfonamide (Santicizer 8) | 11.9 |
| Hydrogenated terphenyl (HB-40) | 9.0 |
| Kronisol | 8.0 |
| Methanol | 14.5 |
| Methyl ethyl ketone | 9.3 |
| Nitromethane | 12.7 |
| n-propyl alcohol | 11.9 |
| Toluene | 8.9 |
| Tributyl phophate | 8.2 |
| 1,1,2-trichloro-1,2,2-trifluoroethane (freon 113) | 7.2 |
| Trichloromethane (chloroform) | 9.2 |
| Tricresyl phosphate | 9.0 |
| Triphenyl phosphate | 9.2 |
| Water | 23.4 |
| Xylene | 8.8 |

## 6.3   Injection Molding

Injection molding is the most important process used to manufacture plastic products. Today, more than one-third of all thermoplastic materials are injection molded and more than half of all polymer processing equipment is for injection molding. The injection molding process is ideally suited to manufacture mass-produced parts of complex shapes requiring precise dimensions. The process goes back to 1872 when the Hyatt brothers patented their stuffing machine to inject cellulose into molds. However, today's injection molding machines are mainly related to the reciprocating screw injection molding machine patented in 1956. A modern injection molding machine with its most important elements is shown in Fig. 6.56. The components of the injection molding machine are the plasticating unit, clamping unit, and the mold.
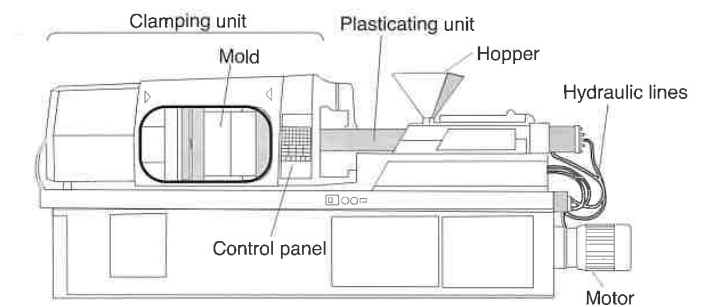


**Figure 6.56**   Schematic of an injection molding machine.

Today, injection molding machines are classified by the following international convention[12]

$$\text{Manufacturer } T / P$$

where $T$ is the clamping force in metric tons and $P$ is defined as

$$P = \frac{V_{max} p_{max}}{1000} \tag{6.26}$$

where $V_{max}$ is the maximum shot size in cm3 and $p_{max}$ is the maximum injection pressure in bar. The clamping forced T can be as low as 1 metric ton for small machines, and as high as 11,000 tons.

---

[12] The old US convention uses MANUFACTURER T-v where T is the clamping force in British tons and v the shot size in ounces of polystyrene.

### 6.3.1  The Injection Molding Cycle

The sequence of events during the injection molding of a plastic part, as shown in Fig. 6.57, is called the injection molding cycle. The cycle begins when the mold closes, followed by the injection of the polymer into the mold cavity. Once the cavity is filled, a holding pressure is maintained to compensate for material shrinkage. In the next step, the screw turns, feeding the next shot to the front of the screw. This causes the screw to retract as the next shot is prepared. Once the part is sufficiently cool, the mold opens and the part is ejected.
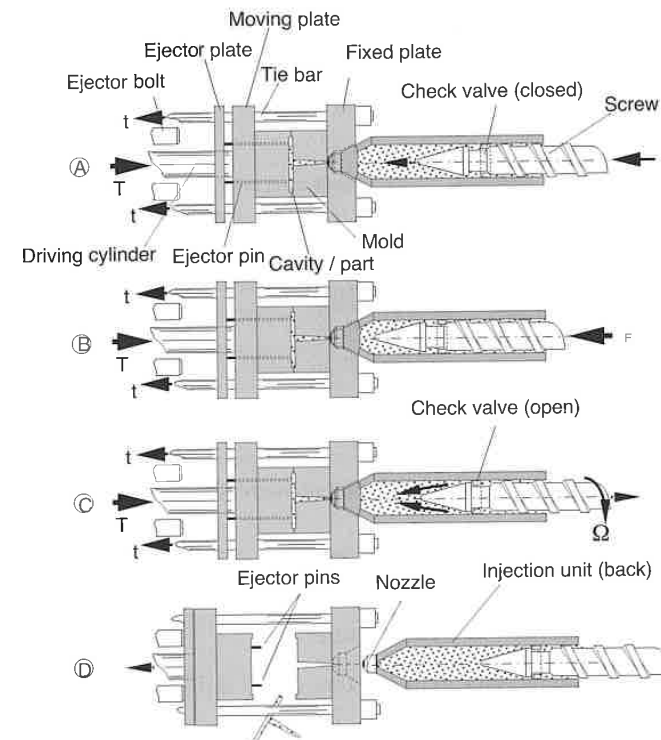


**Figure 6.57**    Sequence of events during an injection molding cycle.

Figure 6.58 presents the sequence of events during the injection molding cycle. The figure shows that the cycle time is dominated by the cooling of the part inside the mold cavity. The total cycle time can be calculated using

$$t_{\text{cycle}} = t_{\text{closing}} + t_{\text{cooling}} + t_{\text{ejection}} \tag{6.27}$$

where the closing and ejection times, $t_{\text{closing}}$ and $t_{\text{ejection}}$, can last from a fraction of second to a few seconds, depending on the size of the mold and machine. The cooling times, which dominate the process, depend on the maximum thickness of the part. The cooling time for a plate-like part of thickness $h$ can be estimated using

$$t_{\text{cooling}} = \frac{h^2}{\pi \alpha} \ln\left( \frac{8}{\pi^2} \frac{T_m - T_w}{T_D - T_w} \right) \tag{6.28}$$

and for a cylindrical geometry of diameter $D$ using

$$t_{\text{cooling}} = \frac{D^2}{23.14\alpha} \ln\left( 0.692 \frac{T_m - T_w}{T_D - T_w} \right) \tag{6.29}$$

where $T_m$ represents the temperature of the injected melt, $T_w$ the temperature of the mold wall, $T_D$ the average temperature at ejection, and $\alpha$ the thermal diffusivity.
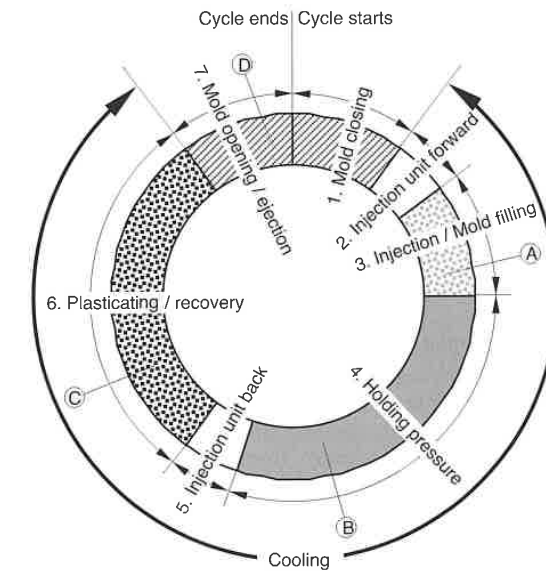


**Figure 6.58**    Injection molding cycle.

Using the average part temperature history and the cavity pressure history, the process can be followed and assessed using the PvT diagram as depicted in Fig. 6.59 [32-33]. To follow the process on the PvT diagram, we must transfer both the temperature and the pressure at matching times. The diagram reveals four basic processes: an isothermal injection (0-1) with pressure rising to the holding pressure (1-2), an isobaric cooling process during the holding cycle (2-3), an isochoric cooling after the gate freezes with a pressure drop to atmospheric (3-4), and then isobaric cooling to room temperature (4-5).
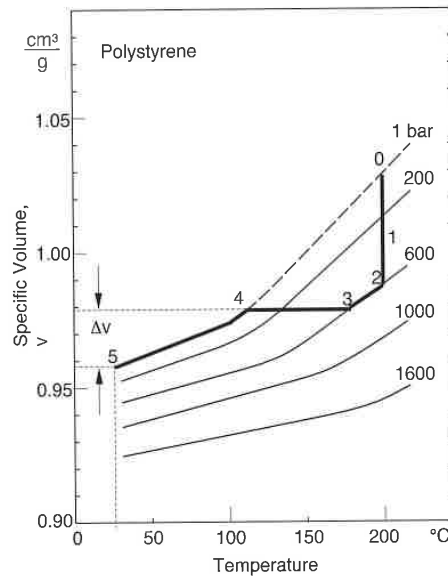


**Figure 6.59**   Trace of an injection molding cycle in a PvT diagram.

The point on the PvT diagram where the final isobaric cooling begins (4), controls the total part shrinkage, $\Delta v$. This point is influenced by the two main processing conditions - the melt temperature, $T_m$, and the holding pressure, $P_H$, as depicted in Fig. 6.60. Here the process in Fig. 6.59 is compared to one with a higher holding pressure. Of course, there is an infinite combination of conditions that render acceptable parts, bound by minimum and maximum temperatures and pressures. Figure 6.61 presents the molding diagram with all limiting conditions. The melt temperature is bound by a low temperature that results in a short shot or unfilled cavity and a high temperature that leads to material degradation. The hold pressure is bound by a low pressure that leads to excessive shrinkage or low part weight, and a high pressure that results in
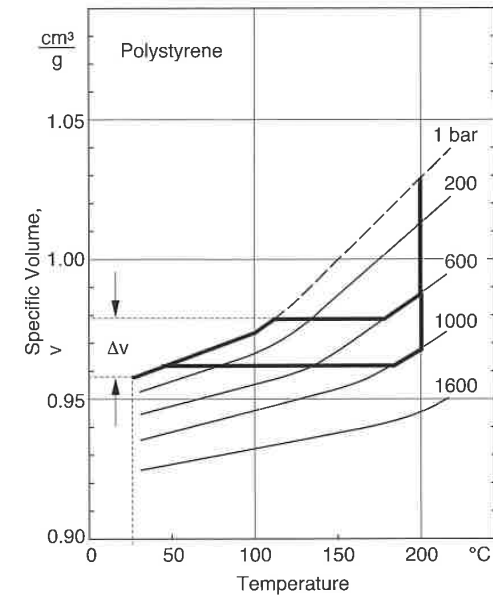
**Figure 6.60**   Trace of two different injection molding cycles in a PvT diagram.
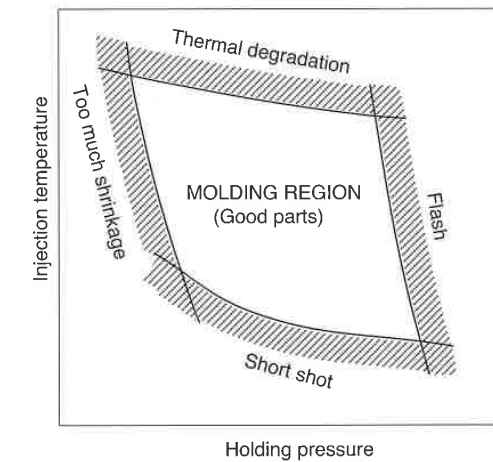


**Figure 6.61**   The molding diagram.

flash. Flash results when the cavity pressure force exceeds the machine clamping force, leading to melt flow across the mold parting line. The holding pressure determines the corresponding clamping force required to size the injection molding machine. An experienced polymer processing engineer can usually determine which injection molding machine is appropriate for a specific application. For the untrained polymer processing engineer, finding this appropriate holding pressure and its corresponding mold clamping force can be difficult.

With difficulty one can control and predict the component's shape and residual stresses at room temperature. For example, sink marks in the final product are caused by material shrinkage during cooling, and residual stresses can lead to environmental stress cracking under certain conditions [35].

Warpage in the final product is often caused by processing conditions that lead to asymmetric residual stress distributions through the part thickness. The formation of residual stresses in injection molded parts is attributed to two major coupled factors: cooling and flow stresses. The first and most important is the residual stress formed as a result of rapid cooling which leads to large temperature variations.

### 6.3.2    The Injection Molding Machine

#### 6.3.2.1    The Plasticating and Injection Unit

A plasticating and injection unit is shown in Fig. 6.62. The major tasks of the plasticating unit are to melt the polymer, to accumulate the melt in the screw chamber, to inject the melt into the cavity, and to maintain the holding pressure during cooling.
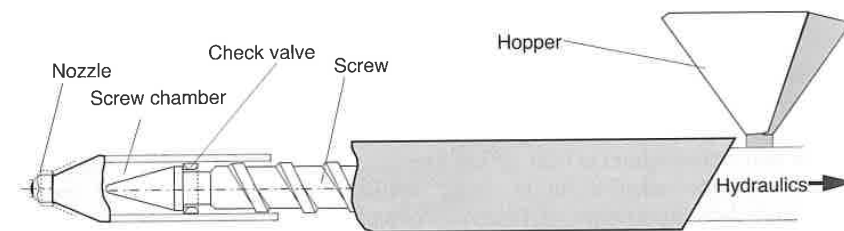


**Figure 6.62**    Schematic of the plasticating unit.

The main elements of the plasticating unit follow:

- Hopper
- Screw
- Heater bands
- Check valve
- Nozzle

The hopper, heating bands, and the screw are similar to a plasticating single screw extruder, except that the screw in an injection molding machine can slide back and forth to allow for melt accumulation and injection. This characteristic gives it the name reciprocating screw. For qquality purposes, the maximum stroke in a reciprocating screw should be set smaller than 3D.

Although the most common screw used in injection molding machines is the three-zone plasticating screw, two stage vented screws are often used to extract moisture and monomer gases just after the melting stage.

The check valve, or non-return valve, is at the end of the screw and enables it to work as a plunger during injection and packing without allowing polymer melt back flow into the screw channel. A check valve and its function during operation is depicted in Fig. 6.57, and in Fig. 6.62. A high quality check valve allows less then 5% of the melt back into the screw channel during injection and packing.

The nozzle is at the end of the plasticating unit and fits tightly against the sprue bushing during injection. The nozzle type is either open or shut-off. The open nozzle is the simplest, rendering the lowest pressure consumption.

#### 6.3.2.2    The Clamping Unit

The job of a clamping unit in an injection molding machine is to open and close the mold, and to close the mold tightly to avoid flash during the filling and holding. Modern injection molding machines have two predominant clamping types: mechanical and hydraulic.

Figure 6.63 presents a toggle mechanism in the open and closed mold positions. Although the toggle is essentially a mechanical device, it is actuated by a hydraulic cylinder. The advantage of using a toggle mechanism is that, as the mold approaches closure, the available closing force increases and the closing decelerates significantly. However, the toggle mechanism only transmits its maximum closing force when the system is fully extended.
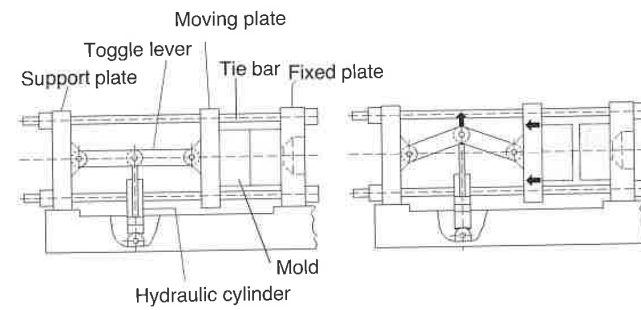
**Figure 6.63**    Clamping unit with a toggle mechanism.

Figure 6.64 presents a schematic of a hydraulic clamping unit in the open and closed positions. The advantages of the hydraulic system is that a maximum clamping force is attained at any mold closing position and that the system can take different mold sizes without major system adjustments.
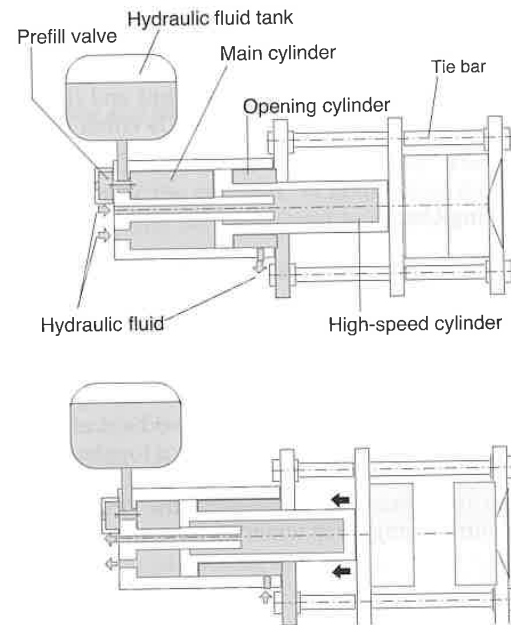


**Figure 6.64**    Hydraulic clamping unit.

### 6.3.2.3  The Mold Cavity

The central point in an injection molding machine is the mold. The mold distributes polymer melt into and throughout the cavities, shapes the part, cools the melt and, ejects the finished product. As depicted in Fig. 6.65, the mold is custom-made and consists of the following elements:

- Sprue and runner system
- Gate
- Mold cavity
- Cooling system (thermoplastics)
- Ejector system
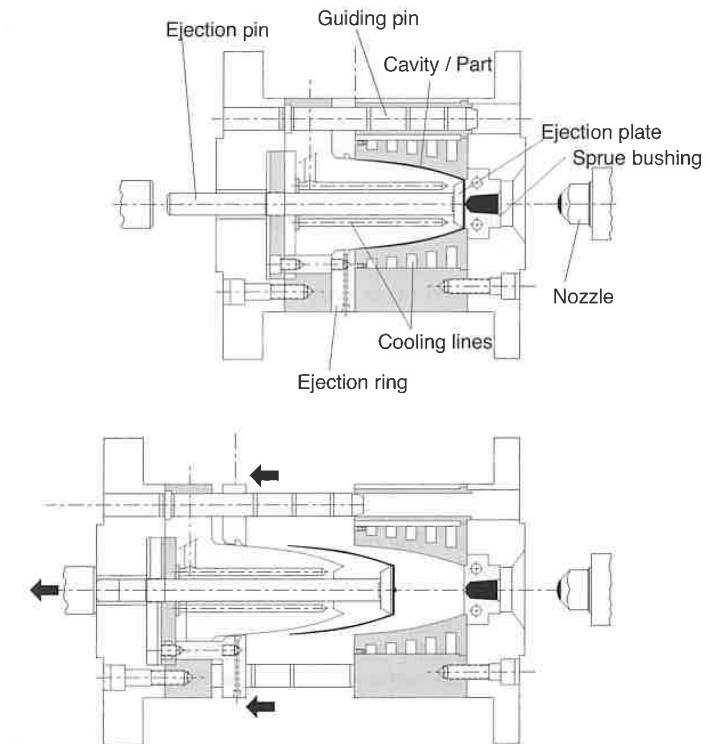


**Figure 6.65**    An injection mold.

During mold filling, the melt flows through the sprue and is distributed into the cavities by the runners, as seen in Fig. 6.66.



(a)

(b)
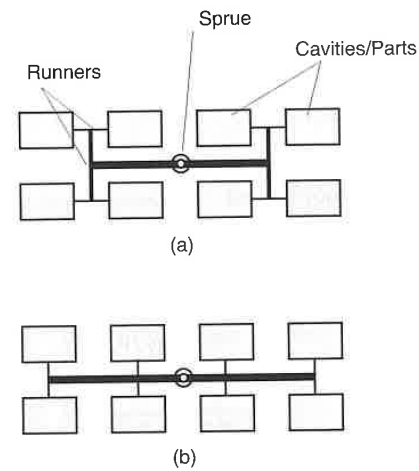
**Figure 6.66**   Schematic of different runner system arrangements.

The runner system in Fig. 6.66 (a) is symmetric where all cavities fill at the same time causing the polymer to fill all cavities in the same way. The disadvantage of this balanced runner system is that the flow paths are long, leading to high material and pressure consumption. On the other hand, the asymmetric runner system shown in Fig. 6.66 (b) leads to parts of different quality. Equal filling of the mold cavities can also be achieved by varying runner diameters. There are two types of runner systems - cold and hot. Cold runners are ejected with the part, and are trimmed after mold removal. The advantage of the cold runner is lower mold cost. The hot runner keeps the polymer at its melt temperature. The material stays in the runner system after ejection, and is injected into the cavity in the following cycle. There are two types of hot runner system: externally and internally heated. The externally heated runners have a heating element surrounding the runner that keeps the polymer isothermal. The internally heated runners have a heating element running along the center of the runner, maintaining a polymer melt that is warmer at its center and possibly solidified along the outer runner surface. Although a hot runner system considerably increases mold cost, its advantages include elimination of trim and lower pressures for injection.

When large items are injection molded, the sprue sometimes serves as the gate, as shown in Fig. 6.67. The sprue must be subsequently trimmed, often

requiring further surface finishing. On the other hand, a pin-type gate (Fig. 6.67) is a small orifice that connects the sprue or the runners to the mold cavity. The part is easily broken off from such a gate, leaving only a small mark that usually does not require finishing. Other types of gates, also shown in Fig. 6.67, are film gates, used to eliminate orientation, and disk or diaphragm gates for symmetric parts such as compact discs.
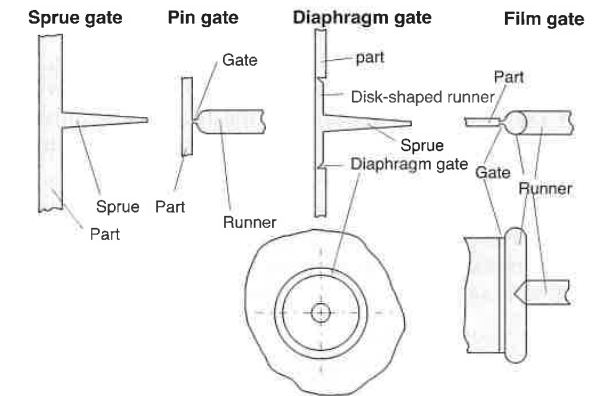


**Figure 6.67**   Schematic of different gating systems.

### 6.3.3   Related Injection Molding Processes

Although most injection molding processes are covered by the conventional process description discussed earlier in this chapter, there are several important molding variations including:

- Multi-color
- Multi-component
- Co-injection
- Gas-assisted
- Injection-compression

Multi-component injection molding occurs when two or more polymers, or equal polymers of different color, are injected through different runner and gate systems at different stages during the molding process. Each component is injected using its own plasticating unit. The molds are often located on a turntable. Multi-color automotive stop lights are molded this way.

In principle, the multi-component injection molding process is the same as the multi-color process. Here, either two incompatible materials are molded or

one component is cooled sufficiently so that the two components do not adhere to each other. For example, to mold a ball and socket system, the socket of the linkage is molded first. The socket component is allowed to cool somewhat and the ball part is injected inside it. This results in a perfectly movable system. This type of injection molding process is used to replace tedious assembling tasks and is becoming popular in countries where labor costs are high. In addition, today, a widely used application is the multi-component injection of a hard and a soft polymer such as polypropylene with a thermoplastic elastomer.

In contrast to multi-color and multi-component injection molding, co-injection molding uses the same gate and runner system. Here, the component that ends as the outer skin of the part is injected first, followed by the core component. The core component displaces the first and a combination of the no-slip condition between polymer and mold and the freezing of the melt creates a sandwiched structure as depicted in Fig. 6.68.

In principle, the gas-assisted injection molding process is similar to co-injection molding. Here, the second or core component is nitrogen, which is injected through a needle into the polymer melt, blowing the melt out of the way and depositing it against the mold surfaces.

Injection-compression molding first injects the material into a partially opened mold, and then squeezes the material by closing the mold. Injection-compression molding is used for polymer products that require a high quality surface finish, such as compact discs and other optically demanding components because it practically eliminates tangential molecular orientation.
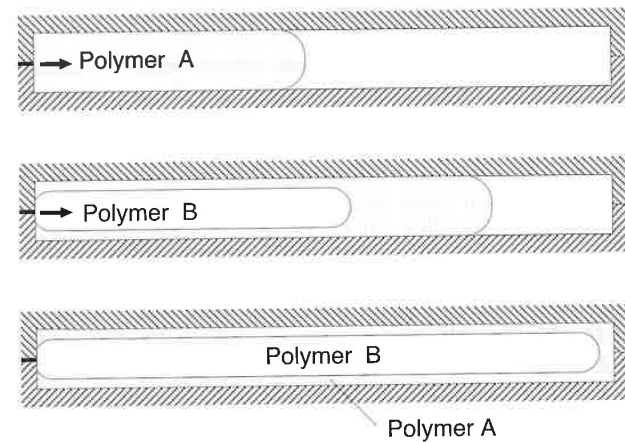


**Figure 6.68**    Schematic of the co-injection molding process.

## 6.4    Secondary Shaping

Secondary shaping operations such as extrusion blow molding, film blowing, and fiber spinning occur immediately after the extrusion profile emerges from the die. The thermoforming process is performed on sheets or plates previously extruded and solidified. In general, secondary shaping operations consist of mechanical stretching or forming of a preformed cylinder, sheet, or membrane.

### 6.4.1    Fiber Spinning

Fiber spinning is used to manufacture synthetic fibers. During fiber spinning, a filament is continuously extruded through an orifice and stretched to diameters of 100 μm and smaller. The process is schematically depicted in Fig. 6.69. The molten polymer is first extruded through a filter or *screen pack*, to eliminate small contaminants. The melt is then extruded through a spinneret, a die composed of multiple orifices. A spinneret can have between one and 10,000 holes. The fibers are then drawn to their final diameter, solidified, and wound onto a spool. The solidification takes place either in a water bath or by forced convection. When the fiber solidifies in a water bath, the extrudate undergoes an adiabatic stretch before cooling begins in the bath. The forced convection cooling, which is more commonly used, leads to a non-isothermal spinning process.
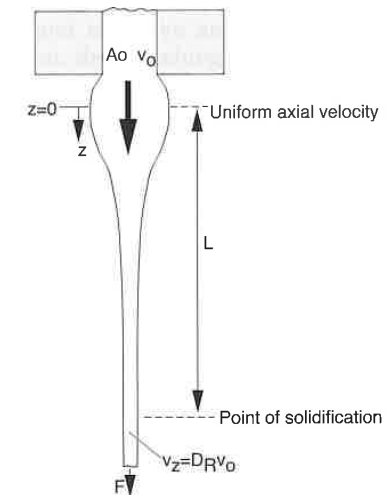


**Figure 6.69**    The fiber spinning process.

The drawing and cooling processes determine the morphology and mechanical properties of the final fiber. For example, ultra high molecular weight HDPE fibers with high degrees of orientation in the axial direction can have the stiffness of steel with today's fiber spinning technology.

Of major concern during fiber spinning are the instabilities that arise during drawing, such as brittle fracture, Rayleigh disturbances, and draw resonance. Brittle fracture occurs when the elongational stress exceeds the melt strength of the drawn polymer melt. The instabilities caused by Rayleigh disturbances are like those causing filament break-up during dispersive mixing as discussed in Chapter 5. Draw resonance appears under certain conditions and manifests itself as periodic fluctuations that result in diameter oscillation.

### 6.4.2    Film Production

#### 6.4.2.1    Cast Film Extrusion

In a cast film extrusion process, a thin film is extruded through a slit onto a chilled, highly polished, turning roll where it is quenched from one side. The speed of the roller controls the draw ratio and final film thickness. The film is then sent to a second roller for cooling of the other side. Finally, the film passes through a system of rollers and is wound onto a roll. A typical film casting process is depicted in Fig. 6.70 and 6.71. The cast film extrusion process exhibits stability problems similar to those encountered in fiber spinning [36].
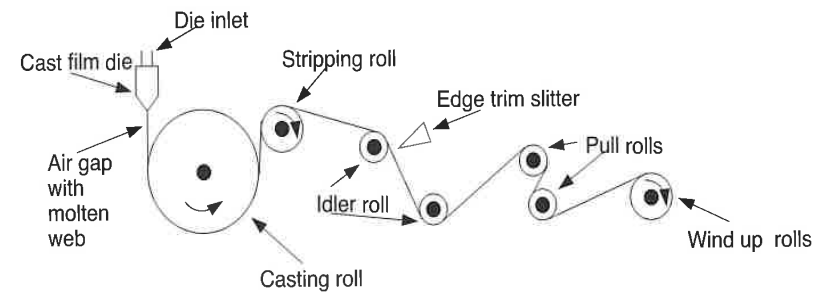


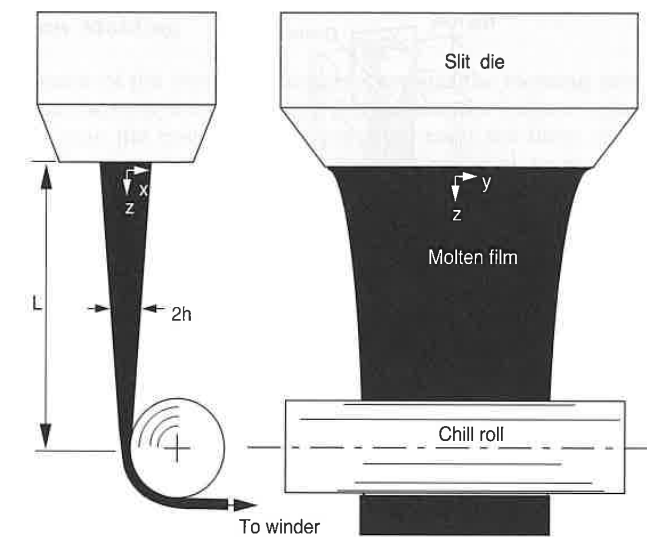Figure 6.70    Schematic of a film casting operation.

Figure 6.71    Film casting.

#### 6.4.2.2    Film Blowing

In film blowing, a tubular cross-section is extruded through an annular die, normally a spiral die, and is drawn and inflated until the freezing line is reached. Beyond this point, the stretching is practically negligible. The process is schematically depicted in Fig. 6.72 [37] and Fig. 6.73. The advantage of film blowing over casting is that the induced biaxial stretching renders a stronger and less permeable film. Film blowing is mainly used with less expensive materials such as polyolefins. Polymers with lower viscosity such as PA and PET are better manufactured using the cast film process.

The extruded tubular profile passes through one or two air rings to cool the material. The tube interior is maintained at a certain pressure by blowing air into the tube through a small orifice in the die mandrel. The air is retained in the tubular film, or bubble, by collapsing the film well above its freeze-off point and tightly pinching it between rollers. The size of the tubular film is calibrated between the air ring and the collapsing rolls.
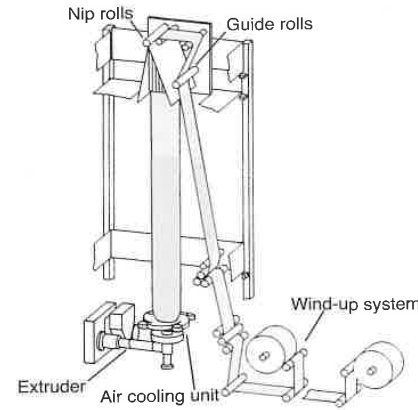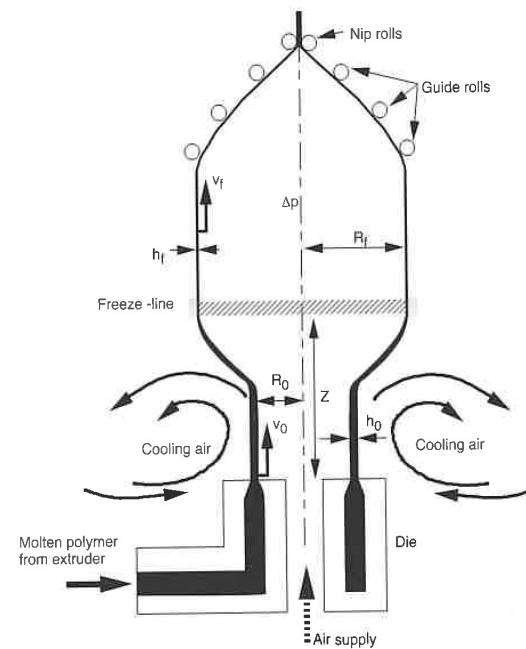
**Figure 6.72**    Film blowing.



**Figure 6.73**    Film blowing.

### 6.4.3    Blow Molding

The predecessor of the blow molding process was the blowing press developed by Hyatt and Burroughs in the 1860s to manufacture hollow celluloid articles. Polystyrene was the first synthetic polymer used for blow molding during World War II and polyethylene was the first material to be implemented in commercial applications. Until the late 1950s, the main application for blow molding was the manufacture of LDPE articles such as squeeze bottles.

Blow molding produces hollow articles that do not require a homogeneous thickness distribution. Today, HDPE, LDPE, PP, PET, and PVC are the most common materials used for blow molding.

#### 6.4.3.1    Extrusion Blow Molding

In extrusion blow molding, a *parison* or tubular profile is extruded and inflated into a cavity with the specified geometry. The blown article is held inside the cavity until it is sufficiently cool. Figure 6.74 [38] presents a schematic of the steps in blow molding.
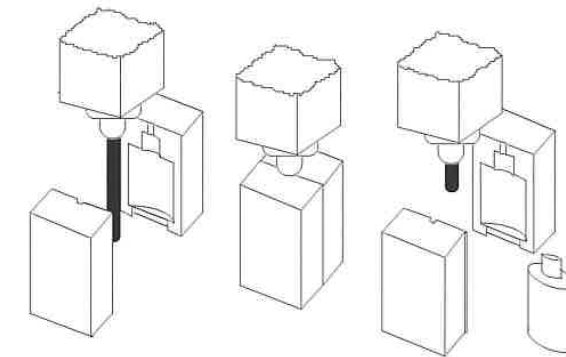


**Figure 6.74**    Schematic of the extrusion blow molding process.

During blow molding, one must generate the appropriate parison length such that the trim material is minimized. Another means of saving material is generating a parison of variable thickness, usually referred to as *parison programming,* such that an article with an evenly distributed wall thickness is achieved after stretching the material. An example of a programmed parison and finished bottle thickness distribution is presented in Fig. 6.75 [39].
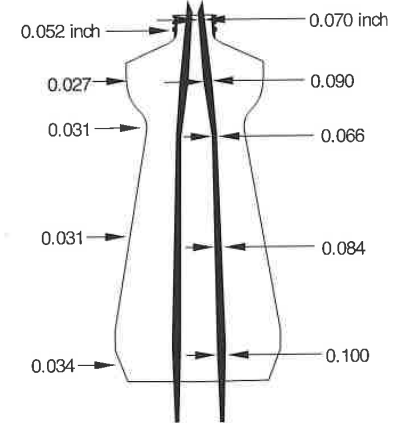
Figure 6.75    Wall thickness distribution in the parison and the part.

A parison of variable thickness can be generated by moving the mandrel vertically during extrusion as shown in Fig. 6.76. A thinner wall not only results in material savings but also reduces the cycle time due to the shorter required cooling times.

As expected, the largest portion of the cycle time is the cooling of the blow molded container in the mold cavity. Most machines wor with multiple molds in order to increase production. Rotary molds are often used in conjunction with vertical or horizontal rotating tables (Fig. 6.77 [37]).
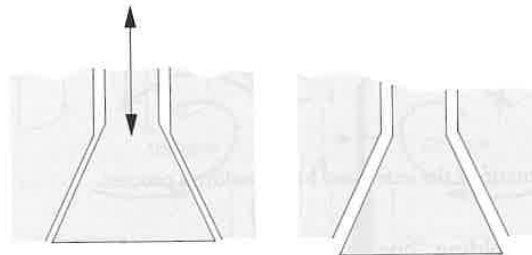


Figure 6.76    Moving mandrel used to generate a programmed parison.
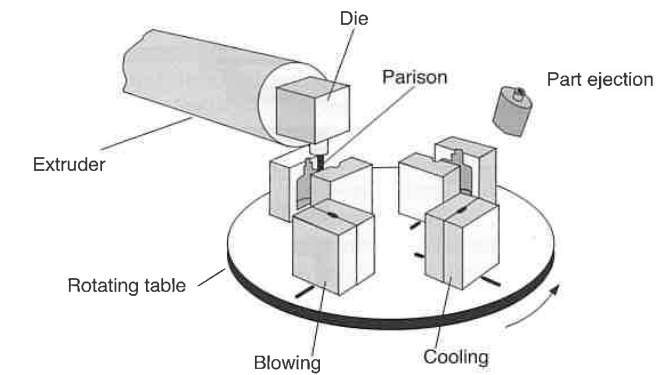
Figure 6.77    Schematic of an extrusion blow molder with a rotating table.

### 6.4.3.2    Injection Blow Molding

Injection blow molding depicted in Fig. 6.78 [38] begins by injection molding the parison onto a core and into a mold with finished bottle threads. The formed parison has a thickness distribution that leads to reduced thickness variations throughout the container. Before blowing the parison into the cavity, it can be mechanically stretched to orient molecules axially, Fig. 6.79 [38]. The subsequent blowing operation introduces tangential orientation. A container with biaxial molecular orientation exhibits higher optical (clarity) and mechanical properties and lower permeability. In the injection blow molding process one can go directly from injection to blowing or one can have a re-heating stage in-between.

The advantages of injection blow molding over extrusion blow molding are:
- Pinch-off and therefore post-mold trimming are eliminated
- Controlled container wall thickness
- Dimensional control of the neck and screw-top of bottles and containers

Disadvantages include higher initial mold cost, the need for both injection and blow molding units and lower volume production.
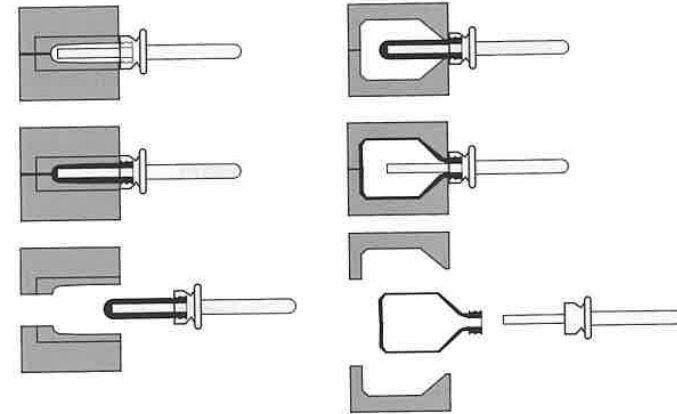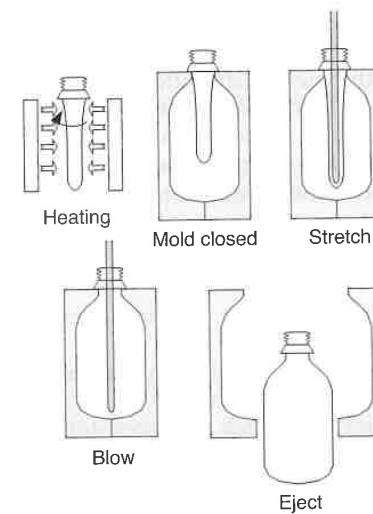
**Figure 6.78**    Injection blow molding.



**Figure 6.79**    Stretch blow molding.

### 6.4.3.3    Thermoforming

Thermoforming is an important secondary shaping method of plastic film and sheet. Thermoforming consists of warming the plastic sheet and forming it into a cavity or over a tool using vacuum, air pressure, and mechanical means. During the 18th century, tortoiseshells and hooves were thermoformed into combs and other shapes. The process was refined during the mid-19th century to thermoform various cellulose nitrate articles.   During World War II, thermoforming was used to manufacture acrylic aircraft cockpit enclosures, canopies, and windshields, as well as translucent covers for outdoor neon signs. During the 1950s, the process made an impact in the mass production of cups, blister packs, and other packaging commodities.    Today, in addition to packaging, thermoforming is used to manufacture refrigerator liners, pick-up truck cargo box liners, shower stalls, bathtubs, as well as automotive trunk liners, glove compartments, and door panels.

A typical thermoforming process is presented in Fig. 6.80 [37].  The process begins by heating the plastic sheet slightly above the glass transition temperature, for amorphous polymers,  or slightly below the melting point, for semi-crystalline materials.  Although, both amorphous and semi-crystalline polymers are used for thermoforming, the process is easiest with amorphous polymers because they have a wide rubbery temperature range above the glass transition temperature. At these temperatures the polymer is easily shaped, but still has enough rigidity to hold the heated sheet without much sagging.  Most semi-crystalline polymers lose their strength rapidly once the crystalline structure breaks up above the melting temperature.

The heating is achieved using radiative heaters and the temperature reached during heating must be high enough for sheet shaping, but low enough so the sheets do not droop into the heaters. One key requirement for successful thermoforming is to bring the sheet to a uniform forming temperature. The sheet is then shaped into the cavity over the tool.  This can be accomplished in several ways. Most commonly a vacuum sucks the sheet onto the tool, stretching the sheet until it contacts the tool surface. The main problem here is the irregular thickness distribution that arises throughout the part. Hence, the main concern of the process engineer is to optimize the system such that the differences in thickness throughout the part are minimized.   This can be accomplished in many ways but most commonly by plug-assist. Here, as the plug pushes the sheet into the cavity, only the parts of the sheet not touching the plug-assist stretch. Since the unstretched portions of the sheet must remain hot for subsequent stretching, the plug-assist is made of a low thermal conductivity material such as wood or hard rubber. The initial stretch is followed by a vacuum for final shaping.  Once cooled, the product is removed.
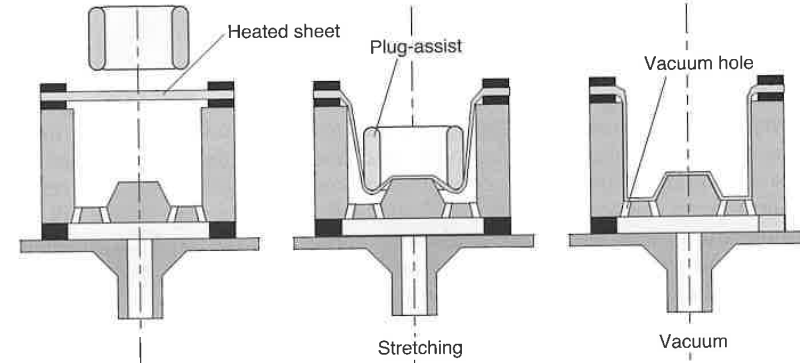
**Figure 6.80**    Plug-assist thermoforming using vacuum.

To reduce thickness variations in the product, the sheet can be pre stretched by forming a bubble at the beginning of the process. This is schematically depicted in Fig. 6.81 [37]. The mold is raised into the bubble, or a plug-assist pushes the bubble into the cavity, and a vacuum finishes the process.
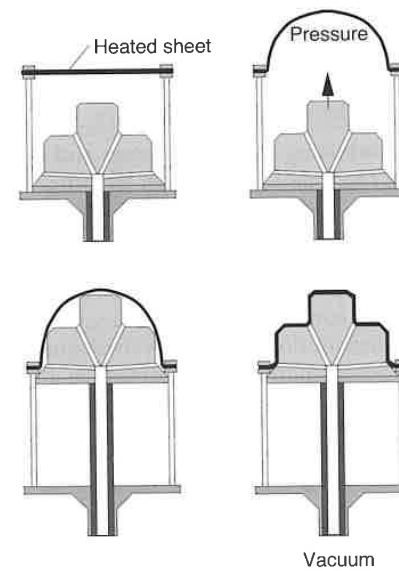


**Figure 6.81**    Reverse draw thermoforming with plug-assist and vacuum.

One of the main reasons for the rapid growth and high volume of thermoformed products is that the tooling costs for a thermoforming mold are much lower than for injection molding.

## 6.5    Calendering

In a calender line, the polymer melt is transformed into films and sheets by squeezing it between pairs of co-rotating high precision rollers. Calenders are also used to produce certain surface textures which may be required for different applications. Today, calendering lines are used to manufacture PVC sheet, floor covering, rubber sheet, and rubber tires. They are also used to texture or emboss surfaces. When producing PVC sheet and film, calender lines have a great advantage over extrusion processes because of the shorter residence times, resulting in a lower requirement for stabilizer. This can be cost effective since stabilizers are a major part of the overall expense of processing these polymers.

Figure 6.82 [37] presents a typical calender line for manufacturing PVC sheet. A typical system is composed of:
- Plasticating unit
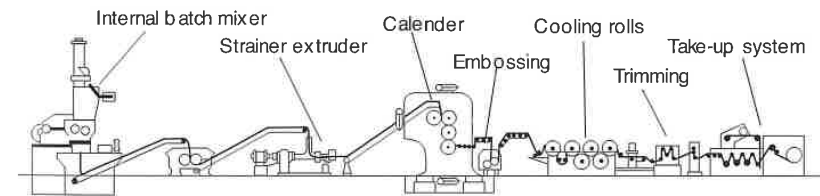- Calender
- Cooling unit
- Accumulator
- Wind-up station



**Figure 6.82**    Schematic of a typical calendering process (Berstorff GmbH).

In the plasticating unit, which is represented by the internal batch mixer and the strainer extruder, the material is melted and mixed and is fed in a continuous stream between the nip of the first two rolls. In another variation of the process, the mixing may take place elsewhere, and the material is simply reheated on the roll mill. Once the material is fed to the mill, the first pair of

rolls control the feeding rate, while subsequent rolls in the calender calibrate the sheet thickness. Most calender systems have four rolls as does the one in Fig. 6.82, which is an inverted L- or F-type system. Other typical roll arrangements are shown in Fig. 6.83 and 6.84. After passing through the main calender, the sheet can be passed through a secondary calendering operation for embossing. The sheet is then passed through a series of chilling rolls where it is cooled from both sides in an alternating fashion. After cooling, the film or sheet is wound.

One of the major concerns in a calendering system is generating a film or sheet with a uniform thickness distribution with tolerances as low as ±0.005 mm. To achieve this, the dimensions of the rolls must be precise. It is also necessary to compensate for roll bowing resulting from high pressures in the nip region. Roll bowing is a structural problem that can be mitigated by placing the rolls in a slightly crossed pattern, rather than completely parallel, or by applying moments to the roll ends to counteract the separating forces in the nip region.

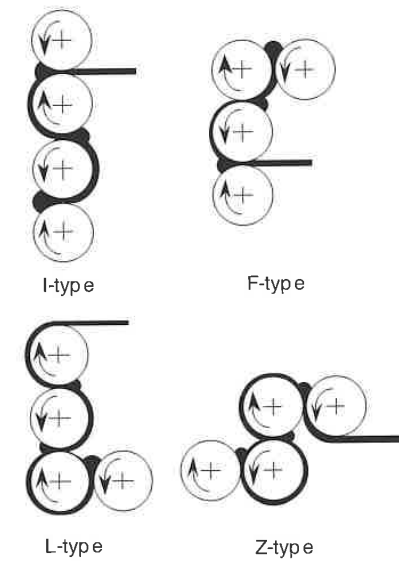Calendering can be modeled by assuming steady state, laminar flow and isothermal conditions.



I-type    F-type

L-type    Z-type
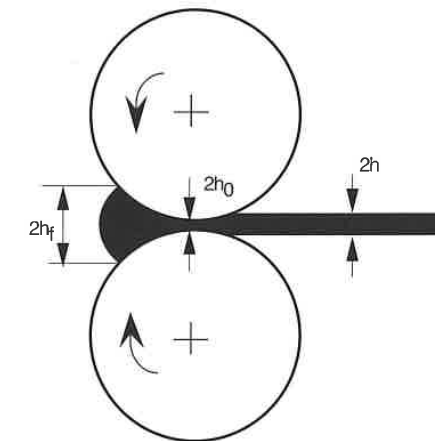
**Figure 6.83**    Calender arrangements.

**Figure 6.84**    Schematic of the calendering process.

## 6.6    Coating

In coating a liquid film is continuously deposited on a moving, flexible or rigid substrate. Coating is done on metal, paper, photographic films, audio and video tapes, and adhesive tapes. Typical coating processes include *wire coating, dip coating, knife coating, roll coating, slide coating,* and *curtain coating.*

In wire coating, a wire is continuously coated with a polymer melt by pulling the wire through an extrusion die. The polymer resin is deposited onto the wire using the drag flow generated by the moving wire and sometimes a pressure flow generated by the back pressure of the extruder. The process is schematically depicted in Fig. 6.85[13]. The second normal stress differences, generated by the high shear deformation in the die, help keep the wire centered in the annulus [40].

Dip coating is the simplest and oldest coating operation. Here, a substrate is continuously dipped into a fluid and withdrawn with one or both sides coated with the fluid. Dip coating can also be used to coat individual objects that are dipped and withdrawn from the fluid. The fluid viscosity and density and the speed and angle of the surface determine the coating thickness.

---

[13]  Other wire coating processes extrude a tubular sleeve which adheres to the wire via stretching and vacuum. This is called tube coating.
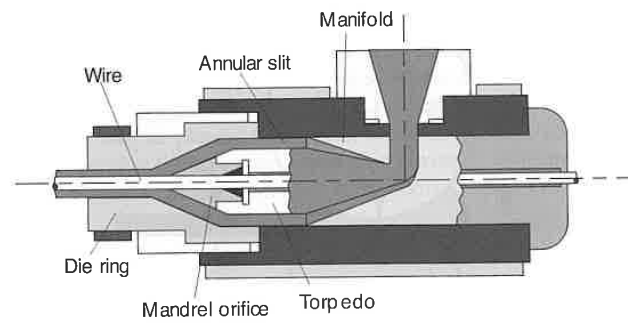
**Figure 6.85**    Wire coating process.

Knife coating, depicted in Fig. 6.86, consists of metering the coating material onto the substrate from a pool of material, using a fixed rigid or flexible knife. The knife can be normal to the substrate or angled and the bottom edge can be flat or tapered. The thickness of the coating is nearly half the gap between the knife edge and the moving substrate or web. A major advantage of a knife edge coating system is its simplicity and relatively low maintenance.

Roll coating consists of passing a substrate and the coating simultaneously through the nip region between two rollers. The physics governing this process is similar to calendering, except that the fluid adheres to both the substrate and the opposing roll. The coating material is a low viscosity fluid, such as a polymer solution or paint and is picked up from a bath by the lower roll and applied to one side of the substrate. The thickness of the coating can be as low as a few μm and is controlled by the viscosity of the coating liquid and the nip dimension. This process can be configured as either forward roll coating for co-rotating rolls or reverse roll coating for counter-rotating rolls (Fig. 6.87). The reverse roll coating process delivers the most accurate coating thicknesses.
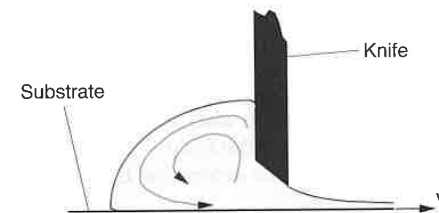


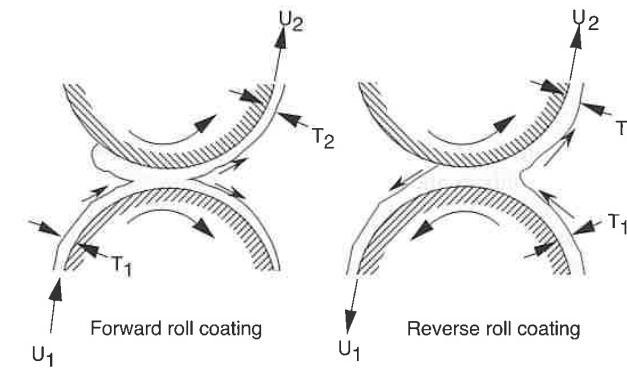**Figure 6.86**    Schematic of a knife coating process.



**Figure 6.87**    Schematic of forward and reverse roll coating processes.

Slide coating and curtain coating, schematically depicted in Fig. 6.88, are commonly used to apply multi-layered coatings. However, curtain coating has also been widely used to apply single layers of coatings to cardboard sheet. In both methods, the coating fluid is pre-metered.
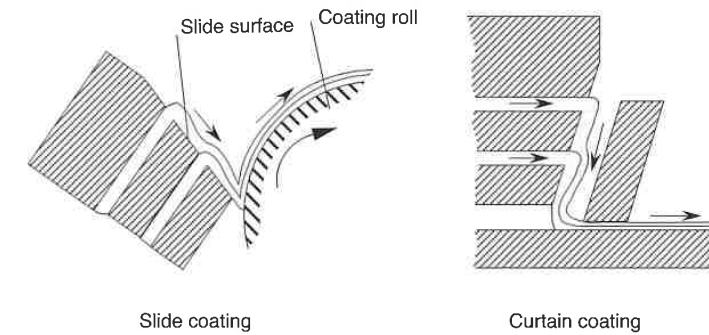


**Figure 6.88**    Slide and curtain coating.

## 6.7 Compression Molding

Compression molding is widely used in the automotive industry to produce parts that are large, thin, lightweight, strong, and stiff. It is also used in the household goods and electrical industries. Compression molded parts are formed by squeezing a charge, often glass fiber reinforced, inside a mold cavity, as depicted in Fig. 6.89. The matrix can be either a thermoset or thermoplastic. The oldest and still widest used material for compression molded products is phenolic. The thermoset materials used to manufacture fiber reinforced compression molded articles is unsaturated polyester sheet or bulk, reinforced with glass fibers, known as sheet molding compound (SMC) or bulk molding compound (BMC). In SMC, the 25 mm long reinforcing fibers are randomly oriented in the plane of the sheet and make up for 20-30% of the molding compound's volume fraction. A schematic diagram of an SMC production line is depicted in Fig. 8.90 [41]. When producing SMC, the chopped glass fibers are sandwiched between two carrier films previously coated with unsaturated polyester-filler matrix. A fiber reinforced thermoplastic charge is often called a glass mat reinforced thermoplastic (GMT) charge. The most common GMT matrix is polypropylene. More recently, long fiber reinforced themoplastics (LFT) have become common. Here, one squeezes sausage shaped charges deposited on the mold by an extruder.
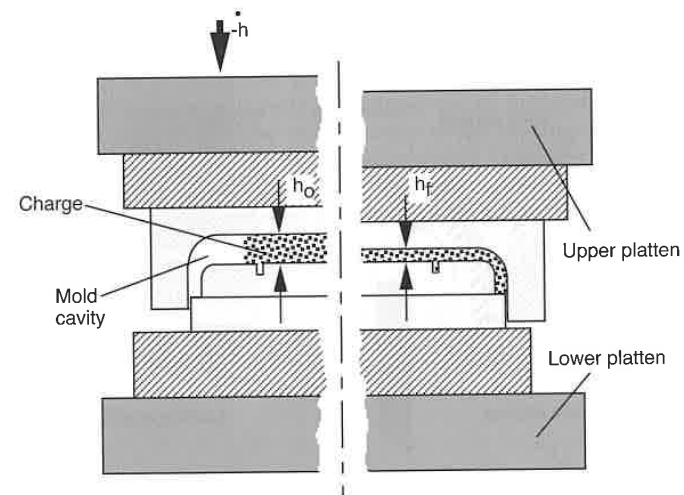
During processing of thermoset charges, the SMC blank is cut from a preformed roll and is placed between heated cavity surfaces. Generally, the mold is charged with 1 to 4 layers of SMC, each layer about 3 mm thick, which initially cover about half the mold cavity's surface. During molding, the initially randomly oriented glass fibers orient, leading to anisotropic properties in the finished product. When processing GMT charges, the preforms are cut and heated between radiative heaters. Once heated, they are placed inside a cooled mold that rapidly closes and squeezes the charges before they cool and solidify.

One of the main advantages of the compression molding process is the low fiber attrition during processing. Here, relatively long fibers can flow in the melt without the fiber damage common during plastication and cavity filling in injection molding.

An alternate process is injection-compression molding. Here, a charge is injected through a large gate followed by a compression cycle. The material used in the injection compression molding process is called bulk molding compound (BMC), which is reinforced with shorter fibers, generally 1 cm long, with an unsaturated polyester matrix. The main benefit of injection compression molding over compression molding is automation. The combination of injection and compression molding leads to lower degrees of fiber orientation and fiber attrition compared to injection molding.
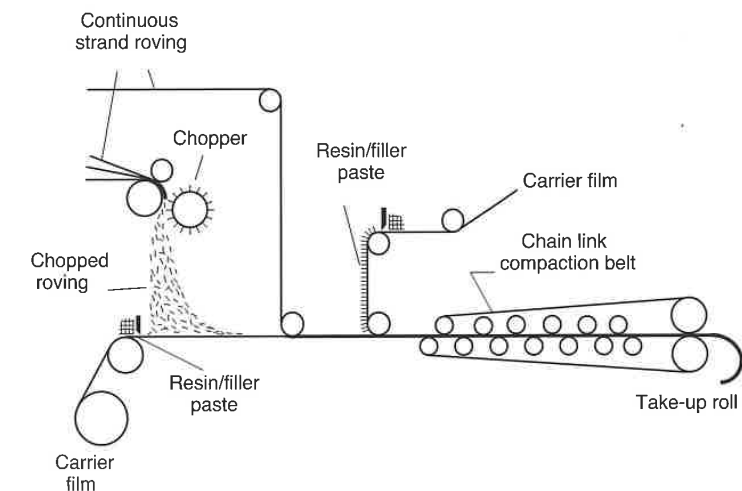


**Figure 6.89** Compression molding process ($h_0$ = charge thickness, $h_f$ = part thickness, and $\dot{h}$ = closing speed).



**Figure 6.90** SMC production line.

## 6.8   Foaming

In foam or a foamed polymer, a cellular or porous structure has been generated through the addition and reaction of *physical* or *chemical blowing agents*. The basic steps of foaming are cell nucleation, expansion or cell growth, and cell stabilization. Nucleation occurs when, at a given temperature and pressure, the solubility of a gas is reduced, leading to saturation, expelling the excess gas to form a bubble. Nucleating agents, such as powdered metal oxides, are used for initial bubble formation. The bubbles reach an equilibrium shape when their inside pressure balances their surface tension and surrounding pressures. The cells formed can be completely enclosed (closed cell) or can be interconnected (open cell).

A physical foaming process is one where a gas such as nitrogen or carbon dioxide is introduced into the polymer melt. Physical foaming also occurs after heating a melt that contains a low boiling point fluid, causing it to vaporize. For example, the heat-induced volatilization of low-boiling-point liquids, such as pentane and heptane, is used to produce polystyrene foams. Also, foaming occurs during volatilization from the exothermic reaction of gases produced during polymerization such as the production of carbon dioxide during the reaction of isocyanate with water. Physical blowing agents are added to the plasticating zone of the extruder or molding machine. The most widely used physical blowing agent is nitrogen. Liquid blowing agents are often added to the polymer in the plasticating unit or the die.

Chemical blowing agents are usually powders introduced in the hopper of the molding machine or extruder. Chemical foaming occurs when the blowing agent thermally decomposes, releasing large amounts of gas. The most widely used chemical blowing agent for polyolefin is azodicarbonamide.

In mechanical foaming, a gas dissolved in a polymer expands upon reduction of the processing pressure.

The foamed structures commonly generated are either homogeneous foams or integral foams. Figure 6.91 [42] presents the various types of foams and their corresponding characteristic density distributions. In integral foam, the unfoamed skin surrounds the foamed inner core. This type of foam can be achieved during injection molding and extrusion and it replaces the sandwiched structure also shown in Fig. 6.91.
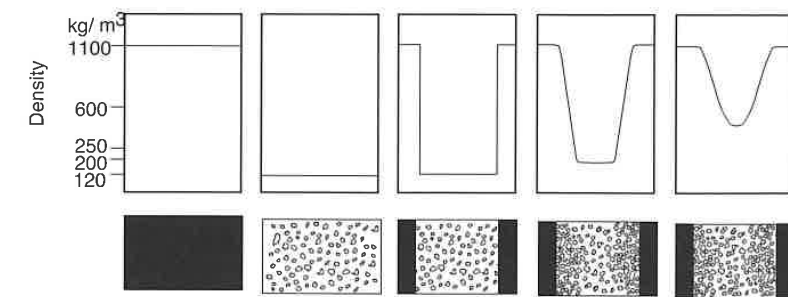
**Figure 6.91**   Schematic of various foam structures.

Today, foams are of great commercial importance and are primarily used in packaging and as heat and noise insulating materials. Examples of foamed materials are polyurethane foams, expanded polystyrene (EPS) and expanded polypropylene particle foam (EPP).

Polyurethane foam is perhaps the most common foaming material and is a typical example of a chemical foaming technique. Here, two low viscosity components, a polyol and an isocyanate, are mixed with a blowing agent such as pentane. When manufacturing semi-finished products the mixture is deposited on a moving conveyor belt where it is allowed to rise, like a loaf of bread contained whithin shaped paper guides. The result is a continuous polyurethane block that can be used, among others, in the upholstery and matress industries.

The basic material to produce expanded polystyrene products are small pearls produced by suspension styrene polymerization with 6-7% of pentane as a blowing agent. To process the pearls they are placed in pre-expanding machines heated with steam until their temperature reaches 80 to 100 °C. To enhance their expansion, the pearls are allowed to cool in a vacuum and allowed to age and dry in ventilated storage silos before the shaping operation. Polystyrene foam is used extensively in packaging, but its uses also extend to the construction industry as a thermal insulating material, as well as for shock absorption in children's safety seats and bicycle helmets.

Expanded polypropylene particle foam is similar in to EPS but is characterized by its excellent impact absorption and chemical resistance. Its applications are primarily in the automotive industry as bumper cores, sun visors and knee cushions, to name a few.

## 6.9    Rotational Molding

Rotational molding is used to make hollow objects. In rotational molding, a carefully measured amount of powdered polymer, typically polyethylene, is placed in a mold. The mold is then closed and placed in an oven where the mold turns about two axes as the polymer melts, as depicted in Fig. 6.92. During heating and melting, which occur at oven temperatures between 250 and 450 °C, the polymer is deposited evenly on the mold's surface. To ensure uniform thickness, the axes of rotation should not coincide with the centroid of the molded product. The mold is then cooled and the solid part is removed from the mold cavity. The parts can be as thick as 1 cm, and still be manufactured with relatively low residual stresses. The reduced residual stress and the controlled dimensional stability of the rotational molded product depend in great part on the cooling rate after the mold is removed from the oven. A mold that is cooled too fast yields warped parts. Usually, a mold is first cooled with air to start the cooling slowly, followed by a water spray for faster cooling.

The main advantages of rotational molding over blow molding are the uniform part thickness and the low cost involved in manufacturing the mold. In addition, large parts such as play structures or kayaks can be manufactured more economically than with injection molding or blow molding. The main disadvantage of the process is the long cycle time for heating and cooling of the mold and polymer.
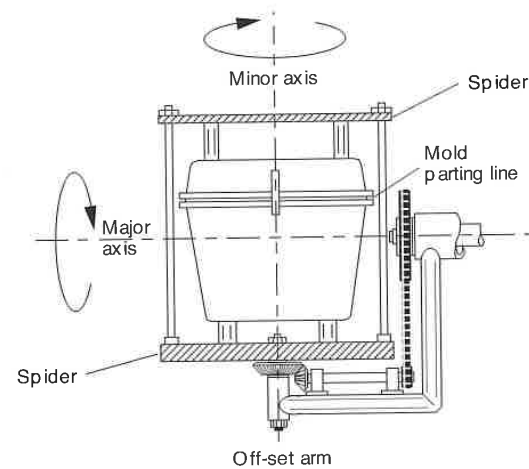


**Figure 6.92**    Schematic of the rotational molding process.

Figure 6.93 presents the air temperature inside the mold in a typical rotational molding cycle for polyethylene powders [43]. The process can be divided into six distinct phases:

1. Induction or initial air temperature rise
2. Melting and sintering
3. Bubble removal and densification
4. Pre-cooling
5. Crystallization of the polymer melt
6. Final cooling

The induction time can be significantly reduced by pre-heating the powder, and the bubble removal and cooling stage can be shortened by pressurizing the material inside the mold. The melting and sintering of the powder during rotational molding depends on the rheology and geometry of the particles. This phenomenon was studied in depth by Bellehumeur and Vlachopoulos [44].
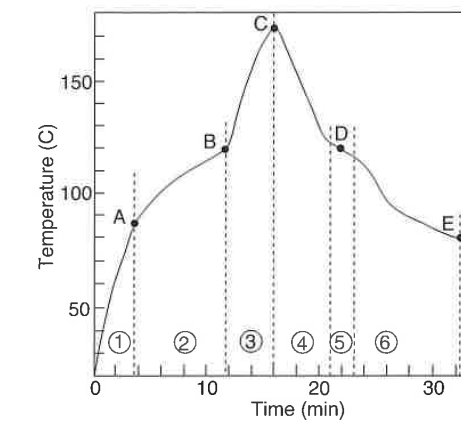


**Figure 6.93**    Typical air temperature in the mold while rotomolding polyethylene parts.

## Examples

6.1  You are to use a 45 mm diameter single screw extruder to create a polymer polycarbonate/polypropylene polymer blend. The maximum screw rotation is 160 rpm and the screw channel depth is 4mm. Assuming a barrel temperature of 300 °C, a surface tension, between the two polymers of $8 \times 10^{-3}$ N/m, and using the viscosity curves given in in the appedix of this book, determine:

- If one can disperse 20% PC into 80% PP
- If one can disperse 20% PP into 80% PC
- The minimum size of the dispersed phase

We start this problem by first calculating the average speed in the extruder using

$$v_0 = \pi D n = \pi (45)(160)(1/60) = 377\,\text{mm}/\text{s}$$

which results in an average rate of deformation of

$$\dot{\gamma} = \frac{v_0}{h} = \frac{377\,\text{mm}/\text{s}}{4\,\text{mm}} = 94\,\text{s}^{-1}$$

From the viscosity curves we get $\eta_{PC} \approx 600\,\text{Pa}-\text{s}$ and $\eta_{PP} \approx 150\,\text{Pa}-\text{s}$. Using Fig. 6.32 we can deduce that one cannot disperse polycarbonte into polypropylene using a single screw extruder that only induces shear deformation, since $\eta_{PC}/\eta_{PP} > 4$. On the other hand, one can disperse polypropylene into polycarbonate using the same single screw extruder.

Using Fig.6.32 we can see that dispersive mixing for a $\eta_{PC}/\eta_{PP} > 0.25$ will occur at $Ca_{crit} \approx 0.7$. Hence, neglecting the effects of coalescence we can calculate the minimun size of the dispersed phase using

$$Ca_{crit} = 0.7 = \frac{\tau R}{\sigma_s} = \frac{600(94)R}{8 \times 10^{-3}} \rightarrow D = 2R = 0.2\,\mu m$$

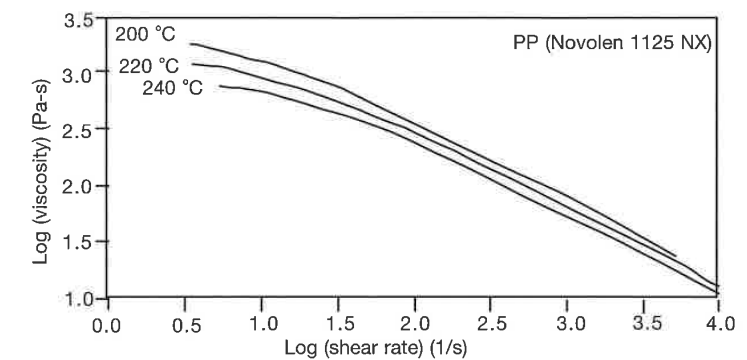To achieve this dispersion we must maintain the stresses for an extended period.

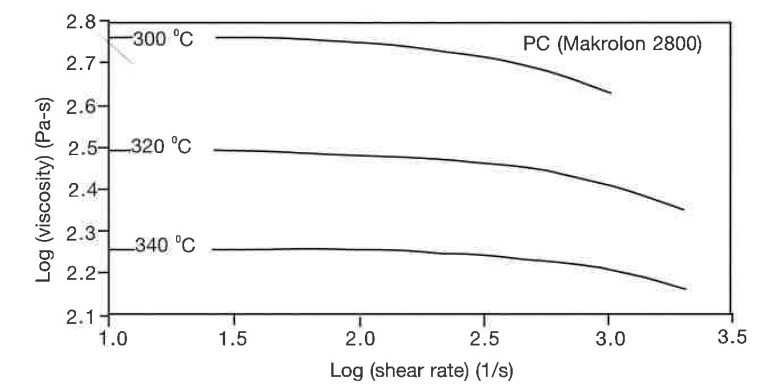**Figure 6.94**   Viscosity curves for a polypropylene.

**Figure 6.95**   Viscosity curves for a polycarbonate.

6.2  You are to determine the maximum clamping force and injection pressure required to mold an ABS suitcase with a filling time, $t_{fill}$, of 2.5 seconds. Use the dimensions shown in Fig. 6.96, an injection temperature, $T_i$, of 227 °C (500 K), and a mold temperature, $T_m$, of 27 °C (300 K). The properties necessary for the calculations are also given below.

**Table 6.8**   Properties for ABS

| | |
|---|---|
| $n = 0.29$ | $\rho = 1020\,\text{kg}/\text{m}^3$ |
| $m_0 = 29 \times 10^6\,\text{Pa}-\text{s}^n$ | $C_p = 2343\,\text{J}/\text{Kg}/\text{K}$ |
| $a = 0.01369/\text{K}$ | $k = 0.184\,\text{W}/\text{m}/\text{K}$ |

To aid the polymer processing engineer in finding required injection pressures and corresponding mold clamping forces, Stevenson [4] generated a set of dimensionless groups and corresponding graphs for non-isothermal mold filling of non-Newtonian polymer melts. We start this problem by first laying the suitcase flat and determining the required geometric factors (Fig. 6.97). From the suitcase geometry, the longest flow path, , is 0.6 m and the radius of the projected area, $R_p$, is 0.32 m.
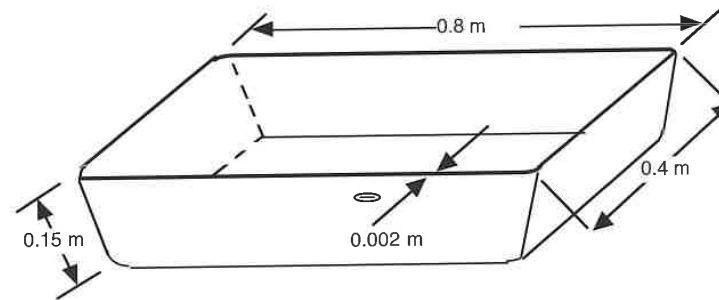


**Figure 6.96**    Suitcase geometry.
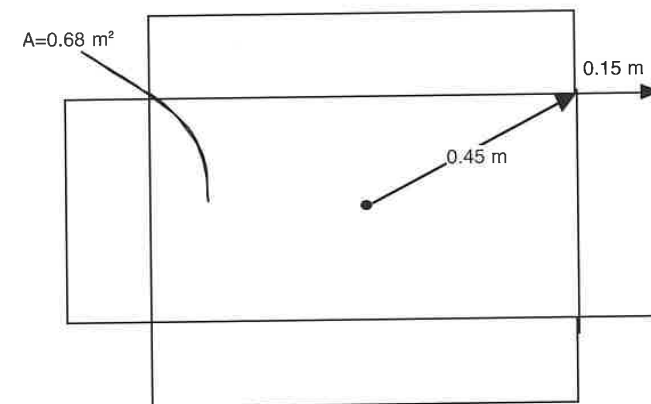


**Figure 6.97**    Layed-flat suitcase.

Using the notation in Fig. 6.25 and a viscosity defined by $\eta = m_0 e^{-a(T - T_{ref})} |\dot{\gamma}|^{n-1}$, four dimensionless groups are defined.

- The dimensionless temperature $\beta$ determines the intensity of the coupling between the energy equation and the momentum balance. It is defined by

$$\beta = a(T_i - T_m) \tag{6.30}$$

where $T_i$ and $T_m$ are the injection and mold temperatures respectively.

- The dimensionless time is the ratio of the filling time, $t_{fill}$, and the time for thermal equilibrium via conduction, defined by

$$\tau = \frac{t_{fill} K}{h^2 \rho C_p} \tag{6.31}$$

- The Brinkman number $Br$ is the ratio of the energy generated by viscous dissipation and the energy transported by conduction. For a non-isothermal, non-Newtonian model it is

$$Br = \frac{m_0 e^{-aT_i} h^2}{k(T_i - T_m)} \left( \frac{R}{t_{fill} h} \right)^{n+1} \tag{6.32}$$

- The power-law index $n$ of the Ostwald and deWaale model reflects the shear thinnng behavior of the polymer melt. Once the dimensionless parameter are calculated, the dimensionless injection pressures $(\Delta p / \Delta p_l)$ and dimensionless clamping forces $(F/F_l)$ are read from Figs. 6.98 to 6.101. The isothermal pressure and force are computed using

$$\Delta p_l = \frac{m_0 e^{-aT_i}}{1-n} \left[ \frac{1+2n}{2n} \frac{R}{t_{fill} h} \right]^n \left( \frac{R}{h} \right) \tag{6.33}$$

and

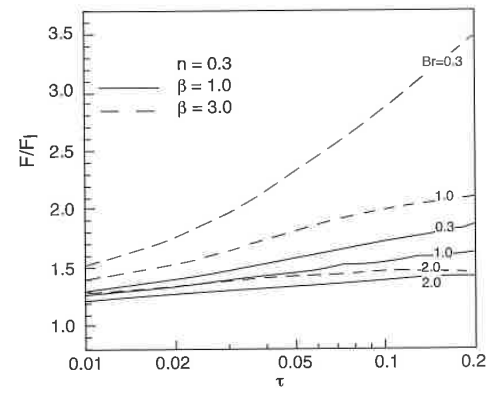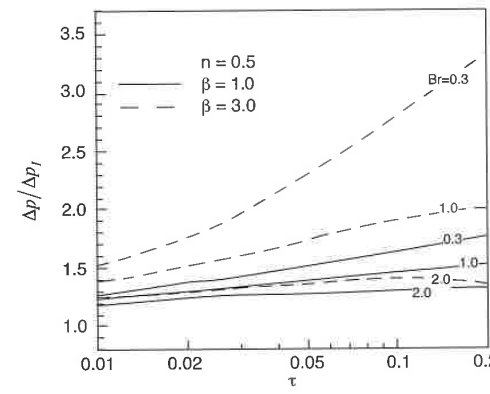$$F_l = \pi R^2 \left( \frac{1-n}{3-n} \right) \Delta p_l \tag{6.34}$$

**Figure 6.98** Dimensionless clamping force versus dimensionless groups.
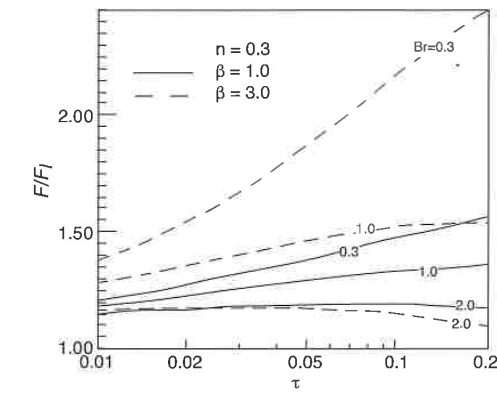


**Figure 6.100** Dimensionless injection pressure versus dimensionless groups.



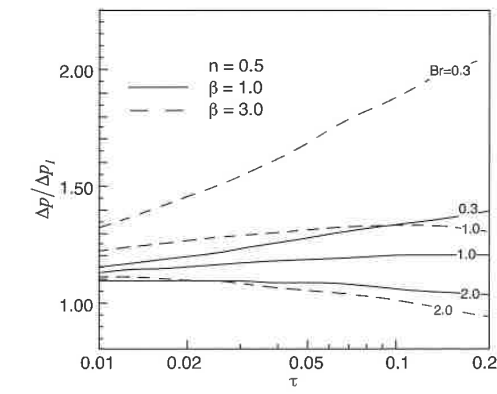**Figure 6.99** Dimensionless clamping force versus dimensionless groups.



**Figure 6.101** Dimensionless injection pressure versus dimensionless groups.

Using the data given for ABS and the dimensions for the laid-flat suitcase we can compute the dimensionless groups as

$$\beta = 0.01369(500-300) = 2.74$$

$$\tau = \frac{2.5(0.184)}{(0.001)^2(1020)(2343)} = 0.192$$

$$Br = \frac{(29x10^6)e^{-0.01369(500)}(0.001)^2}{0.184(500-300)}\left(\frac{0.6}{2.5(0.001)}\right)^{0.29+1} = 0.987$$

The isothermal injection pressure and clampng force are computed using eqs. 6.30 to 6.34.

$$\Delta p_I = \frac{29x10^6 e^{-0.01369(500)}}{1-0.29}\left(\frac{1+2(0.29)}{2(0.29)}\frac{0.6}{2.5(0.001)}\right)^{0.29}\left(\frac{0.6}{0.001}\right) = 171\,\mathrm{MPa}$$

$$F_I = \pi(0.6)^2\left(\frac{1-0.29}{3-0.29}\right)(17.1x10^7) = 50.7x10^6\,\mathrm{N}$$

We now look up $\Delta p/\Delta p_I$ and $F/F_I$ in Figs. 6.98 to 6.101. Since little change occurs between n = 0.3 and n = 0.5, we choose n = 0.3. However, for other values of n we can interpolate or extrapolate. For $\beta = 2.74$, we interpolate between 1 and 3 as

$$\beta = 1 \rightarrow \Delta p/\Delta p_I = 1.36 \text{ and } F/F_I = 1.65$$

$$\beta = 3 \rightarrow \Delta p/\Delta p_I = 1.55 \text{ and } F/F_I = 2.1$$

$$\beta = 2.74 \rightarrow \Delta p/\Delta p_I = 1.53 \text{ and } F/F_I = 2.04$$

$$\Delta p = \left(\frac{\Delta p}{\Delta p_I}\right)\Delta p_I = 262\,\mathrm{MPa} = 2,620\,\mathrm{bar}$$

$$F = \left(\frac{F}{F_I}\right)F_I = 10.3x10^7\,\mathrm{N} = 10,300\,\mathrm{metric\,tons}$$

Since the part are exceeds the projected area, Fig. 6.102 can be used to correct the computed clamping force. The clamping force can be corrected forn an $R_p$= 0.32 m using Fig. 6.102 and $R_p/R = 0.53$.

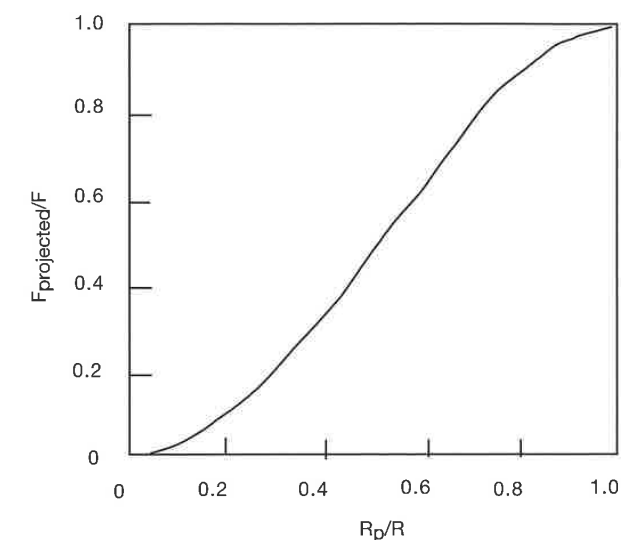$$F_{projected} = (0.52)10,300 = 5,356\,\mathrm{metric\,tons}$$



Figure 6.102   Clamping force correction for the projected area.

For our suitcase cover, where the total volume is 1,360 cc and total part area is 0.68 m$^2$, the above numbers are too high.  A usefull rulo-of-thumb is a maximun allowable clamping force of 2 tons/in$^2$. Here, we have gratly exceeded that number.  Normally, around 3,000 metric tons/m$^2$ are allowed in commercial injection molding machines.  For example, a typical injection molding machine[14] with a shot size of 2,000 cc has a maximun clamping force of 630 metric tons with a maximun injection pressure of 1,400 bar. A machine with much larger clamping forces and injection pressures is suitable for much larger parts.  For example, a mchaine with a shot size of 19,000 cc allows a maximum clamping force of 6,000 metric tons with a maximum injection   pressure of 1,700 bar. For this example we must reduce the pressure and

---

14   MINIFLOW, Injection Molding Simulation, The Madison Groups PPRC, Madison, WI.

clamping force requirements. This can be accomplished by increasing the injection and mold temperatures or by reducing the filling time. Recommended injection temperatures for ABS are between 210 and 240 °C and recommended mold temperatures are between 40 and 90 °C.[15] As can be seen, there is room for adjustment in the processing condition, so one must repeat the above procedure using new conditions.

6.3   Let us consider the multi-cavity injection molding process shown in Fig. 6.103. To achieve equal part quality, the filling time for all cavities must be balanced. For the case in question, we need to balance the cavities by solving for the runner radius. For a balanced runner system the flow rates into all cavities must match. For a given flow rate $Q$, length $L$, and radius $R_1$, we can also solve for the pressure at the runner system junctures. Assuming an isothermal flow of a non-Newtonian shear thinning polymer with viscosity $\eta$, we can compute the radius for a part molded of polystyrene with a consistency index of $2.8 x 10^4$ Pa$-$s$^n$ and a power law index (n) of 0.28.
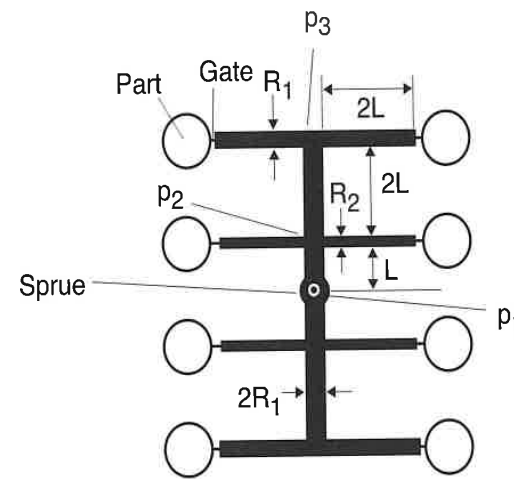


**Figure 6.103**   Runner system lay out.

The flow through each runner section is governed by equation 5.46, and the various sections can be representied using:

---

15   A good reference for such values is the CAMPUS® material data bank. Books such as H. Domininghaus, *Plastics for Engineers*, Hanser Publishers (1992), Munich are also recommended.

Section 1:   $4Q = \left(\dfrac{\pi(2R_1)^3}{s+3}\right)\left(\dfrac{2R_1(P_1 - P_2)}{2mL}\right)^s$

Section 2:   $2Q = \left(\dfrac{\pi(2R_1)^3}{s+3}\right)\left(\dfrac{2R_1(P_2 - P_3)}{2m(2L)}\right)^s$

Section 3:   $Q = \left(\dfrac{\pi R_2^3}{s+3}\right)\left(\dfrac{R_2(P_2 - 0)}{2m(2L)}\right)^s$

Section 4:   $Q = \left(\dfrac{\pi R_1^3}{s+3}\right)\left(\dfrac{R_1(P_3 - 0)}{2m(2L)}\right)^s$

Using values of $L = 10$cm, $R_1 = 4$mm mm, and $Q = 20 cm^3/s$, the unknown parameters, $P_1, P_2, P_3$, and $R_2$ can be obtained using the preciding equations. The equation are non-linear and must be solved in an iterative manner. For the given values, a radius, $R_2$, of 3.4 mm would result in a balanced runner system, with pressures $P_1$ = 265.7 bar, $P_2$ = 230.3 bar, and $P_3$ = 171.9 bar. For comparison, if one had assumed a Newtonian model with the same consistency index and a power law index of 1.0 a radius, $R_2$, of 3.9 mm would have resulted, with much higher required pressures of $P_1$ = 13,926 bar, $P_2$ = 12,533 bar, and $P_3$ = 11,140 bar. The difference is due to shear thinning.

### Problems

6.1   You are to extrude a 100 mm wide high density polyethylene sheet using a 40 mm diameter single screw extruder with distributive as well as dispersive mixing heads. The screw characteristic curve is shown in Fig. 6.104[16].

The die can be approximated with a 100 mm wide and 100 mm long slit. On the graph below draw the die characteristic curves for dies with 1mm and 1.5mm thick slits. Will it be feasible to extrude a sheet through a 1.5mm thick slit? If yes, what screw speed would you choose? What about a 1 mm thick slit.

---

16   Courtesy of ICIPC, Medellín, Colombia.

Why do your die characteristic curves cross over the ones shown in the graph? Note that the data in the graph was measured experimentally with a variable restriction (valve) die.

Typical power law constants for HDPE at 180 °C are m=20,000 Pa-s$^n$ and n=0.41. Use a specific gravity for HDPE of 0.95.
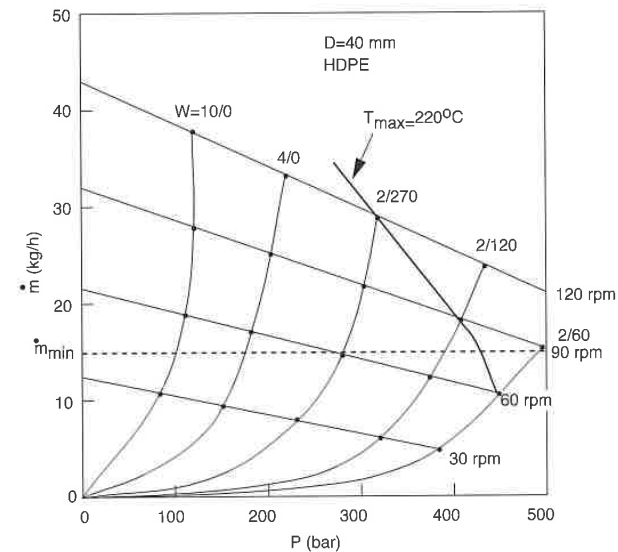


Figure 6.104   Process characteristic curves for a 45 mm diameter conventional extruder.

6.2   Estimate the striation thickness of a 3mm diameter pigmented polystyrene pellet in a polystyrene matrix after traveling through a 20 turn, 45 mm diameter, 5 mm constant channel depth, single screw extruder. Assume open discharge conditions. Use 100 rpm rotational speed.

6.3   Someone in your company proposes to use an existing square pitch 150 mm diameter plasticating single screw extruder as a mixing device for a 40/60 PS/PP polymer blend. The metering section is 5 turns long and has a channel depth of 10 mm. Will dispersion of the polystyrene occur for a screw rotation of 60 rpm? Assume open discharge and a temperature of 220 °C. Use viscosity data given in example 6.1 and Fig. 6.106.

6.4   Someone in your company proposes to use an existing square pitch 150 mm diameter plasticating single screw extruder as a mixing device for a 40/60 PP/PS polymer blend. The metering section is 5 turns long and has a channel depth of 10 mm. Will dispersion of the polypropylene occur for a screw rotation of 60 rpm? Will there be enough time for dispersion? Assume open discharge and a temperature of 220 °C. Use viscosity data given in problems 6.3 and below.
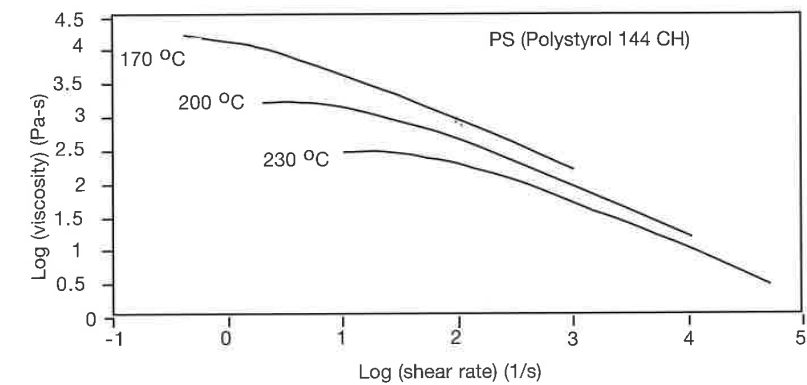


Figure 6.105   Viscosity curves for a polystyrene.

6.5   A thin polyamide 66 component is injection molded under the following conditions:

- The melt is injected at 275 °C to a maximum pack/hold pressure of 800 bar.
- The 800 bar pack/hold pressure is maintained until the gate freezes off, at which point the part is at an average temperature of 175 °C.
- The pressure drops to 1 bar as the part cools inside the cavity.
- The part is removed from the mold and cooled to 25 °C.
- Draw the whole process on the PvT diagram.
- Estimate the final part thickness if the mold thickness is 1 mm. For thin injection molded parts, most of the shrinkage leads to part thickness reduction.

6.6   Does the screw and die characteristic curves, correspond to a conventional or a grooved single screw extruder?

A die can be approximated with a 1 mm diameter and 30 mm long

capillary. On the graph below draw the die characteristic curve for the given die?

Typical power law constants for HDPE at 180 °C are m=20,000 Pa-s$^n$ and n=0.41. Use a specific gravity for HDPE of 0.95.
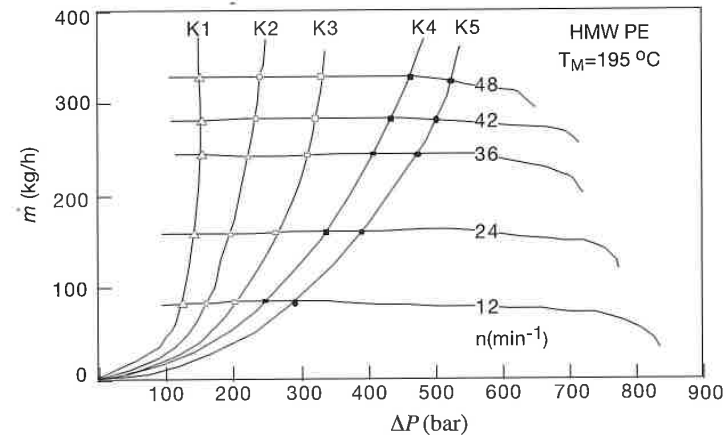


**Figure 6.106**  Process characteristic curves for a 45 mm diameter extruder.

6.7    An internal batch mixer maintains shear rates, $\dot{\gamma}$, of 100 s$^{-1}$ for extended periods. In the mixer you want to disperse LDPE in a PS matrix at 170 °C. What is the size of the dispersed phase? Will the PS still be transparent? Use viscosity data given in Problem 6.4 and below.
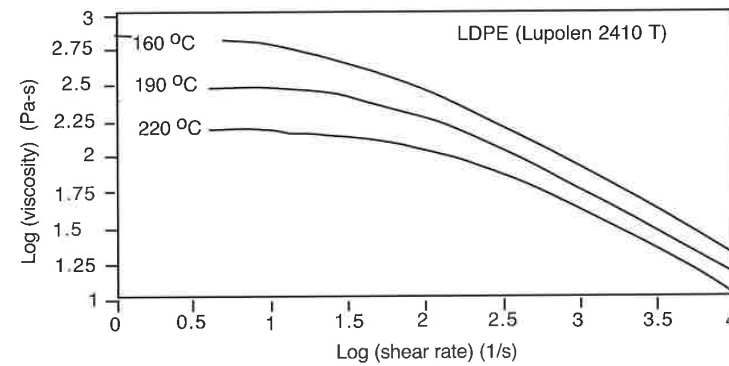


**Figure 6.107**    Viscosity curves for a low density polyethylene.

6.8    Design a balanced runner system for the mold in Example 6.3 if you are to injection mold a polystyrene product. Assume a power-law model with a consistency index, m, of $2.8 \times 10^4$ Pa-s$^n$, and a power-law index, n, of 0.28.

6.9    Estimate the cooling time for the ABS suitcase presented in Example 6.2 if demolding occurs when the average part temperature is below 60 °C.

6.10   What are the required clamping force and injection pressure if the filling time in Example 6.2 is increased from 2.5 s to 3 s?

6.11   What are the required clamping force and injection pressure if the mold temperature in Example 6.2 is increased from 27 °C to 90 °C ?

6.12   What are the required clamping force and injection pressure if the injection temperature in Example 6.2 is increased from 227 to 240 °C?

6.13   Measure and plot the wall thickness distribution on a PE-HD one gallon milk container.

6.14   Measure and plot the wall thickness distribution on a small thermoformed individual coffee cream container.

## References

1.   Tadmor, Z., and Gogos, C.G.,  Principles of Polymer Processing, John Wiley & Sons, New York, (1979).
2.   Rauwendaal, C., *Mixing in Polymer Processing*, Marcel Dekker, Inc., New York, (1991).
3.   Osswald, T.A., Turng, L.S., and Gramann, P.J., Injection Molding Handbook, Hanser Publishers, Munich, (2001).
4.   Menges, G., and Predöhl, W., *Plastverarbeiter, 20*, 79, (1969).
5.   Menges, G., and Predöhl, W., *Plastverarbeiter, 20*, 188, (1969).
6.   Scott, C.E., and Macosko, C.W., *Polymer Bulletin, 26*, 341, (1991).
7.   Gramann, P.J., Stradins, L., and Osswald, T.A., *Intern. Polymer Processing, 8*, 287, (1993).
8.   Osswald, T.A., *Polymer Processing Fundamentals*, Hanser Publishers, Munich, (1998).
9.   Erwin, L., *Polym. Eng. & Sci., 18*, 572, (1978).
10.  Erwin, L., *Polym. Eng. & Sci., 18*, 738, (1978).
11.  Ng, K.Y., Master of Science Thesis, University of Wisconsin-Madison, (1979).
12.  Tadmor, Z., *Ind. Eng. Fundam., 15*, 346, (1976).

13. Cheng, J., and Manas-Zloczower, I., *Internat. Polym. Proc.*, 5, 178, (1990).
14. Grace, H.P., *Chem. Eng. Commun.*, *14*, 225, (1982).
15. Cox, R.G., *J. Fluid Mech.*, 37, 3, 601–623, (1969).
16. Bentley, B.J. and Leal, L.G., *J. Fluid Mech.*, 167, 241–283, (1986).
17. Stone, H.A. and Leal, L.G., *J. Fluid Mech.*, 198, 399–427, (1989).
18. Biswas, A., and Osswald, T.A., unpublished research, (1994).
19. Gramann, P.J., M.S. Thesis, University of Wisconsin-Madison, (1991).
20. Manas-Zloczower, I., Nir, A., and Tadmor, Z., *Rubber Chemistry and Technology*, 55, 1250, (1983).
21. Boonstra, B.B., and Medalia, A.I., *Rubber Age*, March and April, (1963).
22. Rauwendaal, C., *Polymer Extrusion*, Hanser Publishers, Munich, (1990).
23. Menges, G., and Harms, E., *Kautschuk und Gummi, Kunststoffe, 25*, 469, (1972).
24. Rauwendaal, C., *SPE ANTEC Tech. Pap.*, 39, 2232, (1993).
25. Rauwendaal, C., *Mixing in Reciprocating Extruders*, A chapter in *Mixing and Compounding of Polymers*, Eds. I. Manas-Zloczower and Z. Tadmor, Hanser Publishers, Munich, (1994).
26. Elemans, P.H.M., Modeling of the cokneater, A chapter in *Mixing and Compounding of Polymers*, Eds. I. Manas-Zloczower and Z. Tadmor, Hanser Publishers, Munich, (1994).
27. Lim, S. and White, J.L., *Intern. Polymer Processing*, 8, 119, (1993).
28. Lim, S. and White, J.L., *Intern. Polymer Processing*, 9, 33, (1994).
29. Bird, R.B., Steward, W.E., and Lightfoot, E.N., *Transport Phenomena*, John Wiley & Sons, New York, (1960).
30. Erwin, L., *Polym. Eng. & Sci.*, *18*, 1044, (1978).
31. Suetsugu, *Intern. Polymer Processing, 5*, 184, (1990).
32. Greener, J., *Polym. Eng. Sci., 26*, 886 (1986).
33. Michaeli, W., and Lauterbach, M., *Kunststoffe , 79*, 852 (1989).
34. Stevenson, J.F., *Polym. Eng. Sci., 18*, 577 (1978).
35. Osswald, T.A., and Menges, G., *Materials Science of Polymers for Engineers,* Hanser Publishers, Munich (1996).
36. Anturkar, N.R., and Co, A., *J. Non-Newtonian Fluid Mech., 28*, 287 (1988).
37. Menges, G., *Einführung in die Kunststoffverarbeitung*, Hanser Publishers, Munich (1986).
38. Rosato, D.V., *Blow Molding Handbook*, Hanser Publishers, Munich (1989).
39. Modern Plastics Encyclopedia, 53, McGraw-Hill , New York (1976).
40. Tadmor, Z., and Bird, R.B., *Polym.Eng.Sci, 14*, 124 (1973).
41. Denton, D.L, *The Mechanical Properties of an SMC-R50 Composite*, Owens-Corning Fiberglas Corporation (1979).
42. Shutov, F.A., *Integral/Structural Polymer Foams*, Springer-Verlag, Berlin (1986).
43. Crawford, R.J., *Rotational Molding of Plastics*, Research Studies Press, Somerset (1992).
44. Bellehumeur, C.T., and Vlachopoulos, J., *SPE 56th Antec*, (1998).
45. Mascia, L., *The Role of Additives in Plastics*, John Wiley & Sons, New York, (1974).
46. Hildebrand, J. and Scott, R.L., *The Solubility of Non-Electrolytes*, 3rd Ed., Reinhold Publishing Co., New York, (1949).
47. Rosen, S.L., *Fundamental Principles of Polymeric Materials*, 2nd. Ed., John Wiley & Sons, Inc., New York, (1993).
48. Janssen, J.M.H., Ph.D. Thesis, Eindhoven University of Technology, The Netherlands, (1993).
49. van Krevelen, D. W., and Hoftyzer, P.J., *Properties of Polymers*, 2nd ed., Elsevier, Amsterdam, (1976).

# Anisotropy Development During Processing

The mechanical properties and dimensional stability of a molded polymer part are strongly dependent upon the anisotropy of the finished part[1]. The structure of the final part, in turn, is influenced by the design of the mold cavity, e.g., the type and position of the gate, and by the various processing conditions such as injection speed, melt or compound temperatures, mold cooling or heating rates, and others. The amount and type of filler or reinforcing material also has a great influence on the quality of the final part.

This chapter discusses the development of anisotropy during processing of thermoset and thermoplastic polymer parts and presents basic analyses that can be used to estimate anisotropy in the final product.

## 7.1 Orientation in the Final Part

During processing the molecules, fillers, and fibers are oriented in the flow and greatly affect the properties of the final part. Since there are large differences in the processing of thermoplastic and thermoset polymers, the two will be discussed individually in the next two sections.

### 7.1.1 Processing Thermoplastic Polymers

When thermoplastic components are manufactured, the polymer molecules become oriented. The molecular orientation is induced by the deformation of the polymer melt during processing. The flexible molecular chains get stretched, and because of their entanglement they cannot relax fast enough before the part cools and solidifies. At lower processing temperatures this phenomenon is multiplied, leading to even higher degrees of molecular

---

[1] This chapter primarily deals with the anisotropy development of injection and compression molded parts.

orientation. This orientation is felt in the stiffness and strength properties of the polymer component. Orientation also gives rise to *birefringence*, or *double refraction*, a phenomenon discussed in Chapter 12. The various degrees of molecular orientation and the different main directions of orientation in the material introduce a variable refractive index field, n(x,y,z), throughout the part. The value of the refractive index, n, depends on the relative orientation of the molecules, or the molecular axes, to the direction of the light shining through the part.

As polarized light travels through a part, a series of colored lines called *isochromatics* become visible or appear as shown in Fig. 7.1 [1]. The isochromatics are lines of equal molecular orientation and numbered from zero, at the region of no orientation, up with increasing degrees of orientation. A zero degree of orientation is usually the place in the mold that fills last and the degree of orientation increases towards the gate. Figure 7.2 shows schematically how molecular orientation is related to birefringence. The layers of highest orientation are near the outer surfaces of the part with orientation increasing towards the gate.
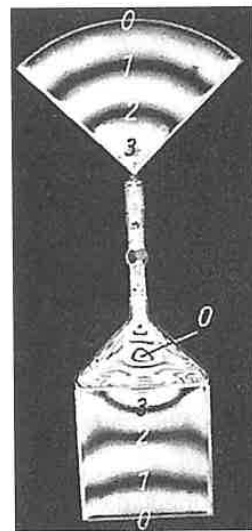


**Figure 7.1**  Isochromatics in a polycarbonate specimen of 1.7 mm wall thickness.

The degree of orientation increases and decreases depending on the various processing conditions and materials. For example, Fig. 7.3 [1] shows quarter disks of various wall thicknesses, molded out of four different materials:

polycarbonate, cellulose acetate, polystyrene, and polymethyl methacrylate. We see that for all materials the degree of orientation increases with decreasing wall thickness. An explanation for this is that the velocity gradients increase when wall thickness decreases. In subsequent sections of this chapter we discuss how orientation is directly related to velocity gradients.

Orientation is also related to the process used to manufacture the part. For example, Fig. 7.4 [1] shows two injection molded polycarbonate parts molded with different injection molders: a piston-type and a screw-type machine. It is obvious that the cover made with the piston-type injection molder has much higher degrees of molecular orientation than the one manufactured using the screw-type injection molder. Destructive tests revealed that it was impossible to produce a cover that is sufficiently crack-proof when molded with a piston-type molding machine.

The articles in Figs. 7.1, 7.3, and 7.4 were injection molded — a common processing method for thermoplastic polymers. Early studies have already shown that a molecular orientation distribution exists across the thickness of thin injection molded parts [2]. Figure 7.5 [2] shows the shrinkage distribution in longitudinal and transverse flow directions of two different plates. The curves demonstrate the degree of anisotropy that develops during injection molding, and the influence of the geometry of the part on this anisotropy.
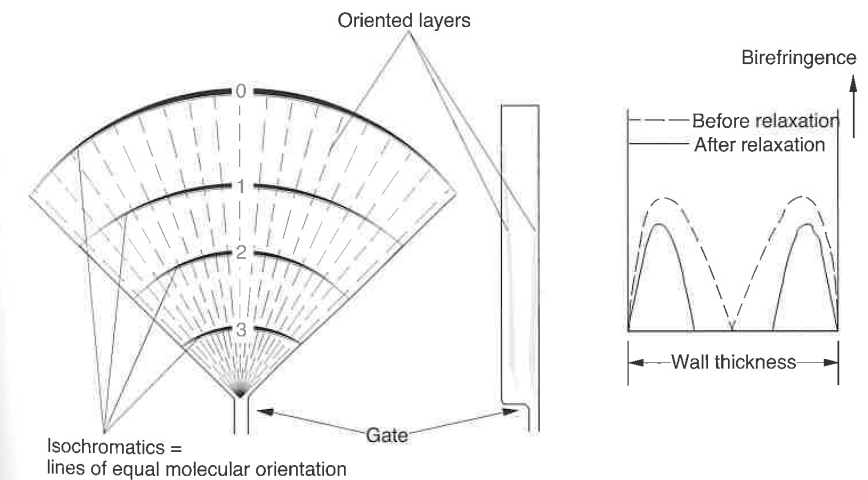


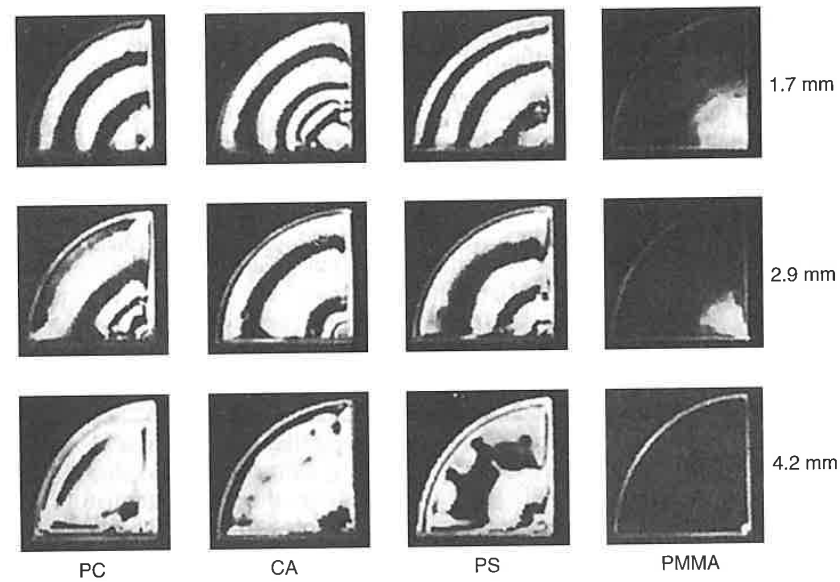**Figure 7.2**  Orientation birefringence in a quarter disk.

**Figure 7.3**   Isochromatics in polycarbonate, cellulose acetate, polystyrene. and polymethyl methacrylate quarter disks of various thicknesses.
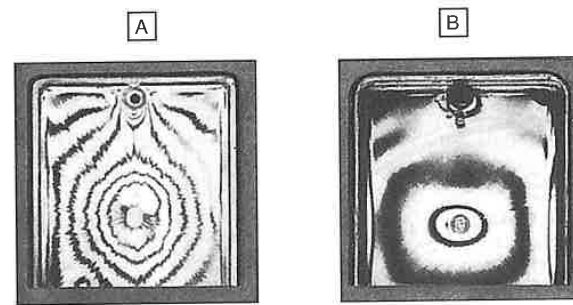


**Figure 7.4**   Isochromatics in polycarbonate parts molded with (left) piston-type and (right) screw-type injection molding machines.
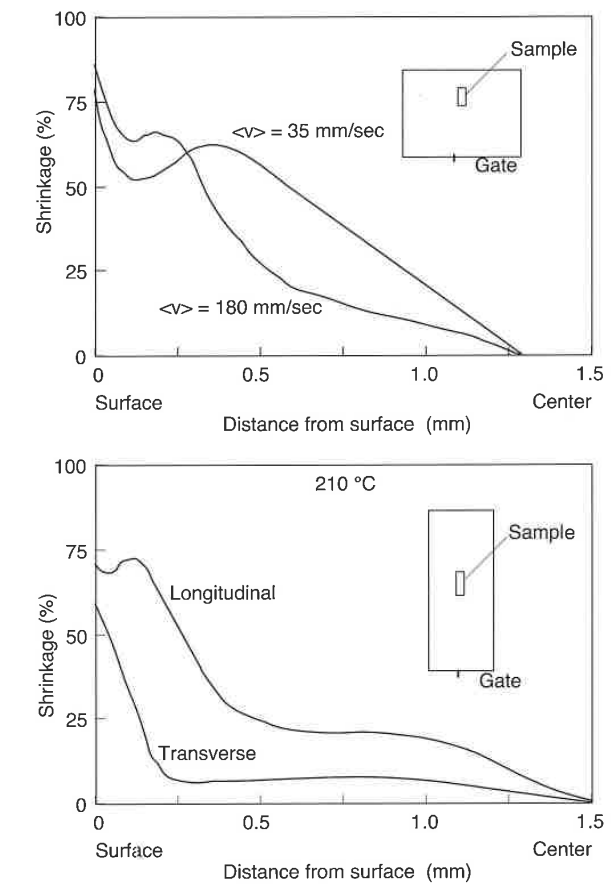


**Figure 7.5**   Shrinkage distribution of injection molded polystyrene plates.

An example of how to use the birefringence pattern of polymer parts to detect severe problems is in the manufacture of polycarbonate compact disks [3, 4]. Figure 7.6 shows the birefringence distribution in the $rz$-plane of a 1.2 mm thick disk molded with polycarbonate. The figure shows how the birefringence is highest at the surface of the disk and lowest just below the surface. Towards the inside of the disk the birefringence rises again and drops somewhat toward the central core of the disk. A similar phenomenon was observed in glass fiber reinforced [5–7] and liquid crystalline polymer [8] injection molded parts which show large variations in fiber and molecular orientation through the thickness.
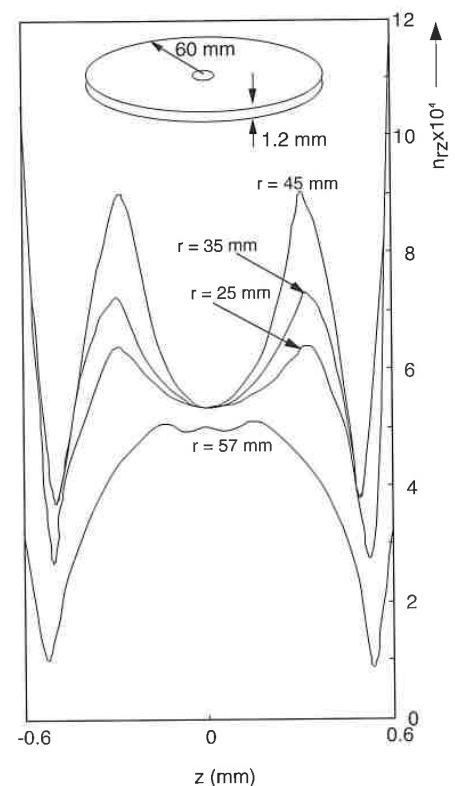
Figure 7.6    Birefringence distribution in the *rz*-plane at various radius positions. Numbers indicate radial position.

All these recent findings support earlier claims that molecular or filler orientation in injection molded parts can be divided into seven layers schematically represented in Fig. 7.7 [1]. The seven layers may be described as follows:

- Two thin outer layers with a biaxial orientation, random in the plane of the disk;
- Two thick layers next to the outer layers with a main orientation in the flow direction;
- Two thin randomly oriented transition layers next to the center core;
- One thick center layer with a main orientation in the circumferential direction.

There are three mechanisms that lead to high degrees of orientation in injection molded parts: fountain flow effect, radial flow, and holding pressure induced flow.

The *fountain flow effect* [9] is caused by the no-slip condition on the mold walls, which forces material from the center of the part to flow outward to the mold surfaces as shown in Fig. 7.8 [10]. As the figure schematically represents, the melt that flows inside the cavity freezes upon contact with the cooler mold walls. The melt that subsequently enters the cavity flows between the frozen layers, forcing the melt skin at the front to stretch and unroll onto the cool wall where it freezes instantly. The molecules which move past the free flow front are oriented in the flow direction and laid on the cooled mold surface which freezes them into place, though allowing some relaxation of the molecules after solidification. Using computer simulation, the fountain flow effect has been extensively studied in past few years [11]. Figures 7.9a and b [12] show simulated instantaneous velocity vectors and streamlines during the isothermal mold filling of a Newtonian fluid.[2] and Figs. 7.9c and d show the velocity vectors relative to the moving flow front. Figure 7.10 [13] presents the predicted shape and position of the tracer relative to the flow front along with the streamlines for a non-Newtonian non-isothermal fluid model. The square tracer mark is stretched as it flows past the free flow front, and is deposited against the mold wall, pulled upward again and eventually deformed into a V-shaped geometry. Eventually, the movement of the outer layer is stopped as it cools and solidifies.
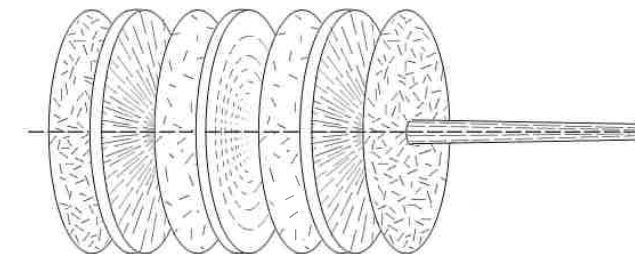


Figure 7.7    Filler orientation in seven layers of a centrally injected disk.

---

[2]    The isothermal and Newtonian analysis should only serve to explain the mechanisms of fountain flow. The non-isothermal nature of the injection molding process plays a significant role in the orientation of the final part and should not be left out in the analysis of the real process.
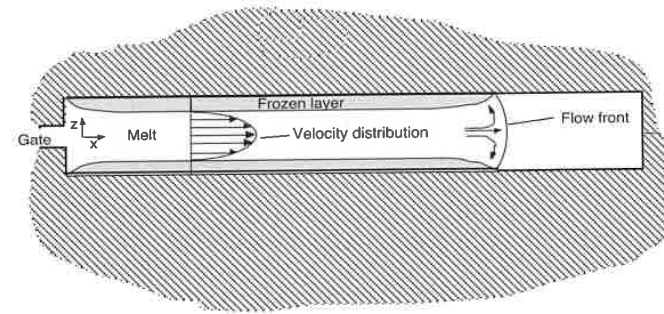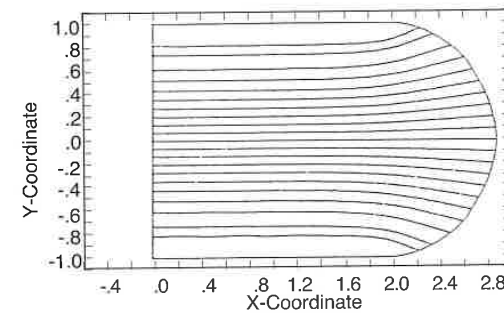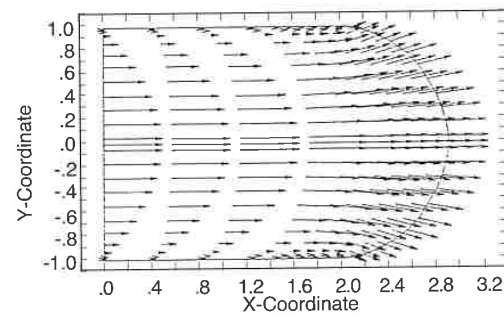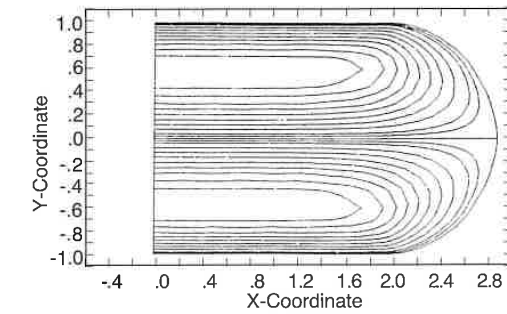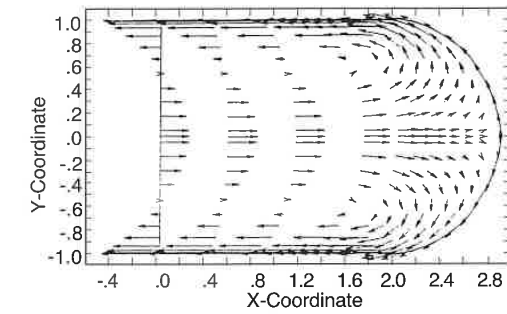
**Figure 7.8**   Flow and solidification mechanisms through the thickness during injection molding.





(b)

**Figure 7.9** *(continued)*   Fountain flow effect: (b) relative to the moving front velocity vectors and streamlines.



(a)

**Figure 7.9**   Fountain flow effect: (a) Actual velocity vectors and streamlines. *(continued)*
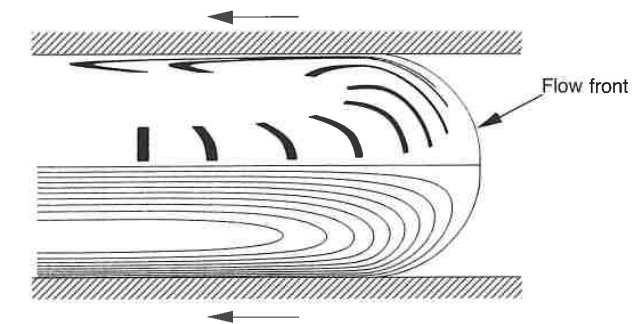


**Figure 7.10**   Deformation history of a fluid element and streamlines for frame of reference that moves with the flow front.

Radial flow is the second mechanism that often leads to orientation perpendicular to the flow direction in the central layer of an injection molded part. This mechanism is schematically represented in Fig. 7.11. As the figure suggests, the material that enters through the gate is transversely stretched while it radially expands as it flows away from the gate. This flow is well represented in today's commonly used commercial injection mold filling software.

Finally, the flow induced by the holding pressure as the part cools leads to additional orientation in the final part. This flow is responsible for the spikes in the curves shown in Figs. 7.5 and 7.6.
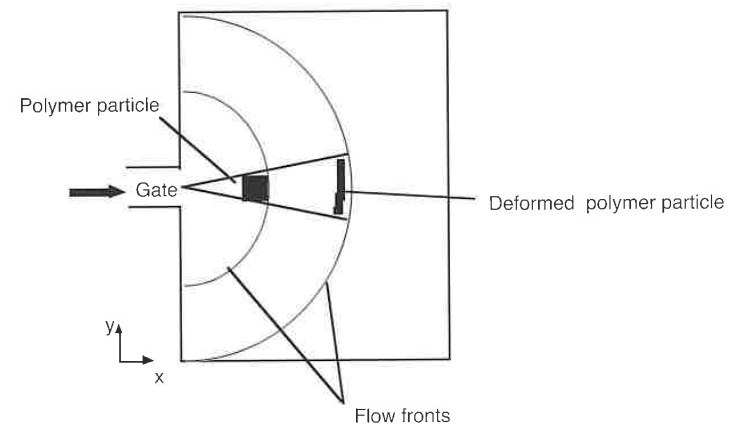


**Figure 7.11**   Deformation of the polymer melt during injection molding.

### 7.1.2  Processing Thermoset Polymers

During the manufacture of thermoset parts there is no molecular orientation because of the cross-linking that occurs during the solidification or curing reaction. A thermoset polymer solidifies as it undergoes an exothermic reaction and forms a tight network of inter-connected molecules.

However, many thermoset polymers are reinforced with filler materials such as glass fiber, wood flour, etc. These composites are molded via transfer molding, compression molding, or injection-compression molding. The properties of the final part are dependent on the filler orientation. In addition, the thermal expansion coefficients and the shrinkage of these polymers are highly dependent on the type and volume fraction of filler being used. Different forms of orientation may lead to varying strain fields, which may cause warpage in the final part. This topic will be discussed in the next chapter.

During the processing of filled thermoset polymers the material deforms uniformly through the thickness with slip occurring at the mold surface as shown schematically in Fig. 7.12 [14]. Several researchers have studied the development of fiber orientation during transfer molding and compression molding of sheet molding compound (SMC) parts [15]. During compression molding, a thin SMC charge is placed in a heated mold cavity and squeezed until the charge covers the entire mold surface. An SMC charge is composed of a polyester resin with around 10% by volume of calcium carbonate filler and 20–50% by volume glass fiber content. The fibers are usually 25 mm long and the final part thickness is 1–5 mm. Hence, the fiber orientation can be described with a planar orientation distribution function.
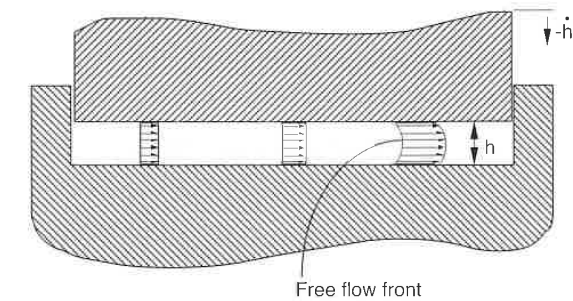


**Figure 7.12**   Velocity distribution during compression molding with slip between material and mold surface.

To determine the relationship between deformation and final orientation in compression molded parts, it is common to mold rectangular plates with various degrees of extensional flow, as shown in Fig. 7.13. These plates are molded with a small fraction of their glass fibers impregnated with lead so that they become visible in a radiograph. Figure 7.14 shows a computer generated picture from a radiograph, taken from a plate where the initial charge coverage was 33% [15, 16]. In Fig. 7.14, about 2000 fibers are visible which through digitizing techniques resulted in the histogram presented in Fig. 7.15 and depict the fiber orientation distribution in the plate. Such distribution functions are very common in compression or transfer molded parts and lead to high degrees of anisotropy throughout a part.

Furthermore, under certain circumstances, filler orientation may lead to crack formation as shown in Fig. 7.16 [1]. Here, the part was transfer molded through two gates which led to a knitline and filler orientation shown in the figure. Knitlines are cracklike regions where there are few or no fibers

bridging across, lowering the strength across the region to that of the matrix material. A better way to mold the part of Fig. 7.16 would be to inject the material through a ring-type gate which would result in an orientation distribution mainly in the circumferential direction.
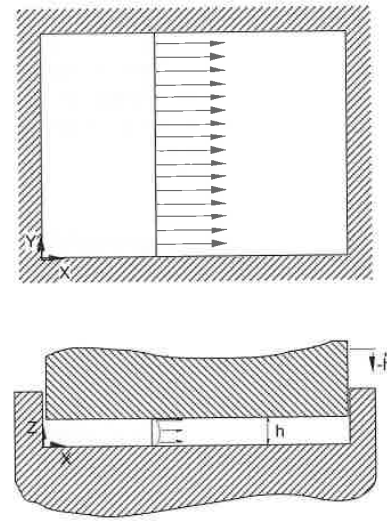


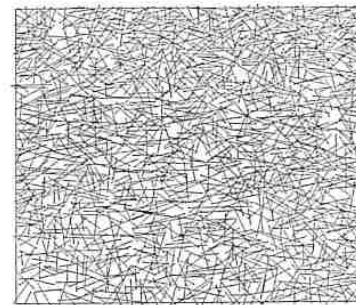**Figure 7.13**    Schematic of extensional flow during compression molding.



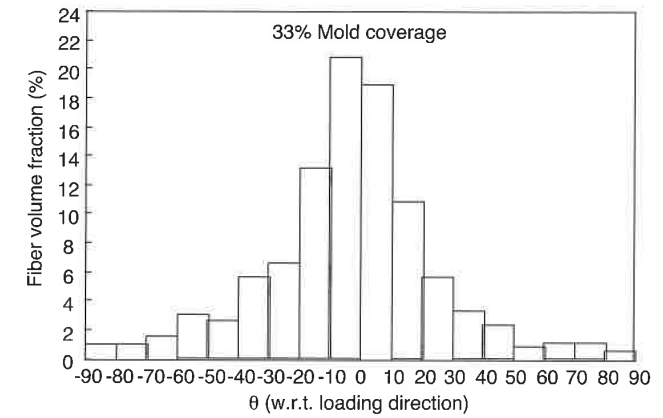**Figure 7.14**    Computer redrawn plot of fibers in a radiograph of a rectangular SMC plate.

**Figure 7.15**    Measured fiber orientation distribution histogram in a plate with 33% initial mold coverage and extensional flow during mold filling.
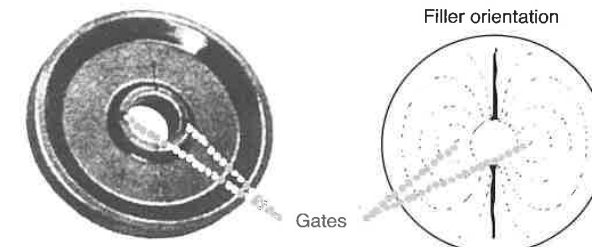


**Figure 7.16**    Formation of knitlines in a fiber filled thermoset pulley.

In compression molding, knitlines are common when multiple charges are placed inside the mold cavity or when charges with re-entrant corners are used, as shown in Fig. 7.17 [18]. However, a re-entrant corner does not always imply the formation of a knitline. For example, when squeezing a very thick charge, an equibiaxial deformation results and knitline formation is avoided. On the other hand, a very thin charge will have a friction dominated flow leading to knitline formation at the beginning of flow. Knitlines may also form when there are large differences in part thickness and when the material flows around thin regions as demonstrated in Fig. 7.18. Here, a crack forms as the material flows past the thinner section of the body panel. It is interesting to point out that usually the thin region will eventually be punched out to give room to headlights, door handles, etc.
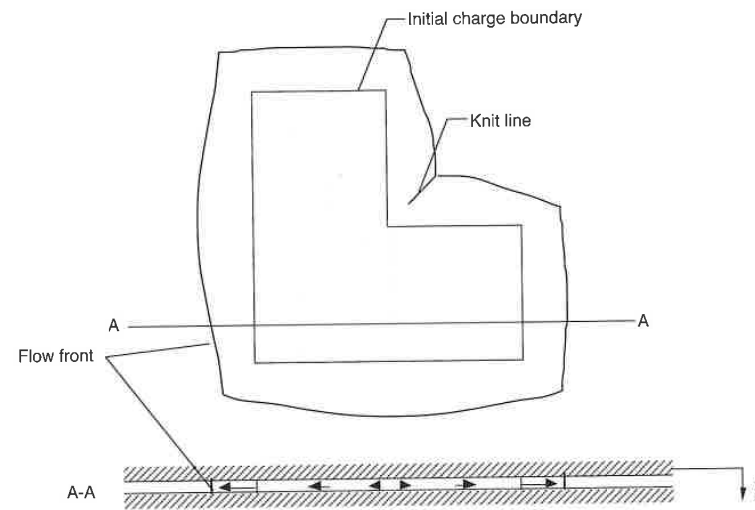
**Figure 7.17**    Knitline formation in an L-shaped charge for a squeeze ratio of 2.
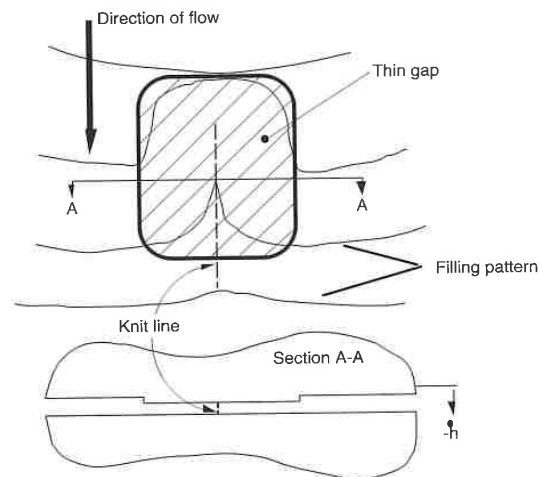


**Figure 7.18**    Schematic of knitline formation as SMC is squeezed through a narrow gap during compression molding.

## 7.2  Predicting Orientation in the Final Part

In general, the orientation of a particle, such as a fiber, is described by two angles, $\phi$ and $\theta$, as shown in Fig. 7.19. These angles change in time as the polymer flows through a die or is stretched or sheared during mold filling. In many cases the angular orientation of a particle can be described by a single angle, $\phi$. This is true since many complex three-dimensional flows can be reduced to planar flows such as the squeezing flow shown in Figs. 7.12 and 7.13 or the channel flow shown in Fig. 7.20. In squeezing flow, the z-dimension is very small compared the other dimensions, whereas in channel flow, the z-dimension is much larger than the other dimensions. Channel flow is often encountered inside extrusion dies, and squeezing flow is common in compression molding where the fiber length is much larger than the thickness of the part. In both cases the fiber is allowed to rotate about the z-axis, with the channel flow having a three-dimensional orientation and the squeezing flow a planar orientation distribution. Due to the simplicity of planar orientation distributions and their applicability to a wide range of applications, we will limit our discussion to two-dimensional systems which can be handled with planar models. However, it should be pointed out that for many polymer articles, such as injection molded parts, a planar orientation is not sufficient to describe the angular position of the fillers or molecules. Since the topic of three-dimensional orientation distribution function is still in the research stages and is therefore beyond the scope of this book, the reader is encouraged to read the literature [6, 7].
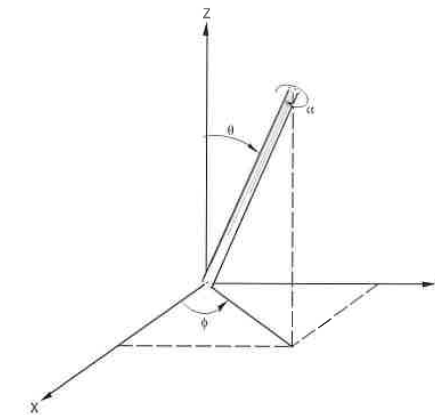


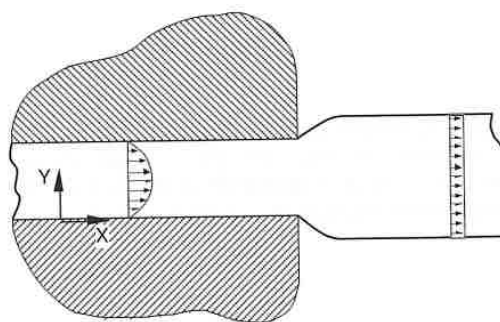**Figure 7.19**    Fiber in a three-dimensional coordinate system.

**Figure 7.20**    Schematic of two-dimensional channel flow.

### 7.2.1  Planar Orientation Distribution Function

The state of particle orientation at a point can be fully described by an orientation distribution function, $\psi(\phi, x, y, t)$. The distribution is defined such that the probability of a particle, located at $x, y$ at time $t$, being oriented between angles $\phi_1$ and $\phi_2$, is given by.

$$P(\phi_1 < \phi < \phi_2) = \int_{\phi_1}^{\phi_2} \psi(\phi, x, y, t)\, d\phi \qquad (7.1)$$

This is graphically depicted in Fig. 7.21. For simplicity, the $x, y, t$ from the orientation distribution function can be dropped.
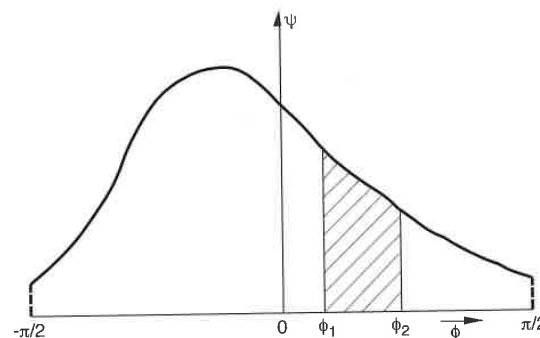


**Figure 7.21**    Orientation distribution function.

Since one end of a particle is indistinguishable from the other, the orientation distribution function must be periodic:

$$\psi(\phi) = \psi(\phi + \pi) \qquad (7.2)$$

Since all particles are located between $-\pi/2$ and $\pi/2$, the orientation distribution function must be normalized such that

$$\int_{-\pi/2}^{\pi/2} \psi(\phi)\, d\phi = 1 \qquad (7.3)$$

The orientation distribution function changes constantly as the particles travel within a deforming fluid element. Assuming the fiber density is homogeneous throughout the fluid and remains that way during processing[3], a balance around a differential element in the distribution function can be performed. This is graphically represented in Fig. 7.22. Here, the rate of change of the fiber density of the differential element, shown in the figure, should be the difference between the number of particles that move into and out of the control volume in a short time period $\Delta t$. This can be written as

$$\frac{\psi(\phi)\Delta\phi}{\Delta t} = \psi(\phi)\dot{\phi}(\phi) - \psi(\phi + \Delta\phi)\dot{\phi}(\phi + \Delta\phi) \qquad (7.4)$$

Letting $\Delta t$ and $\Delta\phi \rightarrow 0$ reduces Eq. 7.4 to

$$\frac{\partial\psi}{\partial t} = -\frac{\partial}{\partial\phi}\left(\psi\dot{\phi}\right) \qquad (7.5)$$

This expression is known as the *fiber density continuity equation*. It states that a fiber which moves out of one angular position must move into a neighboring one, conserving the total number of fibers. If the initial distribution function, $\psi_0$, is known, an expression for the angular velocity of the particle, $\dot{\phi}$, must be found to solve for Eq. 7.5 and determine how the distribution function varies in time. The next sections present various models that can be used to determine the angular rotation of a slender, fiberlike particle.

---

[3]  It is common knowledge that the fiber density is not constant throughout the part. However, this assumption is reasonable for predicting fiber orientation distribution functions.
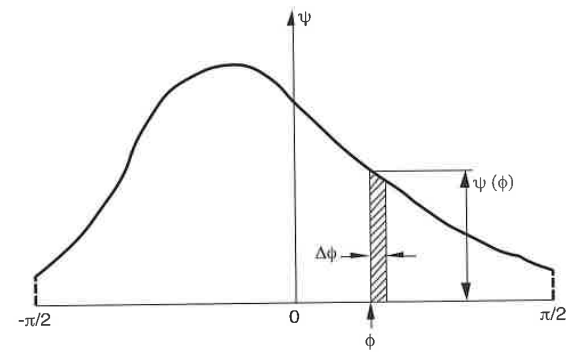
**Figure 7.22** Differential element in an orientation distribution function.

### 7.2.2 Single Particle Motion

The motion of molecules, particles, or fibers can often be described by the motion of a rigid single rod in a planar flow. The analysis is furthermore simplified assuming that the rod is of infinite aspect ratio, that is, the ratio of length to diameter, L/D, is infinite. Using the notation in Fig. 7.23a, the fiber-end velocities can be broken into $x$ and $y$ components and rotational speed of the rod can be computed as a function of velocity gradients and its angular position:

$$\dot{\phi} = -\cos\phi \sin\phi \frac{\partial v_x}{\partial x} - \sin^2\phi \frac{\partial v_x}{\partial y} + \cos^2\phi \frac{\partial v_y}{\partial x} + \sin\phi \cos\phi \frac{\partial v_y}{\partial y} \tag{7.6}$$

Applying this equation to a simple shear flow as shown in Fig. 7.24, the rotational speed reduces to

$$\dot{\phi} = -\frac{\partial v_x}{\partial y} \sin^2\phi \tag{7.7}$$

Figure 7.25 shows the rotational speed, $\dot{\phi}$, as a function of angular position, $\phi$, and Figure 7.26 shows the angular position of a fiber as a function of time for a fiber with an initial angular position of 90°. It should be clear that for this model ($L/D = \infty$) all fibers will eventually reach their 0° position and stay there.
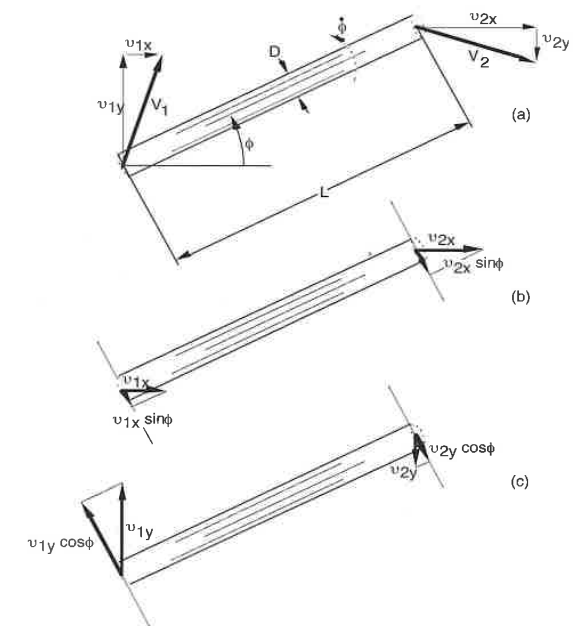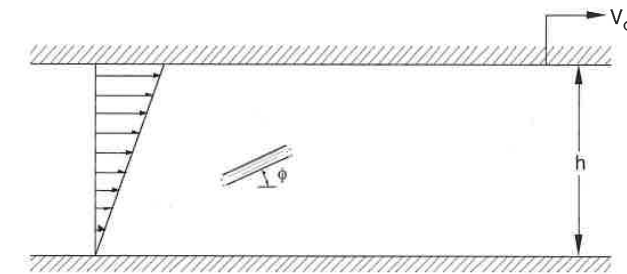
**Figure 7.23** Fiber motion in planar flows.



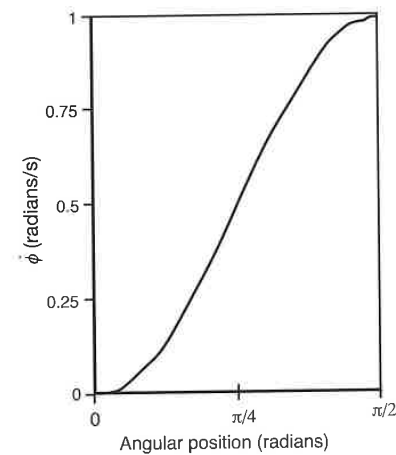**Figure 7.24** Schematic of fiber motion in simple shear flow.

**Figure 7.25**   Rotational speed of a fiber with $L/D = \infty$ in a simple shear flow.
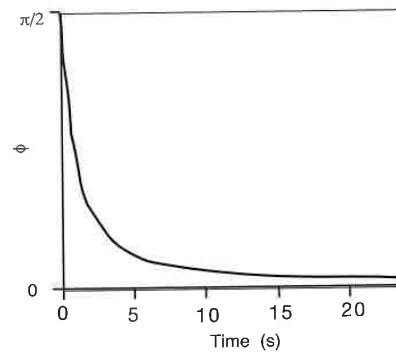


**Figure 7.26**   Angular position of a fiber with $L/D = \infty$ in a simple shear flow.

### 7.2.3 Jeffery's Model

The rotational speed of a single particle, as described in Eq. 7.6, is only valid for an infinite L/D ratio, since the model does not include the rotational speed contribution caused by the thickness dimension of the particle. The thickness term was included in the classical equation derived by Jeffery [19] and describes the rotational motion of a single ellipsoidal particle. His equation was later modified to account for the motion of cylindrical particles or rods [20, 21] and is written as

$$\dot{\phi} = \frac{r_e^2}{r_e^2 + 1}\left(-\sin\phi\cos\phi\,\frac{\partial v_x}{\partial x} - \sin^2\phi\,\frac{\partial v_x}{\partial y} + \cos^2\phi\,\frac{\partial v_y}{\partial x} + \sin\phi\cos\phi\,\frac{\partial v_y}{\partial y}\right)$$
$$- \frac{1}{r_e^2 + 1}\left(-\sin\phi\cos\phi\,\frac{\partial v_x}{\partial x} - \cos^2\phi\,\frac{\partial v_x}{\partial y} + \sin^2\phi\,\frac{\partial v_y}{\partial x} + \sin\phi\cos\phi\,\frac{\partial v_y}{\partial y}\right) \tag{7.8}$$

Here, $r_e$ is the ratio of the major dimensions of the particle, $L/D$. Note that for the infinite $L/D$ case, Eq. 7.8 reduces to Eq. 7.6.

### 7.2.4 Folgar–Tucker Model

A simplification of the Jeffery model is that a dilute suspension is assumed (i.e., very few fibers or fillers are present and do not interact with each other during flow). In polymer processing, this is usually not a valid assumption. In compression molding, for example, in a charge with 20–50% fiber content by volume the fibers are so closely packed that one cannot see through a resinless bed of fibers, even for very thin parts. This means that as a fiber rotates during flow, it bumps into its neighbors making the fiber–fiber interaction a major inhibitor of fiber rotation.

Folgar and Tucker [21, 22] derived a model for the orientation behavior of fibers in concentrated suspensions. For the case of planar flow Folgar and Tucker's model is as follows:

$$\dot{\phi} = \frac{-C_I\dot{\gamma}}{\psi}\frac{\partial\psi}{\partial\phi} - \cos\phi\sin\phi\,\frac{\partial v_x}{\partial x} - \sin^2\phi\,\frac{\partial v_x}{\partial y} + \cos^2\phi\,\frac{\partial v_y}{\partial x} + \sin\phi\cos\phi\,\frac{\partial v_y}{\partial y} \tag{7.9}$$

Here, $\dot{\gamma}$ is the *magnitude of the strain rate tensor* and $C_I$ is a phenomenological coefficient which models the interactions between the fibers. Folgar and Tucker's *interaction coefficient*, $C_I$, varies between 0, for a fiber without interaction with its neighbors, and 1, for a closely packed bed of fibers. For a fiber reinforced polyester resin mat with 20–50% volume fiber content, $C_I$ is usually between 0.03 and 0.06. When Eq. 7.9 is substituted into Eq. 7.5, the transient governing equation for fiber orientation distribution with fiber interaction built-in, becomes

$$\frac{\partial\psi}{\partial t} = -C_I\dot{\gamma}\frac{\partial^2\psi}{\partial\phi^2} - \frac{\partial\psi}{\partial\phi}\left(sc\,\frac{\partial v_x}{\partial x} - s^2\,\frac{\partial v_x}{\partial y} + c^2\,\frac{\partial v_y}{\partial x} + sc\,\frac{\partial v_y}{\partial y}\right)$$
$$- \psi\frac{\partial}{\partial\phi}\left(sc\,\frac{\partial v_x}{\partial x} - s^2\,\frac{\partial v_x}{\partial y} + c^2\,\frac{\partial v_y}{\partial x} + sc\,\frac{\partial v_y}{\partial y}\right) \tag{7.10}$$

where $s$ and $c$ represent sin $\phi$ and cos $\phi$, respectively. The Folgar–Tucker model can easily be solved numerically. Using fiber reinforced thermoset composites as an example, the numerical solution of fiber orientation is discussed in the next section.

### 7.2.5 Tensor Representation of Fiber Orientation

Advani and Tucker [17, 23] developed a more efficient method to represent fiber orientation using orientation tensors. Their technique dramatically reduced the computational requirements when solving orientation problems using the Folgar–Tucker model.

Instead of representing the orientation of a fiber by its angle , $\phi$, Advani and Tucker used the components of a unit vector $p$ directed along the axis of the fiber. The components of $p$ are related to $\phi$,

$$p_1 = \cos\phi \quad \text{and} \tag{7.11a}$$

$$p_2 = \sin\phi \tag{7.11b}$$

where, $p_i$ ($i$=1,2) are the two-dimensional Cartesian components of $p$. A suitably compact and general description of fiber orientation state is provided by the tensor of the form

$$a_{ij} = \left\langle p_i p_j \right\rangle \quad \text{and} \tag{7.12}$$

$$a_{ijkl} = \left\langle p_i p_j p_k p_l \right\rangle \tag{7.13}$$

Here the angle brackets < > represent an average overall possible direction of $p$, weighted by the probability distribution function, and $a_{ij}$ is called the second-order orientation tensor and $a_{ijkl}$ the fourth-order tensor. The properties of these tensors are discussed extensively by Advani and Tucker [24]. For the present, note that $a_{ij}$ is symmetric and its trace equals unity. The advantage of using the tensor representation is that only a few numbers are required to describe the orientation state at any point in space. For planar orientations there are four components of $a_{ij}$, but only two are independent. Advani and Tucker were concerned with planar orientation in SMC only, and used $a_{11}$ and $a_{22}$ to describe the direction and distribution of orientation at a point. Once the orientation tensor $a_{ij}$ is known, the mechanical properties of the composite can be predicted.

The Folgar–Tucker's model for single fiber motion in a concentrated suspension can be combined with the equation of continuity to produce an *equation of change* for the probability function and/or the orientation tensor [17, 25 ,26]. The result of second-order orientation tensors is

$$\frac{Da_{ij}}{Dt} = -\frac{1}{2}\left(\omega_{ik}a_{kj} - a_{ik}\omega_{kj}\right) + \frac{1}{2}\lambda\left(\dot{\gamma}_{ik}a_{kj} + a_{ik}\dot{\gamma}_k - 2\dot{\gamma}_{kl}a_{ijkl}\right) + 2C_i\dot{\gamma}\left(\delta_{ij} - \alpha a_{ij}\right) \tag{7.14}$$

where $\delta_{ij}$ is the unit tensor and $\alpha$ equals 3 for three-dimensional orientation and 2 for planar orientation. Here, $\omega_{ij}$ and $\gamma_{ij}$ are the velocity and the rate of deformation tensors, defined in terms of velocity gradients as

$$\omega_{ij} = \frac{\partial v_j}{\partial x_i} - \frac{\partial v_i}{\partial v_j} \quad \text{and} \tag{7.15}$$

$$\dot{\gamma}_{ij} = \frac{\partial v_j}{\partial x_i} + \frac{\partial v_i}{\partial v_j} \tag{7.16}$$

The material derivative in Eq. 7.14 appears on the left-hand side because the fibers are convected with the fluid. This casts the model of Folgar and Tucker into a useful form for computer simulation.

To calculate components of $a_{ij}$ from Eq. 7.14, $a_{ijkl}$ must be replaced by a suitable closure approximation. Combinations of the unit tensor and the components of $a_{ij}$ can be used to form the approximation. Various closure approximations in planar and three-dimensional flow fields have been extensively tested by Advani and Tucker [17], Verleye and Dupret [27], and Cintra and Tucker [28]. It has been shown that Cintra and Tucker's *orthotropic closure approximation* performs best.

To obtain the orientation state of the fibers during mold filling simulation, Eq. 7.14 can be solved in the context of a finite element/control volume approach filling simulation. Only two equations for $a_{11}$ and $a_{12}$ need be solved. The other components depend on these, and can be replaced on the right-hand side of Eq. 7.14 using $a_{21} = a_{12}$ and $a_{22} = 1 - a_{11}$.

Nodes that lie within the charge at any given time are treated with a conventional Galerkin finite element method. The spatial orientation field is discretized using nodal values of the independent tensor components $a_{11}$ and $a_{12}$ together with element shape function.

The same mesh and linear shape functions that were used in the filling simulation are used for fiber orientation. The resulting finite element equations for fiber orientation may be compactly expressed in a matrix form as

$$\begin{bmatrix} C_{ij} & 0 \\ 0 & C_{ij} \end{bmatrix} \begin{Bmatrix} \dot{a}_{11j} \\ \dot{a}_{12j} \end{Bmatrix} + \begin{bmatrix} K_{Iij} & K_{IIij} \\ K_{IIIij} & K_{IVij} \end{bmatrix} \begin{Bmatrix} a_{11j} \\ a_{12j} \end{Bmatrix} = \begin{Bmatrix} R_i \\ Q_i \end{Bmatrix} \tag{7.17}$$

Here the dot denotes ordinary differentiation with respect to time. This nonlinear system of ordinary differential equation was solved using fully implicit time stepping and a Newton-Raphson technique. The initial condition is provided by the orientation state of the fibers in the initial charge.

Advani [17] compared their model to the experiments and found that, overall, there is a good agreement between experimental and simulation results.

### 7.2.5.1 Predicting Orientation in Complex Parts Using Computer Simulation

Today, computer simulation is commonly used to predict mold filling, fiber orientation, thermal history, residual stresses and warpage in complex parts.

In injection molding, researchers are making progress on solving three-dimensional orientation for complex realistic applications [27, 29]. Crochet and co-workers have solved for the non-isothermal, non-Newtonian filling and fiber orientation in non-planar injection molded parts. They used the Hele–Shaw model [30] to simulate the mold filling and Advani and Tucker's tensor representation for the fiber orientation distribution in the final part. They divided the injection molded part into layers and included the fountain flow effect in the heat transfer and fiber orientation calculations. Figure 7.27 presents the fixed finite element mesh used to represent a 100 x 40 x 1 mm plate and the filling pattern during molding. Figure 7.28 presents the isotherms, the instant of fill, in three layers of the plate shown in Fig. 7.27, and Fig. 7.29 shows the fiber orientation distribution for the same layers.
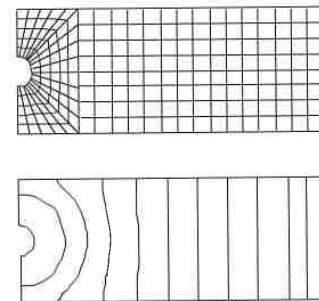


**Figure 7.27**   Fixed finite element mesh used to represent a 100 x 40 x 1 mm plate and temporary mesh adapted to represent the polymer melt at an arbitrary time during filling.
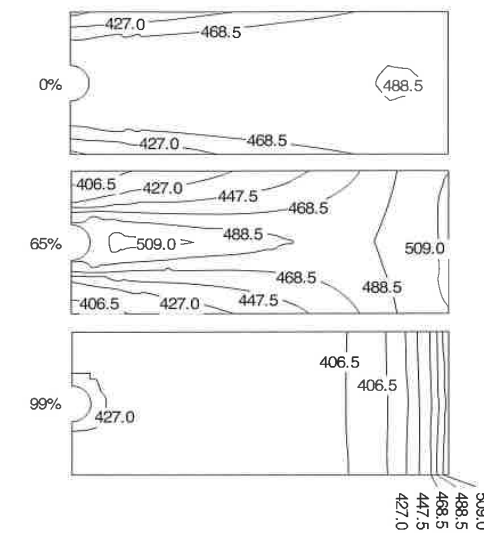


**Figure 7.28**   Isotherms in three layers at, 0 (center-line), 0.65 and 0.99 mm, the instant of fill.
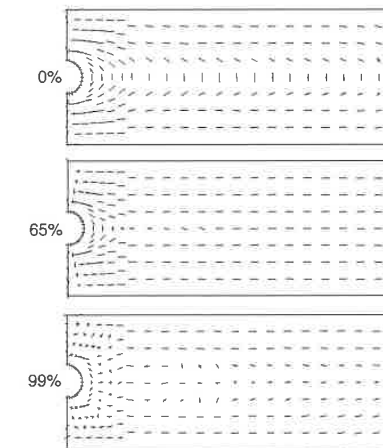


**Figure 7.29**   Fiber orientation in the same three layers shown in Fig. 7.28.

Because planar flow governs the compression molding process, the models described earlier work very well to represent the orientation of the fibers during processing and of the final part. The Folgar–Tucker model, Eq. 7.10, is usually solved using the finite difference technique and the velocity gradients in the equation are obtained from mold filling simulation. The initial condition is supplied by fitting $\psi_i$ ($t = 0$) to the measured initial orientation state. For sheet molding compound charges the starting fiber orientation distribution is usually random, or $\psi_i = 1/\pi$.

The model has proven to work well compared to experiments done with extensional flows described in Section 7.1.2. Figure 7.30 compares the measured fiber orientation distributions to the calculated distributions using the Folgar–Tucker model for cases with 67%, 50%, and 33% initial charge mold coverage. To illustrate the effect of fiber orientation on material properties of the final part, Fig. 7.31 [31] shows how the fiber orientation presented in Fig. 7.30 affects the stiffness of the plates.
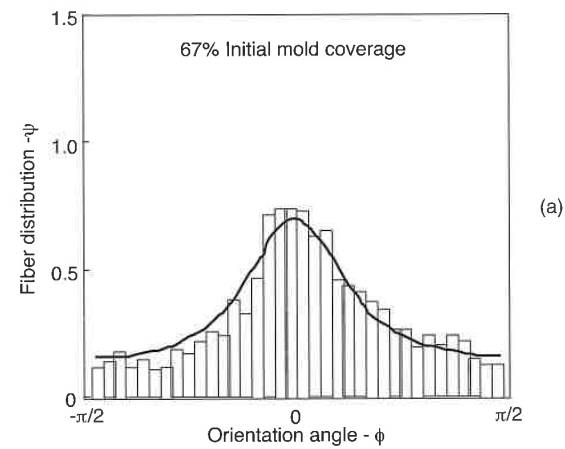


**Figure 7.30**  Comparison of predicted and experimental fiber orientation distributions for SMC experiments with (a) 67% initial mold coverage and $C_I = 0.04$, and (b) 50% initial mold coverage and $C_I = 0.04$ and (c) 33% initial mold coverage and $C_I = 0.04$. *(continued)*
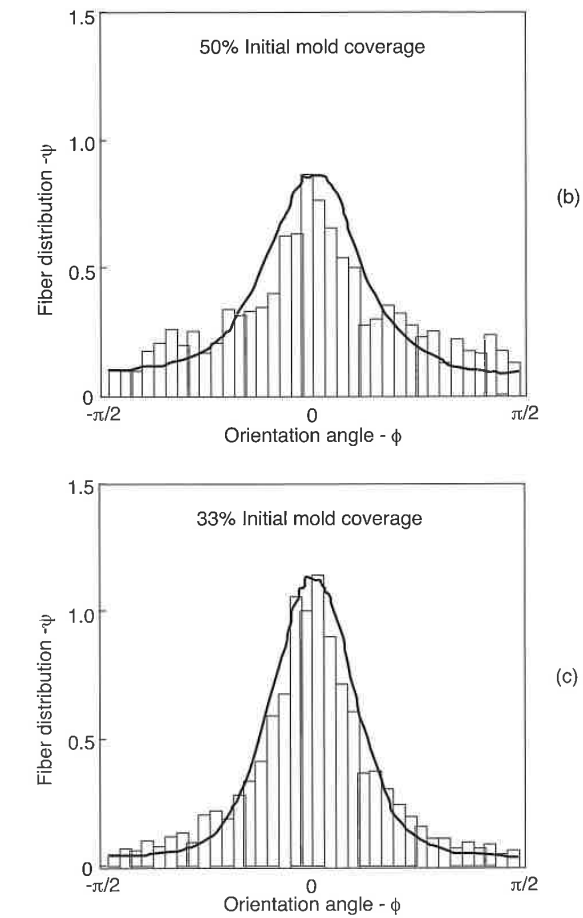




**Figure 7.30** *(continued)*  Comparison of predicted and experimental fiber orientation distributions for SMC experiments with (a) 67% initial mold coverage and $C_I = 0.04$, and (b) 50% initial mold coverage and $C_I = 0.04$, and (c) 33% initial mold coverage and $C_I = 0.04$.
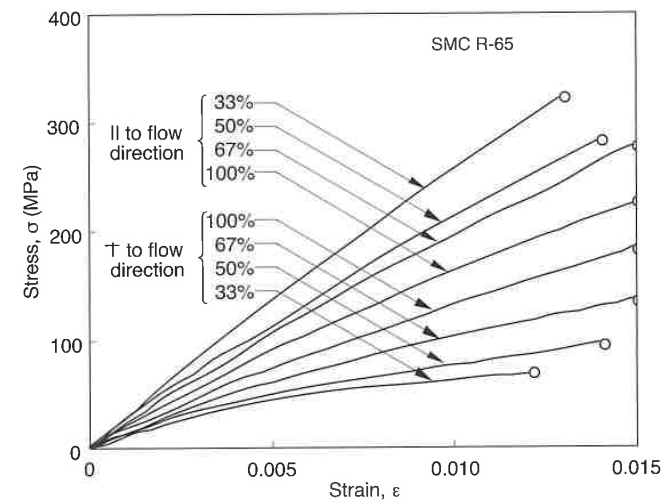
**Figure 7.31**  Stress–strain curves of 65% glass by volume SMC for various degrees of deformation.

The Folgar–Tucker model has been implemented into various, commercially available compression mold filling simulation programs. To illustrate the prediction of fiber orientation distribution in realistic polymer products, the compression molding process of a truck fender will be used as an example. To compute the fiber orientation, the filling pattern must first be computed. This is usually done by using the control volume approach [32]. The initial charge location and filling pattern during compression molding of the fender is shown in Fig. 7.32, and the finite element discretization with which the process was simulated is shown in Fig. 7.33. The fiber orientation distribution field, computed with the Folgar–Tucker model for the compression molded automotive fender under the above conditions is also shown in Fig. 7.33 [33]. For clarity, the orientation distribution function was plotted in polar coordinates from 0 to $2\pi$ and in the center of each finite element that is used for mold filling computation. For more detail about fiber orientation simulation the reader is encouraged to read the literature [34].
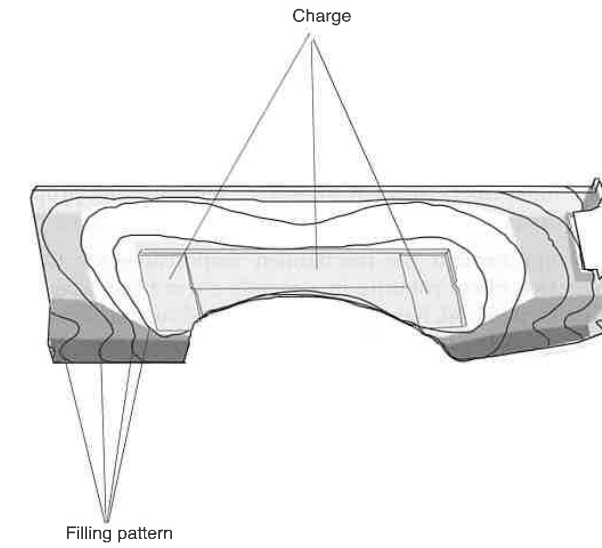
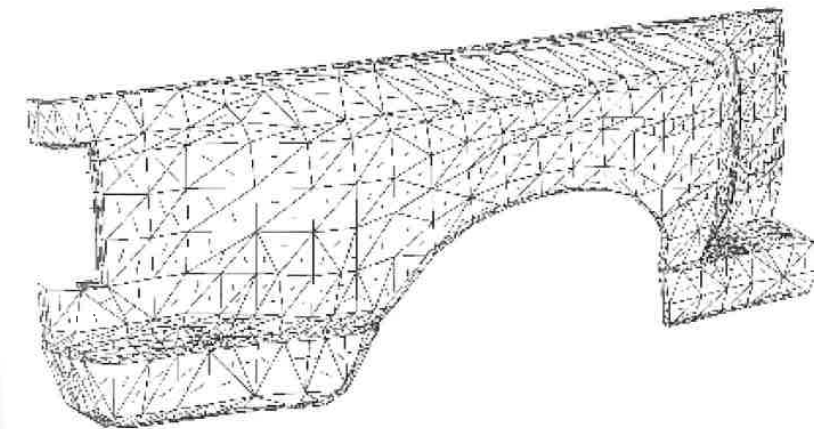**Figure 7.32**  Initial charge and filling pattern during compression molding of an automotive fender.



**Figure 7.33**  Fiber orientation distribution in a compression molded automotive fender.

## 7.3 Fiber Damage

One important aspect when processing fiber reinforced polymers is fiber damage or *fiber attrition*. This is especially true during injection molding where high shear stresses are present. As the polymer is melted and pumped inside the screw section of the injection molding machine and as it is forced through the narrow gate, most fibers shorten in length, reducing the properties of the final part (e.g., stiffness and strength).

Figure 7.34 helps explain the mechanism responsible for fiber breakage. The figure shows two fibers rotating in a simple shear flow: fiber "a", which is moving out of its 0⁰ position, has a compressive loading and fiber "b", which is moving into its 0⁰ position, has a tensile loading. It is clear that the tensile loading is not large enough to cause any fiber damage, but the compressive loading is potentially large enough to buckle and break the fiber. A common equation exists that relates a critical shear stress, $\tau_{crit}$, to elastic modulus, $E_f$, and to the $L/D$ ratio of the fibers

$$\tau_{crit} = \frac{\ln(2L/D) - 1.75}{2(L/D)^4} E_f \qquad (7.18)$$

where $\tau_{crit}$ is the stress required to buckle the fiber. When the stresses are above $\tau_{crit}$ the fiber $L/D$ ratio is reduced. Figure 7.35 shows a dimensionless plot of critical stress versus $L/D$ ratio of a fiber as computed using Eq. 7.18. It is worthwhile to point out that although Eq. 7.18 predicts $L/D$ ratios for certain stress levels, it does not include the uncertainty which leads to fiber $L/D$ ratio distributions– very common in fiber filled systems.
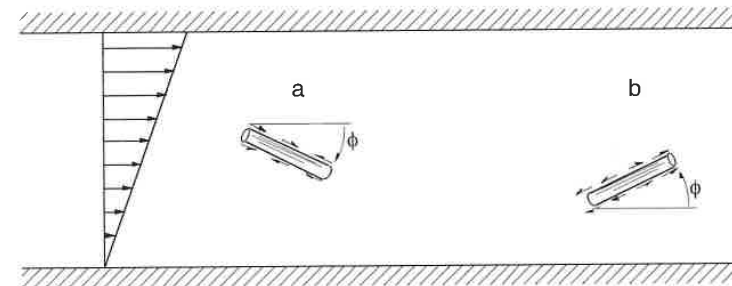


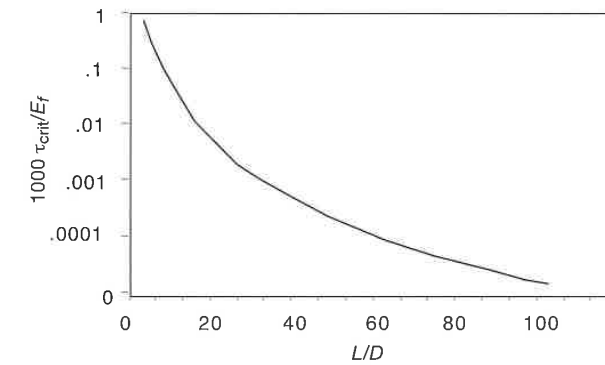**Figure 7.34**   Fiber in compression and tension as it rotates during simple shear flow.



**Figure 7.35**   Critical stress, $\tau_{crit}$, versus fiber $L/D$ ratio.

Figure 7.36 presents findings by Thieltges [35] where he demonstrates that during injection molding most of the fiber damage occurs in the transition section of the plasticating screw. Lesser effects of fiber damage were measured in the metering section of the screw and in the throttle valve of the plasticating machine. The damage observed inside the mold cavity was marginal. However, the small damage observed inside the mold cavity is of great importance since the fibers flowing inside the cavity underwent the highest stresses, further reducing their $L/D$ ratios. Bailey and Kraft [36] also found that fiber length distribution in the injection molded part is not uniform. For example, the skin region of the molding contained much shorter fibers than the core region.
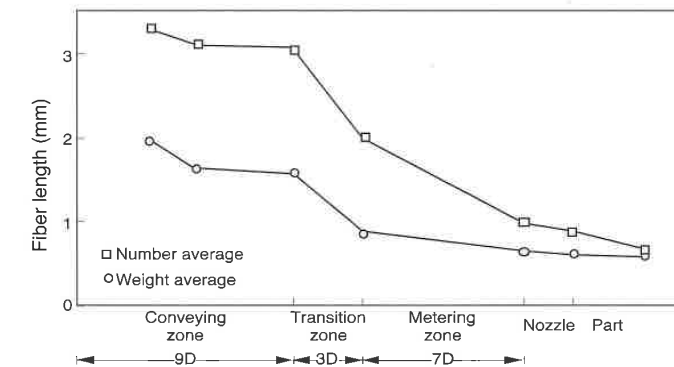


**Figure 7.36**   Fiber damage measured in the plasticating screw, throttle valve and mold during injection molding of a polypropylene plate with 40% fiber content by weight.

Another mechanism responsible for fiber damage is explained in Fig. 7.37 [37], where the fibers that stick out of partially molten pellets are bent, buckled, and sheared-off during plastication.
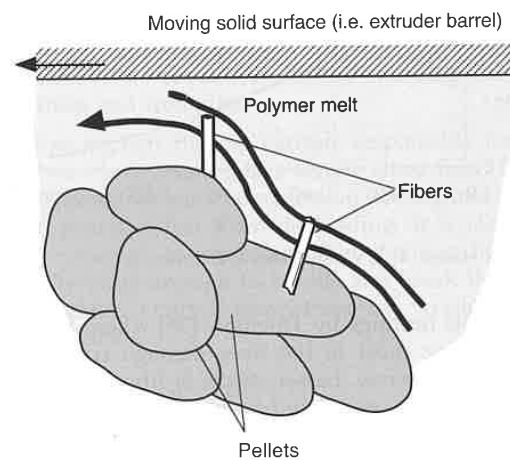


**Figure 7.37**   Fiber damage mechanism is the interface between solid and melt.

**Examples**

7.1   Estimate the fiber length after extruding polyamide 66 reinforced with 33% glass fiber. The initial fiber $L/D$=300, and the fiber diameter is 10 µm. The extruder diameter is 45 mm and the channel depth in the metering section is 5 mm. The extruder rotational speed is 200 rpm. The stiffness of the glass fiber is 90 GPa.

When solving this problem we can assume a simple shear flow in the metering section of the extruder. The maximum speed is computed using

$$v_0 = R\Omega = 22.5\,\text{mm}(200\,\text{rpm})\left(\frac{2\pi}{rev}\right)\left(\frac{1\,\text{min}}{60\,\text{s}}\right) = 471\,\text{mm/s}$$

and the shear with

$$\dot{\gamma} = v_0/h = 471\,\text{mm/s/5mm} = 94\,\text{s}^{-1}$$

At a rate of deformation of 100 s$^{-1}$ the viscosity of PA66 is approximately 66 Pa-s leading to a deviatoric stress of 6204 Pa. We can now either use Eq. 7.18 or Fig. 7.35 with a critical stress equal to 6204 Pa, to find a corresponding $L/D$ of approximately 70.

7.2   Consider a fiber of aspect ratio, $L/D$, of 10 moving in a simple shear flow. Plot the rotational speed of the fiber as a function of angular position, and the angular position as function of time.

If we apply Eq. 7.8 to simple shear flow, it reduces to

$$\dot{\phi} = \frac{1}{r_e^2+1}\cos^2\phi\,\frac{\partial v_x}{\partial y} - \frac{r_e^2}{r_e^2+1}\sin^2\phi\,\frac{\partial v_x}{\partial y} \tag{7.19}$$

When $r_e$ = 10 — typical for a very short, damaged fiber in fiber reinforced composite parts — the equation for rotational speed is

$$\dot{\phi} = 0.01\cos^2\phi\,\frac{\partial v_x}{\partial y} - 0.99\sin^2\phi\,\frac{\partial v_x}{\partial y} \tag{7.20}$$



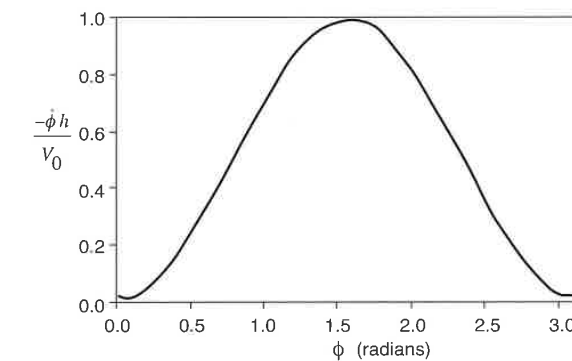**Figure 7.38**   Rotational speed of a fiber with $L/D$ = 10 in a simple shear flow, computed using Jeffery's model.

Figure 7.39 shows the rotation speed, $\dot{\phi}$, as a function of angular position. From Eq. 7.20 it is obvious that, at angular position of 0º, there is a very small rotational speed of $0.01\partial v_x/\partial y$. As the angle moves out of its 0º position it rapidly increases in speed to a maximum of

$0.990 \partial v_x / \partial y$ at 90º. Hence, most of the time a fiber is oriented in its 0º position. Figure 7.38 shows this effect by plotting the angular position of the fiber with respect to time. The effect is further increased for higher $L/D$ ratios. Therefore, in shear dominated flows, most of the fibers will be oriented in the direction of the shear plane on which they are traveling. In polymer processes such as extrusion and injection molding, the main mode of deformation is shear. The relationship in Eq. 7.19 and the behavior seen in Fig. 7.39 apply for each plane with its individual gradient $\partial v_x / \partial y$. In processes such as fiber spinning and compression molding, the main modes of deformation are elongational and a similar analysis as done above may be performed.
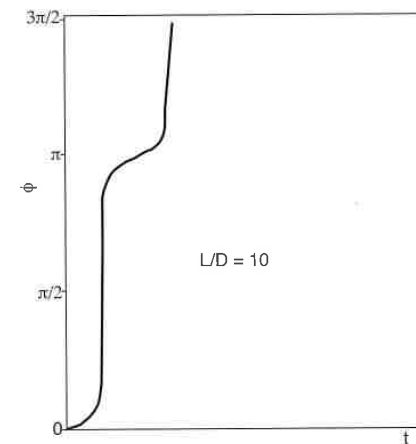


**Figure 7.39**   Angular position of a fiber with L/D = 10 in a simple shear flow, computed using Jefferey's model.

## Problems

7.1   Consider the compression molding process of a circular sheet molding compound (SMC) charge. The charge is composed of 30% by volume 1 in. long glass fibers in an unsaturated polyester resin. The flow field when compression molding a circular charge is described with the following equations: $v_x = x/2$ and $v_y = y/2$. How will the fibers orient if the initial planar orientation is random? Explain.

7.2   Does a lower melt temperature during injection molding lead to higher or lower degrees of molecular orientation? Why?

7.3   Would you use polystyrene to injection mold CD's? Why?

7.4   When manufacturing a component that includes a small lens, would you place the injection gate near the lens edge, or as far as possible from the lens? Why?

7.5   Find an injection molded transparent polystyrene component and observe it through cross-polarizers. Determine the location of the gate. Point out the places of highest and lowest orientation within the part.

7.6   Is there a direct relation between the fringe patterns that you see when observing a transparent component through cross-polarizers and the residual stresses that built up during manufacturing? Why?

7.7   A 45 mm single screw extruder is used to extrude plates manufactured of polyamide 66 filled with 33% glass fiber by volume. Given that the extruder is rotating at 120 rpm and that the channel depth in the metering section is 5 mm, estimate the average final L/D of the fibers.

7.8   Work out example 7.1 for an aspect ratio, L/D, of 100. Plot the rotational speed as a function angular position, and angular position as a function of time.

7.9   The charge location and filling pattern during compression mold filling of a truck wind deflector  is presented in Fig. 7.40 [38]. The part was molded using two sheet molding compound (SMC) charges, one 8 layer charge and another 9 layer charge.

Is there a knitline in the finished product? If yes, sketch a diagram with its approximate location in the finished part.

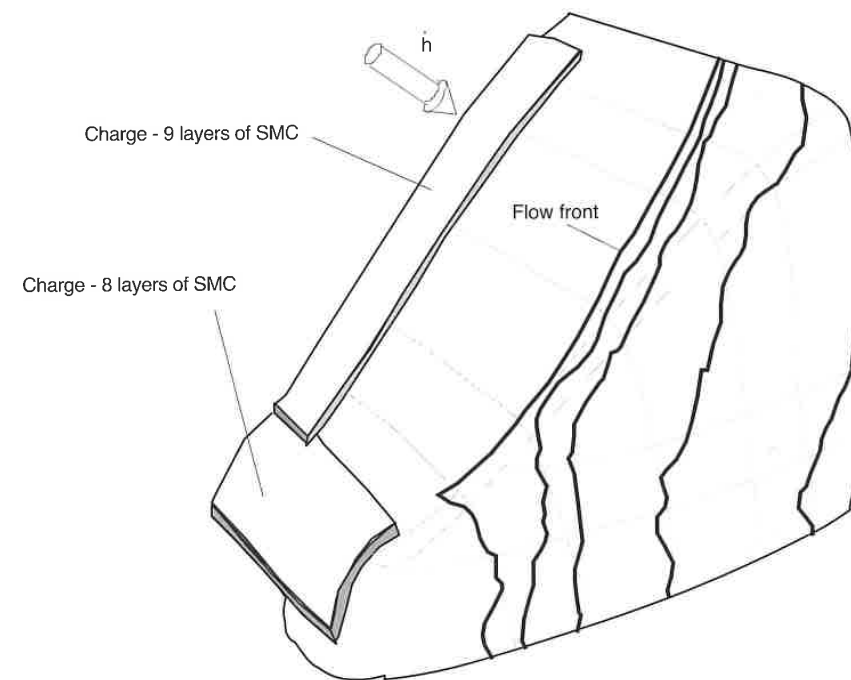Point out the areas of maximum fiber orientation.

**Figure 7.40**   Actual mold filling pattern during compression molding of an SMC truck wind deflector

## References

1. Woebken, W., *Kunststoffe, 51,* 547, (1961).
2. Menges, G., and Wübken, W., *SPE, 31st ANTEC,* (1973).
3. Wimberger-Friedl, R., *Polym. Eng. Sci.,* 30, 813, (1990).
4. Wimberger-Friedl, R., Ph.D. Thesis, Eindhoven University of Technology, The Netherlands, (1991).
5. Menges, G., and Geisbüsch, P., *Colloid & Polymer Science, 260,* 73, (1982).
6. Bay, R.S., and Tucker III, C.L., *Polym. Comp., 13,* 317, (1992a).
7. Bay, R.S., and Tucker III, C.L., *Polym. Comp., 13,* 322, (1992b).
8. Menges, G., Schacht, T., Becker, H., and Ott, S., *Intern. Polymer Processing, 2,* 77, (1987).
9. Leibfried, D., Ph.D. Thesis, IKV, RWTH-Aachen, Germany, (1970).
10. Wübken, G., Ph.D. Thesis, IKV, RWTH-Aachen, (1974).
11. Mavrides, H., Hrymak, A.N., and Vlachopoulos, J., *Polym. Eng. Sci., 26,* 449, (1986).
12. Ibid.
13. Mavrides, H., Hrymak, A.N., and Vlachopoulos, J., *J. Rheol.,* 32, 639, (1988).
14. Barone, M.R., and Caulk, D.A., *J. Appl. Mech.,* 361, (1986).
15. Lee, C.-C., Folgar, F., and Tucker III, C.L., *J. Eng. Ind.,* 186, (1984).
16. Jackson, W.C., Advani, S.G., and Tucker III, C.L., *J. Comp. Mat., 20,* 539, (1986).
17. Advani, S.G., Ph.D. Thesis, University of Illinois at Urbana-Champaign, (1987).
18. Barone, M.R., and Osswald, T.A., *Polym. Comp., 9,* 158, (1988).
19. Jeffery, G.B., *Proc. Roy. Soc., A102,* 161, (1922).
20. Burgers, J.M., *Verh. K. Akad. Wet., 16,* 8, (1938).
21. Folgar, F.P., Ph.D. Thesis, University of Illinois at Urbana-Champaign, (1983).
22. Folgar, F.P., and Tucker III, C.L., *J. Reinf. Plast. Comp., 3,* 98, (1984).
23. Advani, S.G. and Tucker III, C.L., *Polym. Comp., 11,* 164, (1990).
24. Advani, S.G. and Tucker III, C.L., *J. Rheol.,* 31 (1987).
25. Folgar, F. and Tucker III, C.L., *J. Reinf. Plast. Comp., 3,*98 (1984).
26. Jackson, W.C., Advani, S.G., and Tucker III, C.L., *J. Comp. Mat., 20,* :539, (1986).
27. Verleye, V., and Dupret, F., *Proc. ASME WAM,* New Orleans, (1993).
28. Cintra, J. S., and Tucker III, C.L., *J. Rheol.,* forthcoming(1995).
29. Crochet, M.J., Dupret, F., and Verleye, V., *Flow and Rheology in Polymer Composites Manufacturing,* Ed. S.G. Advani, Elsevier, Amsterdam, (1994).
30. Hele-Shaw, H.S., *Proc. Roy. Inst., 16,* 49, (1899).
31. Chen, C.Y., and Tucker III, C.L., *J. Reinf. Compos., 3,* 120, (1984).
32. Osswald, T.A., and Tucker III, C.L., *Int. Polym. Process.,* 5 79, (1989).
33. Gramann, P.J., Sun, E.M., and Osswald, T.A., *SPE 52nd Antec,* (1994).
34. Tucker III, C.L., and Advani, S.G., *Flow and Rheology in Polymer Composites Manufacturing,* Ed. Advani, Elsevier, Amsterdam, (1994).
35. Thieltges, H.-P., Ph.D. Thesis, RWTH-Aachen, Germany, (1992).
36. Bailey, R., and Kraft, H., *Intern. Polym. Proc., 2,* 94, (1987).
37. Mittal, R.K., Gupta, V.B., and Sharma, P.K., *Composites Sciences and Tech.,* 31, 295, (1988).
38. Osswald, T.A., Ph.D. Thesis, University of Illinois at Urbana-Champaign, (1986).

# Solidification of Polymers

Solidification is the process in which a material undergoes a phase change and hardens. The phase change occurs as a result of either a reduction in material temperature or a chemical curing reaction. As discussed in previous chapters, a thermoplastic polymer hardens as the temperature of the material is lowered below either the melting temperature for a semi-crystalline polymer or the glass transition temperature for an amorphous thermoplastic. A thermoplastic has the ability to soften again as the temperature of the material is raised above the solidification temperature. On the other hand, the solidification of a leads to cross-linking of molecules. The effects of cross-linkage are irreversible and lead to a network that hinders the free movement of the polymer chains independent of the material temperature.

## 8.1 Solidification of Thermoplastics

The term "solidification" is often misused to describe the hardening of amorphous thermoplastics. The solidification of most materials is defined at a discrete temperature, whereas amorphous polymers do not exhibit a sharp transition between the liquid and the solid states. Instead, an amorphous thermoplastic polymer vitrifies as the material temperature drops below the glass transition temperature, $T_g$. A semi-crystalline polymer does have a distinct transition temperature between the melt and the solid state, the melting temperature, $T_m$.

### 8.1.1 Thermodynamics During Cooling

As heat is removed from a polymer melt, the molecules loose their ability to move freely, thus making the melt highly viscous. As amorphous polymers cool, the molecules slowly become closer packed, thus changing the viscous